The biology of ADGRL4/ELTD1 in angiogenesis and tumour development

Koon Hwee Ang

Christ Church

University of Oxford

A thesis submitted for the degree of:

Doctor of Philosophy

Trinity Term 2019

Supervisors:

Professor Adrian L. Harris

Professor Alison H. Banham

ABSTRACT

ADGRL4/ELTD1 is an orphan adhesion G protein-coupled receptor that is expressed in both endothelial cells and vascular smooth muscle cells. ELTD1 expression was significantly upregulated in the tumour vasculature and previous studies in our laboratories identified ELTD1 as a novel regulator of tumour angiogenesis. The aims of this project were to further investigate ELTD1's *in vivo* role in the normal and tumour vasculature. In this project, both constitutive and inducible endothelial cell-specific *Eltd1* knockout mouse models were generated using *Tie2-Cre* and *Pdgfb-Cre* lines respectively. Both models exhibited no significant differences in body and organ weights, or other welfare parameters such as behaviour and movement. There were no observed immunohistochemical differences (CD31 and H&E) in the vital organs namely, brain, heart, lung, liver, kidney and spleen. Interestingly, inducible endothelial cell-specific *Eltd1* knockout aortic rings showed inhibition in endothelial cell sprouting that was not observed in the constitutive knockout, suggesting a functional compensatory mechanism in the constitutive model. In both E0771 and MC38 syngeneic tumour models, despite no significant differences in tumour growth curves and survival outcomes, there were observed immunohistochemical differences with generally higher necrosis and hypoxia, and reduction in microvessel density and pericyte coverage in the *Eltd1* knockout tumours. Both genetic and drug induced endothelial-*Eltd1* deletion gave similar results which affirmed the effects of endothelial-*Eltd1* on the tumour vasculature *in vivo.* Single cell sequencing of acute *Eltd1*-depleted lung endothelial cells revealed heterogeneity in *Eltd1*-expressing endothelial cells and showed that lung capillary endothelial cells had higher *Eltd1* expression compared to lung arterial endothelial cells. Interestingly, their differential gene expression profiles were distinct. But in both endothelial cell subsets, there were differentially regulated genes whose functions have been associated with endothelial biology, angiogenesis, tumour development and immunology. In summary, endothelial-*Eltd1* depletion did not cause toxicity but altered the tumour microenvironment. Therefore, ELTD1 could be considered as a potential target for cancer therapy in combination with other therapies targeting hypoxia and angiogenesis.

This thesis is dedicated to

my beloved family and inspiring mentors.

‘I know there is truth opposite to falsehood,

that it may be found if people will, and is worth the seeking,

and is not only the most valuable, but the pleasantest thing in the world.’

- John Locke, *Philosopher* (Christ Church, Oxford)

ACKNOWLEDGMENTS

I would like to express my deepest gratitude to my supervisors, Professor Adrian Harris and Professor Alison Banham for accepting me as their DPhil student and for their patient guidance and support over the years in my DPhil. It has been a pleasure to be under their supervision and I have learnt tremendously in this period.

To my day-to-day supervisors, Dr Esther Bridges and Dr Helen Sheldon, many thanks for the support in the *in vivo* and *in vitro* work that I did in lab. And much appreciation goes towards Dr Massimo Masiero, Dr Amanda Anderson and Dr Demin Li for their advice and help whenever I needed them. It has been a real joy working with Dian Wang, Salwa Lin and Dr David Favara in the lab as students in the ELTD1 project and also other DPhil students like Dr Kate Feldinger, Dr Simon Brooks, Dr Iva Trenevska, Dr Eugene Teoh, Dr Matteo Motti etc, a lot of tears and sweat and encouragements along the way.

The DPhil project would not be possible without the contribution from our collaborators. I thank our collaborators namely, Professor Peter Carmeliet, Professor Paul Riley, Professor Sarah De Val, Professor Francesco Pezzella, Dr Dimitrios Voukantsis, Professor Francesca Buffa and Professor Penny Handford etc.

I would like to thank all Harris lab members (both current and past) namely, Dr Ana Cuervo, Dr Sofia Nascimento dos Santos, Dr Pavitra Kannan, Dr Karim Bensaad, Dr Christos Zois, Dr ShiJie Cai, Dr Syed Haider, Dr Alessandro Valli, Samantha Oats, Penny Berry, Dr Shaunna Beadie, Dr Laurel Jolie for their advice in the lab and Linda and Rose for preparing the reagents and order consumables for us. In addition, I am appreciative for the help rendered by Dr Caroline Fitchett, Katherine Morrison, Andrew Mortimer and Pete Thomas in the daily maintenance of equipment. I would like to give my heartfelt thanks to all Banham Lab members (both current and past) and NDCLS staff namely, Dr Duncan Gascoyne, Dr Ling Felce, Linden Lyne, Hayley Spearman, Carol Bentley, Tasneem Hassanali, Dr Andrew Graham, Stacey Da Silva and Dr Shazia Irshad. It has also been a pleasure interacting with the visiting scientists (students, postdocs and group leaders) in both labs.

I would like to also thank my college friends namely, Caterina, Aurelio, Kris, Sibyl, Rut, Sally and like-minded comrades like Andrew, Isaac, Joseph and Jeff for their awesome company! I would be unimaginably home sick without my Singaporean kakis like Yuen Siang, Shi Yu, Choon Boon and Peter for the frequent meet up on mah-jong, board games and homecooked cuisines. I thank my friends for contributing to this wonderful Oxford experience.

Being an overseas student, I have learnt to appreciate the everyday goodness. I thank my first friends, Linda and Hazel (WIMM reception), several OBC bus '400' conductors, the cleaners in WIMM and NDCLS, the staff in John Radcliffe Hospital canteen, and to emphasize, the marvellous friends I have made in At Thai and Sasi Thai.

Paying a tribute to my inspiring mentors, SB and Mr Tan, thank you for coming into my life and guiding me to somewhere I could only dream of. To my A*STAR mentor, Professor Zeng, thanks for encouraging me in the things I have set out to achieve.

To my grandmothers, Dad, Mum, brother KS, Aunts Esther and Angela, I thank you for allowing me to pursue my dreams without fear and considerations. To my scholarship guarantors, uncle Kevin and cousin Christine, thanks for believing in my passion and my plan to make it a reality.

To the generous funding by the Agency for Science, Technology and Research (A*STAR Singapore), I cannot thank you enough for granting me the scholarship to pursue this aspiration.

TABLE OF CONTENTS

LIST OF FIGURES

LIST OF TABLES

LIST OF ABBREVIATIONS

°C	degrees Celsius
7TM	seven transmembrane domain
aEC	arterial endothelial cell
Ang1	Angiotensin-1
BC	breast cancer
bFGF	Basic fibroblast growth factor
Bp	base pair
BSA	bovine serum albumin
capilEC	capillary endothelial cell
CCRCC	clear cell renal cell carcinoma
cEC	continuum endothelial cell
CIS	Carcinoma *in situ*
CTF	C terminal fragment
DEPC	diethyl pyrocarbonate
DLL4	delta like 4 ligand
DNA	Deoxyribonucleric acid
dNTP	deoxynucleoside triphosphate
EC	endothelial cell
ECD	extracellular domain
EGF	Epidermal growth factor
EGFP	enhanced green fluorescent protein
EGM2	Endothelial growth medium 2
ELTD1	Epidermal growth factor, latrophilin and seven transmembrane domain protein 1
ER	Estrogen receptor
FACS	Fluorescence-activated cell sorting
FB	fibroblast
FBS	Foetal bovine serum
Fl	Floxed

FRET	Fluorescence resonance energy transfer
GAIN	GPCR autoproteolysis inducing domain
GBM	Glioblastoma multiforme
GPCR	G protein-coupled receptor
GPS	GPCR proteolysis site
H&E	Hematoxylin & Eosin
HNSCC	Head and neck squamous cell carcinoma
HRP	Horseradish peroxidase
HTRF	Homogeneous time resolved fluorescence
HUVEC	Human umbilical vein endothelial cell
ICD	Intracellular domain
IF	Immunofluorescence
IHC	Immunohistochemistry
KO	Knockout
LEC	Lymphatic endothelial cell
µg	microgram
µL	microlitre
µM	micromolar
NCBI	National Centre for Biotechnology Information
NTF	N terminal fragment
PAC	P1-derived artificial chromosome
PBS	Phosphate
PC	Pericyte
PCR	Polymerase chain reaction
Pdgfb	Platelet derived growth factor b
PECAM-1	Platelet endothelial cell adhesion molecule-1
qPCR	Quantitative polymerase chain reaction
RCC	Renal cell carcinoma
scRNAseq	Single cell sequencing
siRNA	Small interfering RNA
Tie2	Tyrosine-protein kinase receptor

TKI	Tyrosine kinase inhibitor
TNBC	Triple negative breast cancer
TSO	Template switch oligo
VEGF	Vascular endothelial growth factor
VEGFR2	Vascular endothelial growth factor receptor 2
WHO	World Health Organisation
WT	Wildtype

Chapter 1: Introduction

1.1 Introduction

Cancer is a disease characterised by the abnormal growth of cells that can invade or spread to other parts of the body. According to the World Health Organisation, cancer remains the second leading cause of death and about 9.6 million patients globally were estimated to die of cancer in 2018. The total annual economic cost of cancer in 2010 has been estimated to be US$1.16 trillion. There are many types of cancer. The most common types of cancer in men are lung, prostate and colorectal cancer while breast, colorectal and lung cancer are most common among women. Cancer can also be categorised into different stages from preneoplastic lesions to *in situ* invasive and metastatic, depending on the location and aggressiveness of the tumour. Common causes of cancer have been highlighted such as, smoking and tobacco, diet, radiation and viruses. Current cancer therapies include surgery, chemotherapy, radiotherapy and immunotherapy. Over the years, there has been enormous efforts invested into cancer research. In the past few decades, the advancement of technology has also paved the way for genome sequencing which allows for targeted therapies to correct genetic abnormalities and the development of personalised therapy. However, cancer remains a difficult disease to treat due to several issues such as the clonal evolution of tumour cells (Greaves and Maley, 2012) and the development of resistance to therapies in patients.

Tumours without a blood supply do not grow larger than 2-3 mm^3 (Folkman, 1971) because the diffusion of oxygen and nutrients is limited by distance. In order for the tumours to grow, cancer cells utilise several processes to obtain their blood supply, these typically include vessel co-option (Carmeliet and Jain, 2000) and angiogenesis. Angiogenesis is the process of new blood vessel formation from pre-existing vessels and it is one of the modes of vascularization that has been implicated as one of the hallmarks of cancer that is central to tumour development and metastasis (Fouad and Aanei, 2017) (Figure 1.1). Cancer cells and cancer-associated fibroblasts secrete growth factors, such as vascular endothelial growth factor (VEGF) (Pradeep et al., 2005, Byrne et al., 2005) and basic fibroblast growth factor (bFGF) (Rak and Kerbel, 1997), which activate downstream mechanisms and trigger the

angiogenic switch (Figure 1.2). This signalling to vascular cells encourages endothelial cells and vascular smooth muscle cells to grow towards the cancer cells (Kos and Dabrowski, 2002, Hanahan and Folkman, 1996). This gives an extra blood supply to the tumour, supports abnormal high rates of cellular proliferation and facilitates metastasis. The process of tumour angiogenesis was described in the early 1970s and it was hypothesised that 'starving the cancer' by cutting off the excess blood supply, or 'anti-angiogenic' therapies, could be a way to treat cancer (Folkman, 1971). However, tumours with co-opted vessels may display resistance to anti-angiogenic therapies.

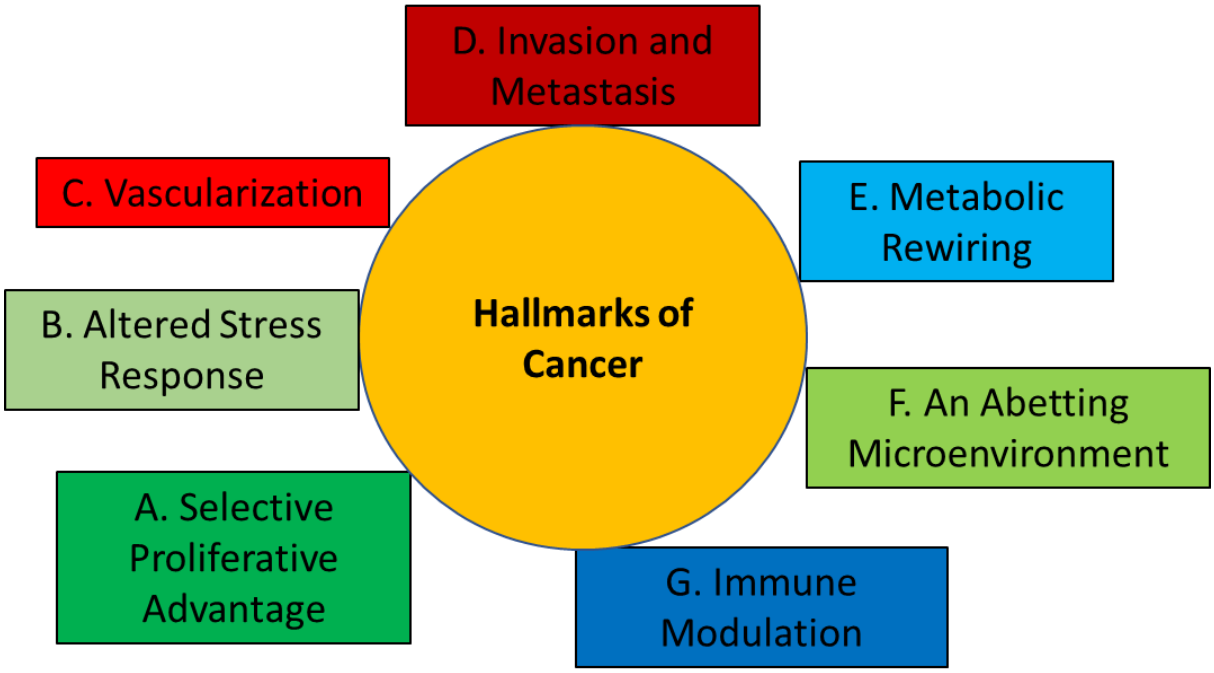

Figure 1.1: The hallmarks of cancer. This illustrates the multiple aspects that are critical in the development of cancer, namely, A) selective proliferative advantage by tapping on the growth promoters and suppressors, B) altered responses to stresses such as, apoptosis and senescence, C) vascularization to support the abnormal growth of cancer cells, D) invasion-metastasis cascade, E) metabolic alterations in cancer cells, F) an abetting microenvironment and G) immune modulation in cancer initiation and progression. (Fouad and Aanei, 2017)

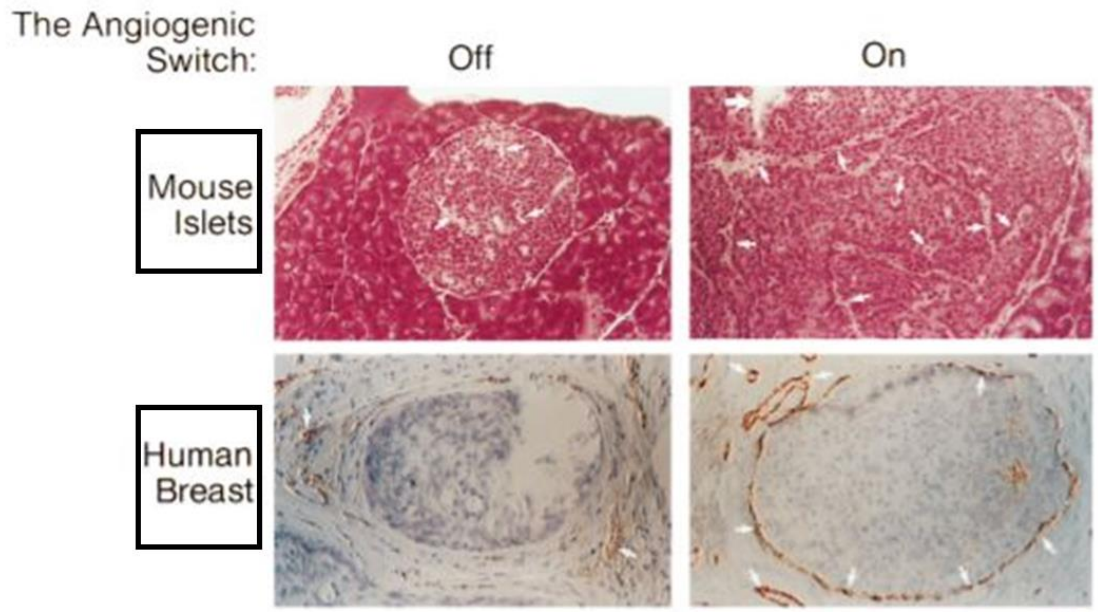

Figure 1.2: Histological illustration of the angiogenic switch. The mouse islets panel (top) shows a hyperplastic mouse islet with vessels in the quiescent state (left) and an islet nodule (right) with more vessels (white arrows) and vascular lacuna (big white arrow) when the angiogenic switch is on. The human breast panel (bottom) shows a CIS (carcinoma *in situ*) duct-associated vessels (left) and CIS lesion with increased neovascularisation (right) when the angiogenic switch is on. The islets sections were stained with haematoxylin and eosin and the breast sections were stained with antisera to an endothelial marker, von Willebrand factor (vWF) and counterstained with haematoxylin. Figure modified from Hanahan & Folkman, 1996.

During embryonic development, vessels are formed from endothelial precursors in a process called vasculogenesis. Following this, the network expands by either sprouting angiogenesis or intussception, the latter involves the insertion of interstitial tissue columns into the lumen of pre-existing vessels (Patan et al., 1996). During tumour development, vessels are formed by sprouting or intussusception from pre-existing vessels (Carmeliet and Jain, 2000). Sprouting angiogenesis is a multi-step process that involves vessel dilation and leakiness in response to VEGF which overcomes the functions of Ang1 and vessel-tightening junctional molecules, such as VE-Cadherin and platelet-endothelial cell-adhesion molecule-1 (PECAM-1). Following this, Ang2 and proteinases facilitate the dissolution of the interstitial matrix and basement membrane to provide an outlet for endothelial cells into new vessels. Various molecules, such as VEGF, bFGF and Ang1 then stimulate the proliferation, migration and assembly of endothelial cells. Several cell-matrix receptors like $\alpha_v\beta_3$ and α_5 integrins also facilitate the migration of endothelial cells. Maturation of these neovessels involves the formation of a new basement membrane and recruitment of pericytes and smooth muscle cells by PDGF-BB. Signalling via TGF-β1 and Ang1/Tie2 assist in the stabilisation of the crosstalk between endothelial cells and smooth muscle cells (Carmeliet and Jain, 2000). The pericytes and smooth muscle cells stabilise the neovessels by wrapping around the endothelial cells and this is a phenotype of mature vessels. Figure 1.3 gives an overview of the angiogenic process (Griffioen and Molema, 2000).

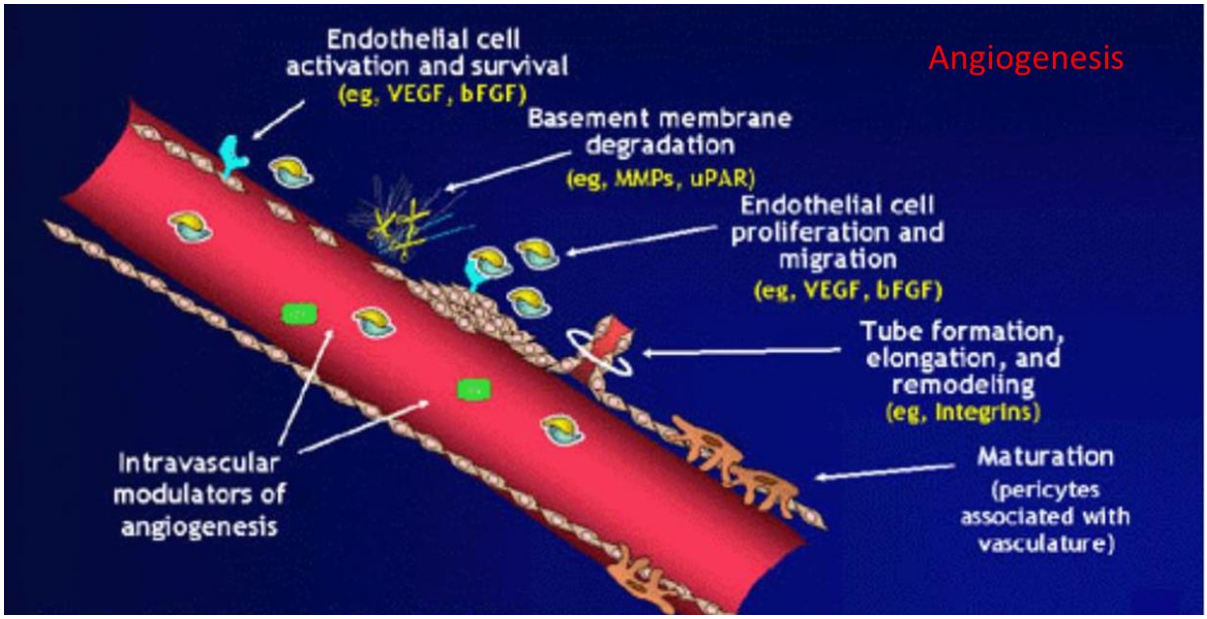

Figure 1.3: Schematic representation of angiogenesis. This illustrates a multi-step process that consists of the activation of endothelial cells by growth factors (VEGF, bFGF), degradation of the basement membrane, proliferation and migration of endothelial cells, formation and elongation of tubes outwards and finally the maturation of neovessels when they become associated with pericytes. Figure modified from Griffioen & Molema, 2000.

However, tumour vessels are structurally and functionally different from normal vessels, and they lack protective mechanism that normal vessels utilise during growth. For instance, tumour vessels may lack functional perivascular cells which protect vessels against changes in oxygen levels or hormonal imbalances, provide essential vasoactive control to support metabolic requirements and induce vascular quiescence (Benjamin et al., 1999). Structurally, the walls of tumour vessels may be made up of cancer cells or a mosaic of cancer and endothelial cells (Carmeliet and Jain, 2000). The presence of these cancer cells in newly formed vessels has important implications for metastasis (Carmeliet and Jain, 2000). Furthermore, due to their structural differences, tumour vessels are often leaky, this compromises their functionality and perfusion is affected which results in a hypoxic core in the tumour and in turn, leads to hypoxia-induced angiogenesis (Harris, 2002). Hypoxia can also select for more aggressive phenotypes in cancer cells by altering their metabolism etc (Petrova et al., 2018). Leaky vessels can also impair drug delivery and thus affects the efficacy of therapy.

This phenomenon led to the emergence of the concept of tumour vessel normalisation (Jain, 2005). By transiently normalising the structurally and functionally abnormal tumour vasculature, it may be possible to restore efficient delivery of oxygen and drugs. This, in turns, leads to a reduced hypoxic core and a less aggressive tumour phenotype.

The mechanistic understanding of tumour angiogenesis has greatly helped in the development of therapeutics against known angiogenic targets. Several VEGF blockers have been approved by the US Food and Drug Administration (FDA) for the treatment of cancer and eye diseases (Tandle and Libutti, 2003, Carmeliet and Jain, 2011a). For instance, the VEGF-neutralising antibody Bevacizumab (Avastin^{TM}) has been approved for the treatment of metastatic breast cancer, metastatic colorectal cancer, metastatic non-squamous non-small-cell-lung cancer, recurrent glioblastoma multiforme (GBM) and metastatic renal cell carcinoma (RCC). Multi-target tyrosine kinase inhibitors (TKIs) which block several signalling pathways including those activated by VEGF, for example, sunitinib (Sutent) has been used in the treatment of metastatic RCC (Carmeliet and Jain, 2011a). VEGF inhibitors prolong the time to tumour progression of responsive patients with cancer but have minimal effect on overall survival. Thus, the clinical use of VEGF blockers has several challenges. For instance, TKIs targeting the VEGF receptor have been shown to be effective as a monotherapy in some

cancers but fail in others, and have turned out to be toxic when used in combination with chemotherapy (Jain et al., 2006, Jain et al., 2009). Most cancer patients are refractory to VEGF inhibition (Bergers and Hanahan, 2008). The extent of refractoriness to treatment varies between cancer types, micro- and macrometastatic diseases and types of VEGF blocker selected. Patients are either intrinsically resistant to therapy or develop acquired-resistance during the course of treatment (Carmeliet and Jain, 2011a, Field et al., 2015). Moreover, there is currently a lack of predictive biomarkers to effectively identify responders (Carmeliet and Jain, 2011a, Jain et al., 2009, Bertolini et al., 2007). To be able to identify responders to therapy remains a very important task as it allows clinicians to better select therapies for specific groups of patients as well as to reduce cost by not administering treatments to non-responders. This is particularly important for patients if the treatments are toxic.

VEGF has been the main angiogenic target, yet clearly inhibiting this pathway alone is insufficient in most patients. Thus, there is a need to identify novel therapeutic targets, signalling pathways and predictive biomarkers in tumour angiogenesis (van Beijnum et al., 2015).

A microarray screen of primary human tumour samples, comprising of 121 primary head and neck squamous cell carcinomas (HNSCCs), 959 primary breast cancers (BCs), and 170 primary clear cell renal cell carcinomas (CCRCCs), was previously reported in 2013 (Masiero et al., 2013). It generated three tumour-specific signatures which correlated with those derived from 15 well-established angiogenesis and/or endothelial 'seed' genes. These signatures were then used to generate a core signature of 43 genes whose association with angiogenesis was consistently top ranked in the tumour types investigated. Gene expression profiling of xenografts treated with anti-VEGF and anti-Notch therapies was then used to experimentally identify which of these core genes showed associations with tumour angiogenesis. This bioinformatic analysis subsequently identified *ELTD1* (*Epidermal growth factor, latrophilin and seven transmembrane containing 1*) as a top-ranked and relatively uncharacterised gene expressed by tumour stromal cells, such as endothelial cells and smooth muscle cells (Masiero et al., 2013). ELTD1 is an orphan G protein-coupled receptor (GPCR) which was discovered in 2001 (Nechiporuk et al., 2001).

1.2 GPCR superfamily and adhesion GPCRs

The GPCR superfamily is the largest family of receptors in the human proteome comprising more than 800 members, and is involved in a repertoire of important physiological functions such as, smell, taste, vision and inflammation etc (Baldwin, 1994, Lefkowitz, 2000). The superfamily is further categorised into five groups, namely glutamate (22 members), rhodopsin (701 members), adhesion (33 members), frizzled (11 members) and secretin (15 members) using a widely adopted system based on the sequence homology of the seven-transmembrane domain (7TM) which is present in all GPCRs (Schioth and Fredriksson, 2005), as shown in Figure 1.4.

ELTD1 is a member of the adhesion GPCR family which have characteristically large extracellular domains containing a variety of adhesion motifs (Bjarnadottir et al., 2004). Adhesion GPCRs have been associated with multiple functions such as cytoskeletal regulation (Oda et al., 1999, Li and Gao, 2003), cell polarity (Usui et al., 1999, Seifert and Mlodzik, 2007), cell adhesion and migration (Fredriksson et al., 2003, Koirala et al., 2009), immunity (Huang et al., 2012, Capasso et al., 2006, Leemans et al., 2004), haematopoiesis and angiogenesis (Masiero et al., 2013, Anderson et al., 2011). However, most adhesion GPCRs are orphan receptors and do not activate canonical GPCR signalling like the receptors in other families. This poses huge difficulties in characterising the functional mechanism of these adhesion GPCRs. Hence, the adhesion GPCR family remains the most poorly understood of the five GPCR families (Promel et al., 2013).

In recent years, there has been a change in the nomenclature of adhesion GPCRs with gene names approved by the International Union of Basic and Clinical Pharmacology (Hamann et al., 2015) which allows for easier identification of adhesion GPCRs. ELTD1 has been named as adhesion GPCR L4 (ADGRL4) (Hamann et al., 2015), however in the following chapters of the thesis, it will be referred to as ELTD1.

Within the adhesion GPCR family, ELTD1 is further categorised into the 1/latrophilin-like subfamily which is based on the 7TM sequence homology and its ability to bind to latrotoxin which is produced by the black widow spider (*Latrodectus mactans*) (Matsushita et al., 1999).

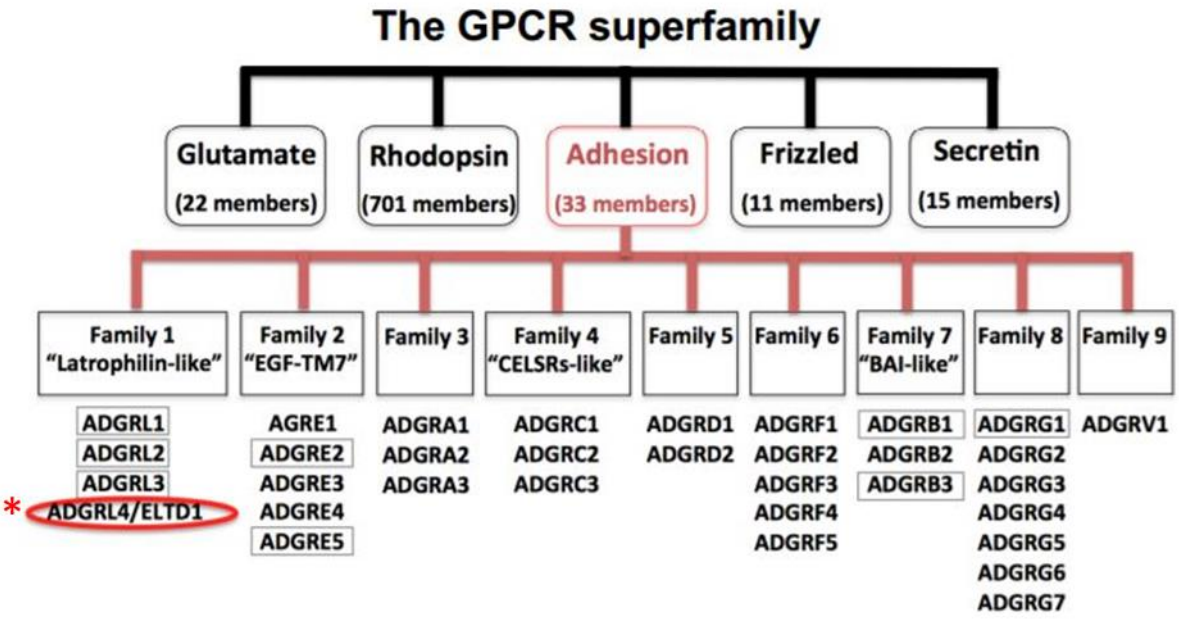

Figure 1.4: Overview of the GPCR superfamily. The GPCR superfamily is comprised of five families namely, glutatmate, rhodopsin, adhesion, frizzled and secretin. Within the adhesion GPCR family, there are nine families in which ELTD1 (*) belongs to the Family 1 'Latrophilin-like'. Boxed members are GPCRs with a known ligand. Figure modified from the thesis of Dr David Favara.

1.3 Structure of ELTD1

The human *ELTD1* gene is found on chromosome 1p31.1 and it encodes a 3527 nucleotide transcript which is translated into a 690 amino acid protein (Flicek et al., 2014). The transcript contains a total of 15 exons with two splice variants encoding a truncated C-terminal segment of the transmembrane domain comprising 149 amino acids (Favara et al., 2014) and another splice variant reported in Ensembl that undergoes nonsense mediated decay. Structurally, ELTD1 is comprised of a large extracellular domain (N-terminal region, EGF-like domain, a calcium-binding domain and a GPCR autoproteolysis inducing domain (GAIN domain)), a seven transmembrane domain (7TM) and a short cytoplasmic tail (intracellular domain) containing a tyrosine kinase phosphorylation site (Figure 1.5) that is suggested to be involved in an intracellular signalling mechanism (Nechiporuk et al., 2001).

Comparatively, the murine *Eltd1* gene is located on chromosome 3 (H3-H4) and it encodes a 4106 nucleotide transcript which is translated into a 739 amino acid protein. The murine *Eltd1* gene consists of a total of 16 exons with six predicted splice variants (Ensembl) of which two mRNAs are putatively predicted to encode proteins. One of those is a full length Eltd1 protein of 739 amino acids and the other truncated protein is made up of 181 amino acids. Tables 1.1 and 1.2 give an overview of human *ELTD1* and mouse *Eltd1* splice variants with their corresponding proteins.

Human *ELTD1*			
Transcript ID	Base pairs (bp)	Amino acids (aa)	Output
ENST00000370742.4	3539	690	Protein coding
ENST00000401034.7	501	149	Protein coding
ENST00000640664.1	2223	158	Nonsense mediated decay

Table 1.1: Human *ELTD1* splice variants and corresponding proteins. Data were obtained from Ensembl.

Mouse *Eltd1*			
Transcript ID	Base pairs (bp)	Amino acids (aa)	Output
ENSMUST00000046977.11	4106	739	Protein coding
ENSMUST00000196970.1	598	181	Protein coding
ENSMUST00000129283.1	625	No protein	Processed transcript
ENSMUST00000198893.1	498	No protein	Processed transcript
ENSMUST00000155652.1	345	No protein	Processed transcript
ENSMUST00000141038.1	783	No protein	Retained intron

Table 1.2: Mouse *Eltd1* splice variants and corresponding proteins. Data were obtained from Ensembl.

Adhesion GPCRs are the only GPCRs which contain a GAIN domain and this is crucial in their protein assembly (Arac et al., 2012). Within the GAIN domain (GPCR autoproteolysis inducing domain), there is a motif known as the 'GPCR proteolysis site' (GPS) which undergoes autoproteolytic cleavage during protein assembly in the endoplasmic reticulum before re-joining non-covalently and being transported to the Golgi apparatus and finally to the cell surface (Lin et al., 2004). It is hypothesized that for some adhesion GPCRs, the autoproteolytic cleavage allows for the swapping of the fragments of extracellular domains between

receptors once at the cell surface (Langenhan et al., 2013) which has been observed in GPR56, EMR2 and latrophilin 1 (Huang et al., 2012, Volynski et al., 2004, Silva et al., 2009) but has not been shown for ELTD1. Other hypothesized roles of the autoproteolytic cleavage are involvement in ligand-receptor interactions and protection of receptor-membrane integrity during mechanical stresses and signalling. Figure 1.5 is a schematic representation of the putative structure of ELTD1.

Currently, the crystal structure of ELTD1 remains unsolved.

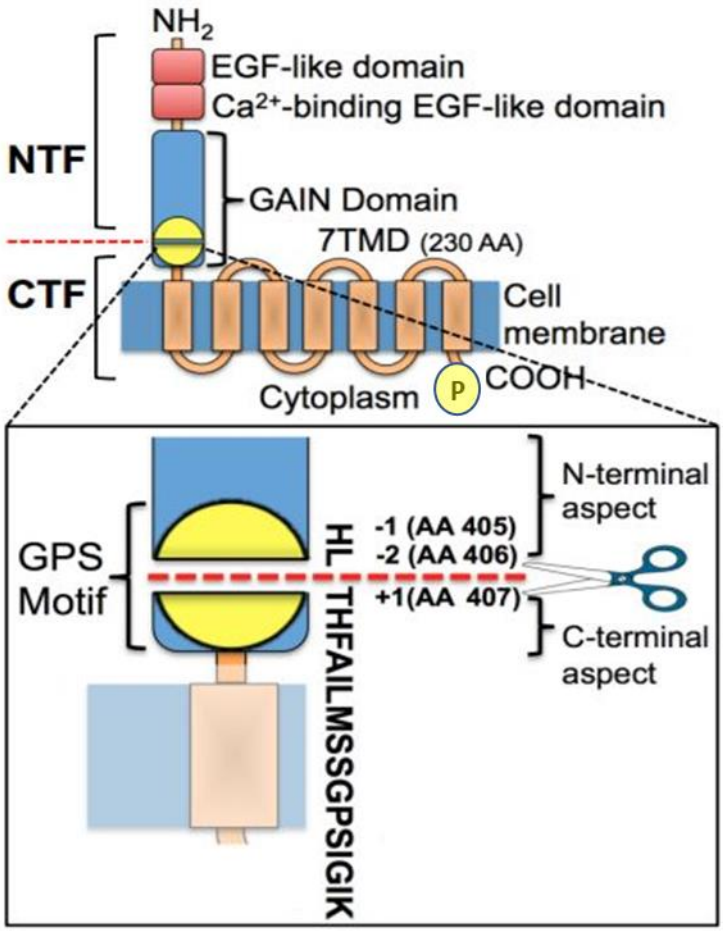

Figure 1.5: Schematic representation of the putative structure of human ELTD1. Like other adhesion GPCRs, the structure of ELTD1 is divided into an N-terminal fragment (NTF) and C-terminal fragment (CTF). The NTF is comprised of an EGF-like domain, Ca-binding EGF-like domain and part of the GAIN (GPCR autoproteolysis inducing domain) domain until the cleavage site (red dotted line) while the CTF consists of the C-terminal end of the GAIN domain, seven transmembrane domain and a short cytoplasmic tail with a tyrosine kinase phosphorylation site (P). At the GPS (GPCR proteolysis site) motif, the cleavage occurs at the autoproteolytic cleavage point situated between amino acids 406 (leucine) and 407 (threonine). Figure modified from the thesis of Dr David Favara.

1.4 Signalling mechanism of ELTD1

Canonical GPCR signalling is extensively studied and involves a multi-step process, starting with an agonist ligand binding to the extracellular domain of the GPCR's 7TM. This binding then triggers a change in conformation of the receptor in which the intracellular domain of the 7TM couples to and activates a heterotrimeric G protein complex. This complex is comprised of three subunits, namely Gα, Gβ and Gγ subunits. In the inactive state, Gα binds to guanosine diphosphate (GDP) along with other parts of the heterotrimeric G protein complex (Hanlon and Andrew, 2015). With the activation and subsequent conformational change of the receptor, Gα binds to an additional guanosine monophosphate (GMP) which then leads to the dissociation of the complex. The guanine triphosphate (GTP) bound Gα subunit then activates a second messenger system triggering the canonical signalling (Ghosh et al., 2015).

A recent insight into adhesion GPCR signalling revealed that both GPR126 (ADGRG6) and GPR133 (ADGRD1) could signal via a mechanism proposed in the Stinger/Stachel hypothesis (Liebscher et al., 2014). This discovery has shed light into the signalling mechanism of adhesion GPCRs which have commonly been poorly understood due to the lack of an agonist ligand.

The Stinger/Stachel Hypothesis proposed that nearly all adhesion GPCRs contain a 10-20 amino acids long tethered agonist located at the C-terminus of the GPS cleavage site, with the exception of GPR123. This tethered agonist acts by mechanically striking the 7TM receptor loops which then triggers downstream canonical GPCR signalling. It can be described metaphorically as the stinging action of a bee ('Stachel' means sting in German). It has also been noted that a modification at the N-terminus of the receptor is required to expose the NTF (N-terminal fragment) end of the CTF (C-terminal fragment) of the tethered agonist either by mechanically pulling off the NTF from the CTF or interacting with a partner molecule (Liebscher et al., 2014). The exposed tethered agonists are able to interact with the 7TM loops which cause a conformational change which then triggers canonical GPCR signalling. Furthermore, it was hypothesized that a mutated adhesion GPCR without the extracellular domain will not be able to signal. Also, It has been proposed that if soluble Stinger/Stachel peptides analogous to the tethered agonist region are added to the cells with these mutated adhesion GPCRs, it is possible to effect the signalling of the adhesion GPCR through the

peptide binding to the 7TM loop. Using the peptides is important as it allowed experimental testing of the hypothesis. Figure 1.6 gives an overview of the Stinger/Stachel Hypothesis.

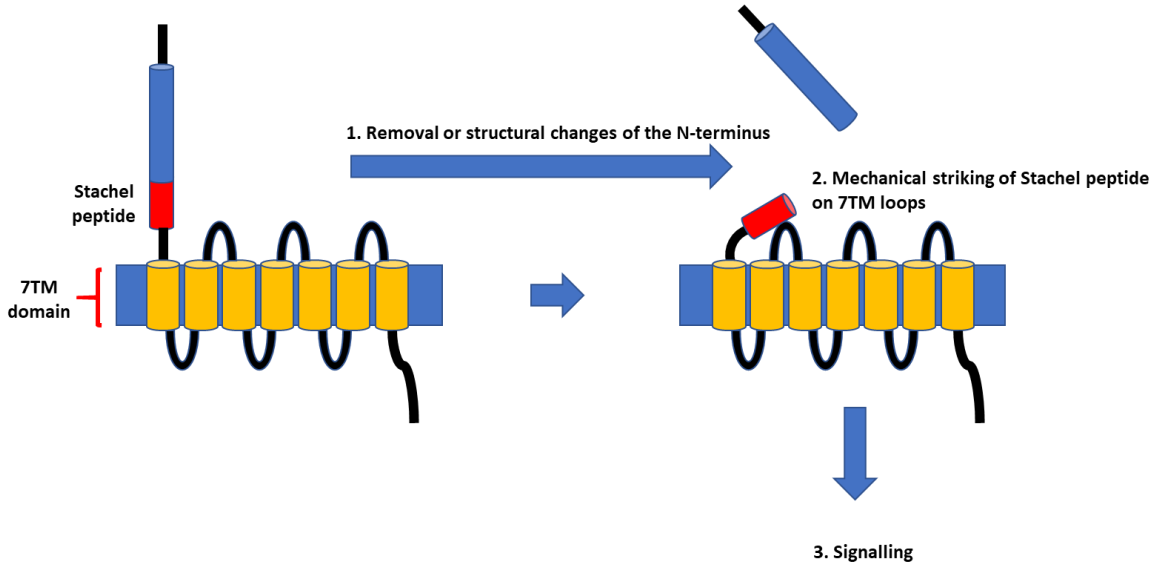

Figure 1.6: Schematic representation of the Stinger/Stachel Hypothesis. This illustrates the activation of adhesion GPCRs by mechanical striking of the Stachel sequence, a tethered peptide agonist (revealed by conformational changes of the N-terminus or removal of the N-terminus), on the seven transmembrane loop.

By experimentally testing the Stinger/Stachel Hypothesis, the G proteins which signal downstream of several adhesion GPCRs have been found. For example, ADGRG6/GPR126 and ADGRD1/GPR133 signal via Gαq (Liebscher et al., 2014) and ADGRG1/GPR56 signal via Gα12/13 (Stoveken et al., 2015). A similar approach was then used to investigate into ELTD1's signalling mechanism by a previous DPhil student in the laboratory, Dr David Favara.

The investigation into ELTD1's signalling mechanism utilised HEK293T cells overexpressing different ELTD1 construct whose design was either 1) a full length form of the receptor, 2) a CTF form of the receptor in which the portion that was N-terminal to the GPS cleavage site was removed and finally 3) a modified 7TM form which lacked the N-terminal portion from

the transmembrane loops and did not contain the region containing a potential tethered agonist (Figure 1.7).

Based on the Stinger/Stachel Hypothesis, the first construct was hypothesized not to signal constitutively, while the second construct was hypothesized to signal constitutively by the mechanical striking of the tethered agonist to the 7TM loops. And the third construct was hypothesized to signal with the exogenous addition of Stinger/Stachel agonist peptides. These ELTD1 overexpressing cells were subject to various signalling assays such as homogeneous time-resolved fluorescence resonance energy transfer (HTRF FRET assays), luciferase reporter assays and AlphaScreen assays which assessed the signalling cascades involving associated G proteins such as Gαq, Gαs, Gαi, Gα12/13 and Gβγ. However, the HTRF FRET assays showed that ELTD1 did not activate Gαq or Gαs and the luciferase reporter assays showed that ELTD1 did not activate Gαq, Gα12/13 or Gαs, either in the CTF truncated form (which should signal constitutively) or in the full-length form. It was proposed that though in the CTF form, the tethered agonist was exposed, the ability to interact with the 7TM loops and generate a signal might be too transient to be detected by the conventional assays. It was proposed that it might give a higher probability to see a signal if the concentration of the tethered agonist was increased dramatically. Stinger/Stachel peptides (21) were synthesized based on the prediction of amino acid sequence of ELTD1's tethered agonist in which each peptide was of varying length starting from the GPS cleavage site and extend towards the predicted start of the first 7TM membrane loop. Figure 1.8 gives an overview of the design of ELTD1's Stinger/Stachel peptides.

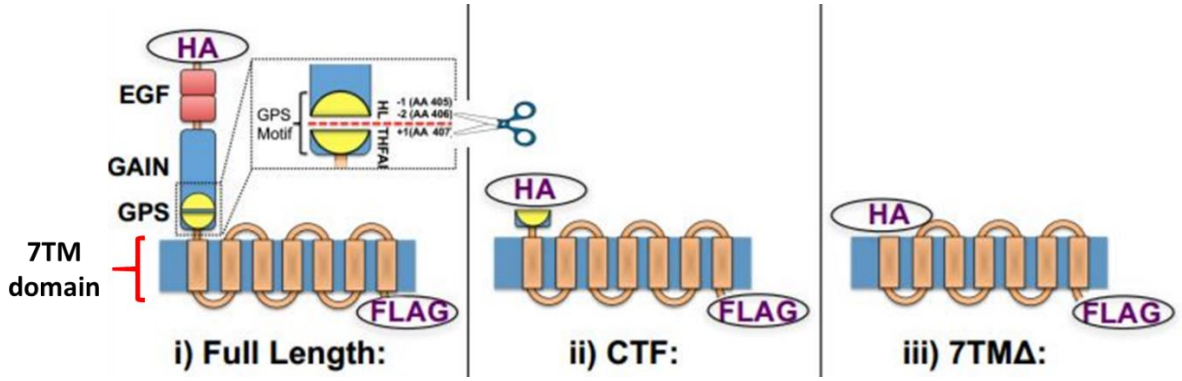

Figure 1.7: Design of the ELTD1 constructs. i) Full length ELTD1; ii) Truncated form of ELTD1 without the fragment that is N-terminal to the GPS (GPCR proteolysis site) motif; iii) Truncated form of ELTD1 without the fragment that is N-terminal to the 7TM loops. In all three constructs, HA and FLAG were tagged to the N-terminus and C-terminus of ELTD1 respectively. Abbreviations: GAIN (GPCR autoproteolysis inducing domain); GPS (GPCR proteolysis site); 7TM domain (seven transmembrane domain). Figure modified from the Thesis of Dr David Favara.

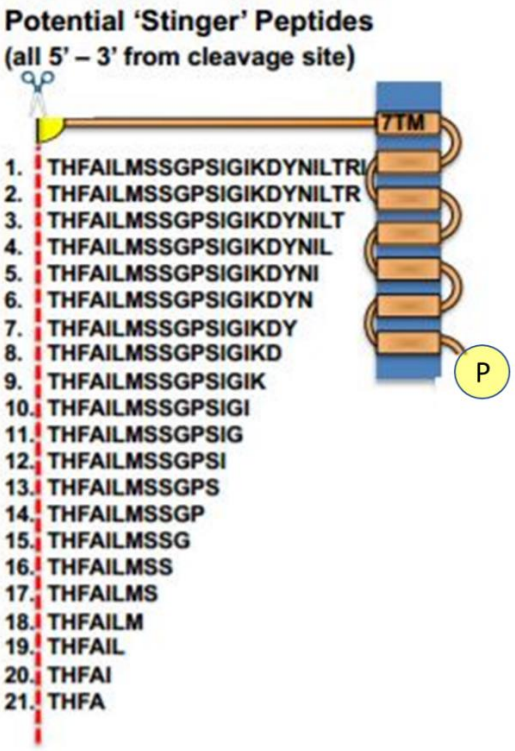

Figure 1.8: Design and the amino acid sequences of the ELTD1 Stinger/Stachel peptides. These peptides were made of amino acid sequences starting from the GPS cleavage site and extending towards the start of the first 7TM loop. Abbreviation: 7TM – seven transmembrane. Figure modified from the Thesis of Dr David Favara.

These ELTD1 Stinger/Stachel peptides were then added to HEK293T cells overexpressing the ELTD1 construct encoding either the full-length form or the 7TM form. HTRF FRET was performed in these cells and showed that ELTD1 Stinger/Stachel peptides did not activate Gαs or Gαi. Considering that the absence of signalling might be due to the lack of the required machinery in HEK293T cells which do not express endogenous ELTD1, the experiment was repeated in HUVECs. However, it was shown that the peptides did not activate Gαs or Gαi in HUVECs either. The luciferase reporter assays in these HEK293T cells also showed that the peptides did not activate Gαq, Gαi or Gαs.

The work described above were performed by Dr David Favara and several expert collaborators namely, Dr. Ali Jazayeri *et al* (Heptares Therapeutics Ltd, United Kingdom), Dr. Ines Liebscher, Professor Torsten Schöneberg *et al* (Rudolf Schönheimer Institute of Biochemistry, University of Leipzig, Germany), Dr. Saskia Nijmeijer and Professor Martine Smith (VU University Amsterdam, The Netherlands).

In summary, our laboratories have demonstrated that ELTD1 did not signal via the canonical GPCR signalling mechanism or the mechanism proposed in the Stinger/Stachel Hypothesis (Unpublished data from thesis of Dr David Favara). Thus, its mechanism of signalling is currently unknown.

1.5 ELTD1 expression in tissues (human and mouse) and human cancer cell lines

It is important to know the location and level of expression of the target gene/protein in the tissues and cells as it helps in the deduction of its function and mechanism of action. Based on the data mining of transcript expression data from online databases (Wu et al., 2009), in human tissues the *ELTD1* transcript is particularly highly expressed in smooth muscles, cardiomyocytes, appendix, thyroid, uterus, lymph nodes, to name a few, as shown in Figure 1.9. In murine tissues *Eltd1* is highly expressed in hematopoietic stem cells, lungs, heart, adrenal gland, adipose, kidney, to name a few (Wu et al., 2009), as shown in Figure 1.10. The two expression profiles do not examine transcript expression in the same set of tissues, thus a direct comparison cannot be made in all tissues. Interestingly, there are differences in the *ELTD1* expression profile of the studied tissues in both humans and mice. For instance, in mice, *Eltd1* expression in the lungs is estimated to be slightly more than two-fold higher than in heart and about four-fold higher than in kidney. However, in humans, the *ELTD1* expression

in lungs, heart and kidney are comparable. In addition, it is worth noting that in mice, the immune cells have low or no *Eltd1* expression. These differing observations could be attributed to several reasons, including the species.

ELTD1 was also reported by antibody staining to have low expression in numerous cancer cell lines and HEK293T cells with telomerase-immortalised microvascular endothelial cells (TIME) having the highest ELTD1 expression by comparison (Serban et al., 2015, Uhlen et al., 2010), as shown in Figure 1.11.

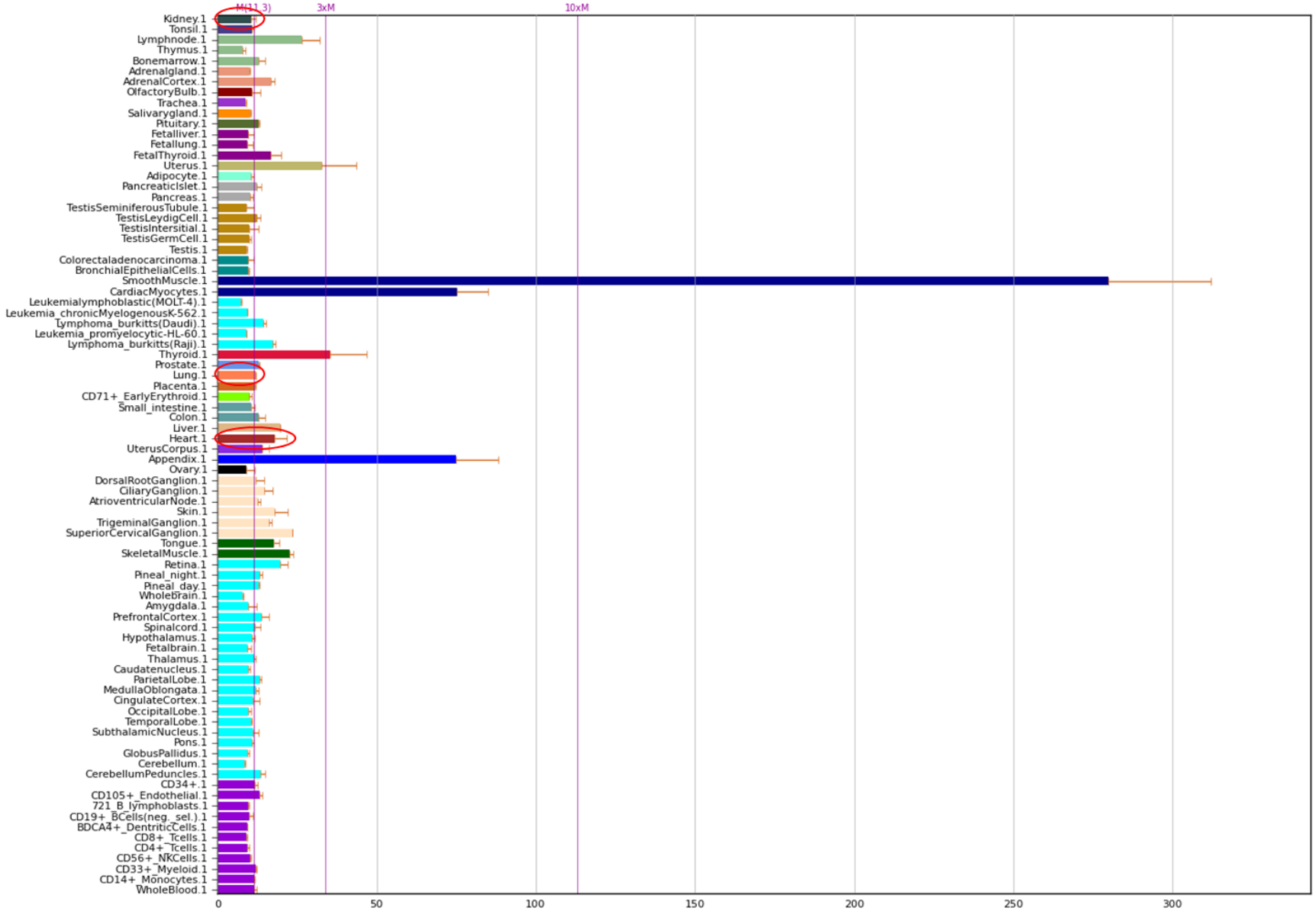
M(11.3)
3xM
10xM
Kidney.1
Tonsil.1
Lymphnode.1
Thymus.1
Bonemarrow.1
Adrenalgland.1
AdrenalCortex.1
OlfactoryBulb.1
Trachea.1
Salivarygland.1
Pituitary.1
Fetalliver.1
Fetallung.1
FetalThyroid.1
Uterus.1
Adipocyte.1
PancreaticIslet.1
Pancreas.1
TestisSeminiferousTubule.1
TestisLeydigCell.1
TestisIntersitial.1
TestisGermCell.1
Testis.1
Colorectaladenocarcinoma.1
BronchialEpithelialCells.1
SmoothMuscle.1
CardiacMyocytes.1
Leukemialymphoblastic(MOLT-4).1
Leukemia_chronicMyelogenousK-562.1
Lymphoma_burkitts(Daudi).1
Leukemia_promyelocytic-HL-60.1
Lymphoma_burkitts(Raji).1
Thyroid.1
Prostate.1
Lung.1
Placenta.1
CD71+_EarlyErythroid.1
Small_intestine.1
Colon.1
Liver.1
Heart.1
UterusCorpus.1
Appendix.1
Ovary.1
DorsalRootGanglion.1
CiliaryGanglion.1
AtrioventricularNode.1
Skin.1
TrigeminalGanglion.1
SuperiorCervicalGanglion.1
Tongue.1
SkeletalMuscle.1
Retina.1
Pineal_night.1
Pineal_day.1
WholeBrain.1
Amygdala.1
PrefrontalCortex.1
Spinalcord.1
Hypothalamus.1
Fetalbrain.1
Thalamus.1
Caudatenucleus.1
ParietalLobe.1
MedullaOblongata.1
CingulateCortex.1
OccipitalLobe.1
TemporalLobe.1
SubthalamicNucleus.1
Pons.1
GlobusPallidus.1
Cerebellum.1
CerebellumPeduncles.1
CD34+.1
CD105+_Endothelial.1
721_B_lymphoblasts.1
CD19+_BCells(neg._sel.).1
BDCA4+_DentriticCells.1
CD8+_Tcells.1
CD4+_Tcells.1
CD56+_NKCells.1
CD33+_Myeloid.1
CD14+_Monocytes.1
WholeBlood.1
0
50
100
150
200
250
300

Figure 1.9: *ELTD1* expression in human tissues and cells. Circled are the *ELTD1* transcript expression in lungs, kidney and heart. Data were obtained from the Biogps online database (http://biogps.org/#goto=genereport&id=170,757) (Wu et al., 2009).

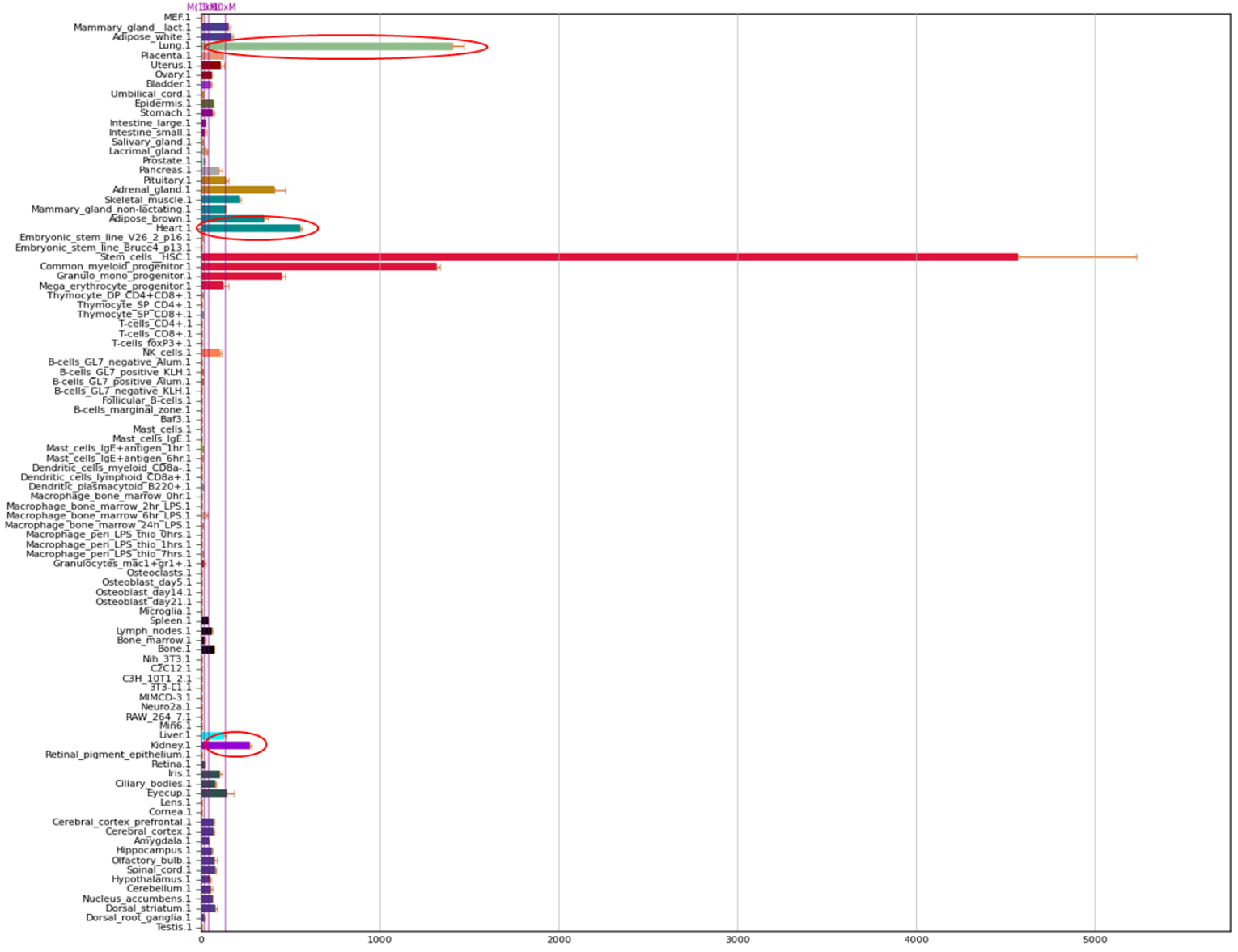
MEF.1
Mammary_gland__lact.1
Adipose_white.1
Lung.1
Placenta.1
Uterus.1
Ovary.1
Bladder.1
Umbilical_cord.1
Epidermis.1
Stomach.1
Intestine_large.1
Intestine_small.1
Salivary_gland.1
Lacrimal_gland.1
Prostate.1
Pancreas.1
Pituitary.1
Adrenal_gland.1
Skeletal_muscle.1
Mammary_gland_non-lactating.1
Adipose_brown.1
Heart.1
Embryonic_stem_line_V26.2_p16.1
Embryonic_stem_line_Bruce4_p13.1
Stem_cells_HSC.1
Common_myeloid_progenitor.1
Granulo_mono_progenitor.1
Mega_erythrocyte_progenitor.1
Thymocyte_DP_CD4+CD8+.1
Thymocyte_SP_CD4+.1
Thymocyte_SP_CD8+.1
T-cells_CD4+.1
T-cells_CD8+.1
T-cells_foxP3+.1
NK_cells.1
B-cells_GL7_negative_Alum.1
B-cells_GL7_positive_KLH.1
B-cells_GL7_positive_Alum.1
B-cells_GL7_negative_KLH.1
Follicular_B-cells.1
B-cells_marginal_zone.1
Baf3.1
Mast_cells.1
Mast_cells_IgE.1
Mast_cells_IgE+antigen_1hr.1
Mast_cells_IgE+antigen_6hr.1
Dendritic_cells_myeloid_CD8a-.1
Dendritic_cells_lymphoid_CD8a+.1
Dendritic_plasmacytoid_B220+.1
Macrophage_bone_marrow_0hr.1
Macrophage_bone_marrow_2hr_LPS.1
Macrophage_bone_marrow_6hr_LPS.1
Macrophage_bone_marrow_24h_LPS.1
Macrophage_peri_LPS_thio_0hrs.1
Macrophage_peri_LPS_thio_1hrs.1
Macrophage_peri_LPS_thio_7hrs.1
Granulocytes_mac1+gr1+.1
Osteoclasts.1
Osteoblast_day5.1
Osteoblast_day14.1
Osteoblast_day21.1
Microglia.1
Spleen.1
Lymph_nodes.1
Bone_marrow.1
Bone.1
Nih_3T3.1
C2C12.1
C3H_10T1_2.1
3T3-L1.1
MIMCD-3.1
Neuro2a.1
RAW_264_7.1
Min6.1
Liver.1
Kidney.1
Retinal_pigment_epithelium.1
Retina.1
Iris.1
Ciliary_bodies.1
Eyecup.1
Lens.1
Cornea.1
Cerebral_cortex_prefrontal.1
Cerebral_cortex.1
Amygdala.1
Hippocampus.1
Olfactory_bulb.1
Spinal_cord.1
Hypothalamus.1
Cerebellum.1
Nucleus_accumbens.1
Dorsal_striatum.1
Dorsal_root_ganglia.1
Testis.1
0
1000
2000
3000
4000
5000

Figure 1.10: *Eltd1* expression in mouse tissues and cells. Circled are the *Eltd1* transcript expression in lungs, kidney and heart. Data were obtained from the Biogps online database (http://biogps.org/#goto=genereport&id=170,757) (Wu et al., 2009).

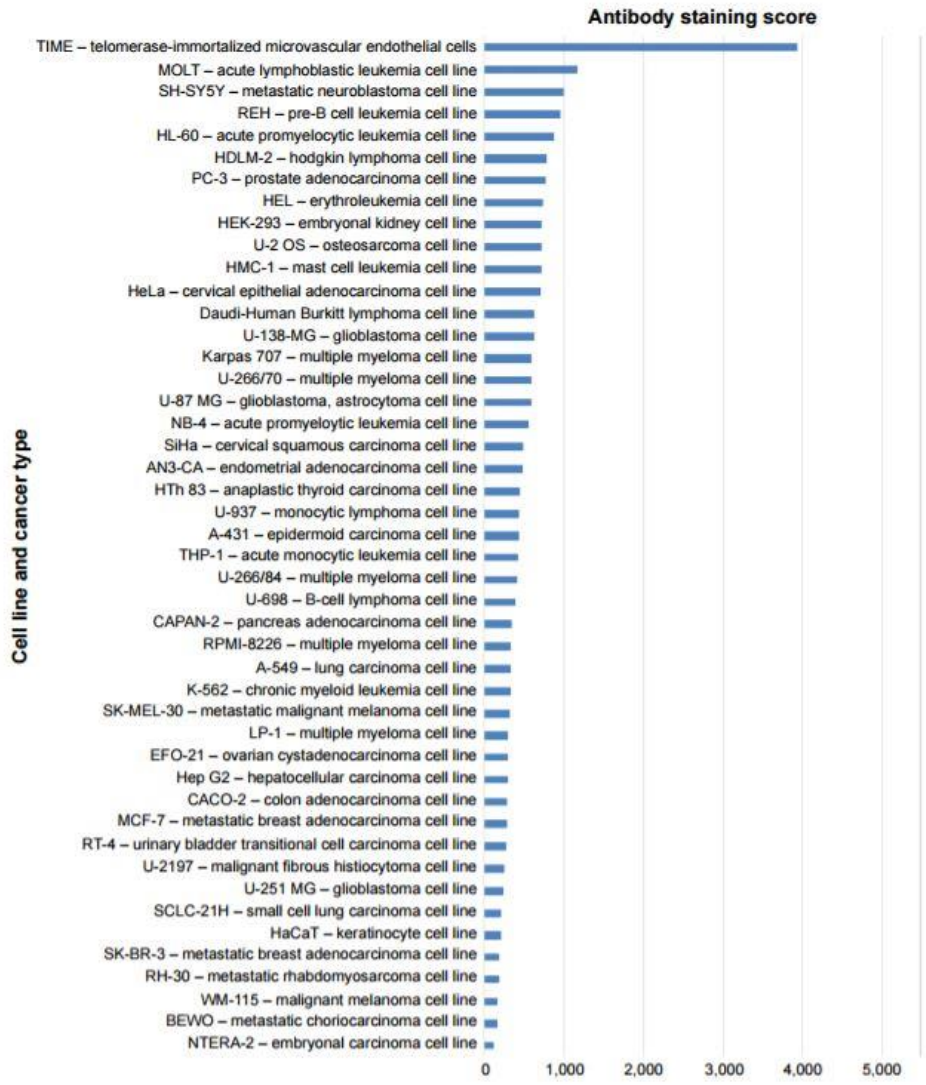

Figure 1.11: ELTD1 protein expression in human cancer cell lines. This illustrates the intensity of antibody staining for ELTD1 in each cancer cell line. Results were obtained from the Human Protein Atlas Database (https://www.proteinatlas.org/ENSG00000162618-ADGRL4/cell).

1.6 Role of ELTD1 in tumour development and angiogenesis

In 2008, 58 genes were identified with specific and broad expression in the mouse microvasculature. A selected subset of the endothelial cell-specific genes included *Eltd1*, which was then confirmed by immunohistochemistry and real time polymerase chain reaction (Wallgard et al., 2008). Additionally, in the same year, it was discovered that ELTD1 was expressed in the normal endothelial transcriptome in humans (Herbert et al., 2008). It was further reported in 2012 that VEGF-A and TGF-β upregulated ELTD1 expression in glioblastoma vessels. Also, it was demonstrated by immunochemistry that the vascular staining intensity of Eltd1 was significantly higher in grade IV glioma-associated vessels compared to control vessels/Grade II vessels (Dieterich et al., 2012). And in 2013, it was reported that ELTD1 could be used as a biomarker for gliomas (Towner et al., 2013, McNamara et al., 2013, Nicolaidis, 2015). It was pointed out that higher ELTD1 levels were associated with high grade and more aggressive gliomas (Towner et al., 2013).

It was highlighted earlier in section 1.1 of this chapter that our laboratories identified *ELTD1* by bioinformatics analysis of a microarray screen of human tumour samples designed to identify novel angiogenic genes. The functional role of ELTD1 in tumour angiogenesis was then evaluated further by *in vitro* and *in vivo* experiments. It was shown by immunohistochemical staining of human primary tumour samples that ELTD1 was expressed largely in the vasculature with a significantly upregulation in tumour-associated endothelial cells compared to those from matched adjacent normal tissues (Masiero et al., 2013). Moreover, it was demonstrated, using *in vitro* and *in vivo* models that VEGF/bFGF and DLL4-Notch, two predominant angiogenic pathways (Li and Harris, 2009, Thurston and Kitajewski, 2008), had opposing effects on ELTD1 expression. ELTD1 expression was upregulated by VEGF, supporting the observation from an earlier report (Dieterich et al., 2012) and downregulated by DLL4 (Masiero et al., 2013). Another study focused on the breast cancer perivascular niche substantiated this antagonism between DLL4 and ELTD1 by demonstrating that NOTCH1 silencing of neovascular sprouts led to an increase in extracellular ELTD1 protein (Ghajar et al., 2013a). *ELTD1* silencing in HUVECs significantly reduced the ability of HUVECs (Human Umbilical Vein Endothelial Cells) to adhere to Matrigel and inhibited their sprouting and acquisition of the tip cell phenotype in a 3-dimensional HUVECs spheroid model. In addition,

ELTD1 silencing in HUVSMCs (Human Umbilical Vein Smooth Muscle Cells) significantly reduced their viability and adhesive properties (Masiero et al., 2013).

In vivo Eltd1-silencing in zebrafish via two different antisense morpholinos targeting the start codon (ATGMO) and a splicing junction (spliceMO) of the *Eltd1* pre-mRNA caused severe vascular defects during the formation of intersegmental vessels (ISV) (Masiero et al., 2013). Furthermore, endothelial *Eltd1*-silencing in mouse xenografts (orthotopic ovarian carcinoma SKOV3ip1 and subcutaneous colorectal HCT116 xenografts) using two independent *Eltd1*-targeting siRNAs incorporated into chitosan nanoparticles significantly reduced tumour growth and improved survival (Masiero et al., 2013). Immunohistochemical analysis of these tumours showed that *Eltd1*-silencing reduced MVD (microvessel density), tumour cell proliferation but increased hypoxia, apoptosis and pericyte coverage.

In 2016, it was reported that ELTD1 was an effective anti-angiogenic target for the treatment of gliomas. By utilizing a commercially available Eltd1 blocking polyclonal antibody in mouse GL261 and human G55 xenograft glioma models, vascularization in tumours was significantly reduced compared with the untreated controls, thus confirming ELTD1's role in tumour angiogenesis (Ziegler et al., 2017). Also, it was shown that *ELTD1* silencing via siRNA transfection in low passage *ex vivo* cultured primary glioblastoma GB8B cells, isolated from fresh tumour tissue fragments from patients with glioblastoma, led to a significant reduction in cell survival after 72 hours of (Serban et al., 2017). In 2018, it was shown by immunohistochemical analyses of patients' hepatocarcinoma (HCC) samples that ELTD1 regulation of disease progression was carcinoma associated fibroblast (CAF)-dependent (Kan et al., 2018). And very recently, it was reported that *in vivo* anti-ELTD1 antibody treatment in G55 glioma xenografts significantly reduced the expression of both ELTD1 and VEGFR2 (Ziegler et al., 2019).

Despite ELTD1's role in tumour angiogenesis and ELTD1-targeting leading to a reduction in tumour growth and MVD in xenografts (Ziegler et al., 2017, Masiero et al., 2013), high ELTD1 endothelial cell protein expression correlated with better prognosis and enhanced survival in human HCC, HNSCC, BC and CCRCC patients (Masiero et al., 2013, Kan et al., 2018). Tumour vessels have been found to be immature, very leaky and functionally abnormal compared to normal vessels (Jain, 2005). It was hypothesised that higher ELTD1 expression in endothelial cells could potentially mediate vascular normalisation. With better perfused vessels prior to

therapy, whether due to more differentiated vessels or less leaky vessels, the tumours would be less hypoxic and potentially less aggressive (Masiero et al., 2013, Goel et al., 2011, Carmeliet and Jain, 2011b, Jain, 2005). Interestingly, a previous study showed that propanolol, a non-specific β-adrenergic receptor inhibitor, was selectively toxic to malignant tumour endothelial cells compared to normal endothelial cells when the drug was administered to SVR angiosarcoma-forming cell line in mice (Favara et al., 2014). Transcriptional profiling showed that propanolol increased the gene expression of endothelial *Eltd1* and *Tek*, which encodes the Tie2 receptor which is known to promote vessel maturation, quiescence and stability (Singh et al., 2011, Helfrich and Schadendorf, 2011). The association between *Eltd1* and *Tek* suggests endothelial *Eltd1*'s involvement in vessel maturation and normalisation.

It was reported recently in 2019 that VEGFR2 is associated with ELTD1. It has been shown that *in vivo* VEGFR2 levels were reduced significantly with treatment using an anti-Eltd1 antibody, and ELTD1 levels were also decreased significantly with VEGFR2-targeted therapy. Interestingly anti-VEGFR2 inhibition did not significantly increase survival, reduce tumour volume or affect tumour perfusion in a glioma model. However, anti-Eltd1 therapy led to a significant improvement in animal survival, reduction in tumour volume and a significant reduction in tumour perfusion (Ziegler et al., 2019).

1.7 Other roles for ELTD1

It was first reported in 2001 that Eltd1 was developmentally regulated in rat and human hearts. Nechiporuk *et al* showed by *in situ* hybridization that *Eltd1* was expressed in rat cardiomyocytes and that there was abundant expression of the protein in vascular and bronchiolar smooth muscle cells (Nechiporuk et al., 2001). In 2012, Xiao *et al* reported that mice lacking *Eltd1* exhibited augmented cardiac hypertrophy in response to pressure overload induced by aortic banding. It was suggested that Eltd1 deficiency increased maladaptive remodeling of the heart by promoting cardiomyocyte hypertrophy and cardiac fibrosis. The study proposed that Eltd1 could be a potential target in the preventive treatment of cardiac diseases (Xiao et al., 2012).

In 2017, it was shown that mice with global double knockout of *Eltd1* and *Gpr116* resulted in an increase in perinatal and postnatal lethality, with cardiovascular malformations consisting

of defects in the septation of the cardiac outflow tract, and renal thrombotic microangiopathy, characterised by a loss of regular glomerular endothelial phenotype. These were, however not seen in endothelial cell-specific *Gpr116* or *Eltd1* double knockout mice (Lu et al., 2017). It was suggested that Gpr116 and Eltd1 might be expressed in cells at certain stages during development which were not captured in the study, also that there might be certain subsets of endothelial cells in the organs studied that did not undergo recombination using VECadherin-Cre (Lu et al., 2017).

Interestingly, *ELTD1* polymorphisms were found in a cohort of Andean people who lived at high altitudes. This suggested that these polymorphisms might play a role in cardio-protective mechanisms against increased cardiac efforts caused by low oxygen levels. These people were also found to have an additional layer of muscles in their pulmonary arteries (Eichstaedt et al., 2014).

In addition to its vascular and cardiac phenotypes there are other miscellaneous associations that may identify other roles for ELTD1. *ELTD1* polymorphisms also increased event-free longevity based on a meta-analysis of 9 genome-wide association studies (GWAS) on aging (Walter et al., 2011). Additionally, *ELTD1* was reported as one of eight genes implicated in subcutaneous fat thickness in humans and pigs (Lee et al., 2011). ELTD1 was also associated with genetic risk of cannabis use disorders (Agrawal et al., 2008) and an *Eltd1* SNP was identified in cattle which were resistant to therapies against tick parasites (Porto Neto et al., 2011). An *ELTD1* SNP was also discovered in patients with risks of developing graft versus host disease after haemopoietic stem cell transplantation (Harkensee et al., 2013). In 2013, a study using complementary DNA microarray discovered that significant *ELTD1* upregulation in patients suffering from ulcerative colitis with dysplastic lesions (Pekow et al., 2013).

In summary, ELTD1 has been associated with many biological observations, however most of the mechanisms underlying these associations remain unidentified.

1.8 Aims

The aim of this thesis is to investigate the *in vivo* functional role of ELTD1 in tumour development and angiogenesis. By developing genetic knockout mouse models, this allows the investigation into the impact of a more complete inactivation of *Eltd1* and an opportunity to investigate the role of endothelial-*Eltd1*. Additionally, these models help to address the safety aspects of long term depletion of endothelial-*Eltd1*.

The thesis will focus on the following areas:

1. Effects of chronic endothelial cell-specific *Eltd1* depletion in mice
    - To generate constitutive endothelial cell-specific *Eltd1* knockout mice
    - To investigate the effects of chronic loss of endothelial-*Eltd1* in normal mouse physiology
    - To investigate the effects of chronic loss of endothelial-*Eltd1* on tumour development and angiogenesis in mice

2. Effects of acute endothelial cell-specific *Eltd1* depletion in mice
    - To generate inducible endothelial cell-specific *Eltd1* knockout mice
    - To investigate the effects of acute loss of endothelial-*Eltd1* in normal mouse physiology
    - To investigate the effects of acute loss of endothelial-*Eltd1* on tumour development and angiogenesis in mice

3. *Ex vivo* gene expression profiling of acute *Eltd1*-depleted mouse lung endothelial cells using single cell sequencing
    - To assess *Eltd1* expression in different subsets of mouse lung endothelial cells
    - To investigate the differential gene expression of lung endothelial cells caused by acute loss of endothelial-*Eltd1* expression
    - To investigate if the differential endothelial gene expressions caused by the loss of endothelial *Eltd1* differs between subsets of lung endothelial cells.

Chapter 2: Materials and Methods

2.1 Cell lines and maintenance

2.1.1 Cell lines used

Human Embryonic Kidney 293 cells expressing the large T antigen (HEK293T) were purchased from Thermo Scientific. MC38 is a cell line derived from C57BL/6 murine colon adenocarcinoma cells and it was given as a gift from Dr Pavitra Kannan (University of Oxford). GL261 cell line is a murine glioma cell line (Perkin Elmer). sEND is a murine endothelial cell line. These cell lines were cultured in Dulbecco's modified Eagle's medium (DMEM) (Gibco, cat. no. 41966-029) supplemented with 10 % heat-inactivated foetal bovine serum (FBS) (Gibco, cat. no. 10500064) and 1 % penicillin-streptomycin (Lonza, DE17-602E). Cells were maintained and medium was changed every 48 hours.

E0771 cell line is a spontaneously developing C57BL/6 murine medullary breast adenocarcinoma and is used as a triple negative breast cancer (TNBC) syngeneic model. It was given as a gift from Professor Ruth Muschel (University of Oxford). E0771 cells were cultured in Roswell Park Memorial Institute (RPMI) 1640 medium (Gibco, cat. no. 21875-034) supplemented with 10 % heat-inactivated foetal bovine serum (FBS) and 1 % penicillin-streptomycin. Tissue culture flasks were coated with poly-l-lysine (Sigma, cat. no. P4707) first before the cells were seeded for culture. Cells were maintained and medium was changed every 48 hours.

2.1.2 Cell culture and maintenance

All cells were cultured in tissue culture incubators at a constant temperature of 37 °C with a humidified atmosphere of 5% and 95% filtered atmospheric air. Cells were cultured on sterile, tissue culture grade, plastic cell culture ware (Corning). Culture medium used was presented in the section 2.1.1.

Cells were passaged once they reached 70-90 % confluence. Passaging was performed by aspirating medium, washing the adherent cells with phosphate buffered saline (PBS, composed of 10 mM sodium phosphate, 137 mM sodium chloride and 2.7 mM potassium chloride) followed by incubating in trypsin-EDTA at 37 °C for 5 minutes to detach the cells from the flask surface. Trypsin-EDTA was neutralised by adding medium containing 10 % heat-

inactivated foetal bovine serum (FBS). Cells were centrifuged for 5 minutes at 1500 rpm, medium aspirated and pellet re-suspended in fresh medium. Cells were usually split 1:3 to 1:10 and re-seeded. Medium was changed every 48 hours.

2.1.3 Cell counting

All cell counting was performed using a Cellometer Auto T4 cell counter (Nexcelcom Bioscience) as per the manufacturer's instructions. 20 µL of cell suspension was pipetted onto a Cellometer counter chamber and analysed by the Cellometer machine. The cell suspension was then diluted to the required concentration and seeded into sterile tissue culture plastic ware.

2.1.4 Freezing and thawing cells

For long term storage, cells were trypsinised, washed and spun into pellets which were then resuspended in freezing medium that was comprised of 90 % of heat inactivated foetal calf serum and 10 % of dimethyl sulfoxide (DMSO, Sigma-Aldrich) and transferred to a cryovial. To allow for gradual freezing and to prevent initial freeze associated damage to cells, cryovials were transferred to a Mr. Frosty™ Freezing Container (Thermo Fisher Scientific) for 24 hours and kept in a -80 °C freezer. After 24 hours, the cryovials were transferred to a liquid nitrogen storage tank for long-term storage.

Thawing of cells involved retrieving cryovials from liquid nitrogen storage tank and warming the cryovials in a 37 °C water bath for 3 minutes till the contents were fully thawed. The cryovials were transferred to a sterile hood with the lids of cryovials facing away from the researcher. The lids were gently opened to release the pressure and the cell suspension was transferred into a falcon tube with 5 mL of pre-warmed cell culture medium. The tube was centrifuged for 3 minutes at 1500 rpm and the medium was aspirated out, and the cell pellet was resuspended in 15 mL of fresh pre-warmed medium in a T75 tissue culture flask (Corning). Cells were used for experiments after a passage.

2.1.5 Mycoplasma testing

The cell cultures were kept in complete media without antibiotics for about a week, with the change of media every three days. The media was collected and tested for mycoplasma infection using the MycoAlert™ Mycoplasma Detection Kit, as per the manufacturer's instructions.

2.2 Design of murine Eltd1 over-expressing plasmid

pIRES-eGFP plasmid containing full-length murine *Eltd1* cDNA was used for overexpression in HEK293T cells. As shown in Figure 2.1, the plasmid comprised of an N-terminal flag tagged full length murine *Eltd1* and an independent eGFP feature in the vector. This plasmid was generated by Dr Demin Li (University of Oxford).

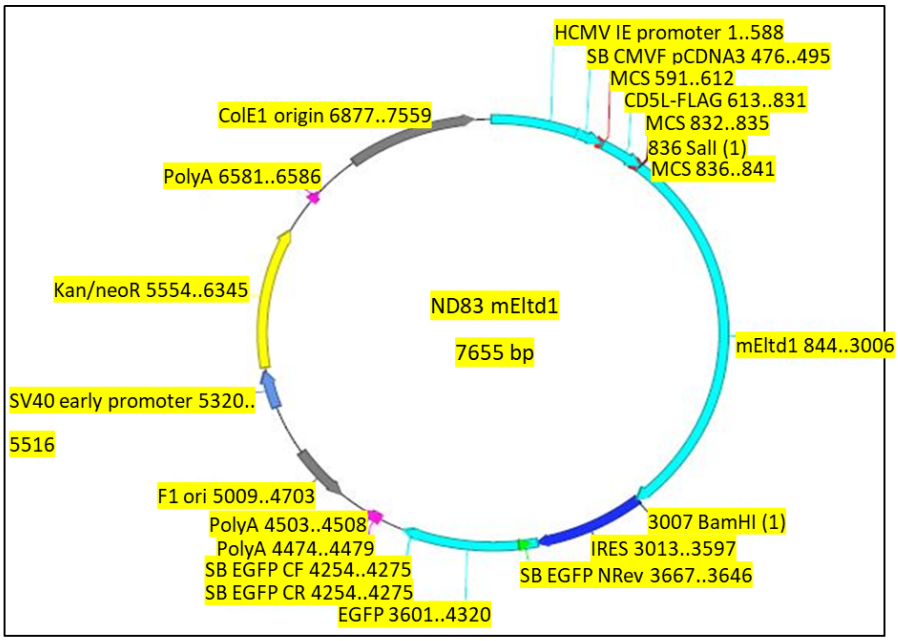

Figure 2.1: Schematic representation of pIRES-eGFP plasmid containing full length murine *Eltd1*.

2.3 Transient transfection

HEK293T cells were used in the transient transfection of pIRES-eGFP plasmid containing full-length murine *Eltd*1 as described in section 2.2. Lipofectamine LTX (Thermofisher, cat. no. 15338500) was used as the transfection reagent and the protocol was conducted as per the manufacturer's instruction. In brief, 5×10^5 HEK293T cells were seeded in each well of 6-well plate and incubated at 37 °C overnight. On the following day, a mixture of 2.5 µg plasmid and 6.25 µL Lipofectamine LTX in Opti-MEMTM I reduced serum medium (Thermofisher, cat. no. 31985070) was prepared and added dropwise into each well. The plate was then incubated at 37 °C for two days before the cells were harvested for protein analysis.

2.4 Generation of rabbit polyclonal antibodies against murine Eltd1

2.4.1 Rationale

A reliable antibody was important in characterising Eltd1 knockout in the tumours and tissues of the Eltd1 knockout mice. At this point, m174, a commercially available antibody (Santa cruz, sc292226) targeting the extracellular domain of Eltd1, had been validated in the detection of recombinant Eltd1 in Eltd1-overexpressing HEK293T cells. However, m174 gave background in endogenous Eltd1 detection by Western blotting and immunohistochemistry of cell lysates and murine tissues which rendered it unreliable for further investigation (Figure 2.3). This prompted the generation of new polyclonal antibodies against Eltd1.

2.4.2 Design of the immunogen

The immunogen was an existing recombinant murine Eltd1 protein, comprising the three EGF domains from the extracellular domain, as shown in Figure 2.2. The recombinant protein was expressed in *Escherichia coli*, purified and re-folded by Dr Patricia Whiteman in the laboratory of Professor Penny Handford (Department of Biochemistry, University of Oxford).

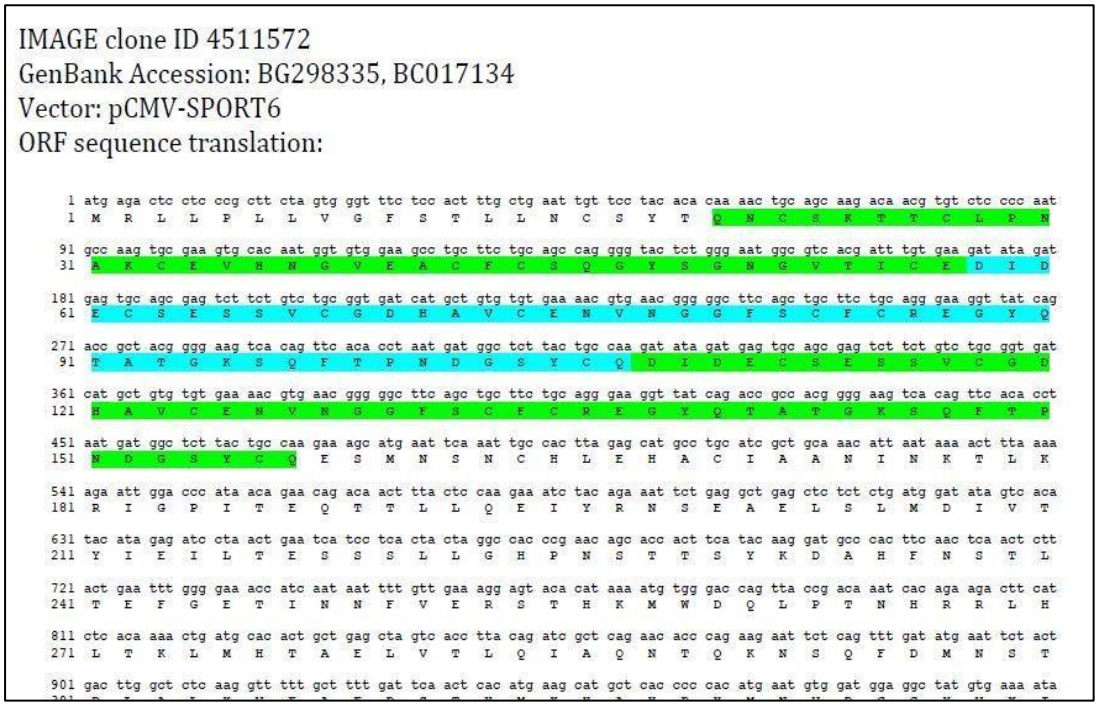

Figure 2.2: Protein sequence of murine Eltd1 immunogen. The highlighted regions indicate the three EGF domains of murine Eltd1 which constituted the immunogen.

2.4.3 Screening of pre-immune sera from rabbits

Cambridge Research Biochemicals (CRB) was contracted to make rabbit polyclonal antibodies against this murine Eltd1 immunogen. Pre-immune sera from five rabbits were received and screened by Western blotting and immunohistochemistry to assess any background antibody activity with endothelial cells. Two rabbits whose pre-immune sera gave the least background in the two techniques, as shown in Figure 2.3, were selected for antibody production (F01 and F04). Each rabbit was given five immunizations of 100 µg protein each time, with two weeks gap between two separate immunizations.

In Figure 2.3, the pre-immune sera of F01 and F04, at 1:1000 dilution, gave very little background in the Western blotting (A) and immunohistochemistry (B) of Eltd1-overexpressing HEK293T cell lysates and endogenous Eltd1-expressing murine endothelial cell lysates (sEND) and murine kidney tissue. Therefore, it was decided that these two rabbits, F01 and F04 were suitable for generating polyclonal antibodies against Eltd1.

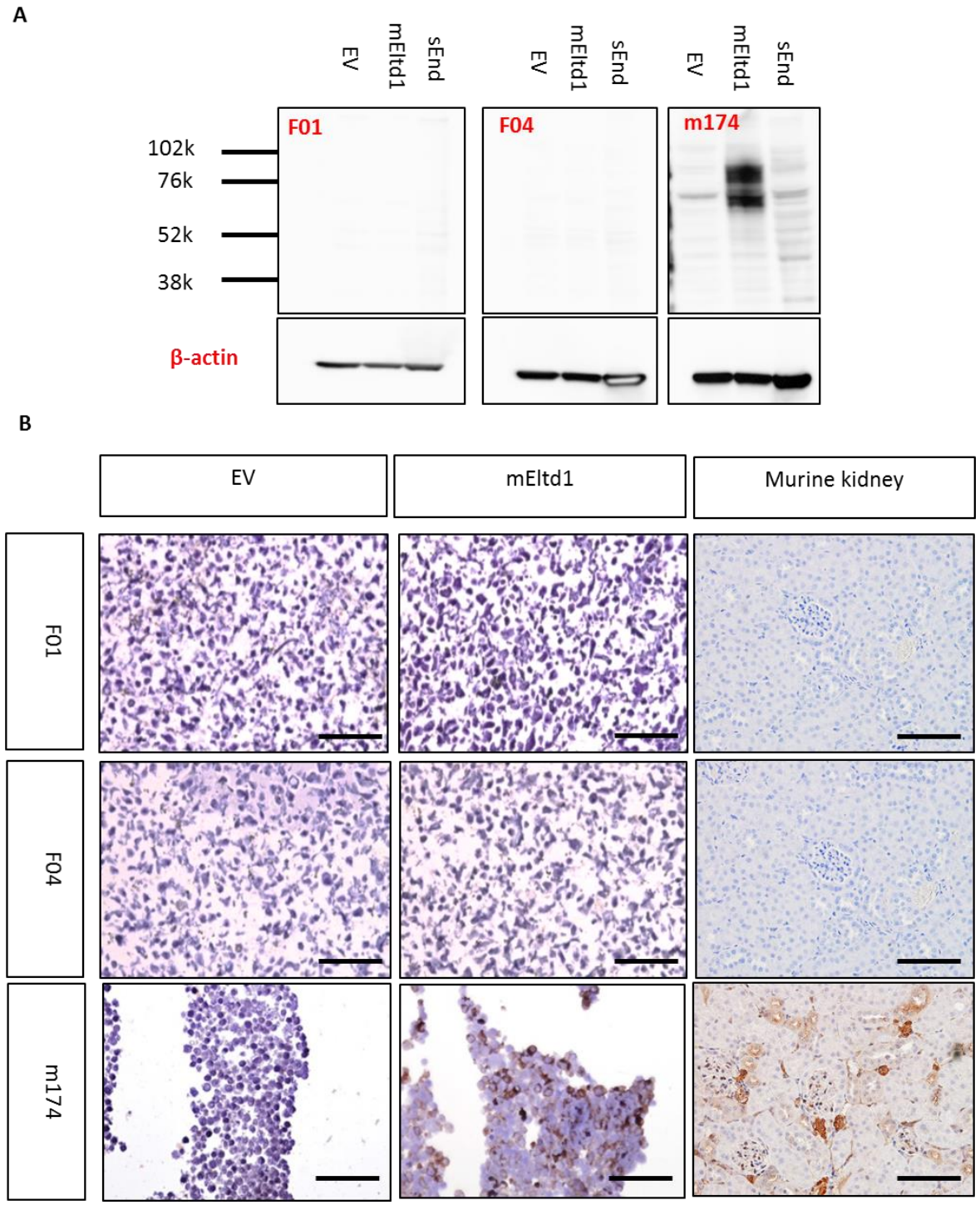

Figure 2.3: Screening of pre-immune sera by Western blotting and immunohistochemistry. F01 and F04 gave the least background in the two techniques namely, A) Western blotting and B) immunohistochemistry (Scale bar: 50 µm). sEND, murine heart and kidney tissues were used for the detection of endogenous Eltd1. m174 is a commercially available antibody that targets the extracellular domain of Eltd1 and was used as a positive control. EV: HEK293T cells

transfected with empty vector (pIRES-eGFP); mEltd1: HEK293T cells overexpressing Eltd1; sEND: murine endothelial cell line.

2.4.4 Testing various applications of polyclonal antibodies

The final F01 and F04 bleeds were screened for the detection of Eltd1 overexpression and endogenous Eltd1 in Western blotting and immunohistochemistry. In Figure 2.4A, F01 and F04 showed 2 strong bands around 76 kDa (two glycosylated forms of Eltd1) which were also seen in the blot stained with m174 in Figure 2.3A. In Figure 2.4B, F01 and F04 showed vessel staining in murine kidney sections and F04 showed membrane staining of Eltd1-overexpressing HEK293T cell pellet. Interestingly, F04 was a stronger antibody in Western blotting while F01 gave a stronger signal in Immunohistochemistry.

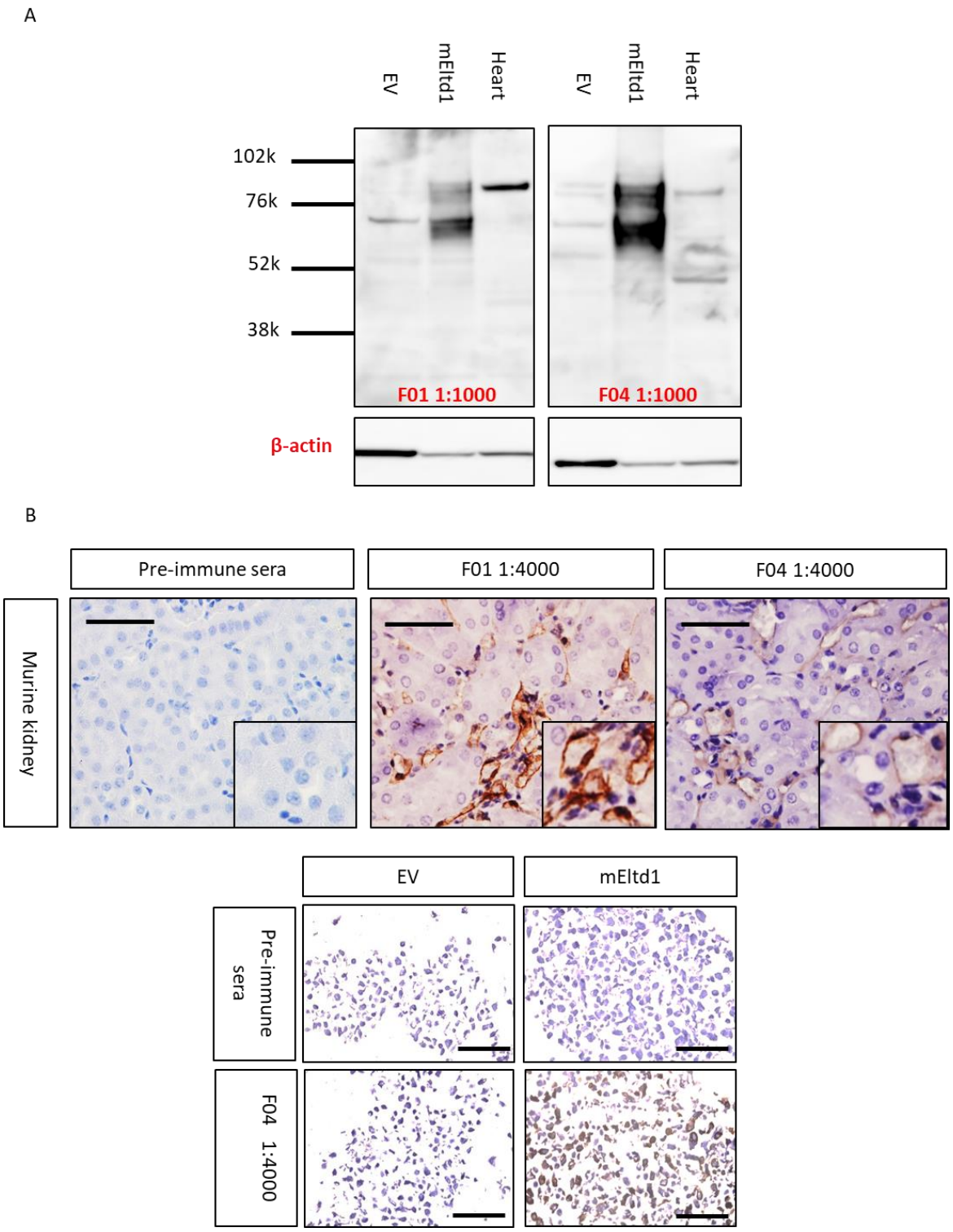

Figure 2.4: Screening of final bleeds of F01 and F04 in Western blotting and Immunohistochemistry. Heart and kidney tissues were used for the detection of endogenous Eltd1. EV: HEK293T cells transfected with empty vector (pIRES-eGFP); mEltd1: HEK293T cells overexpressing Eltd1; Scale bar: 100 µm (kidney), 50 µm (transfected HEK293T cells).

2.5 Protein analysis

2.5.1 Extraction of proteins and quantification

Cells were washed with chilled PBS on ice and were lifted by cell lifters (Corning, cat. no. 3008) in appropriate volume of RIPA buffer (Sigma, cat. no. R0278) with 1X cOmplete™ protease inhibitor cocktail (Roche, 04693116001). These were then incubated on ice for 30 minutes and then centrifuged at 15000 rpm for 15 minutes at 4 °C. Supernatants were collected and quantified by Bio-Rad protein assay (BioRad, 5000001) with absorbance measured at 595 nm using a µQuant microplate reader (Bio-Tek). The protein concentration was calculated based on the absorbance reading and the standard curve generated with a serial dilution of bovine serum albumin (Sigma, cat. no. A3059). Samples were then stored at -20 °C.

2.5.2 Western blotting: SDS-PAGE electrophoresis and transfer to membrane

Protein samples were mixed with appropriate amounts of loading buffer comprised of 4X LDS Sample buffer (Invitrogen, NP0007) and 10 % β-mercaptoethanol (Sigma, cat. no. M3148). The samples were then heated to 95 °C for 5 minutes and then centrifuged briefly to spin down liquid on the lids. The samples were mixed briefly and loaded into a 4-12 % NuPAGE Bis Tris polyacrylamide gel (Invitrogen, NP0335) in a tank containing 1X MOPS Running buffer (Invitrogen, NP0001-02) and ran for 1.5 hours at 120 V. The proteins were then transferred from the gel onto the polyvinylidene difluoride (PVDF) membrane (Millipore) using the Novex semi-dry blotter machine (Invitrogen).

2.5.3 Western blotting: Incubation with primary and secondary antibodies

After the semi dry transfer, the membrane was incubated in milk blocking buffer that contained 10 % milk in TBS/0.2 % tween-20 (TBS-T) for 2 hours at room temperature. The membranes were then incubated in primary antibodies diluted in 10 % bovine serum albumin/TBS-T overnight at 4 °C on a roller. Following this, the membrane was washed thrice with TBS-T, each wash involved shaking for 15 minutes. The membrane was then incubated in secondary antibody, conjugated to Horseradish peroxidase (HRP), diluted in milk blocking buffer for 1 hour at room temperature. The primary and secondary antibodies used in this application are listed in Table 2.1.

2.5.4 Western blotting: Detection

HRP detection on the membrane was done using the ECL Prime chemiluminescent reagent system (GE Healthcare), as per the manufacturer's instructions. Visualisation was performed using the ImageQuant LAS4000 digital imaging system (GE Healthcare).

Antibodies	Dilution for Western blotting	Company (cat. no.)
Primary antibodies		
Eltd1 – F01 (produced in rabbit)	1:1000	In-house polyclonal
Eltd1 – F04 (produced in rabbit)	1:1000	In-house polyclonal
Eltd1-m174	1:1000	Santa cruz (sc292226)
β-actin conjugated to horseradish peroxidase (HRP)	1:25000	Sigma (3854)
Secondary antibodies		
Anti-rabbit conjugated to HRP	1:1000	DAKO (P044801-2)

Table 2.1: Antibodies used for Western blotting

2.6 RNA Analysis

2.6.1 Extraction of RNA and quantification

RNA was extracted using Tri Reagent (Sigma) according to the manufacturer's instructions. In brief, cells were washed with chilled PBS on ice, lifted by cell lifters in Tri reagent and transferred to 1.5 mL eppendorf tubes. Mouse tissues were minced in tubes using a micropestle (Sigma, cat. no. SIAL501ZZ0). Chloroform was then added and the tubes were vigorously shaken for 15 seconds. After which, the tubes were left to stand for 10 minutes and then centrifuged at 15000 rpm for 15 minutes. The top layer was collected in fresh tubes and equal amount of isopropanol was added and mixed. The mixture was centrifuged and

washed with 70% ethanol. After which, the mixture was centrifuged once more and supernatant was aspirated and air dried for 10 minutes before resuspending pellets in nuclease-free water (Severn Biotech, cat. no. 020-9000-01). RNA samples were stored at -20 °C.

For FACS sorted cells of at least 10,000 cells, the RNA was extracted using Trizol (Invitrogen, cat. no. 5596-018) as per manufacturer's instructions. In brief, cells were sorted into 800 µL TRIzol. The mixture was vortexed and spun down at 16100 g for 30 seconds. 160 µL of chloroform was added to the mixture using a micropipette. Following this, the mixture was vortexed and allowed to sit ambient for 3 minutes. The samples were spun at 12000g at 4 °C for 15 minutes. 1 µL of Linear Poly Acrylamide (LPA, 25 ug/ul, Sigma, cat. no. 5-6575) was added into each RNAse free tube. The aqueous phase of the mixture was transferred to the tube and 500 µL of isopropanol was added and mixed thoroughly. The samples were then allowed to sit ambient for 10 minutes before being spun down at 16100g for 10 minutes. The supernatant was removed, and the pellet was washed with 500 µL of 70% ethanol. Finally, the supernatant was removed and the pellet was resuspended with 20 µL of nuclease-free water.

RNA quantification was performed using a NanoDrop 1000 spectrophotometer (NanoDrop Technologies) measuring absorbance at 260 nm.

2.6.2 Conversion to cDNA

Reverse transcription was performed using the High Capacity cDNA Reverse Transcription kit (Applied Biosystems) as per the manufacturer's instructions. Each reaction comprised 1X reverse transcription buffer, 1X random primers, 4mM deoxynucleotide triphosphates (dNTP), 5 units of reverse transcriptase enzyme, diethyl pyrocarbonate (DEPC) treated water and 1000 ng of RNA, in a total of 20 µL volume. For thermal cycling, a GeneAmp PPCR System 9700 system (Applied Biosystems) was used. The cycle used was: 25 °C (10 minutes), 37 °C (120 minutes), 85 °C (5 minutes) and 4 °C (infinite).

For the RNA extracted from FACS sorted cells, reverse transcription was conducted using SuperScript™ VILO™ cDNA synthesis kit (Invitrogen, 11754-050). Each reaction consisted of 5X VILO™ reaction mix, 10X SuperScriptTM enzyme mix, RNA (up to 2.5 µg) and DEPC-treated water. The cycle used was: 25 °C (10 minutes), 42 °C (60 minutes) and 85 °C (5 minutes).

2.6.3 Real-time quantification polymerase chain reaction (qPCR)

Real-time quantification polymerase chain reaction was conducted using the SensiFAST SYBR No Rox kit (Bioline) as per the manufacturer's guidelines. qPCR primers, including both forward and reverse primers, were prepared in nuclease-free water to a concentration of 10 µM. *β-Actin* was used as the housekeeping gene. qPCR primer sequences were designed using the NCBI website and were synthesised by Invitrogen. cDNA was diluted by 1:10 with nuclease-free water. 2 µL of the diluted cDNA was added into the 1X SYBR master mix with qPCR forward and reverse primers to make up a final volume of 10 µL. The final concentration of qPCR primers was 0.3 nM. These samples were then run by QuantStudio qPCR machine (Applied biosystems) in a 384-well format and the reaction consisted of 50 °C for 2 minutes, 10 °C for 10 minutes, followed by 50 cycles (95 °C for 15 seconds and 60 °C for 1 minute). After the completion of the reaction, the raw threshold cycle (C_t) values were analysed using the 2-[delta][delta]C_t method to obtain fold changes. Table 2.2 provides a list of qPCR primers used in the study.

Primer	Forward	Reverse
Eltd1 (pre-deletion exons)	CCTCCCGCTTCTAGTGGGTT	GCACTTCGCACTTGGCATTG
Eltd1 (deleted exons)	CCACGGGGAAGTCACAGTT	GGCATGCTCTAAGTGGCAAT
Eltd1 (post-deletion exons)	ACATGAAGCATGCTCACCCC	ACTACATTGCCAGTTGTGCCA
Tie2	GCCGCGGACTGACTACGAGC	GGAGGAGGGAGTCCGATAGACGC
Pdgfb	ATCGCCGAGTGCAAGACGCG	AAGCACCATTGGCCGTCCGA
β-actin	ATGCTCTCCCTCACGCCATC	CACGCACGATTTCCCTCTCA

Table 2.2: List of qPCR primers used.

2.7 Isolation of endothelial cells from murine tissues

Murine tissues (lungs and aortas) were harvested from mice and collected in Hank's Balanced Saline Solution (HBSS), with calcium and magnesium, (Thermo Fisher Scientific, cat. no. 24020117) on ice. Tissues were transferred into sterile petri dishes under the hood. Using two disposable scalpels (Swann-Morton, cat. no. 0503), the tissues were minced into small pieces which were then transferred to at least 3 mL of collagenase mixture, comprised of 3 mg/mL of collagenase type 1 (Worthington, LS004194) and collagenase type 3 (Worthington, LS004180) dissolved in HBSS. The mixtures were then incubated in a 37 °C incubator for 30 minutes with occasional shaking until a homogenous mixture was achieved. The mixtures were then pipetted several times to dissociate the remnants of the tissues further and then put through a filter (Sysmex, cat. no. 04-004-2327) attached to a 15 mL falcon tube. The filtrate was topped up with 5 mL of staining buffer (PBS and 10% FBS) and centrifuged at 450

g for 5 minutes. The pellet was washed twice with staining buffer to yield a pellet of endothelial cells isolated from the tissues.

2.8 Isolation of mouse aortic vascular smooth muscle cells

This isolation method was followed as described in (Churchman and Siow, 2009). Aortas were harvested from mice and collected in Hank's Balanced Saline Solution (HBSS), with calcium and magnesium, (Thermo Fisher Scientific, cat. no. 24020117) on ice. Under the dissection microscope, the aorta was removed from connective tissues and then cut open longitudinally with a small scissors, keeping the luminal surface facing upwards. The endothelium was removed by scraping the cell layer off with a sterile scalpel blade or cotton bud. After which, the tissue was placed in a petri dish of HBSS. The aorta was then cut into 2 mm cubes with tweezers and scalpel and subsequently the luminal surfaces were placed on the wall of a 25 cm^2 tissue culture flask using a sterile Pasteur pipette. The flask was then placed upright and added with 5 mL of Dulbecco's modified Eagle's medium (DMEM) supplemented with 10 % heat-inactivated foetal bovine serum (FBS) and 1 % penicillin-streptomycin. A minimum of 12-16 cubes was placed in a 25 cm^2 flask kept in a 37 °C incubator with a humidified atmosphere of 5% and 95% filtered atmospheric air. The explants were left undisturbed for about 3-4 days and then media was changed. After 3-4 weeks, the smooth muscle cells reached an adequate density and the explants were removed.

2.9 *In vitro* cre recombination

The aortic vascular smooth muscle cells isolated from *Eltd1*$^{fl/fl}$ mice were treated with TAT-CRE recombinase (Millipore, SCR508). In brief, 5 x 10^4 aortic vascular smooth muscle cells were cultured in each well of a 12-well culture plate. Different concentrations (0.5 µM, 2 µM and 8 µM) of TAT-CRE recombinase was added into each well and cells were further cultured for 2 weeks before they were harvested for analysis.

2.10 Extraction of DNA from cells

The *ex vivo* cultured aortic vascular smooth muscle cells were harvested and DNA was extracted using the QIAamp DNA micro kit (Qiagen, 56304) as per manufacturer's instructions.

2.11 Flow cytometry

2.11.1 Detection of cell surface antigens by flow cytometry

Flow cytometry was used to detect the expression of cell surface antigens. *Ex vivo* isolated cell pellets, as described in section 2.7, was resuspended in 100 µL of primary antibody diluted in staining buffer that comprised of PBS and 5 % FBS. The antibodies used are listed in Table 2.3. A control sample was used as the negative stain control and was not stained with primary antibody. Cells were incubated for 30 minutes in the dark on ice, after which the cells were washed with 1 mL of staining buffer and pelleted by centrifugation at 1500 rpm for 5 minutes. The wash was done thrice. The pellets were then resuspended in 500 µL of staining buffer. As the primary antibodies used were conjugated with fluorophores, there was no need for a separate incubation with secondary antibody. The samples were then analysed by the flow cytometer (BD FACSAria^{TM} Fusion). Data was obtained and analysed using FlowJo.

2.11.2 Detection of GFP-expressing cells by flow cytometry

Detection of GFP (Green Fluorescent Protein)-expressing cells by flow cytometry was conducted using the same procedure as described in section 2.11.1, except that in this method, there is no GFP primary antibody staining required as the GFP fluorescence in the cells was the readout. In this method, non GFP-expressing cells were used as negative control. The cells were harvested and analysed directly using flow cytometer. Data was obtained and analysed as described in 2.11.1.

2.11.3 FACS sorting into single cells for single cell sequencing

After the samples have been analysed by the flow cytometer, the cells that were EGFP^{+}, CD31^{+} and VECadherin^{+} were sorted into 96-well plates by the sorter. A dummy plate was used to calibrate the sorter to ensure that every drop fell in the centre of each well of the plate. Once the calibration was completed, the samples were analysed using the method described in 2.11.1 and 2.11.2, the triple positive cells were then added singly in drops into the 96-well plates. Once the plates were filled, they were immediately transported in dry ice and stored in -80 °C. These samples were then submitted to the Dr Neil Ashley in the Single Cell Sequencing facility (Weatherall Institute of Molecular Medicine) for single cell sequencing (Picelli et al., 2014).

Conjugated primary antibodies	Dilution	Cat. no.
CD31-PerCPef710 (clone 390)	1:250	Invitrogen (14-0311-82)
VECadherin-APC (clone BV13)	1:300	Biolegend (138011)

Table 2.3: List of antibodies used in flow cytometry.

2.12 Smartseq2 single cell sequencing preparation

The preparation was performed by Dr Neil Ashley after the single cells have been sorted into 96-well plates as described in section 2.11.3. In brief, the sample preparation was carried out in the clean room and before use, the hood and pipettes were wiped with RNAse Away. First, first strand synthesis reverse transcriptase reaction buffer was prepared which consisted of SuperScript II first strand buffer (5X), DTT (100 mM), Betaine (5 M), $MgCl_2$ (1 M), Rnase inhibitor (40 U/µl), TSO (100 µM), SuperScript II reverse transcriptase (200 U/µl) and water. Second, the samples were thawed on ice and heated to 72 °C for 3 minutes before cooling on ice and then centrifuged. Next, 6 ul of first strand synthesis buffer was added to each sample. Following this, the samples were incubated at 42 °C for 90 minutes followed by 10 x 2 minute cycles of 50 °C and 2 minutes at 42 °C and finally 15 minutes at 70 °C. Following cDNA synthesis, 15 µl of PCR mix (KAPA Hifi HS Ready Mix 2X, ISPCR primers 10 µM and water) was added to each reaction. The samples were placed in a PCR machine and the PCR reaction consisted of 1 cycle of 98 °C for 3 minutes, 26 cycles of 98 °C for 20 seconds, 67 °C for 15 seconds and 72 °C for 6 minutes, 1 cycle of 72 °C for 5 minutes and hold at 4 °C. After which, the PCR products were cleaned up using a 1:1 volume of Ampure SPRI beads to sample. Beads were warmed to room temperature and dispensed into a V bottom plate. PCR reaction samples were added and mixed by pipetting. Both beads and PCR samples were incubated for 8 minutes at room temperature and placed on magnet for 2 minutes. Supernatant was removed gently without disturbing the beads. Next, 200 µl of freshly made 80% ethanol was added and incubated for 30 seconds before removing. The samples were then resuspended in 17.5 µl of elution buffer EB (Qiagen). The cDNA was then analysed on an Agilent High Sensitivity DNA microfluidic chip using a BioAnalyser.

2.13 Immunostaining of mouse tissues & tumour samples

For all the immunostaining, omission of primary antibody was used as the negative control.

2.13.1 Preparation of formalin fixed paraffin-embedded blocks

Cell pellets and mouse tissue samples were fixed in 4 % paraformaldehyde (PFA) (Sigma) at 4 °C overnight, washed with PBS thrice and processed using the tissue processor (Tissue-Tek® VIP™ 5 JR.) the following day. These samples were then embedded in paraffin wax using moulds and chilled on a cold pad until they were fully solidified. After which, the blocks were removed from the moulds and stored at room temperature indefinitely.

2.13.2 Preparation of sections

Formalin fixed paraffin embedded (FFPE) cytospin cells and mouse tissue sections were processed and sectioned to 4 µm in thickness onto charged glass slides (VMR SuperFrost® Plus). After which, they were air dried in 37 °C incubator and kept at 4 °C for maximum of two months.

The chilled FFPE slides were first warmed at 60 °C and then dewaxed and rehydrated as follows:

Twice in Histolene Clearing Agent (CellPath, cat. no. EGB-0500-00A) for 5 minutes each, twice in 100 % Industrial Methylated Spirit (IMS) (Fisher, cat. no. M/4450/PB17) for 3 minutes each, once in 70 % IMS for 3 minutes, once in 50 % IMS for 3 minutes and once in water for 3 minutes. Tables 2.4 and 2.5 give an overview of the IHC antibodies used on mouse tumour and tissue samples, and IF antibodies used on mouse tumour and tissue samples respectively.

2.13.3 Staining protocols

2.13.3.1 Immunohistochemistry

2.13.3.1.1 H&E, Eltd1, CA9, CD31, Ki67

For Hematoxylin & Eosin staining, mouse tissue and tumour samples were incubated in Eosin for 10 seconds and then rinsed in tap water. The samples were then counterstained with Hematoxylin for 10 seconds and finally rinsed in tap water. The sections were mounted with cover slips using DPX mountant (Sigma 06522). The slides were then air dried overnight and kept at room temperature for long term storage.

Mouse tumour and tissue samples were antigen retrieved in the Decloaker Chamber with citrate buffer (pH 6.0) and peroxidase blocked for 5 minutes. Primary antibodies (Table 2.4)

were prepared in antibody diluent solution. The sections were then incubated with primary antibody solution for an hour at room temperature or overnight at 4 °C. After which, the slides were washed with washing buffer thrice and appropriate secondary HRP antibody was added. The slides were incubated for 1 hour at room temperature and then washed thrice with washing buffer. The DAB/substrate buffer was then added onto the sections and incubated for 5 minutes. After which the slides were washed thrice with washing buffer and counterstained with Hematoxylin for 10 seconds and washed in tap water. The sections were mounted with cover slips using DPX mountant (Sigma 06522). The slides were then air dried overnight and kept at room temperature for long term storage.

H&E staining of mouse tissues was also assessed by a qualified histopathologist, Professor Francesco Pezzella to observe any abnormalities in the architecture of tissues. H&E staining of mouse tumour samples was used to score the area of necrosis. Images of the H&E staining were taken at 4X magnification. Multiple non-overlapping images were taken for each tumour section to cover the entire tumour section. The area of necrosis was then analysed using FIJI software such that the necrotic area was quantified as a percentage of the entire tumour section in each image. The percentage necrosis of the tumour section was calculated as the average of the percentage of necrosis in all images of the section.

CD31 and Eltd1 were scored by 5 randomly chosen fields, at 40X magnification, with the highest vessel density. The number of vessels stained positively with CD31 or Eltd1 was then counted manually and the data was presented as the total number of vessels in 5 fields.

CA9 was scored by the percentage of CA9-positive cells (total expression) staining in the tumour section. Ki67 was scored by the percentage nuclear positivity in the tumour section. Both CA9 and Ki67 were scored by Professor Francesco Pezzella.

Primary antibodies	Dilution	Company (Cat. No.)	Secondary antibodies	Dilution	Company (Cat. No.)
Eltd1 – F01 (produced in rabbit)	1:4000	In-house	Envision+System-HRP labelled anti-rabbit polymer	Use neat	Dako (K4003)
Eltd1 – F04 (produced in rabbit)	1:2000	In-house	Envision+System-HRP labelled anti-rabbit polymer	Use neat	Dako (K4003)
CA9 (Clone M75)	1:100	Absolute antibody	Envision™ FLEX/HRP	Use neat	Dako (SM802)
CD31 (Clone SZ31)	1:100	Dianova (DIA-310)	Simple stain mouse MAX PO (Rat) Immuno-peroxidase polymer	Use neat	Histofine (414311F)
Ki67 (Clone TEC-3)	1:100	Dako (M7249)	Simple stain mouse MAX PO (Rat) Immuno-peroxidase polymer	Use neat	Histofine (414311F)

Table 2.4: IHC antibodies used on mouse tumour and tissue samples.

2.13.3.2 Immunofluorescence

2.13.3.2.1 CD31 and αSMA (double staining)

Both mouse tissue/tumour samples were antigen retrieved in the Decloaker Chamber with citrate buffer (pH 6.0) and peroxidase blocked for 5 minutes. After which, the slides were blocked with 5 % Horse serum (AbD Serotec, C09SA) for 30 minutes at room temperature. CD31 and Cy3-conjugated αSMA antibodies were diluted in 5% horse serum (Table 2.5). The sections were incubated with the antibody mixture at room temperature in the dark for 1 hour. Following this, the sections were washed with washing buffer thrice and incubated in secondary antibody solution diluted in 5% horse serum. The sections were then washed with wash buffer thrice and counterstained with Hoechst 33342 (Invitrogen, H3570) (diluted in PBS) for 5 minutes. The sections were rinsed with washing buffer thrice and coverslips were finally mounted onto the slides with mounting medium (Vector H-1000). The edges were sealed with

clear nail polish. The slides were air dried overnight in the dark and kept at 4 °C. Could be kept at -20 °C for longer term storage (a month).

Primary antibodies	Dilution	Company (Cat. No.)	Secondary antibodies	Dilution	Company (Cat. No.)
CD31 (mouse), clone SZ31)	1:100	Dianova (DIA-310)	Alexa Fluor goat anti-rat IgG 488	1:100	Invitrogen (A11006)
Cys-αSMA	1:200	Sigma (C6198)	N.A.	N.A.	N.A.
Hoechst	1:1000	Invitrogen (H3570)	N.A.	N.A.	N.A.

Table 2.5: IF antibodies used on mouse tumour and tissue samples. N.A.: not applicable

2.14 *In situ* hybridisation (RNAscope® technology) of *Eltd1* probe

The *in situ* hybridisation protocol using the RNAscope® technology was conducted as per the manufacturer's instruction. Murine tissues (kidney and lung) were harvested and collected in 4 % PFA at room temperature for 24 hours. After which, the tissues were processed, embedded and sectioned as described in sections 2.13.1 and 2.13.2. The sections were first baked at 60 °C for an hour and deparaffinised with xylene twice and 100 % ethanol twice. After which, the sections were blocked by hydrogen peroxidase for 10 minutes at room temperature and washed with distilled water for 3-5 times. Following this, the sections were submerged into a beaker of boiling 1X antigen retrieval solution for 15 minutes and were then incubated with protease plus at 40 °C for 30 minutes. Following this, the sections were washed in distilled water 3-5 times. The sections were then stained with the probe and sequential incubation with amplifiers (Amp). The process was as follow: *Eltd1* probe at 40 °C for 2 hours, Amp 1 at 40 °C for 30 minutes, Amp 2 at 40 °C for 15 minutes, Amp 3 at 40 °C for 30 minutes, Amp 4 at 40 °C for 15 minutes, Amp 5 at room temperature for 30 minutes and Amp 6 at room temperature for 15 minutes. Between each incubation, the sections were washed in 1X wash buffer twice. Following this, to detect the signal, a fast red reagent was prepared and added onto the sections for 10 minutes at room temperature. After which, the

sections were washed in distilled water for 3-5 times. The sections were then counterstained by 50 % Hematoxylin for 10 seconds and washed in distilled water for 3-5 times. The slides were left to dry in 60 °C oven and mounted with coverslip using VectorMount™ permanent mounting medium (Vector, cat. no. H-5000) and left to dry overnight.

The RNAscope® staining intensity was then semi-quantitatively assessed under the light microscope. 5 randomly chosen fields at 40X magnification were taken and scores were given based on the number of pink dots or dot clusters (comprised of many dots in a cluster) observed. Table 2.6 is the scoring guideline, adapted from RNAscope® 2.5 HD Detection9 Reagent - RED User Manual.

Staining score	Microscope Objective Scoring
0	No staining or less than 1 dot to every 10 cells (40X magnification)
1	1-3 dots/cell (visible at 20-40X magnification)
2	4-10 dots/cell. Very few dot clusters (visible at 20-40X magnification)
3	> 10 dots/cell. Less than 10% positive cells have dot clusters (visible at 20X magnification)
4	> 10 dots/cell. More than 10% positive cells have dot clusters (visible at 20X magnification)

Table 2.6: Scoring guideline of RNAscope® staining intensity. Adapted from RNAscope® 2.5 HD Detection Reagent - RED User Manual.

2.15 Confocal microscopy

Confocal microscopy was executed using the Zeiss LSM 780 Confocal Microscopy and was used in the assessment of the pericyte coverage of vessels in the human and mouse tumour PPFE sections. Endothelial cells were stained with CD31 antibody. Pericyte coverage around the vessels was assessed by staining with Cy3-conjugated αSMA marker. Fluorescent microscopy images were taken for three tile scans of 5 by 5 images at 25X magnification each per tumour section, such that most part of the tumour was considered in the assessment. Vessel density was scored by the number of CD31 positive vessels in the tile scans. Percentage of pericyte coverage was calculated by the number of double positive vessels for CD31 and αSMA over total number of CD31 positive vessels multiplied by 100.

2.16 Animal breeding and colony maintenance

2.16.1 Animal husbandry

In this project, the strain of mice used was C57BL/6 and these mice were grown in a specific pathogen free (SPF) facility. These mice were taken care of daily by the researchers and supported by the technicians in the animal facility. All the animal experiments conducted in this project adhered to all relevant ethics guidelines for animal care and experimentation under the project license (30-3197).

2.16.2 DNA extraction from ear notches

Ear notches of mice were harvested and collected in 1.5 mL eppendorf tubes by the technicians in the animal facility. Each ear notch was incubated in 75 µL of 'Hot Shot' buffer (25 mM sodium hydroxide (NaOH) and 0.2 mM ethylenediaminetetraacetic acid (EDTA)) for an hour at 99 °C. Following this, the tubes were centrifuged briefly at top speed and the reaction was stopped by adding 75 µL of 'Neutralisation Buffer' (40 mM Tris-HCl, pH 7.4). The extracted DNA was kept at -20 °C for long term storage.

2.16.3 Genotyping of mice by polymerase chain reaction (PCR)

Genotyping of mice was carried out by polymerase chain reaction (PCR) using the extracted DNA from the ear notches of mice, designed primers (Table 2.8) and the mixture of DNA polymerase and dNTPs. In brief, 12.5 µL of Go Taq Green Master Mix (Promega, cat. no. M7113), consisting of DNA polymerase, dNTPs and loading dye, 1 µL of forward primer (10 µM), 1 µL of reverse primer (10 µM), 5.5 µL of nuclease-free water and 5 µL of extracted DNA were prepared in a PCR tube. The PCR tubes were then gently flicked to ensure well mixing of the reaction mixture and spun down briefly to ensure that the mixture was at the bottom of the tubes. Following this, the tubes were placed in a thermal cycler and run under the programme of 94 °C for 2 minutes, 94 °C for 30 seconds, 55 °C for 30 seconds, 72 °C for 1 minute followed by 35 cycles of 94 °C for 30 seconds, 72 °C for 10 minutes and 12 °C infinitely.

The annealing temperature operated in Step 3 was dependent on different primer pairs. The optimised annealing temperature for each primer pair is listed in Table 2.7. Once the reaction was complete, the mixtures were run in 1 % agarose gel (Invitrogen, cat. no. 16500-500) in a gel electrophoresis tank (BioRad) for 20 minutes at 120 V. Following this, the gel was imaged using GBox (Syngene).

Primer		Sequence	Annealing temperature (°C)
LoxP	Forward	TAAATCTTAAGAGAGTTGAATCAC	53.6
	Reverse	ATCTAAGATGTAACAGTTAGTTCT	
Eltd1 locus	Forward	TAAATCTTAAGAGAGTTGAATCAC	53.9
	Reverse	TGTGGTACTGGATCTGAGCCTATG	
Cre	Forward	CCAGCCGCCGTCGCAACT	59
	Reverse	GCCGCCGGGATCACTCTCG	

Table 2.7: List of genotyping PCR primers used.

2.17 Aortic ring angiogenesis assay

Age-matched mice of 7-8 weeks were chosen in this assay (Baker et al., 2011). The mice were sacrificed, and the aortas were harvested and collected in EGM2 medium (Endothelial Basal Medium 2 (EBM^{TM} 2) (Lonza, cat. no. 00190860) supplemented with Endothelial Growth Medium 2 (EGM^{TM} 2) Endothelial SingleQuots^{TM} kit (Lonza, cat. no. CC-4176)). Using tweezers and disposable scalpels, the extraneous fat, tissue and branching vessels were removed and then the aorta was cut into rings of 1 mm in length. A layer of growth factor-reduced Matrigel (Corning, cat. no. 354230) was added into a 96-well plate and incubated at 37 °C. Once solidified, another layer of Matrigel was added and the rings were embedded such that they faced upwards. The plate was then incubated at 37 °C for 30 minutes to ensure that Matrigel had solidified. These aortic rings were cultured in EGM2 medium at 37 °C. Medium was changed the following day. Images, at 4X magnification, of the rings were taken at day 5 and day 9 using the EVOS microscope. The images were analysed using FIJI software such that the total area (including the ring and sprouting area) and the area of the ring were quantified. The sprouting area was then calculated by subtracting the area of the ring from the total area.

2.18 Tamoxifen preparation and induction

Tamoxifen (Sigma, cat. no. T5648) was dissolved in 100% ethanol, by pipetting and warming in a water bath at 37 °C to achieve a concentration of 100 mg/mL. This stock was then aliquoted into 100 µL volumes in 1.5 mL eppendorf tubes. On the day of tamoxifen induction, 900 µL of sunflower seed oil (Sigma, S5007) was mixed with 100 µL of tamoxifen. 100 µL of

the mixture was injected between the inner thigh and genitals of each experimental mouse to ensure no organs were punctured. The mice were then monitored closely for any welfare problems. The experimental mice were given intraperitoneal injections of tamoxifen, 1 mg, for 5 consecutive days.

2.19 Syngeneic tumour models

Syngeneic tumour models were generated by subcutaneous injection of syngeneic cancer cell lines (E0771 or MC38) into C57BL/6 mice. Two models have been chosen to avoid model-dependent observations. For each mouse, either 5×10^5 E0771 cells or 1×10^6 MC38 cells were used. Dr Esther Bridges assisted by performing the subcutaneous injection of tumour cells.

The cells were cultured for several passages and checked for mycoplasma infection before they were subcutaneously injected into the mice. On the day of injection, the experimental mice were anaesthetised with isoflurane. During this time, the right flank of the back of the mouse was shaved to allow for better visibility of the skin. After which, 100 µL of E0771 cells in Matrigel with growth factors (Corning, cat. no. 354234) or 100 µL of MC38 cells in PBS were prepared using a 1 mL syringe on ice. Following this, the skin of the mice was pinched and lifted gently and the cell suspension in the syringe was gently injected such that it formed a bulge under the skin. The mice were then removed from anaesthesia and kept in the cage. They were monitored for at least half an hour for any welfare issue pertaining to abnormal behaviour such as unconsciousness or disturbed movements. Over the course of the experiment, the experimental mice were monitored and tumour size measurements were taken every alternate day when the tumours were small, and daily when the tumours were nearing endpoint size of gross medium dimension (GMD = (length X breadth X height)$^{1/3}$) of 10 mm towards the end of the experiment. The tumours were measured using the calliper, taking note of the length, breadth and height of the tumours. The GMD of the tumours and the welfare condition of the mice were recorded. Once the endpoint of the experiment was reached, the mice were given intraperitoneal injection of pimonidazole (2 mg/100 µL). One and a half hour later, the mice were then injected with 100 µL of a mixture solution of Hoechst (6 mg/mL) and tomato lectin (1 mg/mL) via tail vein for 2 minutes before they were sacrificed. The tumours and the vital organs (brain, heart, lung, liver, kidney and spleen) were then

harvested. All animal work was conducted under the relevant ethics guidelines for animal care and experimentation.

2.20 Statistical analyses using Prism

Prism 7 (Graphpad Software) was used in the data analysis from wet lab and *in vivo* experiments. In the comparison of two groups, the Student's *t*-test was used. For unpaired data, an unpaired Student's *t*-test was performed. Kaplan-Meier survival analyses were computed for all survival comparisons. Significance was denoted as: * $p \leq 0.05$, ** $p \leq 0.01$, *** $p \leq 0.001$, **** $p \leq 0.0001$.

Chapter 3: Investigation into the *in vivo* effects of chronic endothelial-*Eltd1* depletion

3.1 Introduction

3.1.1 Rationale

It has been previously reported that *in vivo* targeting of endothelial cells using *Eltd1* siRNA, incorporated into chitosan nanoparticles (CH-NP) in orthotopic ovarian and subcutaneous colorectal xenografts resulted in a reduction in microvessel density, cell proliferation and increases in hypoxia, pericyte coverage and endothelial cell apoptosis (Masiero et al., 2013). However, this experiment was performed on immunocompromised nude mice that are not sufficiently reflective of therapy, as it disregards the potential involvement of Eltd1 in the immune activity in the tumour microenvironment. Hence it would be useful to generate *Eltd1* knockout mice with a functional immune capability for further investigation. It has also been reported that Eltd1 depletion in mice did not cause any developmental defects (Xiao et al., 2012) even though striking vascular defects were seen in *Eltd1* knockout zebrafish embryos (Masiero et al., 2013). This might suggest that there could be acquired functional compensation during evolution which is in line with the expansion of the receptor family that could substitute the functions of existing receptors in higher vertebrates (Kwakkenbos et al., 2004). However, the knockout strategy previously used (Xiao et al., 2012) retained the entire extracellular domain of Eltd1 which could still have functional activity and could mask or diminish the phenotype of the knockout. Therefore, it was critical to re-examine the *in vivo* functions of Eltd1 in immunocompetent mice more carefully with a knockout strategy that leads to the loss of function/expression of the bulk of the protein including the extracellular domain.

Cre/loxP-mediated recombination technology has been used widely to generate tissue-specific conditional knockout mice (Bouabe and Okkenhaug, 2013). This methodology requires the use of two genetically modified mouse strains namely, a floxed mouse and a cre mouse. In the floxed mouse, the gene of interest is flanked by *loxP* sites. In the cre mouse,

the expression of the cre recombinase is under a relevant tissue-specific promoter and can be conditional which allows for the deletion of the floxed DNA to occur at a specific time and in a specific tissue (Ray et al., 2000), as shown in Figure 3.1. An endothelial cell-specific *Eltd1* knockout model was generated to investigate the role of Eltd1 in endothelial cell-mediated tumour development, pathological and physiological angiogenesis in immunocompetent mice.

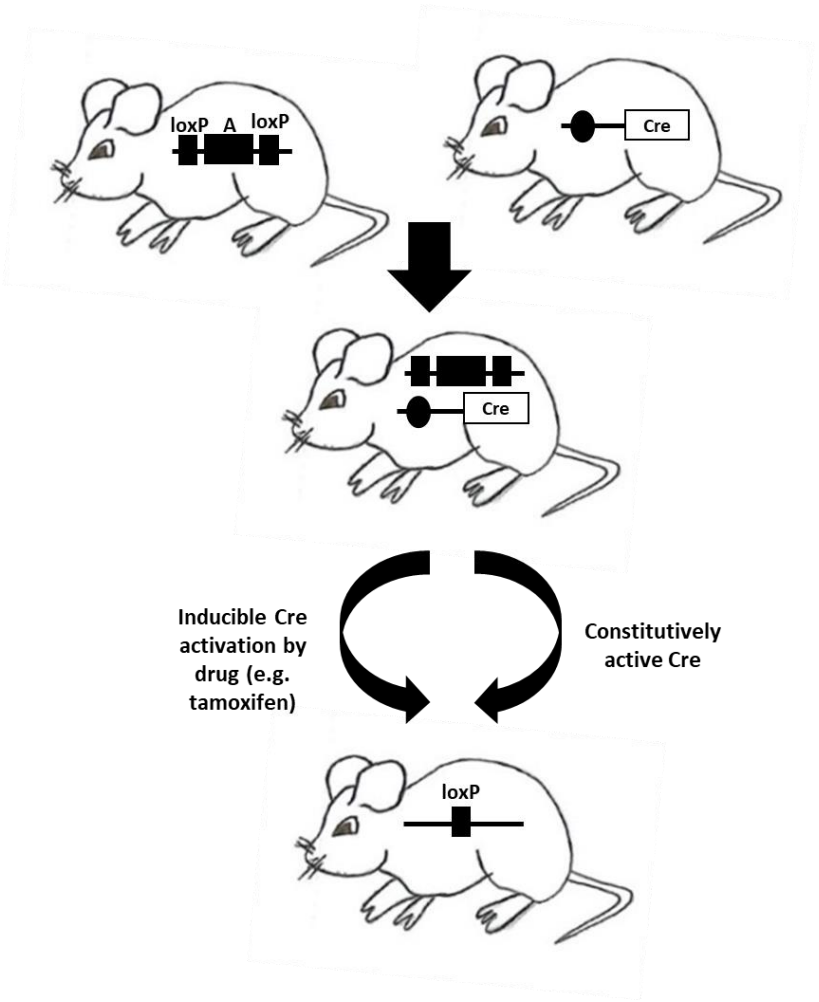

Figure 3.1: Schematic representation of Cre/loxP-mediated recombination technology. In this technology, a floxed mouse, with a target gene flanked by *loxP* sites, is generated. The floxed mouse is then crossed with a cre mouse, in which the expression of the cre recombinase is driven by a tissue-specific promoter. The activity of the cre recombinase can be either constitutively active or drug induced. The cre recombinase catalyses the recombination event of the *loxP* sites, leading to the excision of the target gene A.

3.1.2 *In vivo* endothelial cell-specific *Eltd1* knockout strategy

Based on The European Conditional Mouse Mutagenesis Program (EUCOMM), we selected the construct in which the *loxP* sites flanked exons 4 and 5 of *Eltd1* (covering the second and third EGF domains of murine Eltd1) and into which a premature stop codon was inserted which would result in a frameshift mutation preventing expression of the bulk of the Eltd1 protein, as shown in Figure 3.2.

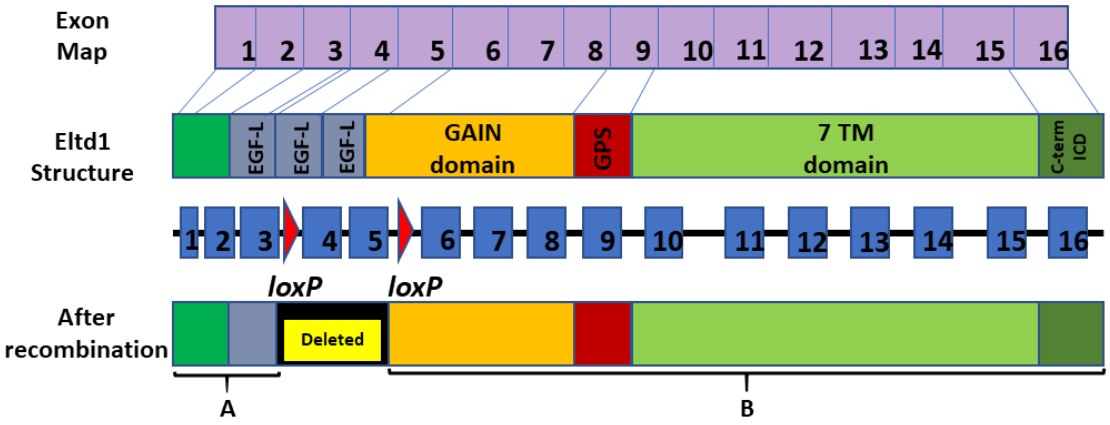

Figure 3.2: *In vivo* mouse *Eltd1* knockout strategy. A small N-terminal fragment of Eltd1 (A) is retained but it is unlikely to have any functionality and may have reduced expression if the transcript is subject to nonsense-mediated decay. With the deletion of exons 4 and 5, a premature stop codon and a frameshift mutation result in the loss of expression of the bulk of Eltd1 (B). EGF-L: Calcium binding EGF-like domain; GAIN domain: GPCR Autoproteolysis Inducing Domain; GPS: GPCR Proteolysis Site; 7 TM domain: 7 Transmembrane domain; C-term ICD: C-terminus Intracellular domain; EUCOMM: The European Conditional Mouse Mutagenesis Program.

3.2 Generation of constitutive endothelial cell-specific *Eltd1* knockout model using *Tie2-Cre* mice

3.2.1 Breeding of *Eltd1* floxed mice

Our collaborator (Professor Peter Carmeliet's laboratory, CCB-KU Leuven Center for Cancer Biology) had generated the *Eltd1* floxed mice prior to the start of this DPhil project, based on the design illustrated in 3.1.2. Heterozygous *Eltd1* floxed mice ($Eltd1^{fl/WT}$) were then provided to Oxford.

To generate *Eltd1* homozygous floxed mice ($Eltd1^{fl/fl}$), these mice were bred with each other generating pups with the three different genotypes s shown in Figure 3.3. DNA extraction from ear notches and genotyping PCR protocols were optimised to determine the genotypes of the pups. The insertion of *loxP* site resulted in a larger band of 346 bp while the absence of *loxP* site gave a band of 223 bp. Hence for the $Eltd1^{fl/fl}$ (homozygote), a strong band at 346 bp was expected while for the $Eltd1^{WT/WT}$ (wildtype), a strong band was expected at 223 bp. Both bands were expected for the $Eltd1^{fl/WT}$ (heterozygotes).

During the colony expansion, we observed that the pups exhibited either a black or brown coat colour due to the mixed background of the 129S6 and C57BL/6 strain. To maintain a high C57BL/6 background, only the black mice were kept for further breeding. After three rounds of breeding, all the subsequent litters were black.

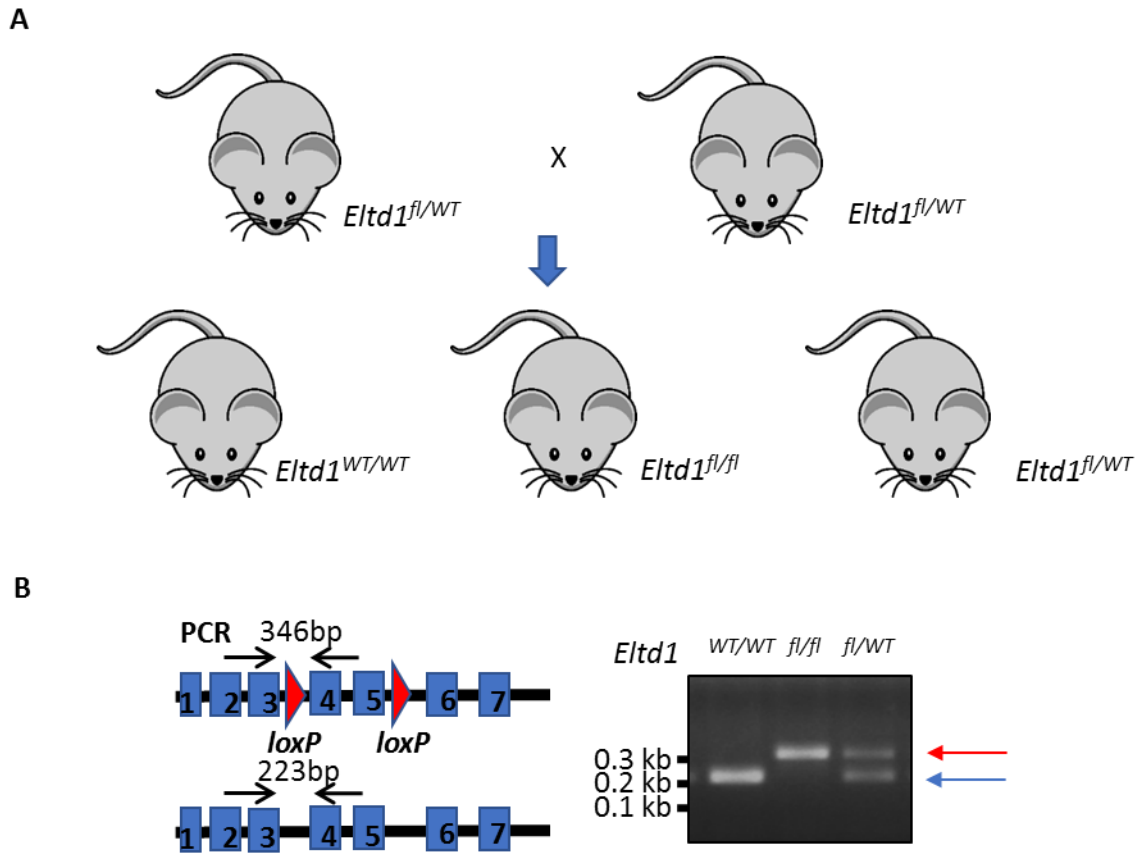

Figure 3.3: Generation and expansion of *Eltd1* floxed mouse colony. A) *Eltd1*$^{fl/WT}$ mice have been generated by our collaborator (Professor Peter Carmeliet's laboratory). Once received, *Eltd1*$^{fl/WT}$ mice were crossed yielding three different genotypes namely, *Eltd1*$^{WT/WT}$, *Eltd1*$^{fl/fl}$ and *Eltd1*$^{fl/WT}$, in the ratio of 1:1:2. B) Genotyping DNA gel image showing the bands of the different genotypes. The red arrow indicates a band at 346 bp and the blue arrow points to the band at 223 bp.

3.2.2 Proof of concept of the knockout strategy

To investigate if the design of the *Eltd1* floxed locus enabled deletion of exons 4 and 5, an *in vitro* experiment was conducted in which *ex vivo* cultured aortic vascular smooth muscle cells isolated from *Eltd1*$^{fl/fl}$ (homozygous) mice were treated with tat-cre recombinase. In the *Eltd1*$^{fl/fl}$ mice, all the *Eltd1*-expressing cells would contain *loxP* sites flanking exons 4 and 5 of *Eltd1*. The genotyping PCR strategy was designed such that forward primer started from the 5' end to the *loxP* site flanking exon 4 and the reverse primer started from the 3' end of the *loxP* site flanking exon 5, illustrated in Figure 3.4. Using different concentrations of the

recombinase, 0.5 µM, 2 µM and 8 µM, there was an increase in the band intensity at the band indicative of the deleted locus (276 bp) while the wildtype locus of 1.4 kb was diminished at 8 µM (Figure 3.4). GL261 is a murine glioma cell line reported to have endogenous *Eltd1* expression (Ziegler et al., 2017) and was used in this experiment as a control. Since the *Eltd1* sequence was unmodified, the PCR product would give a distinct band lower than that of the wildtype locus due to the absence of the *loxP* sites. There were two other bands observed in the GL261 which could be non-specific PCR products. This experiment demonstrated that the design of knockout strategy worked successfully to enable deletion of *Eltd1* exons 4 and 5.

A

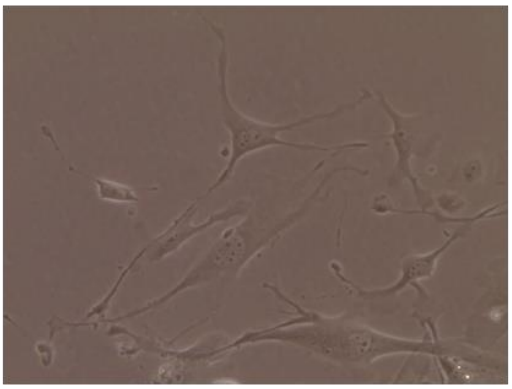

B

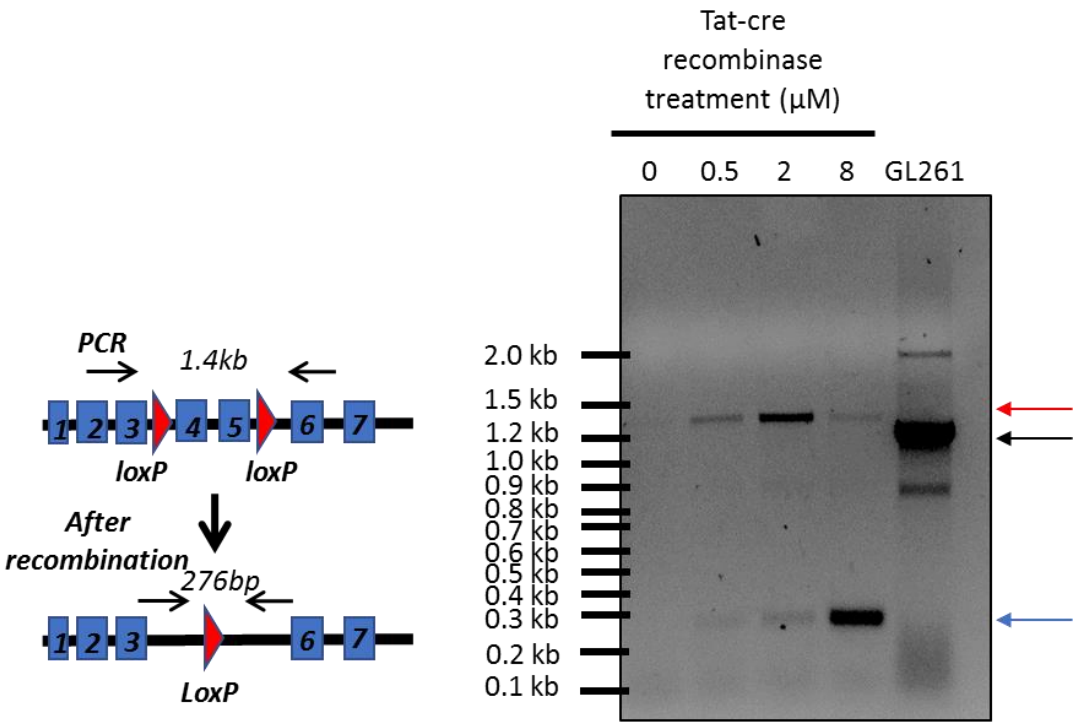

Figure 3.4: *In vitro loxP* recombination of *ex vivo* cultured aortic vascular smooth muscle cells. A) Image of *ex vivo* cultured aortic vascular smooth muscle cells isolated from *Eltd1*$^{fl/fl}$ mice, taken at 40X magnification. B) Representative genotyping PCR of the wildtype (1.4 kb) and deleted *Eltd1* locus (276 bp) in the aortic vascular smooth muscle cells treated with different concentrations of tat-cre recombinase (0.5 µM, 2 µM and 8 µM), n=3. GL261 is a murine glioma cell line with endogenous *Eltd1* and was used as a control of unmodified *Eltd1* locus. The red and blue arrows indicate the wildtype locus (1.4 kb) and deleted *Eltd1* locus (276 bp) respectively while the black arrow points to the unmodified *Eltd1* locus.

3.2.3 Generation of constitutive endothelial cell-specific *Eltd1* knockout model

Tie2-Cre was selected for endothelial-*Eltd1* deletion as these mice have been used extensively and successfully for generating endothelial cell-specific knockout models (Kisanuki et al., 2001). The *Tie2-Cre* strain we selected had the allele of Tek^{12Flv} and was a constitutive line in which the Cre recombinase in *Tie2*-expressing cells is active from around E8 embryonic stage without needing any drug treatment to stimulate its expression. It was advised by our collaborator (Professor Sarah De Val, Ludwig Cancer research, University of Oxford) that *Tie2-Cre* breeding should be performed with hemizygous males as double copies of the *Cre* recombinase could be lethal. Importantly, one copy of the Cre recombinase would produce sufficient levels of the recombinase to effectively target the *loxP* sites at both *Eltd1* loci. As there are reports that *Tie2* is also expressed in macrophages (Chen et al., 2016) and other hemopoietic cells (Tang et al., 2010), this must be considered when analysing downstream functional phenotypes.

The breeding strategy required to generate the constitutive endothelial cell-specific *Eltd1* knockout mice is illustrated in Figure 3.5. Two crosses were required to yield the $Eltd1^{fl/fl}$;$Tie2\text{-}Cre^{+/-}$ mice.

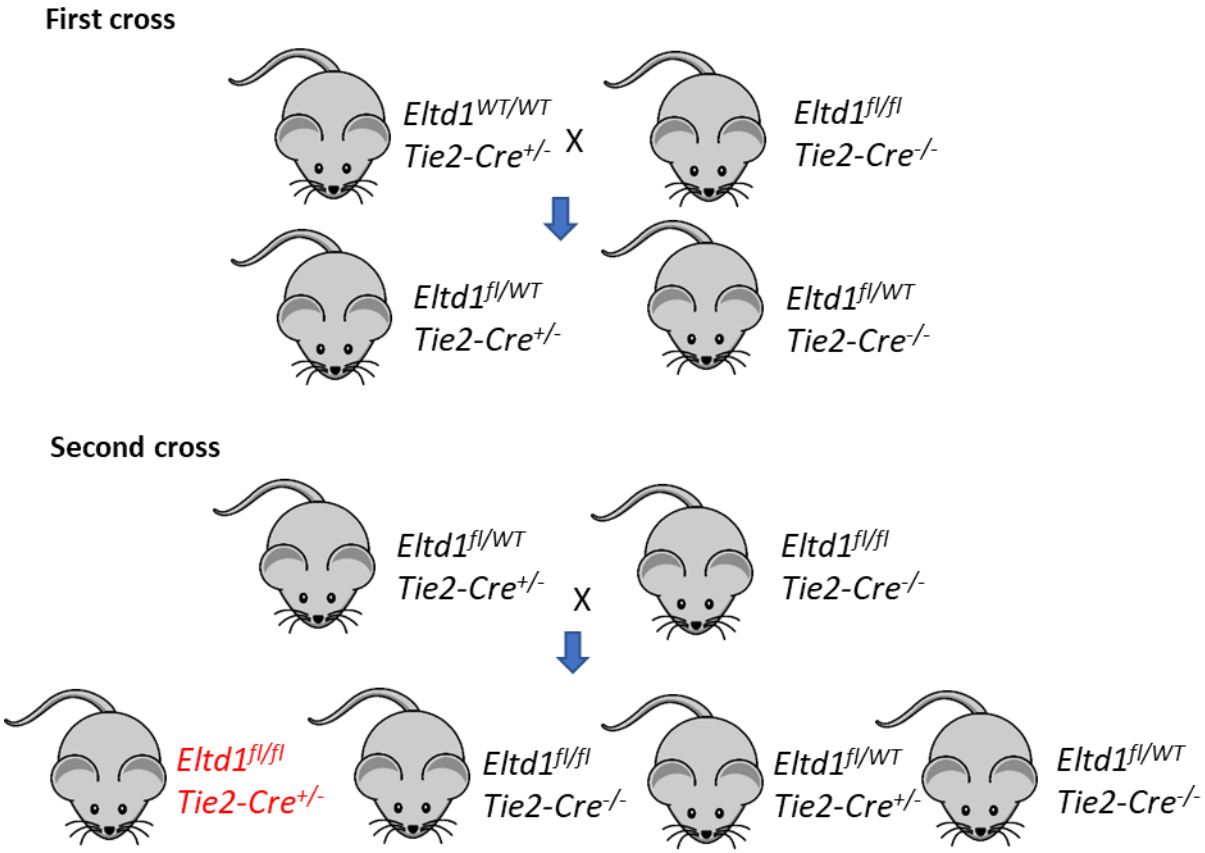

Figure 3.5: Schematic representation of the generation of constitutive endothelial cell-specific *Eltd1* knockout mice (*Eltd1*$^{fl/fl}$;*Tie2-Cre*$^{+/-}$). The first cross created mice heterozygous for both floxed *Eltd1* and *Tie2-Cre*, while the second generated mice homozygous for floxed *Eltd1* and heterozygous for *Tie2-Cre* (highlighted in red).

Once the *Eltd1*$^{fl/fl}$;*Tie2-Cre*$^{+/-}$ mice had been generated, additional breeding was carried out to generate experimental mice. As illustrated in Figure 3.6, this strategy generated 50% of the mice with *Tie2-Cre* and *Eltd1* deletion, and 50% that lacked *Tie2-Cre* which were suitable littermate controls for subsequent experiments.

In this chapter, *Eltd1*$^{fl/fl}$;*Tie2-Cre*$^{-/-}$ mice are referred to as 'Control' while *Eltd1*$^{fl/fl}$;*Tie2-Cre*$^{+/-}$ mice are named as 'EC KO'.

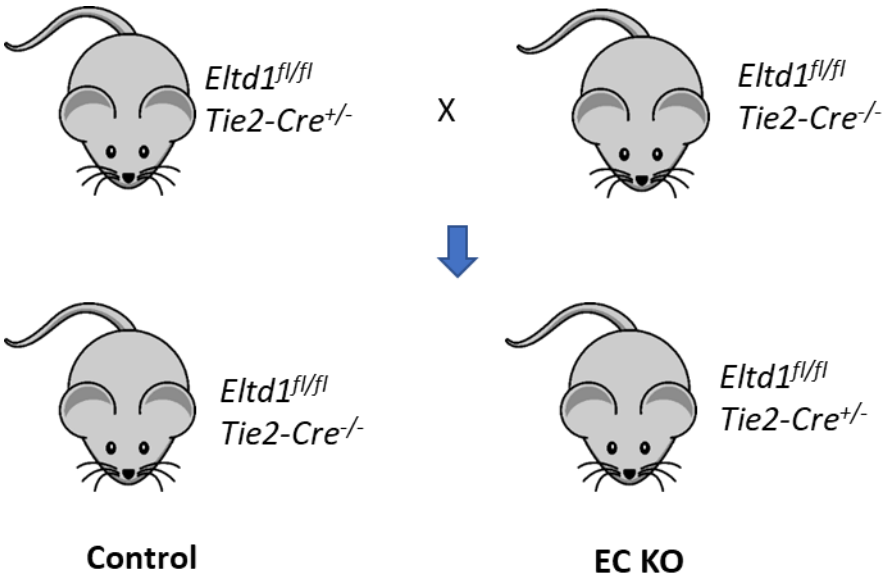

Figure 3.6: Schematic representation of the generation of the experimental mice. This cross created all mice homozygous for floxed *Eltd1*, 50% of which were heterozygous for *Tie2-Cre* while the other 50% did not express *Tie2-Cre*. These mice were then used for downstream functional experiments. Legend: Control mice: *Eltd1$^{fl/fl}$;Tie2-Cre$^{-/-}$* and EC KO mice: *Eltd1$^{fl/fl}$;Tie2-Cre$^{+/-}$*.

3.3 Validation of the constitutive endothelial cell-specific *Eltd1* knockout model

Deletion of *Eltd1* in the *Eltd1$^{fl/fl}$;Tie2-Cre$^{+/-}$* mice was initially validated at the genomic level by performing genotyping PCR using DNA extracted from the ear notches of these mice. The genotyping PCR strategy detecting the deletion of *Eltd1* exons 4 and 5 has been described earlier in section 3.2.2. By comparing the *Eltd1$^{fl/fl}$;Tie2-Cre$^{+/-}$* and *Eltd1$^{fl/fl}$;Tie2-Cre$^{-/-}$* mice, *Eltd1* deletion was detected by a 276 bp in the knockout but not the control, the latter gave a faint band of higher molecular weight derived from the wildtype locus (1.4 kb), illustrated in Figure 3.7. The wildtype locus was also expected to be observed in the knockout, due to this model being an endothelial cell-specific and not a total knockout model. However, the relatively small PCR product of 276 bp was preferentially amplified and thus the intensity of the 1.4 kb, band was much lower and sometimes undetectable.

At this stage of the project, the commercially available antibodies had already been tested for their specificity for Eltd1 detection by western blotting and immunohistochemistry but none

of the antibodies was reliable. Hence, it was decided to evaluate the *Eltd1* knockout at the transcript levels using the RNA *in situ* hybridisation. This approach was selected, rather than PCR in a bulk tissue, to enable the validation of *Eltd1* deletion occurring in the expected cell types. The probe chosen targeted exons 9-15, downstream of the deleted exons. Due to the high cost of probe customisation, an 'off-the-shelf' probe that had been validated by the Company was selected, rather than having an untested custom probe designed to the deleted exons 4 and 5. It was expected that hybridisation using this probe would give a lower signal through nonsense mediated decay of the deleted transcript, this would add confidence that a knockout model had been generated. The RNA *in situ* hybridisation experiment was performed on kidney and lung sections of the mice as these tissues have high *Eltd1* expression (Regard et al., 2008) and are highly vascularised. In both kidney and lung sections, there was a significant reduction in the staining (unpaired Student's *t* test, kidney: $p \leq 0.001$; lung: $p \leq 0.01$) which suggested that deletion of exons 4 and 5 did cause mRNA decay of the *Eltd1* transcript. This data supported the efficiency of the *in vivo Eltd1* knockout strategy and the constitutive endothelial cell-specific *Eltd1* knockout model.

Since an antibody against murine Eltd1 would be very useful in assessing Eltd1 knockout in the tissues and tumours generated from the *in vivo* experiments in future, rabbit polyclonal antibodies against Eltd1 were generated with the help of Cambridge Research Biochemicals (CRB) using a recombinant murine Eltd1 protein (EGF domains) that was generated by Professor Penny Handford's laboratory (Department of Biochemistry, University of Oxford). Details on the protein design, immunisation protocol and validation of the bleeds in Western blotting and immunohistochemistry applications are described in the chapter 2.

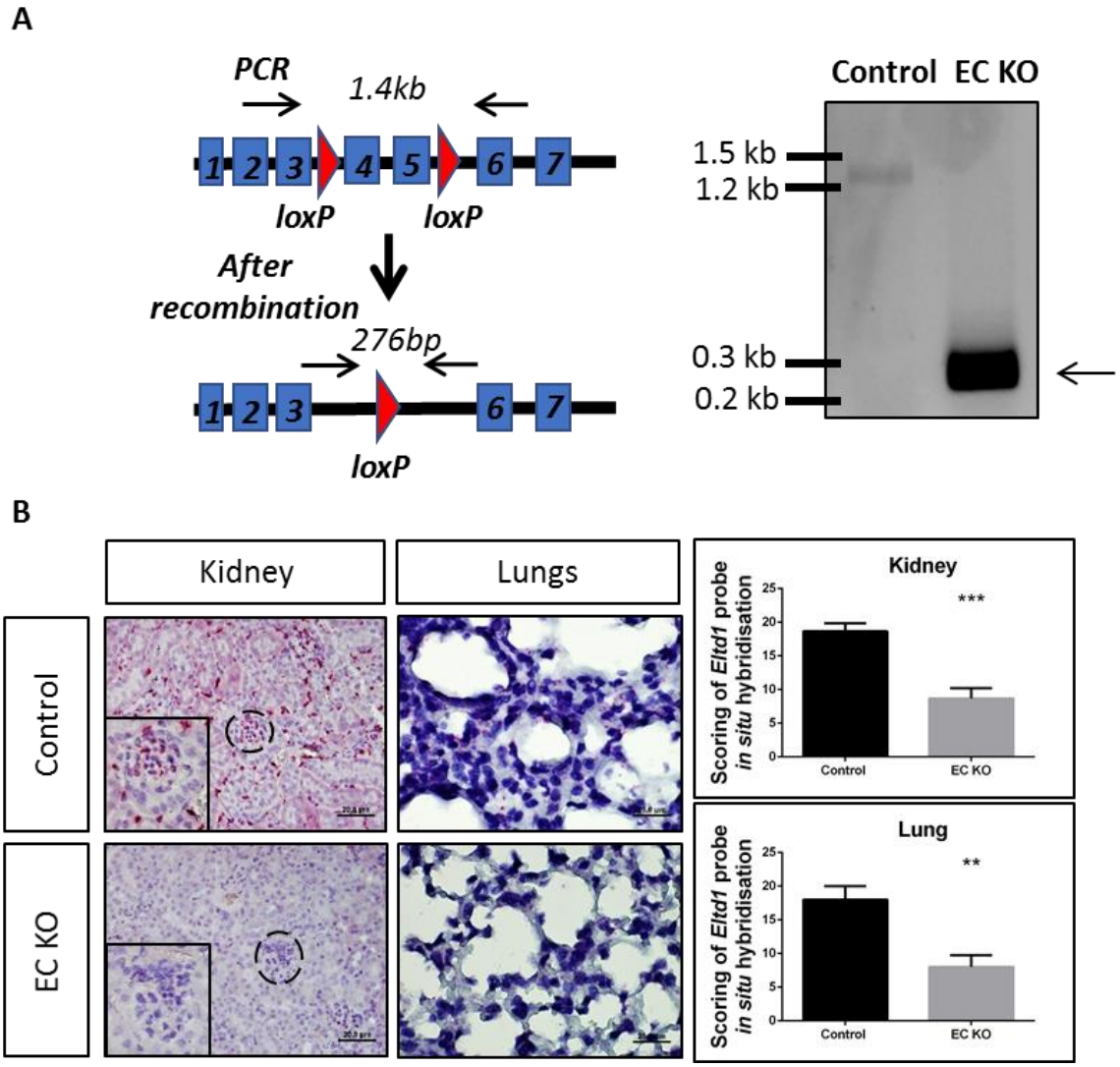

Figure 3.7: Validation of constitutive endothelial cell-specific *Eltd1* knockout model. A) Representative genotyping PCR of the *Eltd1* deleted locus, identified by a strong low molecular weight band of 276 bp indicated by an arrow. B) *In situ* hybridization of *Eltd1* probe on murine kidney and lung sections. The kidney glomeruli (highlighted in black) and the lungs are rich in endothelial cells which express *Eltd1*, indicated by punctate red dots in which each dot represents an RNA molecule of *Eltd1*. There was a marked reduction in *Eltd1* staining in the glomeruli and lungs (unpaired Student's *t* test, kidney: $p \leq 0.001$; lung: $p \leq 0.01$) of EC KO compared to Control mice. Data represented as mean ± SD (**=$p \leq 0.01$; ***=$p \leq 0.001$) (n=3).

3.4 Effects of *loxP* insertion on *Eltd1* expression and architectural integrity of vital organs of the mice

For the littermates to be suitable experimental controls we needed to confirm that the *loxP* insertion itself did not result in differential *Eltd1* expression or any morphological changes in the vital organs of the *Eltd1* floxed mice. Therefore, qPCR analysis of *Eltd1* transcript levels was performed on lungs and kidneys and H&E staining was done on heart, lungs and kidneys in which *Eltd1* has been reported to have a functional role and high expression (Xiao et al., 2012; Lu et al., 2017). Hematoxylin & Eosin (H&E) staining showed no abnormalities in these vital organs and there was no significant difference in *Eltd1* expression between the three different *Eltd1* genotypes as shown in Figure 3.8. The H&E staining was verified by an experienced clinical histopathologist (Professor Francesco Pezzella, University of Oxford).

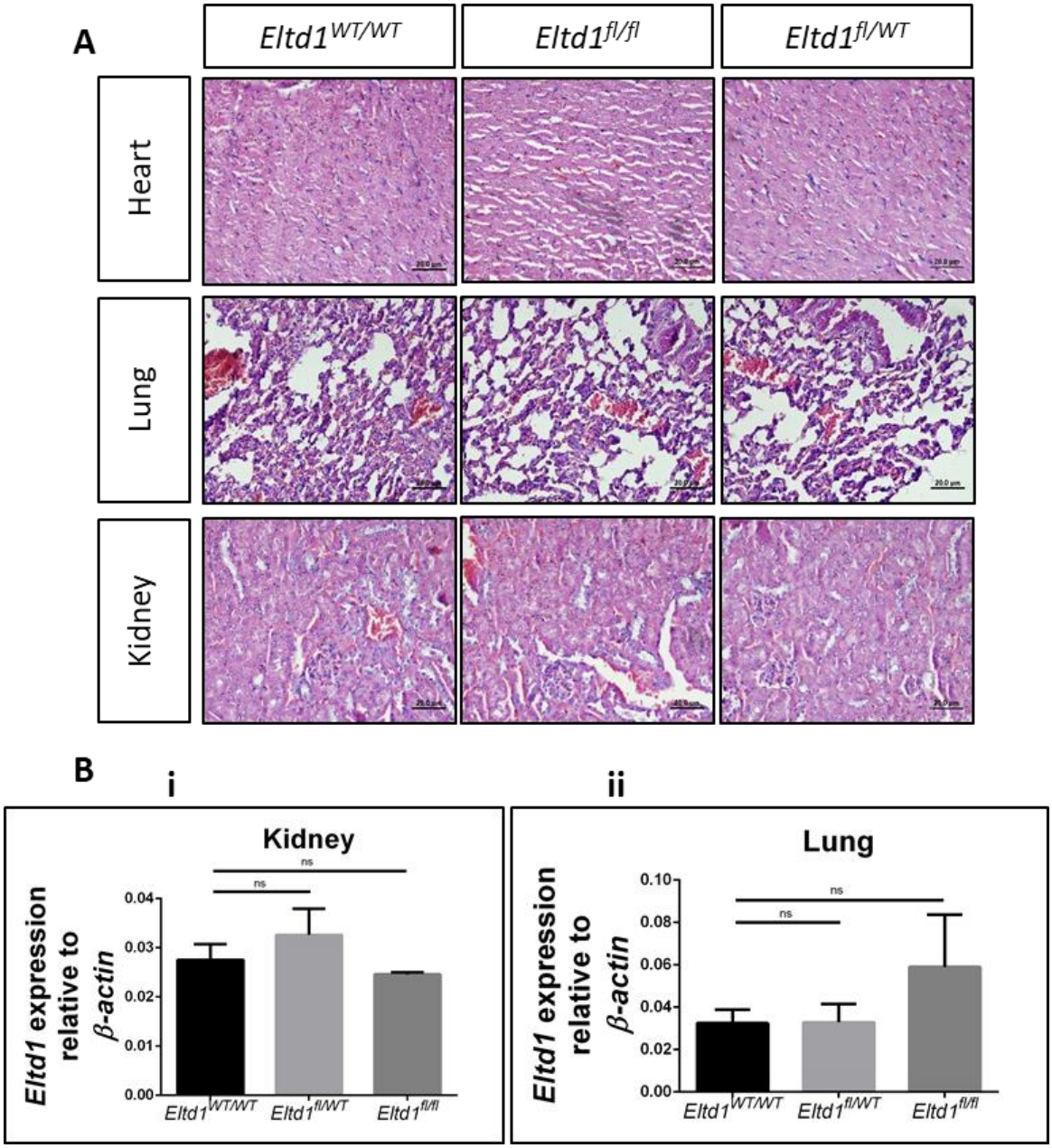

Figure 3.8: Effects of *loxP* insertion on architectural integrity and *Eltd1* mRNA expression of vital organs of the mice. A) H&E staining showed no significant differences in the architectural integrity of heart, lung and kidney between *Eltd1*$^{WT/WT}$, *Eltd1*$^{fl/fl}$ and *Eltd1*$^{fl/WT}$ mice (Scale bar: 20 µm). B) qPCR analysis showed no significant differences in *Eltd1* expression in kidney (i) and lung (ii) of *Eltd1*$^{WT/WT}$, *Eltd1*$^{fl/WT}$ and *Eltd1*$^{fl/fl}$ mice.

3.5 Variable levels of *Eltd1* reduction, by qPCR, was observed across different normal tissues.

To assess the levels of *Eltd1* transcript reduction in normal tissues, lungs and kidneys were harvested from three 8-week-old male mice (n=3 mice per group). Lungs and kidney from *Eltd1$^{fl/fl}$;Tie2-Cre$^{+/-}$* mice exhibited different levels of *Eltd1* reduction relative to *Tie2* gene expression as compared to *Eltd1$^{fl/fl}$;Tie2-Cre$^{-/-}$* mice (unpaired Student's *t* test: lungs, $p = 0.021$; kidney, $p = 0.039$), as shown in Figure 3.9. The reduction in the transcript level of *Eltd1* exons 4 and 5 gave confidence that a constitutive endothelial cell-specific *Eltd1* knockout model had been established. The variable levels of *Eltd1* reduction could suggest that different organs might have endothelium made up of different proportion of *Tie2*-expressing endothelial cells in which the deletion of *Eltd1* exons occur.

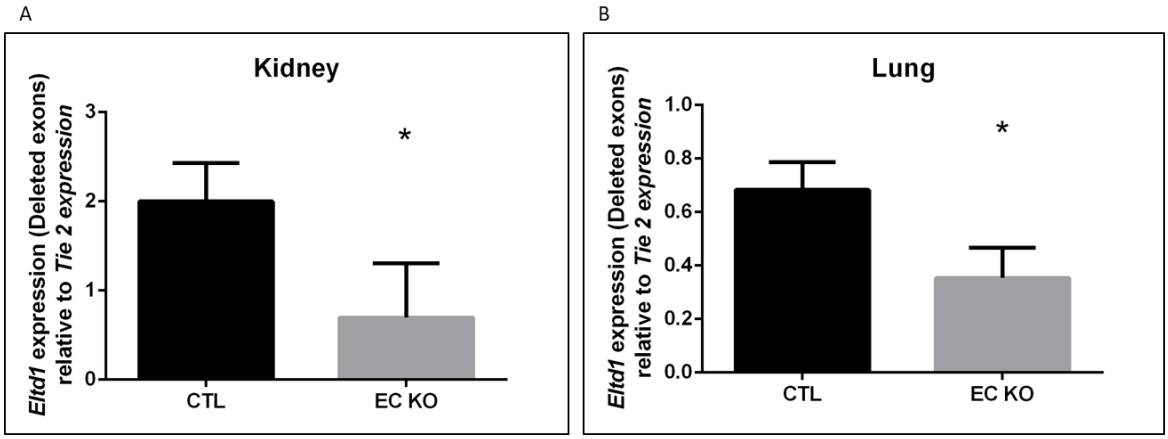

Figure 3.9: Assessment of *Eltd1* mRNA reduction in lungs and kidneys of the constitutive endothelial cell-specific *Eltd1* knockout mice compared to those of littermate control mice. This was achieved by assessing *Eltd1* expression relative to *Tie2* gene expression normalized to *β-actin* expression. Both lung and kidney showed significant reduction (unpaired Student's *t* test: lungs, $p = 0.021$; kidney, $p = 0.039$) in the expression of *Eltd1* exons 4 and 5 (deleted exons). Data represented as mean ± SD (*=$p \leq 0.05$) (n=3 male mice per group).

3.6 Constitutive endothelial cell-specific *Eltd1* knockout mice did not exhibit significant differences in body weight and general physiological parameters compared to littermate controls

Having confirmed genomic *Eltd1* deletion and loss of transcript expression in endothelial cells, further studies were performed to identify any marked phenotypic changes. As the crossing of *Eltd1*$^{fl/fl}$;*Tie2-Cre*$^{+/-}$ mice gave the control and EC KO mice in the expected ratio of 1:1, there was no suggestion of loss of any *Eltd1*-deleted embryos during development or prior to adulthood. The constitutive endothelial cell-specific *Eltd1* knockout mice did not show signs of distress and there was no significant change in body weight over a duration of 103 days (Figure 3.10). This was consistent with the literature in which total *Eltd1* knockout mice did not show significant changes in organ-to-body weight ratios and signs of distress (Xiao et al., 2012).

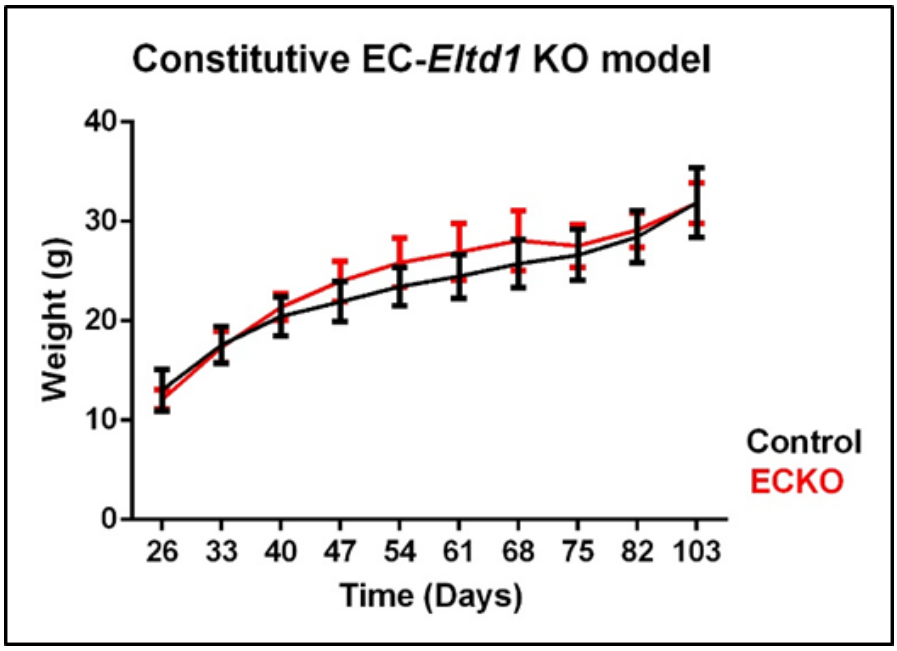

Figure 3.10: Body weight comparison between constitutive endothelial cell-specific *Eltd1* knockout and littermate control mice. There was no significant differences in body weight between constitutive endothelial cell-specific *Eltd1* knockout and littermate control mice over a duration of 103 days (n=5 male mice per group).

3.7 Constitutive endothelial cell-specific *Eltd1* knockout mice did not exhibit significant differences in organ/body weight ratios

Vital organs (brain, heart, lung, kidney, liver and spleen) were harvested and weighed when the mice were 8-week-old (n=6). There was no observed significant difference in the organ-to-body weight ratios in the *Eltd1* knockout group (Figure 3.11).

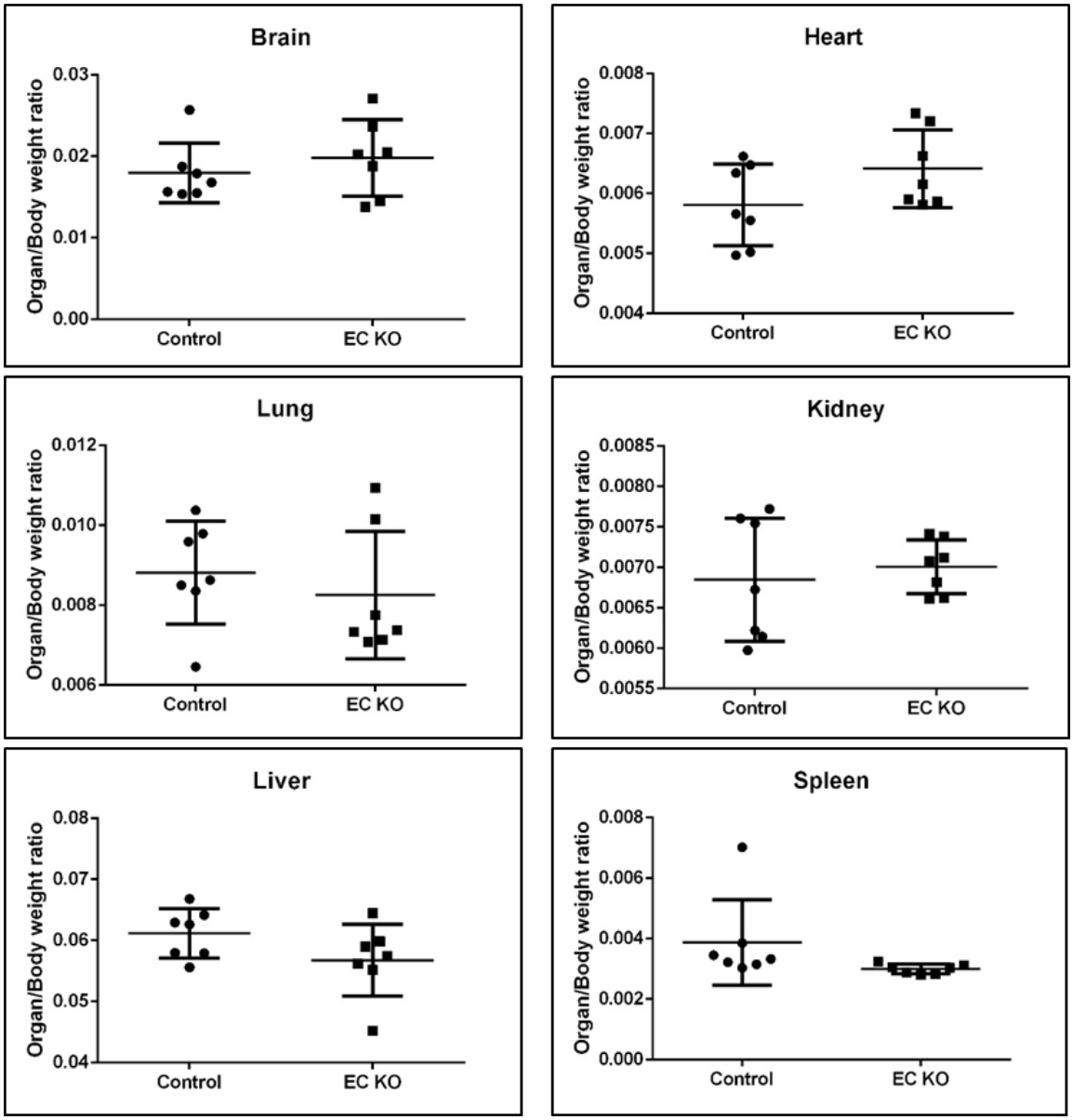

Figure 3.11: Organ/Body weight comparison between constitutive endothelial cell-specific *Eltd1* knockout and littermate control mice. No significant differences (unpaired Student's *t* test) in organ/body weight ratios of the constitutive endothelial cell-specific *Eltd1* knockout mice were observed (n=6 male mice per group).

3.8 Constitutive endothelial cell-specific *Eltd1* knockout mice did not exhibit significant differences in the architecture or vessel morphology of vital organs

Vital organs (brain, heart, lung, kidney, liver and spleen) from constitutive endothelial cell-specific *Eltd1* knockout mice exhibited similar vessel morphology with comparable CD31 staining intensity and distribution (Figure 3.13), no compromise of the architectural integrity of the tissues by H&E staining and no signs of necrosis as compared to the littermate controls (Figure 3.12). Three male mice were used per group in this assessment and my conclusions were verified by an experienced clinical histopathologist (Professor Francesco Pezzella, University of Oxford).

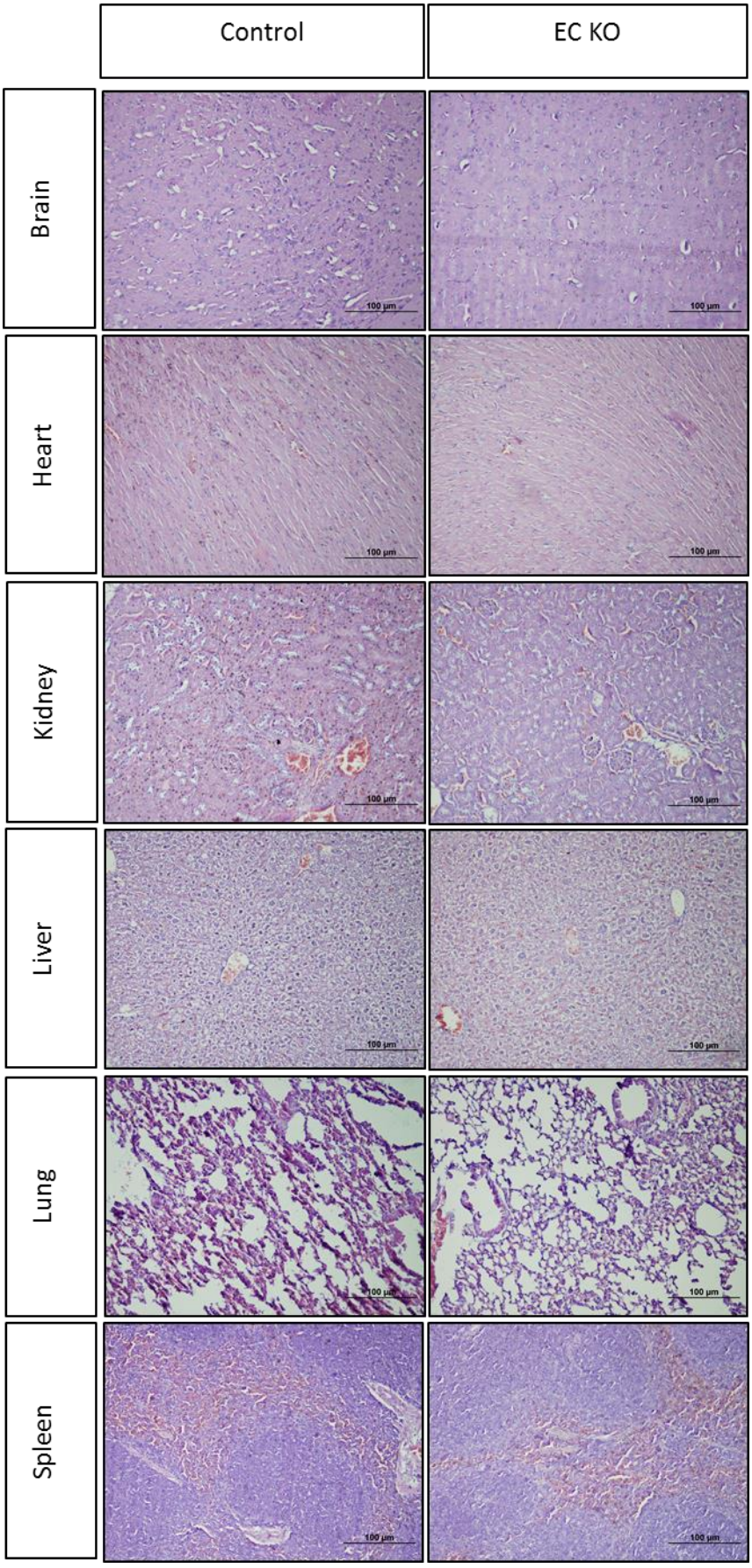
Control
EC KO
Brain
Heart
Kidney
Liver
Lung
Spleen
100 µm

Figure 3.12: Histological analysis of vital organs between constitutive endothelial cell-specific *Eltd1* knockout and littermate control mice. H&E staining showed no difference in architectural integrity of vital organs (brain, heart, lung, liver, kidney and spleen) between the two groups (n=3 male mice per group)(Scale bar: 100 μm).

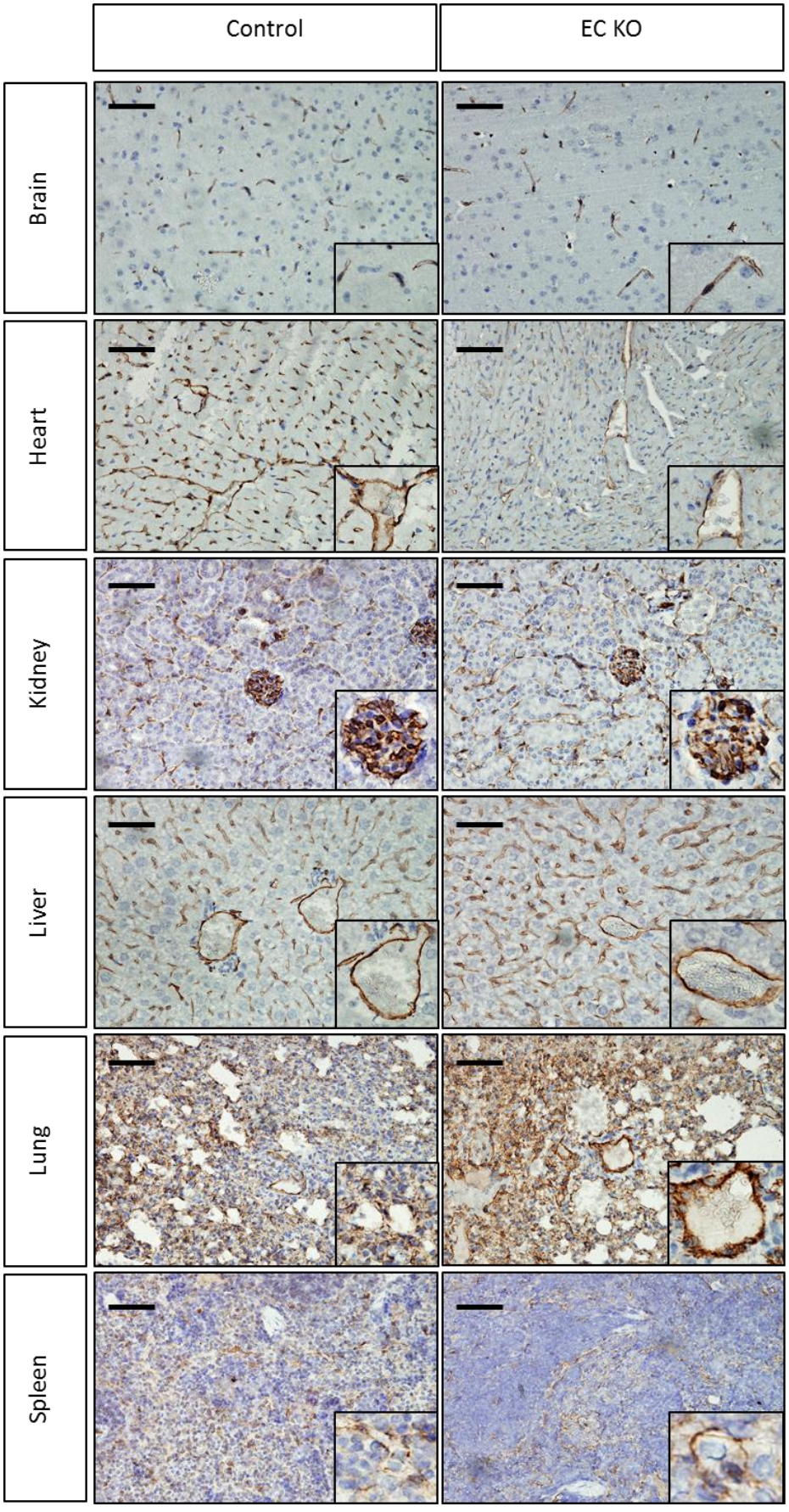
Control
EC KO
Brain
Heart
Kidney
Liver
Lung
Spleen

Figure 3.13: Immunohistochemical (CD31) analysis of vessels in vital organs (brain, heart, lung, liver, kidney and spleen) between constitutive endothelial cell-specific *Eltd1* knockout and littermate control mice. CD31 staining of vital organs showed no difference in vessel morphology or the vessel density of vital organs between the two groups (n=3 male mice per group) (Scale bar = 20 μm).

3.9 No significant difference in endothelial cell sprouting was observed in *ex vivo* cultured aortic rings isolated from constitutive endothelial cell-specific *Eltd1* knockout mice compared to those of littermate controls

Eltd1 has an established role in physiological angiogenesis and it was important to determine whether the endothelial cells lacking Eltd1 might exhibit functional differences. An *ex vivo* model was adopted which better capitulates the *in vivo* setting, such as the interactions of different cell types as compared to *in vitro* assays, and this is less complex than *in vivo* assays. Furthermore, in the endothelial cell-specific *Eltd1* knockout model, we decided to adopt an *ex vivo* assay in which vascular cells predominate so as to specifically investigate the endothelial-*Eltd1* contribution to the phenotype. Based on these considerations, the aortic ring assay for endothelial cell sprouting activity was chosen.

In this assay slices of the aorta (rings) were layered between Matrigel and subsequent endothelial sprouting was quantified. The assay was performed three times and no significant change in the area of vessel outgrowth in the constitutive endothelial cell-specific *Eltd1* knockout aortic rings was observed when compared to those of the littermate control group (Figure 3.14).

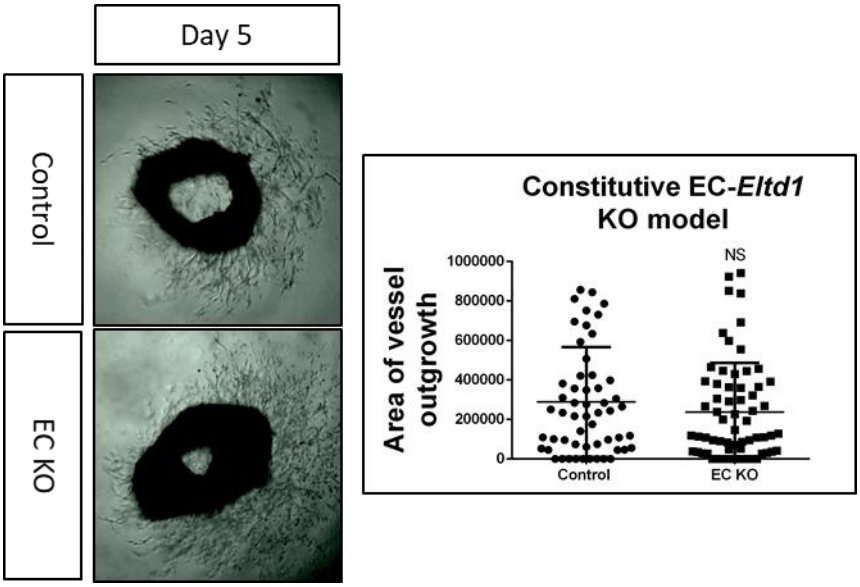

Figure 3.14: *Ex vivo* aortic ring assays. There was no significant difference (unpaired Student's *t* test) in the area of vessel outgrowth at day 5 between constitutive endothelial cell-specific *Eltd1* knockout and littermate control mice. n=3, 3 mice were used in each group, 5 rings per aorta.

3.10 Syngeneic tumour models

3.10.1 Introduction

We next studied *in vivo* tumour growth in this model. The genetically modified C57BL/6 mice generated in the study were immunocompetent and thus syngeneic tumour cell lines had to be used to avoid tissue rejection by the immune system. In this investigation, two cell lines were used, E0771 is a medullary breast adenocarcinoma cell and MC38 is derived from a C57BL/6 murine colon adenocarcinoma. Different models were chosen to avoid model-dependent observations and to compare different cancer types.

3.10.2 Syngeneic E0771 tumour model

3.10.2.1 Experimental design

In this study, five age-matched 5-6 week old female mice per group (*Eltd1*$^{fl/fl}$*;Tie2-Cre*$^{+/-}$ and *Eltd1*$^{fl/fl}$*;Tie2-Cre*$^{-/-}$) were used. 5 x 10^5 tumour cells resuspended in Matrigel were injected subcutaneously into the back of the mice (Figure 3.15) and tumour growth was recorded every two days. Tumours were harvested at individual endpoints when each tumour had reached a gross median dimension (GMD = $(LxBxH)^{1/3}$) of 10 mm. These conditions were chosen based on a pilot study done using E0771 in which we found that subcutaneous injection of E0771 tumours showed a higher frequency of engraftment and grew better than orthotopic tumours inoculated into the mammary fat pad and tumours harvested at GMD 10 mm showed less ulceration and necrosis within the tumours compared to larger GMD. This facilitated the immunohistochemical analyses of the tumours.

Figure 3.15: Schematic diagram of subcutaneous tumour inoculation in mice. Tumour cells, suspended in Matrigel or PBS, were inoculated on the left flank at the back of the mice.

3.10.2.2 No significant difference was observed in tumour growth curves and animal survival between constitutive endothelial cell-specific *Eltd1* knockout and littermate control groups

The experiment was carried out until all the tumours had reached the end point GMD of 10 mm which was 42 days. However, there was no significant difference in tumour growth curves and survival outcome of tumour-bearing constitutive endothelial cell-specific *Eltd1* knockout mice as compared to the littermate controls (Figure 3.16). Average tumour volume was analysed until day 14 when the first mouse was culled due to tumour volume reaching the GMD of 10 mm, which reduced the group size.

A

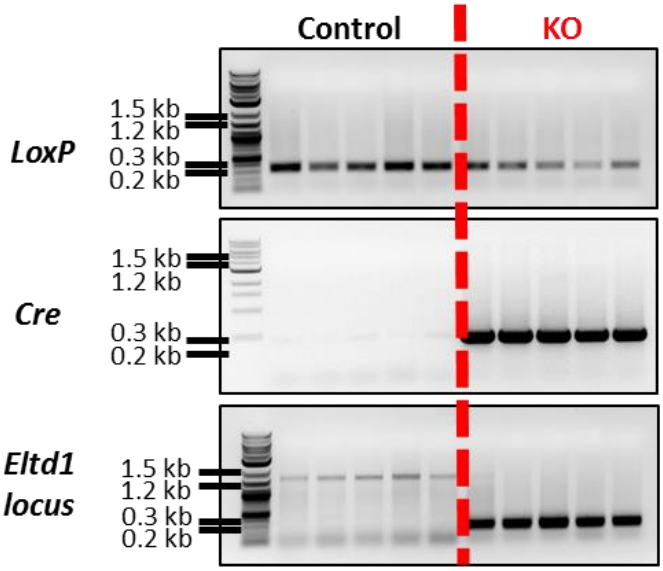
Control
KO
LoxP
1.5 kb
1.2 kb
0.3 kb
0.2 kb
Cre
1.5 kb
1.2 kb
0.3 kb
0.2 kb
Eltd1
locus
1.5 kb
1.2 kb
0.3 kb
0.2 kb

B

i

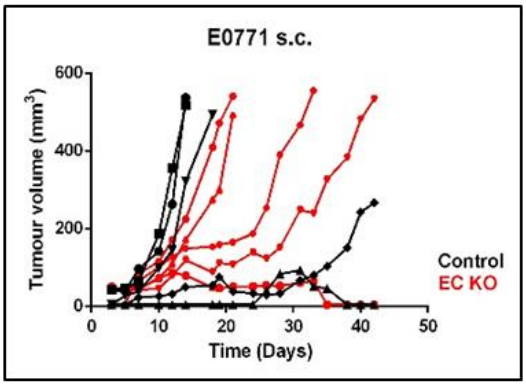
E0771 s.c.
Tumour volume (mm3)
600
400
200
0
0
10
20
30
40
50
Time (Days)
Control
EC KO

ii

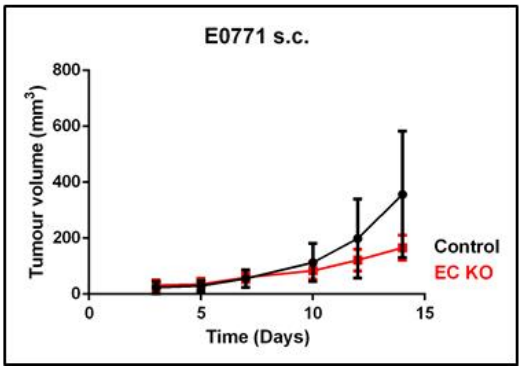
E0771 s.c.
Tumour volume (mm3)
800
600
400
200
0
0
5
10
15
Time (Days)
Control
EC KO

iii

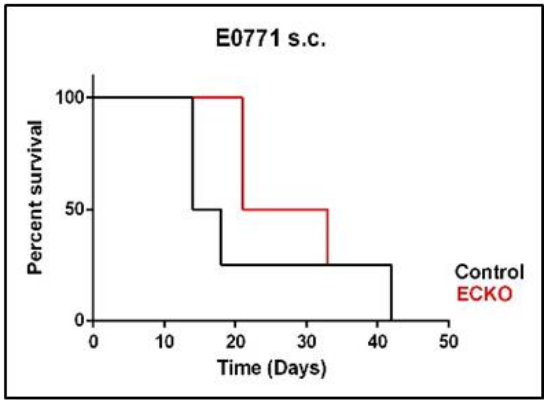
E0771 s.c.
Percent survival
100
50
0
0
10
20
30
40
50
Time (Days)
Control
ECKO

Figure 3.16: Analysis of E0771 syngeneic tumour model. A) Genotyping PCR of experimental mice B) Tumour growth curves (i. raw data; ii. average tumour volume at day 14; iii. Survival plot) showed no significant difference in tumour growth and survival between constitutive endothelial cell-specific *Eltd1* knockout and littermate control mice (n=5 female mice were used in each group). However, one mouse in each group did not take up the tumour successfully and these were excluded in the analysis.

3.10.2.3 Constitutive endothelial cell-specific *Eltd1* knockout tumours had reduced microvessel density and pericyte coverage, increased hypoxia and a trend towards necrosis but there was no change in tumour proliferation.

In this analysis, only four tumours per group were used, as two mice (one per group) did not take up the tumour successfully. Despite that there being no significant change in tumour growth curves and survival outcome in the endothelial cell-specific *Eltd1* knockout mice, interestingly, there was a significant increase in hypoxia (CA9) (fold change = 1.5, unpaired Student's *t* test: $p = 0.028$), with a trend towards increased necrosis in the knockout group (Figure 3.17). Microvessel density (CD31) (fold change= -0.38, unpaired Student's *t* test: $p = 0.022$), and pericyte coverage (CD31/αSMA) (fold change= -0.28, unpaired Student's *t* test: $p = 0.0024$), was significantly reduced in the knockout group (Figure 3.18). Eltd1 depletion was validated in the tumours by IHC using in-house rabbit polyclonal antibodies against murine Eltd1 (F01: fold change = -1.00, unpaired Student's *t* test: F01: $p \leq 0.001$; F04: fold change = -1.00, unpaired Student's *t* test: F04: $p \leq 0.01$) (Figure 3.18). Interestingly, there was a larger reduction in $Eltd1^+$ vessels than $CD31^+$ vessels, which would suggest that the remaining vessels lacked Eltd1. Ki67 analysis was performed on the tumour rather than vasculature and was not significantly different in the endothelial cell-specific *Eltd1* knockout tumours.

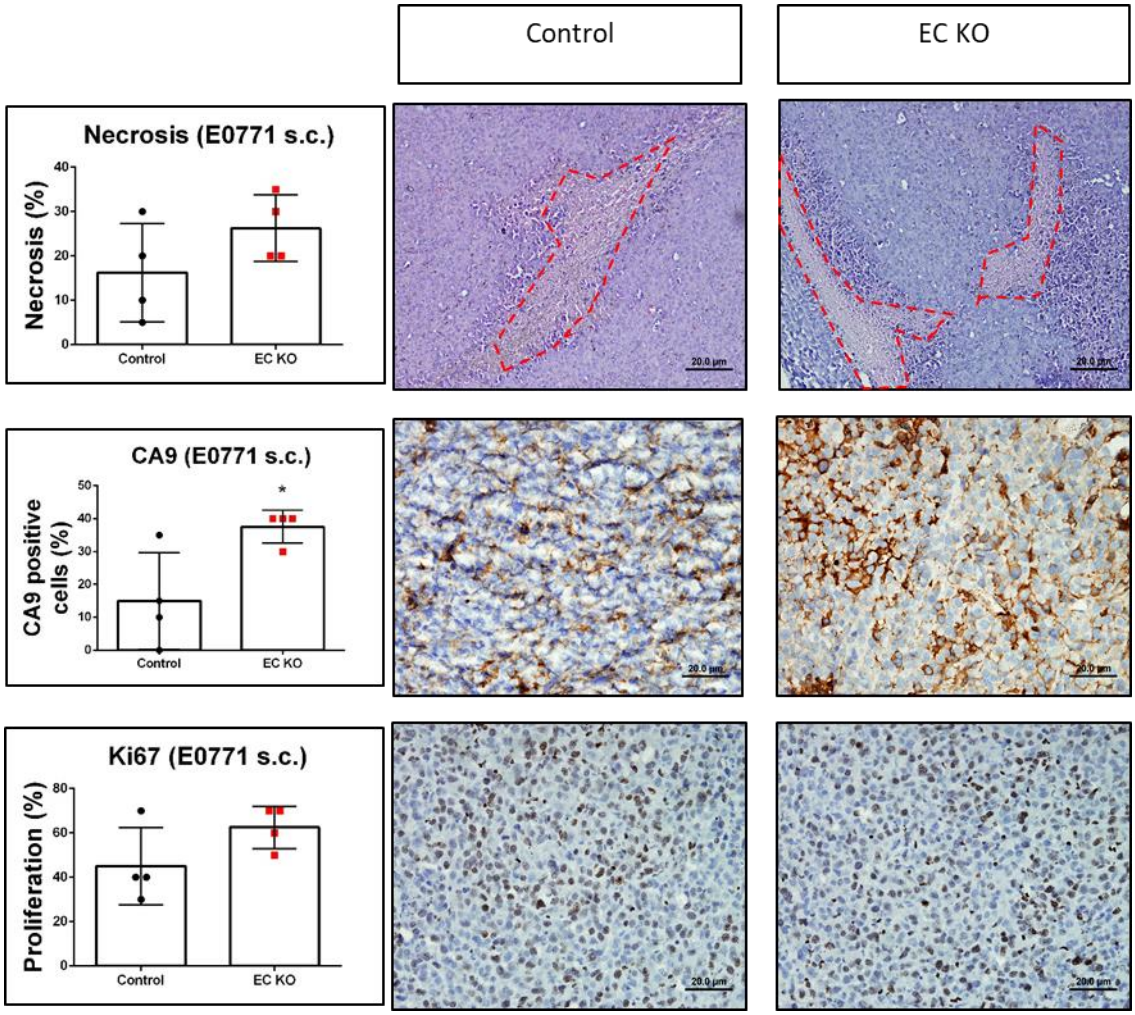

Figure 3.17: Immunohistochemical analyses of necrosis, hypoxia and proliferation in the E0771 syngeneic tumour model. Immunohistochemical analysis showed a significant increase in CA9 (fold change = 1.5, unpaired Student's *t* test: $p = 0.028$), a trend towards increased necrosis and no change in proliferation in the tumours of constitutive endothelial cell-specific *Eltd1* knockout compared to those of littermate control mice. Four tumours per group were used in the analysis (Scale bar: 20 µm). Data represented as mean ± SD (*=$p < 0.05$).

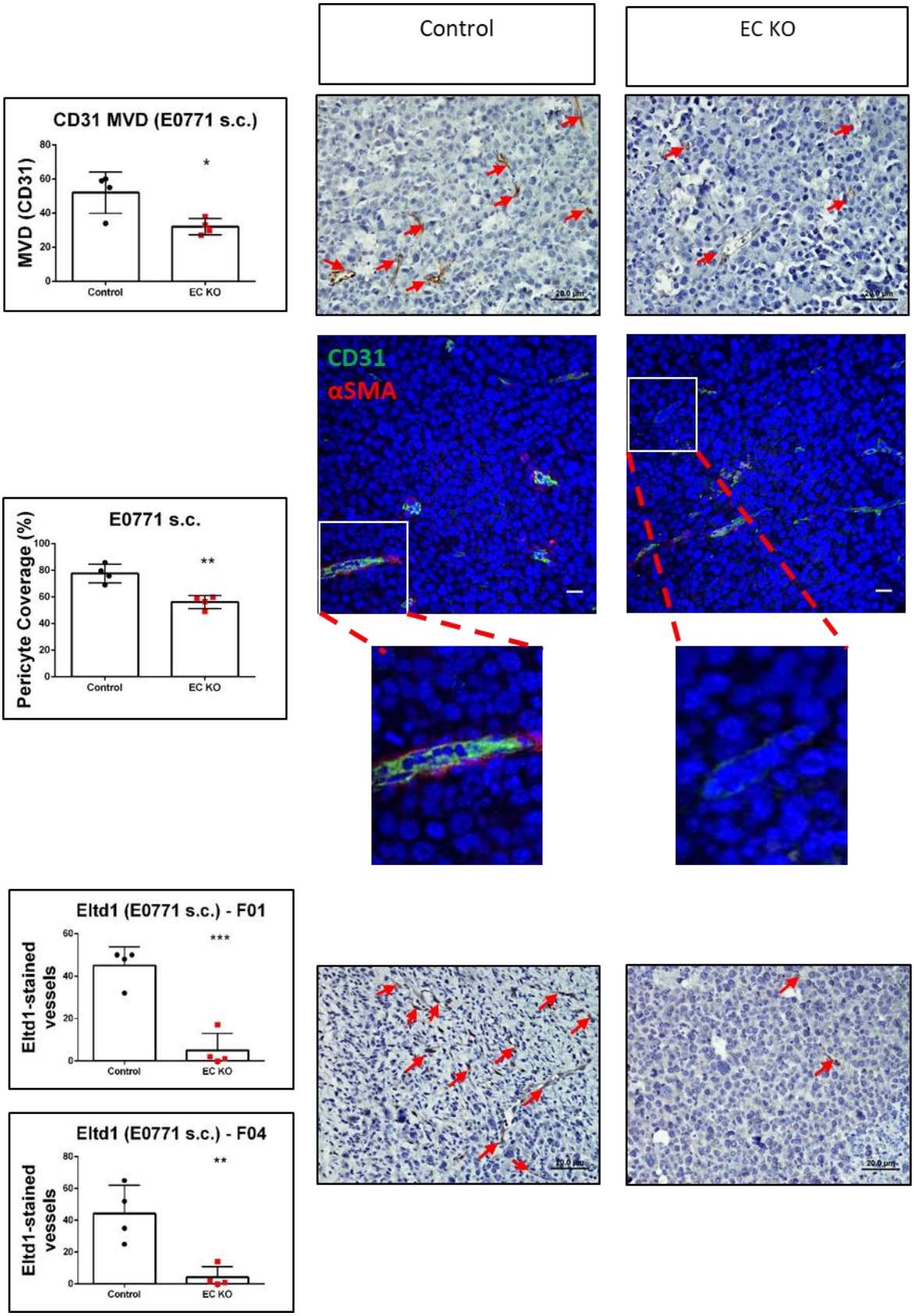
Control
EC KO
CD31 MVD (E0771 s.c.)
MVD (CD31)
80
60
40
20
0
*
Control
EC KO
CD31
αSMA
E0771 s.c.
Pericyte Coverage (%)
100
80
60
40
20
0
**
Control
EC KO
Eltd1 (E0771 s.c.) - F01
Eltd1-stained vessels
60
40
20
0
***
Control
EC KO
Eltd1 (E0771 s.c.) - F04
Eltd1-stained vessels
80
60
40
20
0
**
Control
EC KO

Figure 3.18: Immunohistochemical analysis of vasculature in E0771 syngeneic tumour model. Immunohistochemical analysis showed a significant reduction in microvessel density (CD31) (fold change= -0.38, unpaired Student's *t* test: p = 0.022), pericyte coverage (CD31/αSMA) (fold change= -0.28, unpaired Student's *t* test: p = 0.0024) and Eltd1 (F01: fold change = -1.00, unpaired Student's *t* test: F01: $p \leq 0.001$; F04: fold change = -1.00,unpaired Student's *t* test: F04: $p \leq 0.01$) in the tumours of inducible endothelial cell-specific *Eltd1* knockout compared to those from littermate control mice. Four tumours per group (Control and EC KO) were used in the analysis (Scale bar: 20 µm). Data represented as mean ± SD (*=$p < 0.05$; **=$p \leq 0.01$; ***=$p \leq 0.001$). F01 and F04 are in-house polyclonal antibodies targeting Eltd1.

3.10.3 Syngeneic MC38 tumour model

3.10.3.1 Experimental design

In this study, 10 age-matched 8 week old mice (5 males and 5 females) per group (*Eltd1*$^{fl/fl}$*;Tie2-Cre*$^{+/-}$ and *Eltd1*$^{fl/fl}$*;Tie2-Cre*$^{-/-}$) were used to study growth of the syngeneic MC38 tumour model. 1 x 10^6 cells resuspended in PBS and were used as described above.

It has been reported that the syngeneic MC38 model can be used in both male and female mice (Zigmond et al., 2011, Lau et al., 2017). We wanted to assess if gender plays a role in tumour growth between the control and endothelial cell-specific *Eltd1* knockout mice, so that all the offspring could be used in future animal studies that utilise MC38 cells.

3.10.3.2 No significant difference was observed between constitutive endothelial cell-specific *Eltd1* knockout and littermate control groups in male and female mice

As shown in Figure 3.19, there was no significant difference in tumour growth between constitutive endothelial cell-specific *Eltd1* knockout and littermate control groups in both sexes. Hence, the tumour growth and histology data of both males and females could be combined in the analysis.

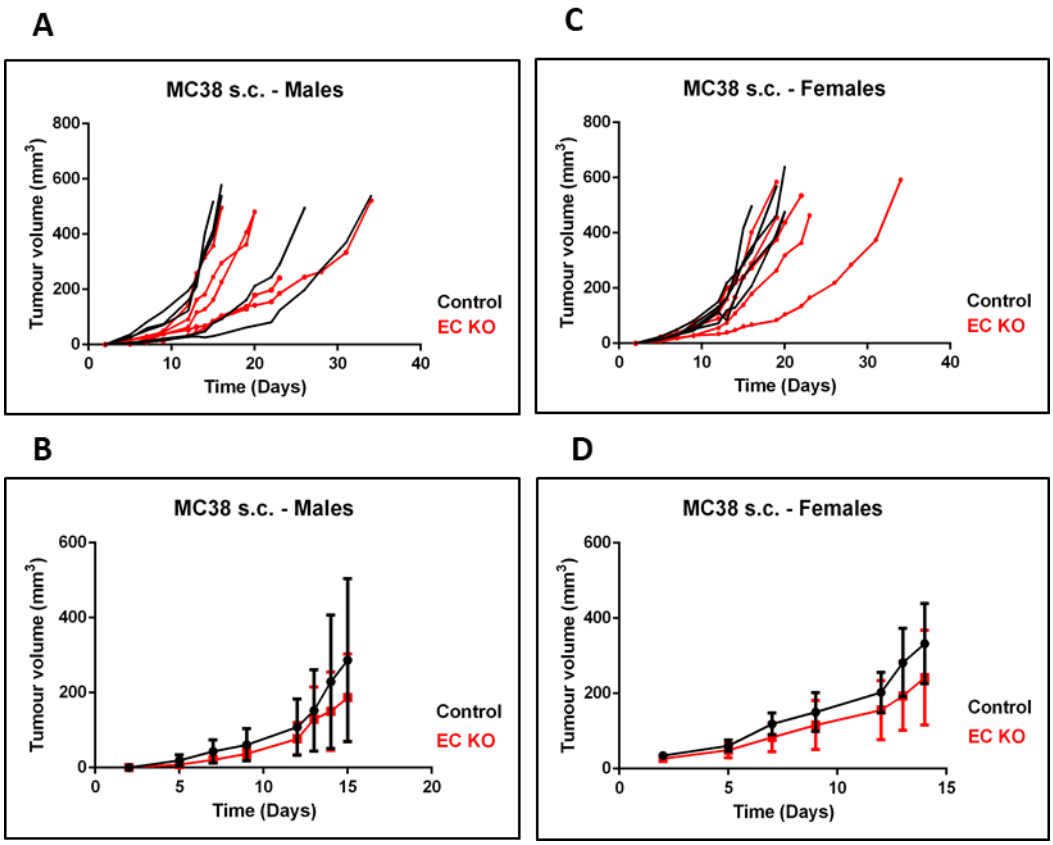

Figure 3.19: Comparison of gender effects on MC38 tumour growth curves in endothelial cell-specific *Eltd1* knockout and littermate control groups. There were no significant differences in MC38 tumour growth between male and female mice (both in control and knockout), hence there was no gender effect on MC38 tumour growth.

3.10.3.3 No significant difference was observed in tumour growth curves and survival plot between constitutive endothelial cell-specific Eltd1 knockout and littermate control groups

The experiment was carried out till the tumours reached the end point GMD of 10 mm, which lasted 34 days. However, there was no significant difference in the growth curves and survival of constitutive endothelial cell-specific *Eltd1* knockout tumours as compared to those of littermate control as shown in Figure 3.20. Average tumour volume was plotted till day 15 when the first mouse was culled due to tumour volume reaching the endpoint size of 10 mm.

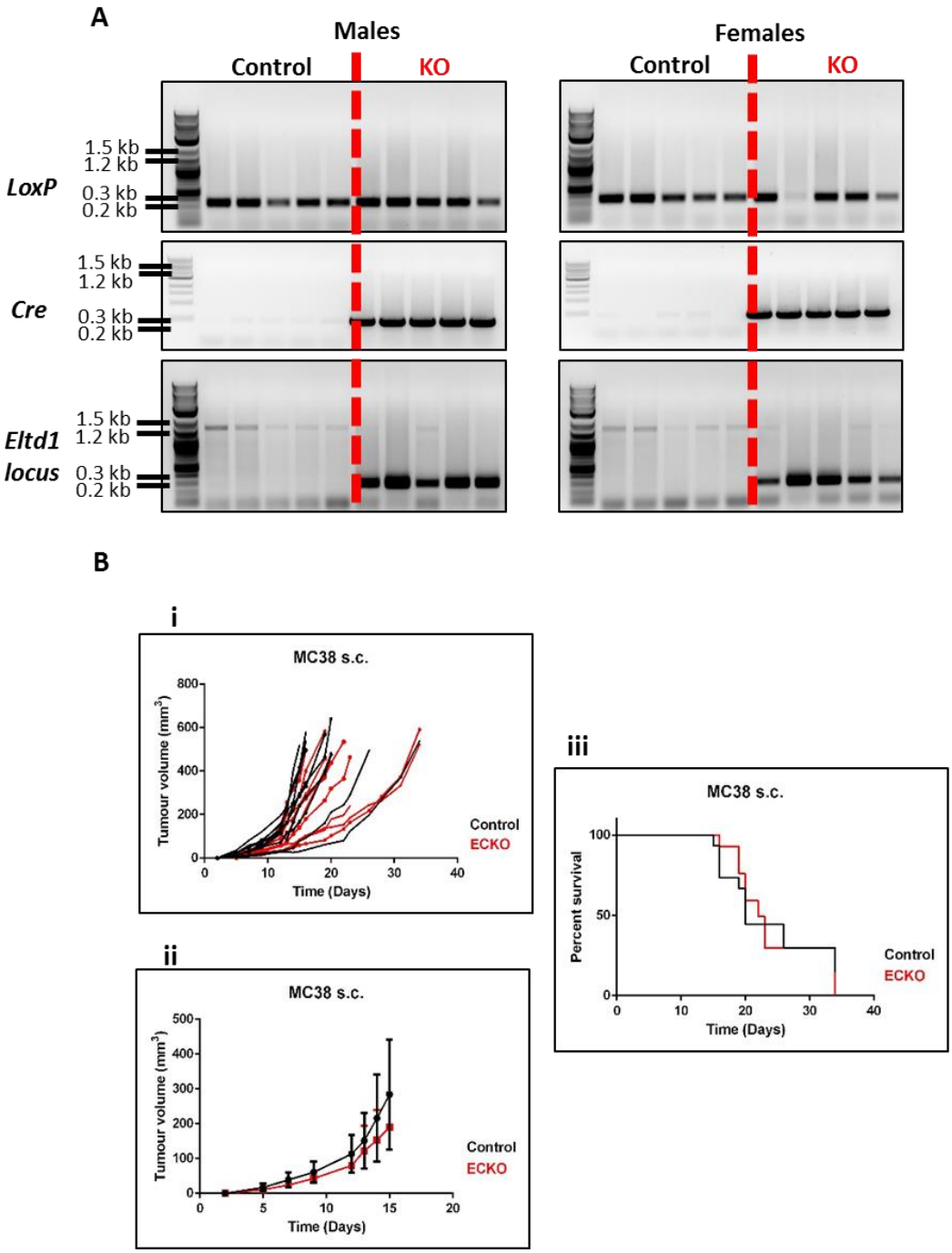

Figure 3.20: Analysis of MC38 syngeneic tumour model. A) Genotyping PCR of experimental mice B) Tumour growth curves (i. raw data; ii. average tumour volume at day 15; iii. Survival plot) showed no significant difference in tumour growth and survival between constitutive endothelial cell-specific *Eltd1* knockout and littermate control mice. Ten mice (five males and five females) were used in each group.

3.10.3.4 Constitutive endothelial cell-specific *Eltd1* knockout tumours were more hypoxic and necrotic with lower microvessel density but there was no change in tumour proliferation

In this analysis, ten tumours per group were used. Despite no significant change in tumour growth curves, there were histological differences in the tumours with significantly higher necrosis (fold change= 2.22, unpaired Student's *t* test: $p = 0.0183$) and hypoxia (CA9)(fold change= 1.48, unpaired Student's *t* test: $p = 0.012$), as shown in Figure 3.21. Also, there was a significant reduction in microvessel density (CD31) (fold change= -0.55, unpaired Student's *t* test: $p \leq 0.001$) and pericyte coverage (CD31/ αSMA)(fold change= -0.39, unpaired Student's *t* test: $p = 0.0018$) in the endothelial cell-specific *Eltd1* knockout mice. The Eltd1 knockout was validated by significant reduction in murine Eltd1 staining in tumour endothelium (F01: fold change = -0.98, unpaired Student's *t* test: $p \leq 0.0001$; F04: fold change = -0.90, unpaired Student's *t* test: $p \leq 0.0001$), as shown in Figure 3.22. This finding was similar in trend as those in the E0771 tumour model and shows that constitutive endothelial cell-specific *Eltd1* depletion has an impact on the tumour microenvironment.

Similarly, to the E0771 model described in section 3.10.2.3, there was a larger reduction in $Eltd1^+$ vessels than $CD31^+$ vessels. Ki67 analysis was performed on the tumour rather than its vasculature and was not significantly different in the endothelial cell-specific *Eltd1* knockout tumours.

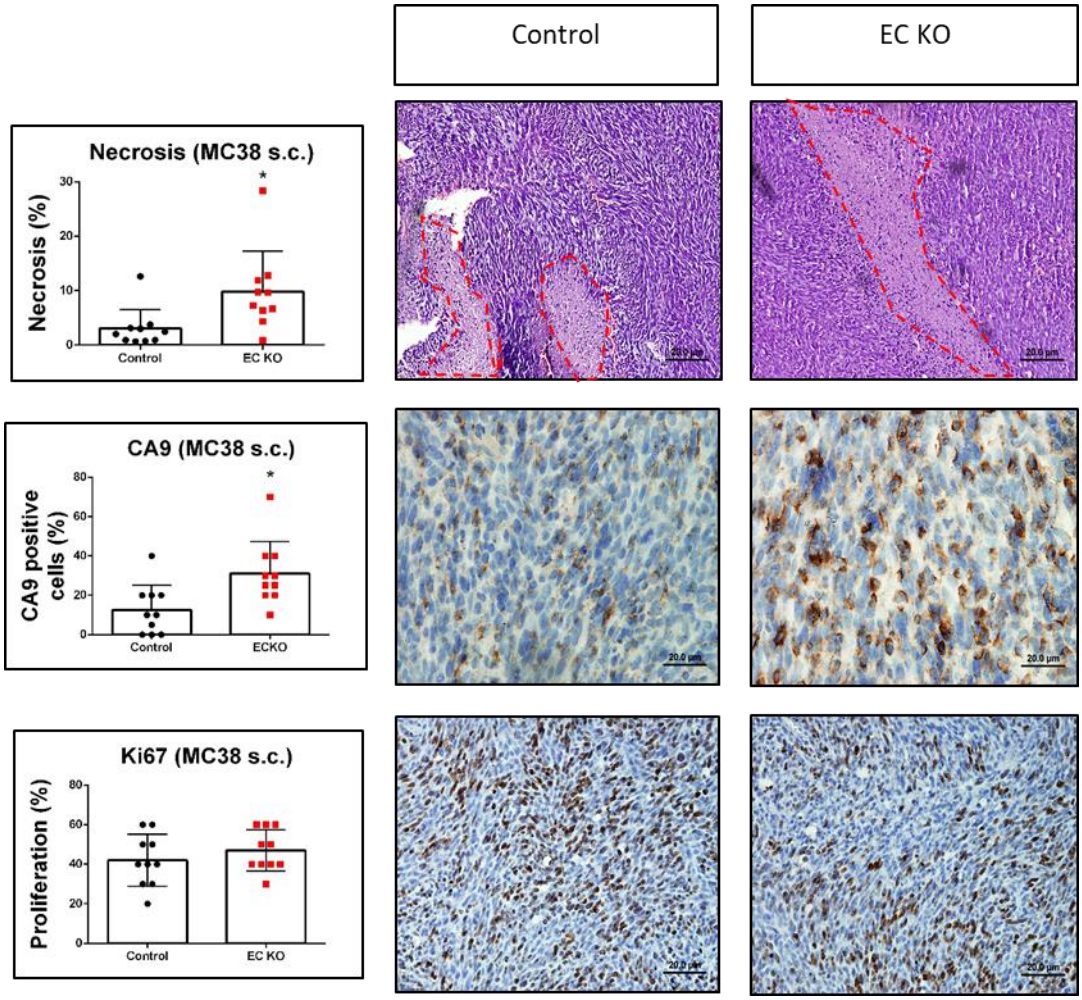

Figure 3.21: Immunohistochemical analyses of necrosis, hypoxia and proliferation in the MC38 syngeneic tumour model. Immunohistochemical analysis showed a significant increase in hypoxia (CA9) (fold change= 1.48, unpaired Student's *t* test: $p = 0.012$) and necrosis (H&E) (fold change= 2.22, unpaired Student's *t* test: $p = 0.0183$) in the tumours of constitutive endothelial cell-specific *Eltd1* knockout compared to those of littermate control mice. Ki67 analysis was done on tumour and did not show significant difference in the endothelial cell-specific *Eltd1* knockout tumours. 10 tumours in each group were used in the analysis (Scale bar: 20 µm). Data represented as mean ± SD (*=$p \leq 0.05$).

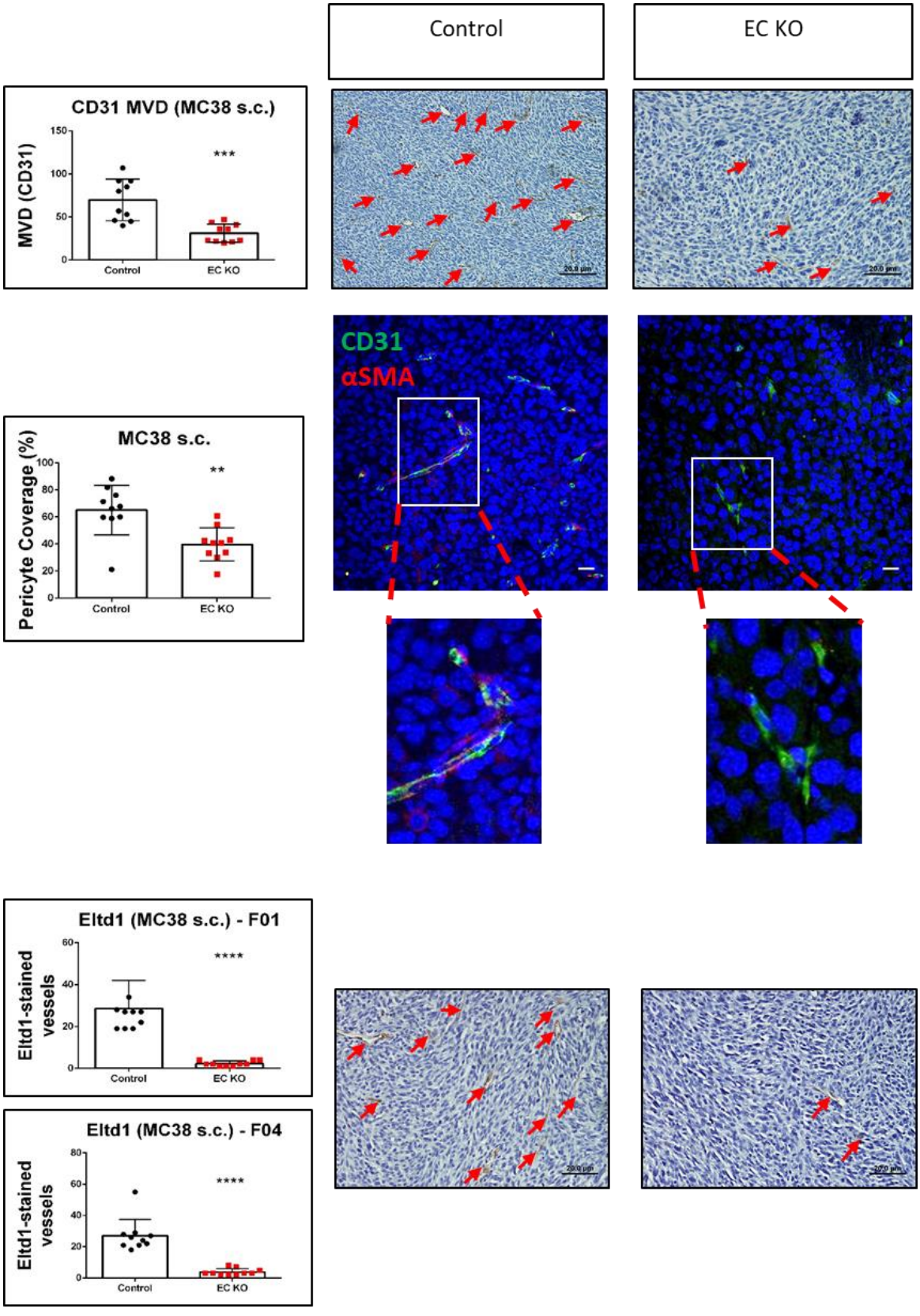
Control
EC KO
CD31 MVD (MC38 s.c.)
MVD (CD31)
150
100
50
0
***
Control
EC KO
CD31
αSMA
MC38 s.c.
Pericyte Coverage (%)
100
80
60
40
20
0
**
Control
EC KO
Eltd1 (MC38 s.c.) - F01
Eltd1-stained vessels
60
40
20
0
****
Control
EC KO
Eltd1 (MC38 s.c.) - F04
Eltd1-stained vessels
80
60
40
20
0
****
Control
EC KO

Figure 3.22: Immunohistochemical analysis of vasculature in MC38 syngeneic tumour model. Immunohistochemistry analysis showed a significant reduction in microvessel density (CD31) (fold change= -0.55, unpaired Student's *t* test: $p \leq 0.001$), pericyte coverage (CD31/αSMA) (fold change= -0.39, unpaired Student's *t* test: $p = 0.0018$) and Eltd1 (F01: fold change = -0.98, unpaired Student's *t* test: $p \leq 0.0001$; F04: fold change = -0.90, unpaired Student's *t* test: $p \leq 0.0001$) in the tumours of constitutive endothelial cell-specific *Eltd1* knockout group compared to those of littermate control. 10 tumours in each group were used in the analysis (Scale bar: 20 µm). Data represented as mean ± SD (**=$p \leq 0.01$; ***=$p \leq 0.001$; ***=$p \leq 0.0001$). F01 and F04 are in-house polyclonal antibodies targeting Eltd1.

3.11 Discussion

In this study, a constitutive endothelial cell-specific *Eltd1* knockout model was generated and validated. It was observed that both kidneys and lung had varying degrees of reduction in the expression of transcripts containing *Eltd1* exons 4 and 5. As the constitutive knockout model was generated using *Tie2-Cre* mouse, the difference in *Eltd1* reduction in kidneys and lung may be attributed to the endothelium of the organs comprising of different proportion of $Tie2^{+}$ endothelial cells.

To date, there were two published reports on genetic *Eltd1* knockout mice (Lu et al., 2017, Xiao et al., 2012). In the report by Xiao *et al*, the total *Eltd1* knockout strategy adopted was constitutive and retained the entire extracellular domain of Eltd1 which could have functional activity and mask the phenotype of *Eltd1* knockout in mice. However, the emphasis of the study was on cardiac hypertrophy and there was no report on the vasculature. In 2017, Lu *et al* reported no significant differences observed in cardiovascular or kidney function in a constitutive endothelial cell-specific *Eltd1* knockout model using a strategy which deleted exon 5 (Lu et al., 2017). In this report, the focus was on developmental vascular remodelling and postnatal kidney function. In short, both studies focused on a different disease model compared to the work performed in this thesis.

In our model, constitutive endothelial cell-specific *Eltd1* depletion did not cause any defects in vasculature or architectural integrity of the vital organs (brain, heart, lung, kidney, liver and spleen) and no apparent change in body weight and no sign of distress were seen in the knockout mice as compared to the littermate control. These observations were in line with published reports on total and endothelial cell-specific *Eltd1* knockout models (Xiao et al., 2012; Lu et al., 2017).

Furthermore, the *ex vivo* aortic ring assay did not show any significant difference in the area of vessel outgrowth in the endothelial cell-specific *Eltd1* knockout aortas as compared to those from control mice.

It was previously reported that the loss of *Eltd1* resulted in augmented cardiac hypertrophy under cardiac overload but under normal conditions, total *Eltd1* knockout mice developed normally and the *Eltd1* knockout hearts did not display any difference in size and histology as compared to those of the littermate control (Xiao et al., 2012). This suggested that the

functional activity of Eltd1 could be observed more significantly under certain pathological conditions such as aortic banding and tumour contexts in which there is an element of mechanical stress or matrix stiffness in the tumour microenvironment. In the future it could be worth performing the aortic ring assays in different matrices such as fibronectin and type IV collagen to assess the potential of Eltd1 depletion to affect aortic sprouting in matrices of different stiffness. Under normal physiological conditions, *Eltd1* depletion does not cause any defect, which makes it a good therapeutic target in terms of lack of toxicity in normal tissues.

Aortic banding experiment was not performed using the constitutive endothelial cell-specific *Eltd1* knockout model as the phenotype observed in (Xiao et al., 2012) might be due to Eltd1-expressing cardiomyocytes and may not be mediated by endothelial cells. But it could be considered in the future to investigate the contribution of endothelial-Eltd1 to the cardiac hypertrophy phenotype seen in the report.

Both syngeneic E0771 and MC38 tumour models showed no significant differences in tumour growth curves or survival outcome with endothelial-*Eltd1* depletion. But there were significant histological differences in both the endothelial cell-specific *Eltd1* knockout tumours, higher necrosis and hypoxia as indicated by CA9, and significant reduction in microvessel density (CD31) and pericyte coverage (CD31/αSMA). The endothelial cell-specific *Eltd1* knockout tumours showed as expected significant reduction in Eltd1, by two in-house rabbit polyclonal antibodies, which suggested strongly that the histological phenotypes were due to the depletion of endothelial-*Eltd1*. Moreover, the larger reduction in $Eltd1^+$ vessels compared to $CD31^+$ vessel suggested that the remaining vessels were $Eltd1^-$. The similar immunohistochemical results in both models showed concordance and the effect of *in vivo* endothelial-Eltd1 depletion on tumour histology was not sex or tumour type-dependent.

There are several reasons why significant histological differences might not have any effects on the overall growth of the tumours in endothelial cell-specific-*Eltd1* depleted mice

Firstly, E0771 and MC38 cell lines are highly proliferative and *in vivo*, these tumours reached endpoint of GMD 10 mm in 21-28 days post tumour cell injection. With the tumour cells proliferating and expanding, the reduction in microvessel density might not be sufficient to cause a delay in tumour growth. With lower microvessel density, the tumours were less

perfused and were more hypoxic which led to higher necrosis. It will be of future interest to analyse tumours at earlier stages.

Secondly, the constitutive knockout model has its limitations. Having a gene knocked out during early developmental stages could lead to functional compensation by other genes as seen by the expansion of this receptor family in higher vertebrates through evolution (Kwakkenbos et al., 2004). This might mask or diminish the phenotype of the knockout. Importantly the published reports on *Eltd1* knockout models also adopted constitutive knockout models. Also, in the previous study conducted by Masiero *et al* (2013), *Eltd1* silencing via the delivery of chitosan nanoparticles containing siRNA reduced tumour growths and improved survival outcome in xenograft models using immunocompromised mice. *Eltd1*-silenced tumours had similar histological differences compared to the constitutive endothelial-*Eltd1* depleted tumours, such as increased hypoxia and necrosis and reduced microvessel density. Despite similar histological observations, constitutive endothelial-*Eltd1* depleted tumours did not show significant difference in growth or survival outcome. This could be due to the immune status of the host or the effects of constitutive deletion suggesting possible functional compensation. In addition, it is important to note that Eltd1 is upregulated in tumour-associated endothelial cells which was targeted by the siRNA that was given to the established tumours. However, in the constitutive knockout model, there was no opportunity for endogenous *Eltd1* upregulation in the tumour-associated endothelial cells. This opened up a new question of whether the therapeutic effects of *Eltd1*-targeting could only be observed when upregulated *Eltd1* was targeted.

The reduction in the pericyte coverage of existing vessels in the tumours suggested that the vessels in the tumours might be immature and could be leaky. The follow up study on this would be to investigate into the functionality of the vessels by analysing the tomato lectin stains using the confocal microscope. If the tumour vessels were functional, they would be perfused with blood and thus positively stained with tomato lectin introduced into the tail vein.

Interestingly, though constitutive endothelial-*Eltd1* depletion led to a reduction in vessels and pericyte coverage of the remaining vessels in the tumours but there were no functional vascular sprouting changes in the aortic ring assay. There could be several possibilities. Firstly, tumour endothelial cells have different biology as compared to aortic endothelial cells.

Secondly, there could be different angiogenic processes that affect vessels or tumour microenvironment compared to normal tissues.

Considering the clinical relevance of the inducible knockout model as well as circumventing the potential issue of functional compensational in this constitutive knockout model, it could be worth generating the inducible endothelial cell-specific *Eltd1* knockout model and perform the same *ex vivo* and *in vivo* assays on these mice.

3.12 Conclusion

Constitutive endothelial-*Eltd1* depletion in mice does not cause defects under normal physiological conditions. In the tumour models, constitutive endothelial loss of *Eltd1* results in significant differences in histology with lower microvessel density and pericyte coverage, higher hypoxia and necrosis despite no significant change in tumour growth and survival outcomes.

Chapter 4: Investigation into the *in vivo* effects of acute endothelial-*Eltd1* depletion

4.1 Introduction

Data presented in chapter 3 indicated that constitutive endothelial cell-specific *Eltd1* depletion did not cause apparent physiological defects or significant differences in syngeneic tumour growth curves and survival plots. Interestingly, tumours from constitutive endothelial cell-specific *Eltd1* knockout mice were histologically different when compared to those from $Cre^{-/-}$ littermate control. However, constitutive knockout models have their disadvantages. It has been reported (El-brolosy et al., 2017) that knocking out certain genes constitutively could result in the differential expression of other genes, which could then potentially functionally compensate for the deleted target genes. This eventually masks the phenotype initially caused by the loss of the target gene. Furthermore, a constitutive knockout model does not reflect the induced inhibition of a target when exploring targets for therapy in the clinic.

To have a more clinically relevant model and to further examine the possibility of functional compensation in the constitutive endothelial-*Eltd1* knockout model, an inducible endothelial-*Eltd1* knockout model was developed using the *PdgfbiCreER*^{T2} strain, a tamoxifen-inducible endothelial cell-specific cre line (Claxton et al., 2008).This would enable the investigation into *in vivo* functions of *Eltd1* commences shortly after *Eltd1* deletion to prevent a large enough window for functional compensation to occur. This could perhaps allow us to observe more significant differences in various parameters both physiological and pathological. Furthermore, an inducible knockout model is more reflective on therapy as the induction of knockout with a drug can be initiated at any time of the experimentation.

At the time of experimentation, the *PdgfbiCreER*^{T2} strain was available in the University of Oxford, it was selected as the *Pdgfb* promoter is more specific to endothelial cells than the *Tie2* promoter. A collaboration was started with Professor Paul Riley (Department of Physiology, Anatomy and Genetics, University of Oxford) who had the *PdgfbiCreER*^{T2} strain, a tamoxifen-inducible endothelial cell-specific cre line (Claxton et al., 2008). It was planned to

conduct the same studies in the constitutive endothelial cell-specific *Eltd1* knockout mice, in chapter 3, on the inducible endothelial cell-specific *Eltd1* knockout mice.

4.2 Generation of tamoxifen-inducible endothelial cell-specific *Eltd1* knockout model using *Pdgfb-Cre* mice

4.2.1 Design of the *PdgfbiCreER^{T2}* strain

PdgfbiCreER^{T2} strain is the tamoxifen-inducible endothelial cell-specific cre line that was generated by the laboratory of Professor Frutigger (University College London, United Kingdom) and was given by our collaborator, Professor Paul Riley (University of Oxford, United Kingdom). In this strain, a sequence consisting of *iCreER^{T2}*, an *IRES* element, *EGFP* and an FRT-flanked chloramphenicol resistance cassette were recombined into the open reading frame of the *Pdgfb* gene in a phage artificial chromosome (PAC) in which the cassette was subsequently removed (Calxton et al., 2008), as shown in Figure 4.1. In this transgenic strain, all *Pdgfb*-expressing cells also express cre recombinase (*iCreER^{T2}*), the enzyme that catalyses the recombination of the *loxP* sites, and EGFP as a fluorescent reporter. The recombination event will only occur with tamoxifen administration. Tamoxifen binds to the iCreER^{T2} protein which is then translocated to the nucleus to catalyse the recombination of the *loxP* sites. In the absence of tamoxifen, the iCreER^{T2} protein remains sequestered by HSP90 in the cytoplasm.

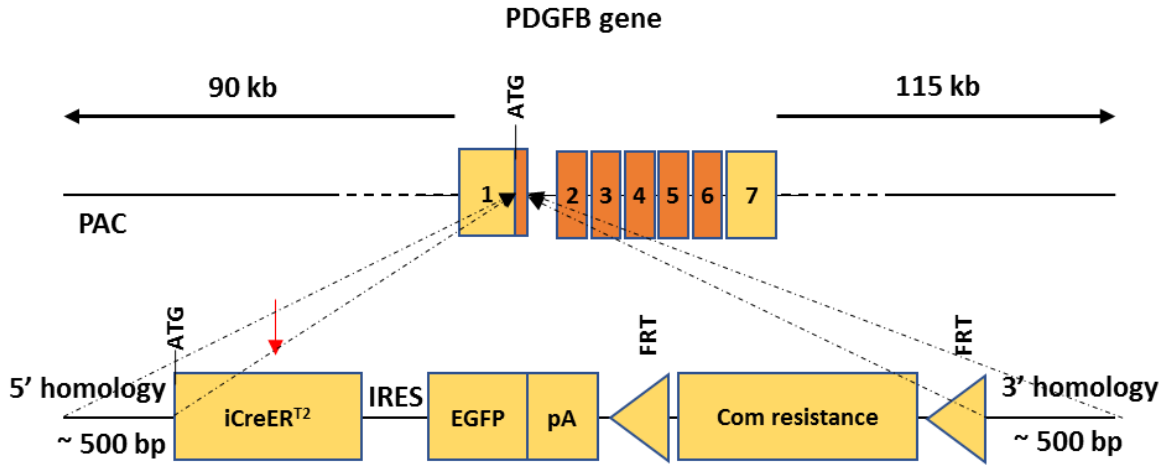

Figure 4.1: Structure of construct used in transgenesis in the development of the *PdgfbiCreERT2* strain. In this construct, a sequence comprising of *iCreER*^{T2} (red arrow), *IRES*, *EGFP* and an FRT-flanked chloramphenicol resistance cassette was recombined into the open reading frame of the *Pdgfb* gene in a PAC. After the chloramphenicol selection cassette was removed, the PAC was used for transgenesis via pronuclear injection in the development of the *PdgfbiCreER*^{T2} strain. Figure redrawn from Claxton et al (2008).

4.2.2 Breeding strategy to generate a tamoxifen-inducible endothelial cell-specific *Eltd1* knockout model

The breeding strategy to generate the inducible endothelial cell-specific *Eltd1* knockout mice is illustrated in Figure 4.2. Two crosses were required to yield the *Eltd1*$^{fl/fl}$*;Pdgfb-Cre*$^{+/-}$ mice and in each cross, hemizygous (*Pdgfb-Cre*$^{+/-}$) male mice were used to provide one copy of the *cre* recombinase.

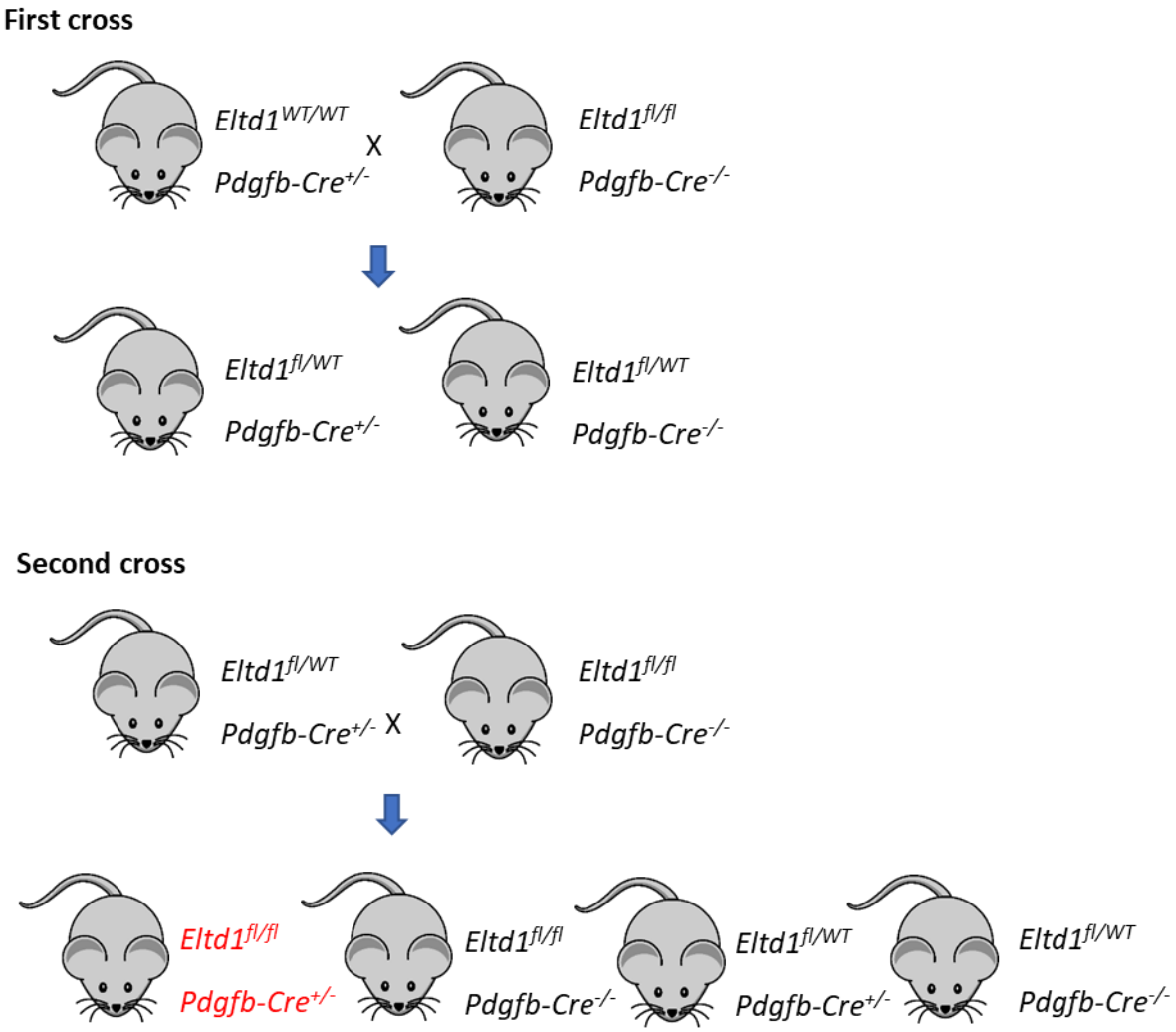

Figure 4.2: Schematic representation of the generation of *Eltd1*$^{fl/fl}$;*Pdgfb-Cre*$^{+/-}$ mice. This was achieved by breeding the inducible *Cre* onto the *Eltd1* floxed strain. Two crosses were required. In the first cross, mice heterozygous for both *Cre* and *Eltd1* floxed were generated and used for the second cross, in which these mice were crossed with mice homozygous for the *Eltd1* floxed allele to yield the *Eltd1*$^{fl/fl}$;*Pdgfb-Cre*$^{+/-}$ mice, as highlighted in red.

Once *Eltd1*$^{fl/fl}$;*Pdgfb-Cre*$^{+/-}$ mice had been generated, these were then used to generate the experimental mice. This strategy generated 50% of the mice with *Tie2-Cre* and *Eltd1* deletion, and 50% that lacked *Tie2-Cre* which were suitable littermate controls for subsequent experiments, as shown in Figure 4.3.

In this chapter, *Eltd1*$^{fl/fl}$*;Pdgfb-Cre*$^{-/-}$ mice are referred to as 'Control' while *Eltd1*$^{fl/fl}$*;Pdgfb-Cre*$^{+/-}$ mice (after tamoxifen induction) are named as 'EC KO'.

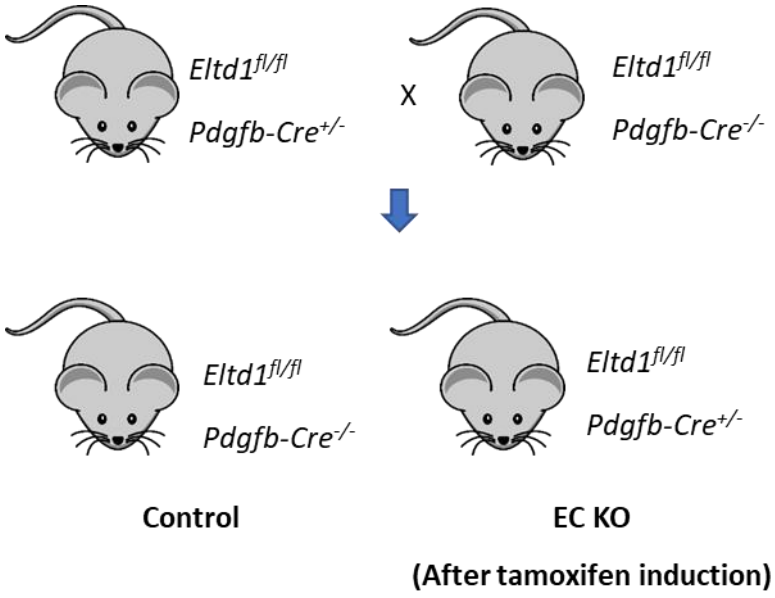

Figure 4.3: Schematic representation of the generation of the experimental mice (*Eltd1*$^{fl/fl}$*;Pdgfb-Cre*$^{-/-}$ and *Eltd1*$^{fl/fl}$*;Pdgfb-Cre*$^{+/-}$). In this breeding, we observed the expected ratio of progeny, 50% of the litter were *Eltd1*$^{fl/fl}$*;Pdgfb-Cre*$^{-/-}$ and 50% were *Eltd1*$^{fl/fl}$*;Pdgfb-Cre*$^{+/-}$. These mice were then all given intraperitoneal injection of tamoxifen to induce the *Eltd1* deletion in the EC KO group prior to downstream functional experiments.

4.2.3 Detection of the EGFP signal in *Eltd1*$^{fl/fl}$*;Pdgfb-Cre*$^{+/-}$ mice

EGFP could be used as a reporter to identify *Cre*$^{+/-}$ *Eltd1* knockout cells (after *in vivo* tamoxifen induction) isolated from the *Eltd1*$^{fl/fl}$*;Pdgfb-Cre*$^{+/-}$ mice. An experiment was initially conducted to confirm detection of the EGFP signal in the *Eltd1*$^{fl/fl}$*;Pdgfb-Cre*$^{+/-}$ mice (without tamoxifen induction). The lungs and aortas of both *Eltd1*$^{fl/fl}$*;Pdgfb-Cre*$^{-/-}$ and *Eltd1*$^{fl/fl}$*;Pdgfb-Cre*$^{+/-}$ mice were harvested and unpurified endothelial cell suspensions were prepared from the tissues. The samples were then analysed by flow cytometry and the endothelial cell suspensions

isolated from *Cre*$^{+/-}$ mice were shown to be positive for EGFP as compared to those of the *Cre*$^{-/-}$ littermate control as shown in Figure 4.4.

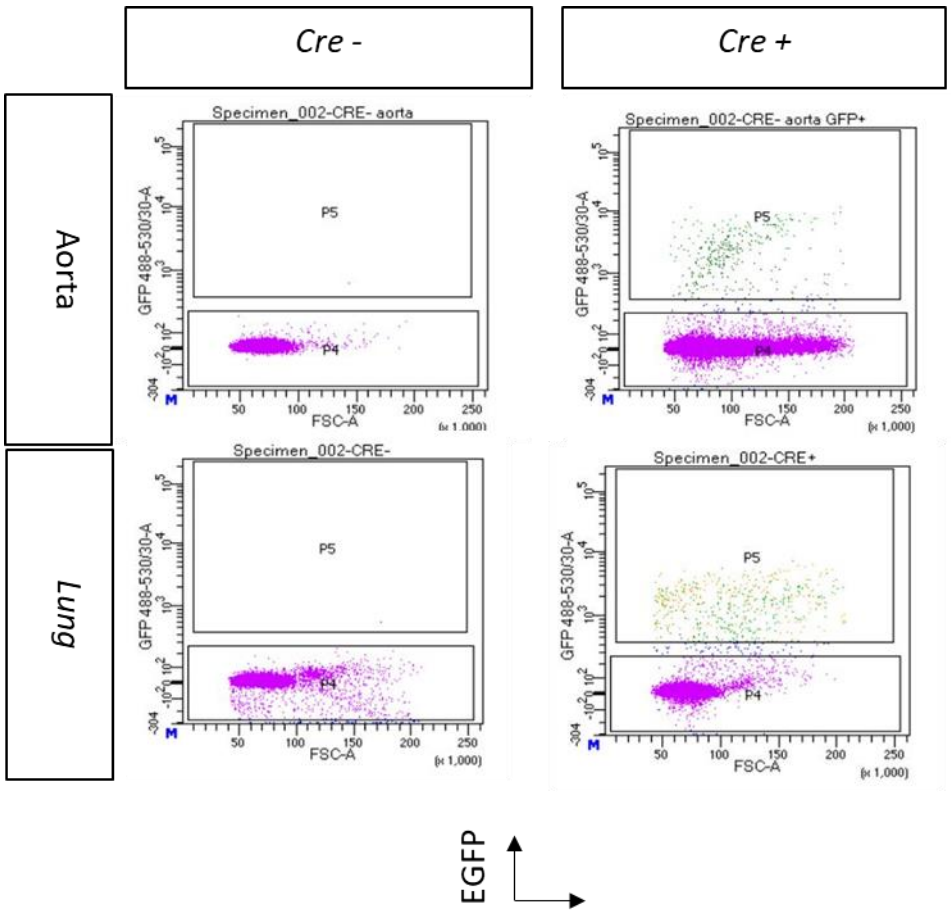

Figure 4.4: Detection of EGFP expression in isolated endothelial cells from aortas and lungs in *Pdgfb-Cre*$^{+/-}$ mice. FACS analysis (EGFP against forward scatter plot) showed an EGFP signal in the isolated endothelial cells (aorta and lung) from *Pdgfb-Cre*$^{+/-}$ mice but not from those of *Pdgfb-Cre*$^{-/-}$ mice.

4.3 Validation of tamoxifen induction protocol to generate endothelial cell-specific *Eltd1* knockout model

Once the *Eltd1*$^{fl/fl}$*;Pdgfb-Cre*$^{+/-}$ mice were generated, an experiment was initially conducted to validate the protocol for tamoxifen induction to generate the endothelial cell-specific *Eltd1* knockout mice.

4.3.1 Validation of the inducible endothelial cell-specific *Eltd1* knockout model by ear notch genotyping and *Eltd1 in situ* hybridisation (RNAscope).

Tamoxifen can be delivered using several different protocols, either intraperitoneal injection of 4-hydroxytamoxifen, 1 mg, for 3 alternate days or intraperitoneal injection of tamoxifen, 1 mg, for 5 consecutive days. The metabolised form of tamoxifen, 4-hydroxytamoxifen (4-HT) is more potent than the unmetabolized form but was considered to be too expensive for the number of *in vivo* experiments to be executed during this project.

Intraperitoneal injection of the unmetabolized form of tamoxifen, dose 1 mg, for 5 consecutive days was evaluated. Before the commencement of the protocol, the weights of the experimental mice, namely *Eltd1*$^{fl/fl}$*;Pdgfb-Cre*$^{-/-}$ and *Eltd1*$^{fl/fl}$*;Pdgfb-Cre*$^{+/-}$ mice, were recorded. 3 days after the last dose of tamoxifen injection, the mice were weighed again and observed for any welfare issues till the endpoint of the experiment (day 15). The mice were then allowed to rest for 10 days after the last dose of tamoxifen to allow for the excretion of tamoxifen from the body. At this time point, the mice were sacrificed and ear notches as well as tissues were harvested to assess the efficiency of *Eltdt1* knockout (Figure 4.5). Only *Eltd1*$^{fl/fl}$*;Pdgfb-Cre*$^{+/-}$ mice exhibited the deleted *Eltd1* locus, a band of 276 bp, in the ear notch DNA genotyping and significant reduction in *Eltd1 in situ* hybridisation staining was seen in both kidney glomeruli (fold change= -0.54, unpaired Student's *t* test: p = 0.012) and lung sections (fold change= -0.56, unpaired Student's *t* test: p = 0.003) of *Eltd1*$^{fl/fl}$*;Pdgfb-Cre*$^{+/-}$ mice but not *Cre*$^{-/-}$ littermate controls. The *Eltd1* probe used in the *in situ* hybridisation experiment targets exons 9-15 (was described in the previous chapter), which was downstream of the deletion in exons 4-5. The reduction seen in the *in situ* hybridisation signal was likely due to premature nonsense mediated decay of the downstream mRNA and gave confidence in that the adopted tamoxifen induction protocol generated an endothelial cell-specific *Eltd1* knockout model.

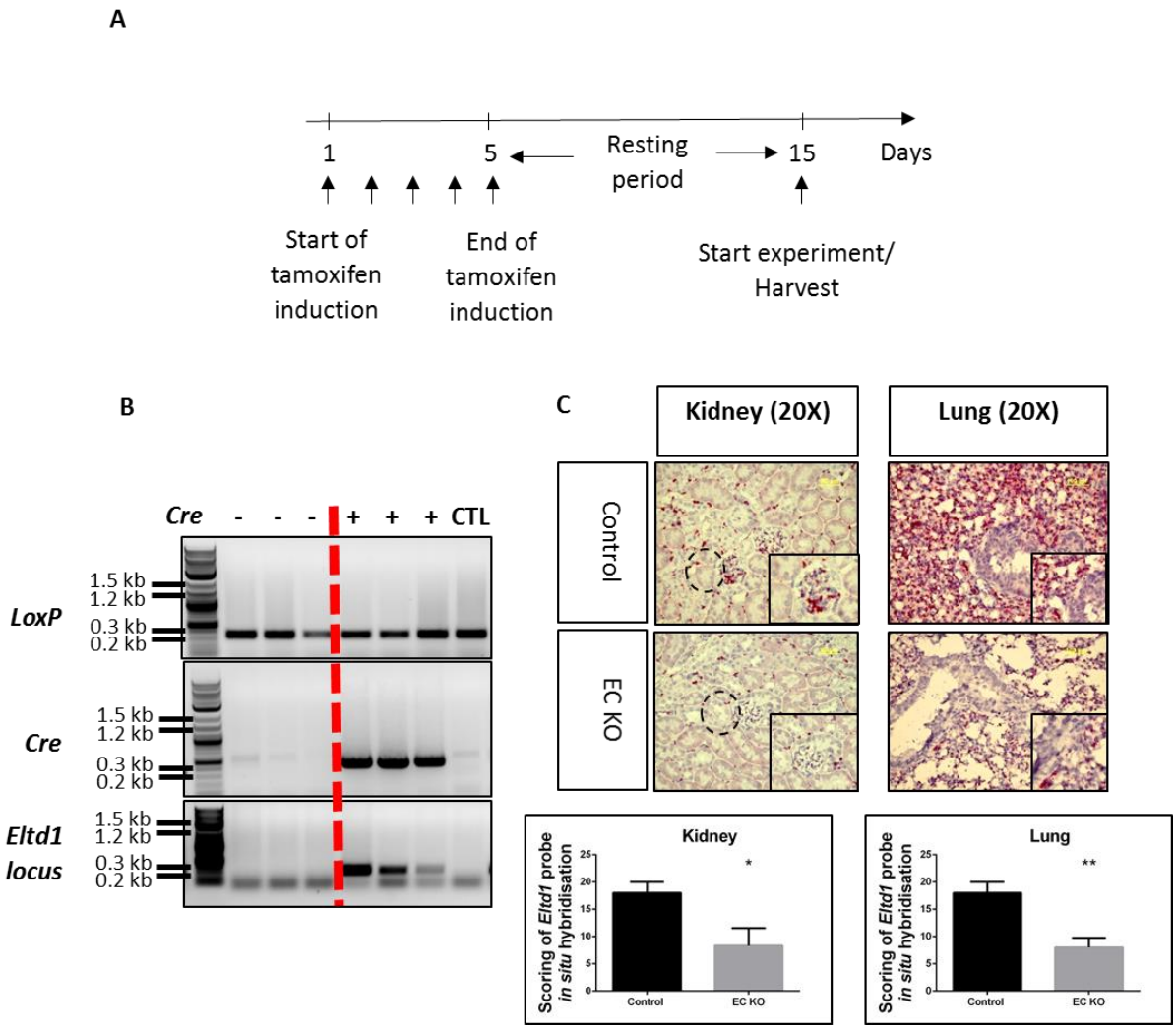

Figure 4.5: Validation of tamoxifen induction protocol. A) Schematic representation of tamoxifen induction protocol (5 consecutive days of intraperitoneal injection of tamoxifen); B) Ear notch genotyping PCR gels showed a deleted *Eltd1* locus, identified by a strong low molecular weight band of 276 bp, in *Pdgfb-Cre*$^{+/-}$ mice but not in *Pdgfb-Cre*$^{-/-}$ mice after tamoxifen induction. C) *In situ* hybridization of an *Eltd1* RNAscope probe on murine kidney and lung sections. The kidney glomeruli (highlighted in black) and the lungs are rich in endothelial cells which express *Eltd1*, indicated by punctate red dots in which each dot represents an *Eltd1* RNA molecule. There is a marked reduction in *Eltd1* staining in the glomeruli (fold change= -0.54, unpaired Student's *t* test: $p = 0.012$) and lungs (fold change= -0.56, unpaired Student's *t* test: $p = 0.003$) of EC KO compared to Control mice. Images were taken at 20X magnification. Data represented as mean ± SD (*: $p \leq 0.05$; **: $p \leq 0.01$). Three mice were used per group.

4.3.2 Validation of the inducible endothelial cell-specific *Eltd1* knockout model by qPCR analysis of the EGFP$^+$ sorted lung endothelial cells

To further substantiate *Eltd1* deletion in the endothelial cells of the inducible endothelial cell-specific *Eltd1* knockout model, endothelial cell suspensions were prepared from the lungs of the mice. Lungs were chosen for this preparation as it was reported that there was high *Eltd1* expression in mouse lungs (Regard et al., 2008). Six *Eltd1*$^{fl/fl}$;*Pdgfb-Cre*$^{+/-}$ mice were used and only three were injected with tamoxifen to induce *Eltd1* knockout. Following this, 10,000 EGFP$^+$ endothelial cells from the lung cell preparations were sorted from each mouse using a flow cytometer. As shown in Figure 4.6, qPCR analysis of these cells showed significant reduction in the expression of the targeted exons 4-5 of *Eltd1* (fold change= -0.97, unpaired Student's *t* test: $p = 0.0084$), the exons 5' to the deletion (1-2) and 3' to the deletion (8-9)(fold change= -0.87, unpaired Student's *t* test: $p = 0.013$) also showed a reduction in abundance, supporting the *in situ* hybridisation results indicating a reduction in *Eltd1* transcripts from the lungs and kidneys of the knockout mice.

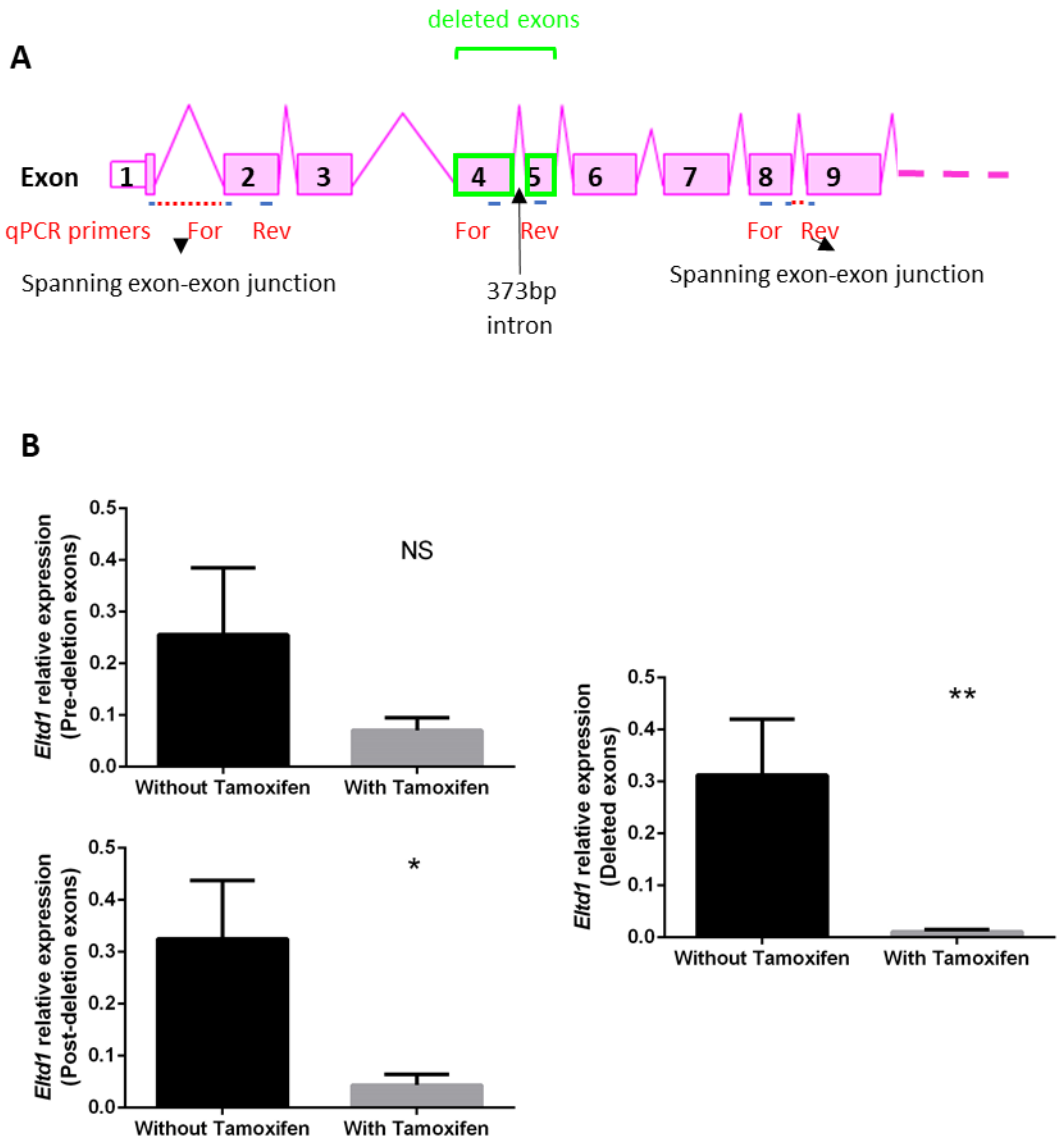

Figure 4.6: Validation of tamoxifen induction protocol by qPCR of EGFP⁺ lung endothelial cells. A) Schematic representation of qPCR primer sequences in which pre-deletion qPCR primer set spans exons 1-2, deletion qPCR primer set spans exons 4-5 and post-deletion set spans exons 8-9. B) *Eltd1* expression (exons 1-2 (5' to the deleted exons), exons 4-5 (deleted exons) (fold change= -0.97, unpaired Student's *t* test: $p = 0.0084$) and exons 7-8 (3' to the deleted exons) (fold change= -0.87, unpaired Student's *t* test: $p = 0.013$)) of EGFP⁺ lung endothelial cells isolated from *Pdgfb-Cre*$^{+/-}$ mice, both untreated and tamoxifen-treated. qPCR showed varying degree of *Eltd1* downregulation depending on the regions analysed in EGFP⁺ cells of *Pdgfb-Cre*$^{+/-}$ mice treated with tamoxifen. Data represented as mean ± SD (*: $p \leq 0.05$; **: $p \leq 0.01$). Three mice were used per group.

4.3.3 The inducible endothelial cell-specific *Eltd1* knockout model was highly specific to endothelial cells as shown by flow cytometry analyses.

As described earlier, Cre-expressing cells in this model are $EGFP^+$. To determine if the $EGFP^+$ Cre-expressing cells were largely endothelial populations, cell suspensions prepared from *Eltd1*$^{fl/fl}$*;Pdgfb-Cre*$^{+/-}$ mouse lungs were stained with the endothelial markers CD31 and VE-Cadherin and then analysed by flow cytometry. Greater than 80% of the $EGFP^+$ cells were positive for both CD31 and VECadherin (unpaired Student's *t* test: $p \leq 0.0001$), while $EGFP^-$ cells were largely negative for both CD31 and VECadherin (Figure 4.7). This showed that the inducible endothelial cell-specific *Eltd1* knockout model was highly specific to endothelial cells. The 80% positivity for both CD31 and VECadherin in the $EGFP^+$ population could be due to the strict gating in the flow cytometry analysis as well as due to different subsets of endothelial cells having different expression levels of endothelial markers (He et al., 2018).

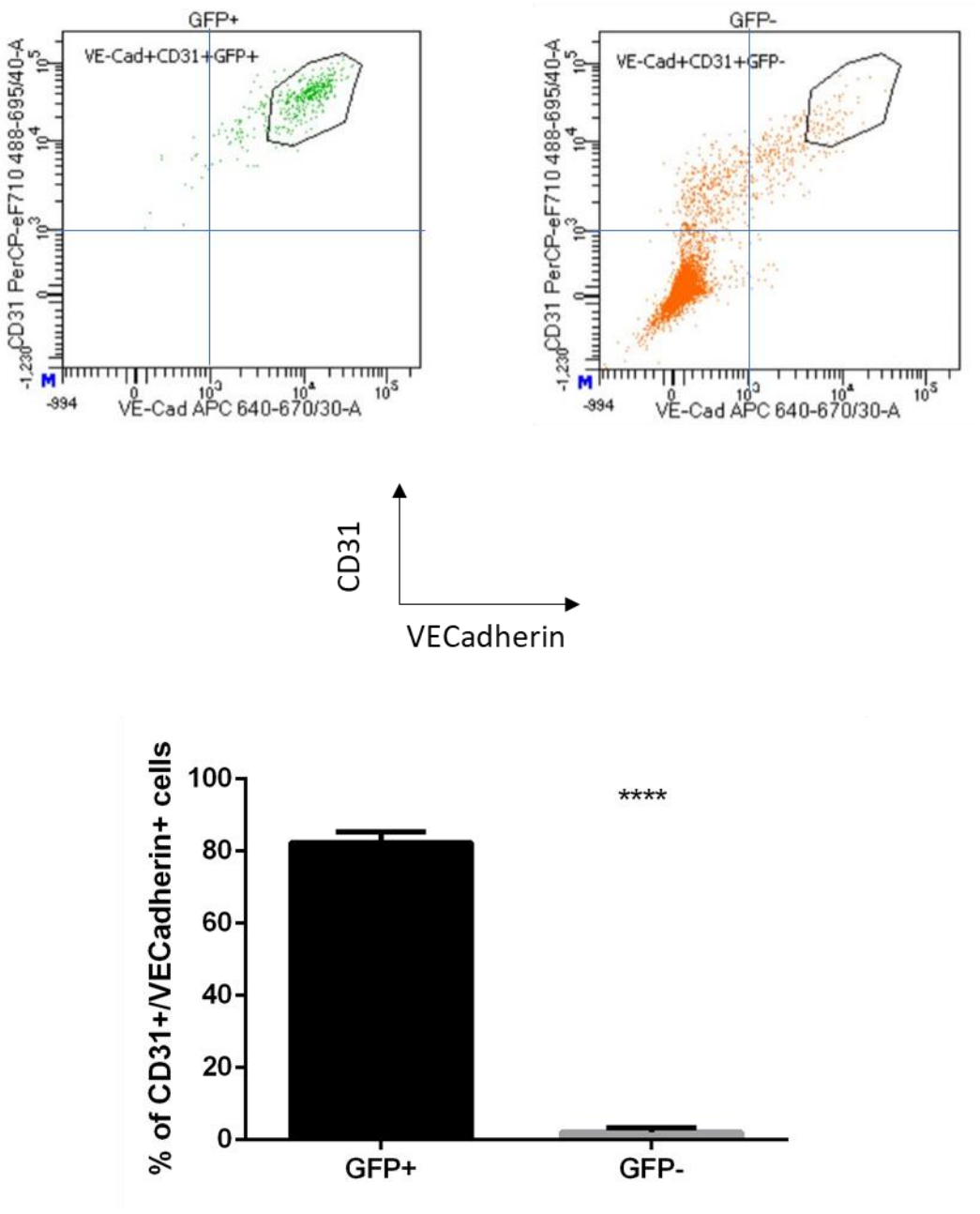

Figure 4.7: Assessment of the percentage (%) of CD31$^+$/VECadherin$^+$ cells in EGFP$^+$ fraction of lung endothelial cell preparations from *Pdgfb-Cre*$^{+/-}$ mice by flow cytometry. Analysis showed that EGFP$^+$ cells were predominantly CD31$^+$ and VECadherin$^+$(unpaired Student's *t* test: $p \leq 0.0001$), indicative of endothelial cells. Data represented as mean ± SD (****: $p \leq 0.0001$). Nine mice were used in the analysis.

4.4 Variable levels of *Eltd1* reduction, by qPCR, was observed across different normal tissues.

Vital organs (brain, heart, lung and kidney) from *Eltd1*$^{fl/fl}$*;Pdgfb-Cre*$^{+/-}$ mice exhibited different levels of *Eltd1* reduction relative to *Pdgfb* gene expression as compared to *Eltd1*$^{fl/fl}$*;Pdgfb-Cre*$^{-/-}$ mice harvested at day 10 post tamoxifen treatment (Figure 4.8). This could suggest that the tamoxifen penetrance might vary across different organs and/or that different organs might have endothelium made up of different proportion of *Pdgfb*-expressing endothelial cells in which the deletion of *Eltd1* exons occur. Heart (fold change= -0.95, unpaired Student's *t* test: $p = 0.008$) and kidneys (fold change= -0.7, unpaired Student's *t* test: $p = 0.022$) had significant reduction in the expression of *Eltd1* exons 4 and 5.

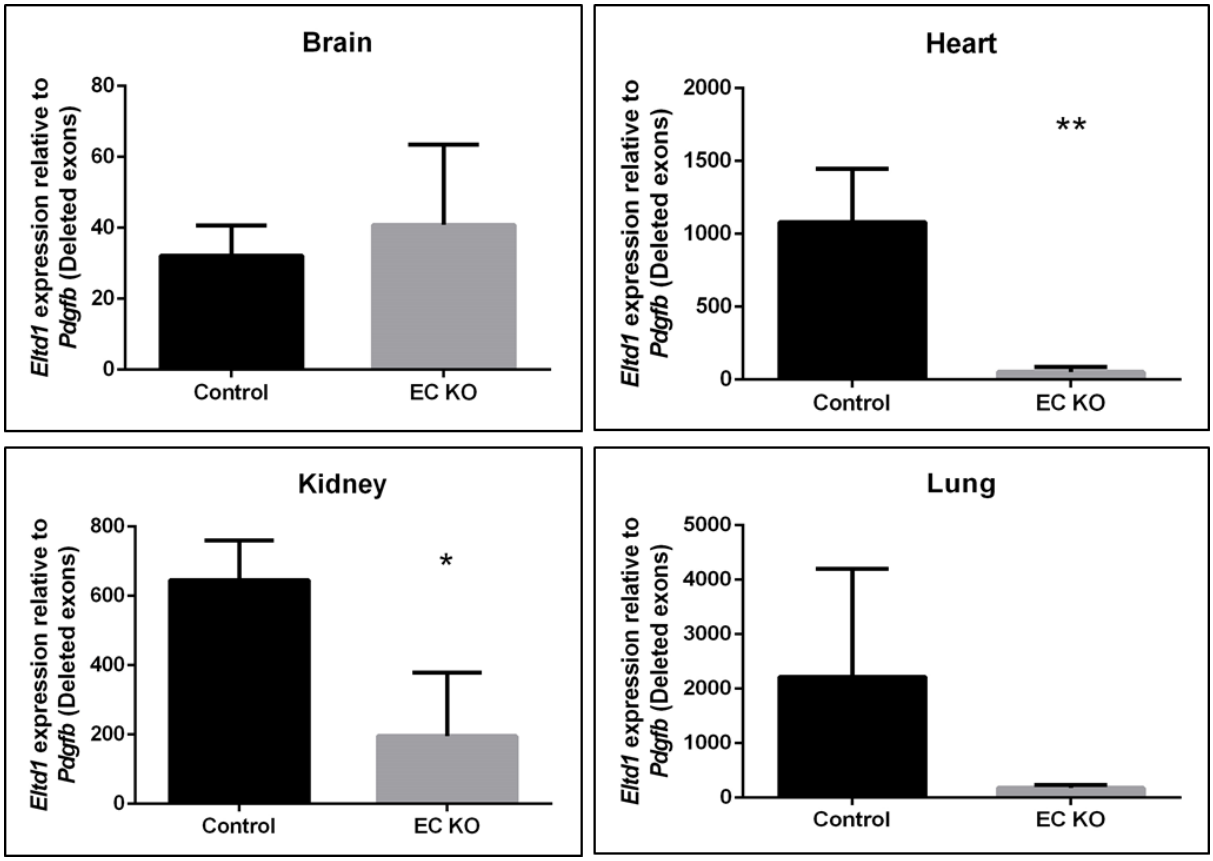

Figure 4.8: Assessment of *Eltd1* mRNA reduction in vital organs of the inducible endothelial cell-specific *Eltd1* knockout mice compared to those of littermate control mice. This was achieved by assessing *Eltd1* expression relative to *Pdgfb* gene expression normalized to β-actin expression. *Eltd1* expression was significantly reduced in heart (fold change= -0.95, unpaired Student's t test: $p = 0.008$) and kidney (fold change= -0.70, unpaired Student's t test: $p = 0.022$). Data represented as mean ± SD (*: $p \leq 0.05$; **: $p \leq 0.01$). Three mice were used per group.

4.5 Tamoxifen-inducible endothelial cell-specific *Eltd1* knockout mice did not exhibit significant differences in body weight and general physiological parameters compared to littermate controls

The inducible endothelial cell-specific *Eltd1* knockout male mice (n=7) did not show any signs of altered behaviour or distress and there was no significant difference in body weight over 40 days post tamoxifen treatment from the control group (Figure 4.9).

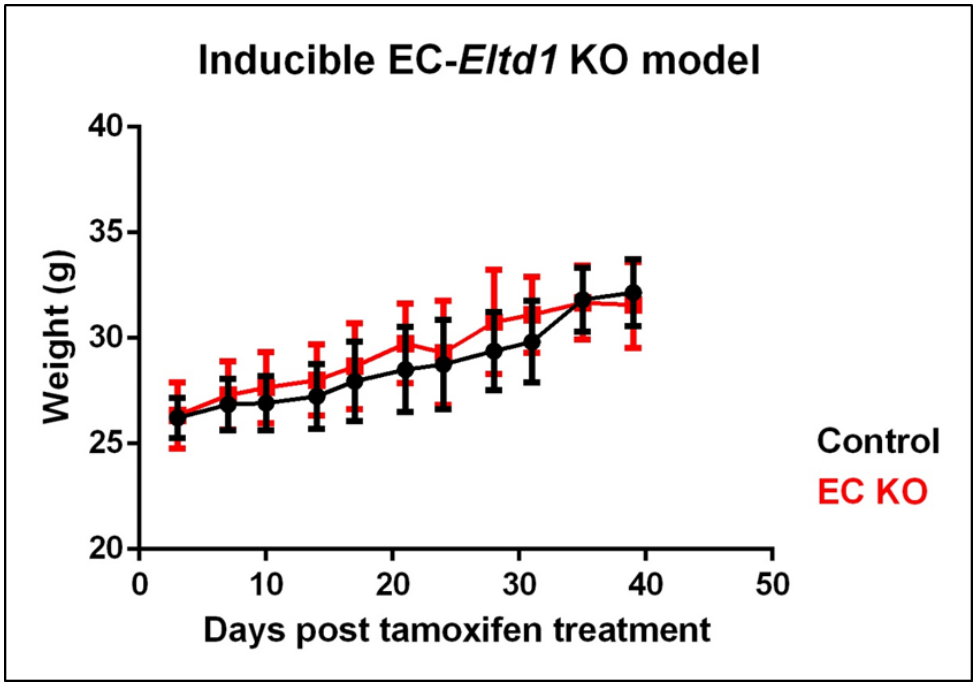

Figure 4.9: Body weight comparison between inducible endothelial cell-specific *Eltd1* knockout and littermate control mice over a duration of 40 days post tamoxifen treatment. No significant difference in body weight was observed between the two groups (n=7 male mice per group).

4.6 Tamoxifen-inducible endothelial cell-specific *Eltd1* knockout mice did not exhibit significant differences in organ/body weight ratios

Vital organs (brain, heart, lung, kidney, liver and spleen) were also harvested and weighed at 10 days post tamoxifen treatment (n=6). There was no observed significant difference in the organ-to-body weight ratios in the *Eltd1* knockout group (Figure 4.10).

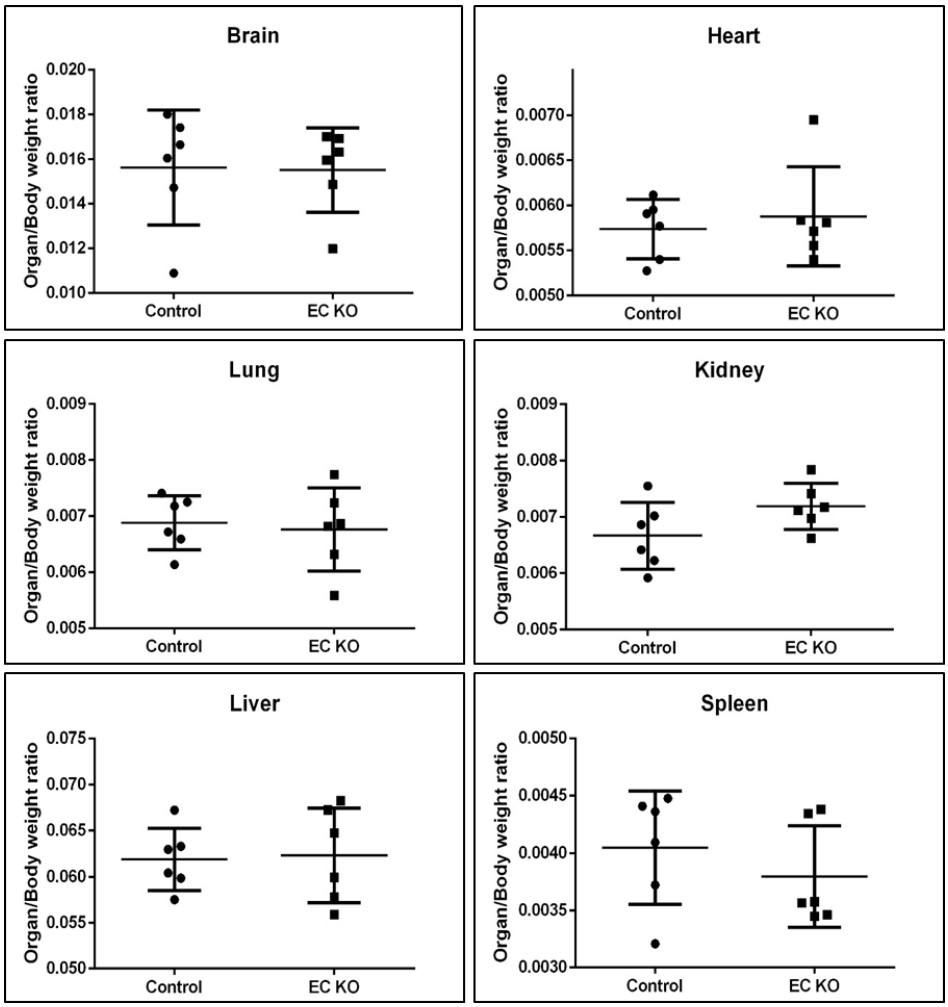

Figure 4.10: Organ/body weight comparison between inducible endothelial cell-specific *Eltd1* knockout and littermate control mice. No significant differences (unpaired Student's *t* test) in organ/body weight ratios of the inducible endothelial cell-specific *Eltd1* knockout mice were observed (n=6 male mice per group)

4.7 Tamoxifen-inducible endothelial cell-specific *Eltd1* knockout mice did not exhibit significant differences in the architecture or vessel morphology of vital organs

Vital organs (brain, heart, lung, kidney, liver, spleen) from inducible endothelial cell-specific *Eltd1* knockout mice (n=3) had similar vessel morphology with comparable CD31 staining intensity and distribution, no compromise of the architectural integrity by H&E staining and no signs of necrosis as compared to littermate controls (Figures 4.11 and 4.12). These findings were verified by an experienced histopathologist pathologist (Professor Francesco Pezzella, University of Oxford). The lack of phenotype was consistent with the knockout mice having no obvious phenotypic differences from the littermate controls.

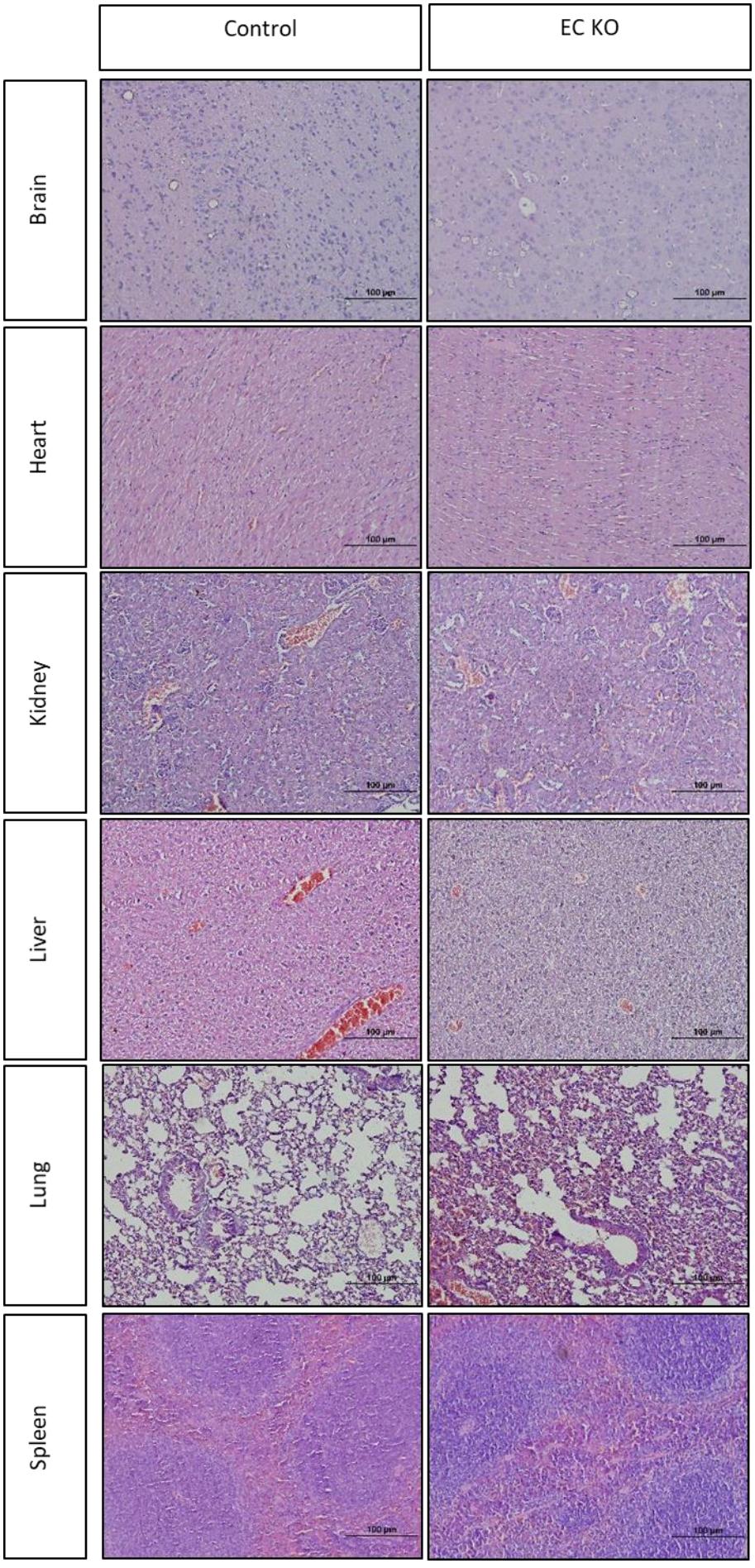
Control
EC KO
Brain
Heart
Kidney
Liver
Lung
Spleen

Figure 4.11: Histological analysis of vital organs (brain, heart, lung, liver, kidney and spleen) between inducible endothelial cell-specific *Eltd1* knockout and littermate control mice. Haematoxylin & Eosin staining (H&E) showed no difference in architectural integrity of vital organs between the two groups (n=3 mice per group)(Scale bar: 100 μm).

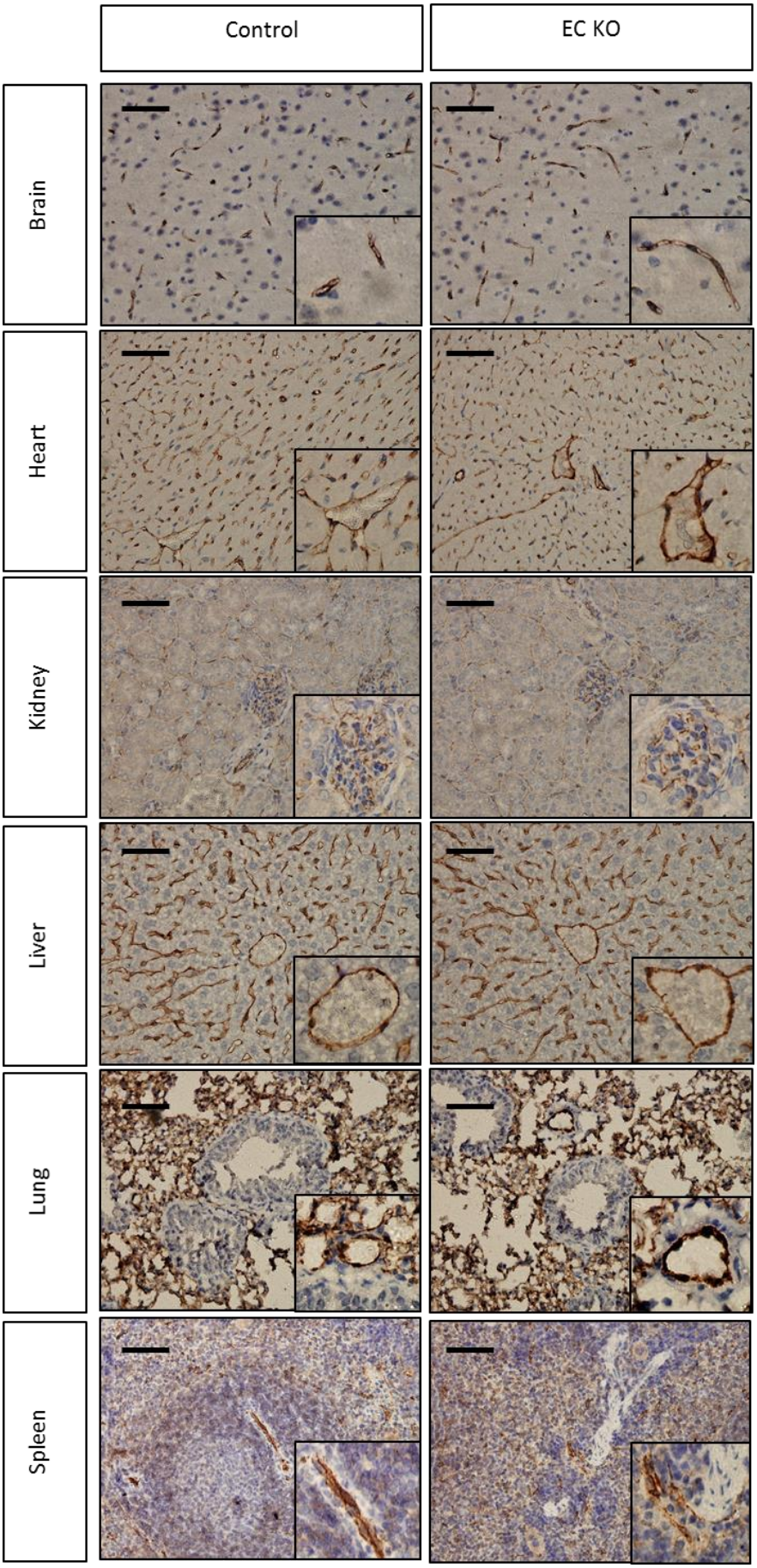
Control
EC KO
Brain
Heart
Kidney
Liver
Lung
Spleen

Figure 4.12: Immunohistochemical (CD31) analysis of vital organs (brain, heart, lung, liver, kidney and spleen) between inducible endothelial cell-specific *Eltd1* knockout and littermate control mice. CD31 staining of vital organs showed no difference in vessel morphology or the vessel density of vital organs between the two groups (n=3 mice per group) (Scale bar: 20 μm).

4.8 Endothelial cell sprouting was impaired from *ex vivo* cultured aortic rings isolated from tamoxifen-inducible endothelial cell-specific *Eltd1* knockout mice compared to littermate controls

The rationale of adopting the *ex vivo* aortic ring angiogenesis assay was described in chapter 3 where the assay was used to demonstrate that endothelial cell sprouting was unaffected in the mice with constitutive endothelial *Eltd1* deletion. However, in triplicate experiments, the inducible endothelial cell-specific *Eltd1* knockout aortas showed a significant reduction (fold change= -0.54, unpaired Student's *t* test: $p = 0.045$) in endothelial sprouting compared to aortas from littermate controls (Figure 4.13).

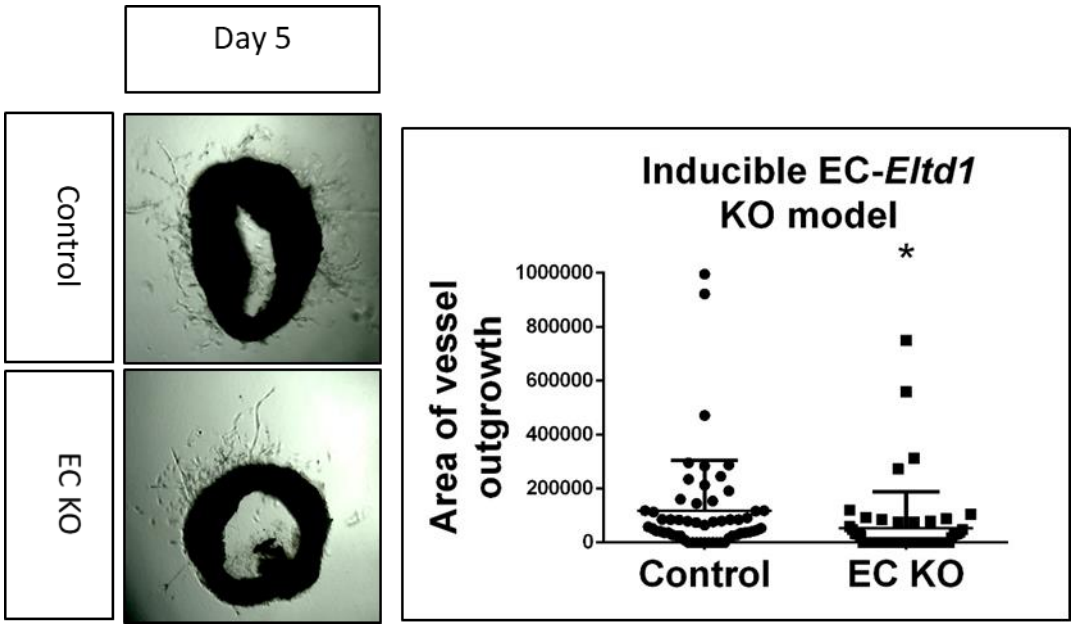

Figure 4.13: *Ex vivo* aortic ring assays. A significant difference (fold change= -0.54, unpaired Student's *t* test: $p = 0.045$) in the area of vessel outgrowth at day 5 between inducible endothelial cell-specific *Eltd1* knockout and littermate control mice was observed. Data represented as mean ± SD (*: $p \leq 0.05$). Three mice were used in each group, 6-8 rings per aorta (n=3 experiments).

4.9 Syngeneic E0771 tumour model

4.9.1 Experimental design

To investigate whether inducible endothelial cell *Eltd1* deletion affected tumour growth *in vivo*, the syngeneic E0771 breast cancer model was analysed. In this study, eight age-matched 5-6 week old female mice per group (*Eltd1*$^{fl/fl}$*;Pdgfb-Cre*$^{+/-}$ and *Eltd1*$^{fl/fl}$*;Pdgfb-Cre*$^{-/-}$) were used. The mice were given intraperitoneal injections of tamoxifen, 1mg, for 5 consecutive days. Tumour inoculation was conducted 10 days post tamoxifen treatment. 5 x 10^5 E0771 cells resuspended in Matrigel was injected subcutaneously at the back of the mice and tumour growth was measured three times per week with calipers and tumours were harvested as they each reached an endpoint of gross median dimension (GMD = $(LxBxH)^{1/3}$) of 10 mm. These conditions were chosen based on the pilot study performed using E0771 that was described in the previous chapter.

4.9.2 No significant difference was observed in tumour growth curves and survival plot between inducible endothelial cell-specific *Eltd1* knockout and littermate control groups

The experiment lasted 34 days and over this period there were no significant differences in tumour growth curves, average tumour volume at day 22 (before loss of any animals from the study) and survival plots of inducible endothelial cell-specific *Eltd1* knockout tumours as compared to those of the littermate control group (Figure 4.14).

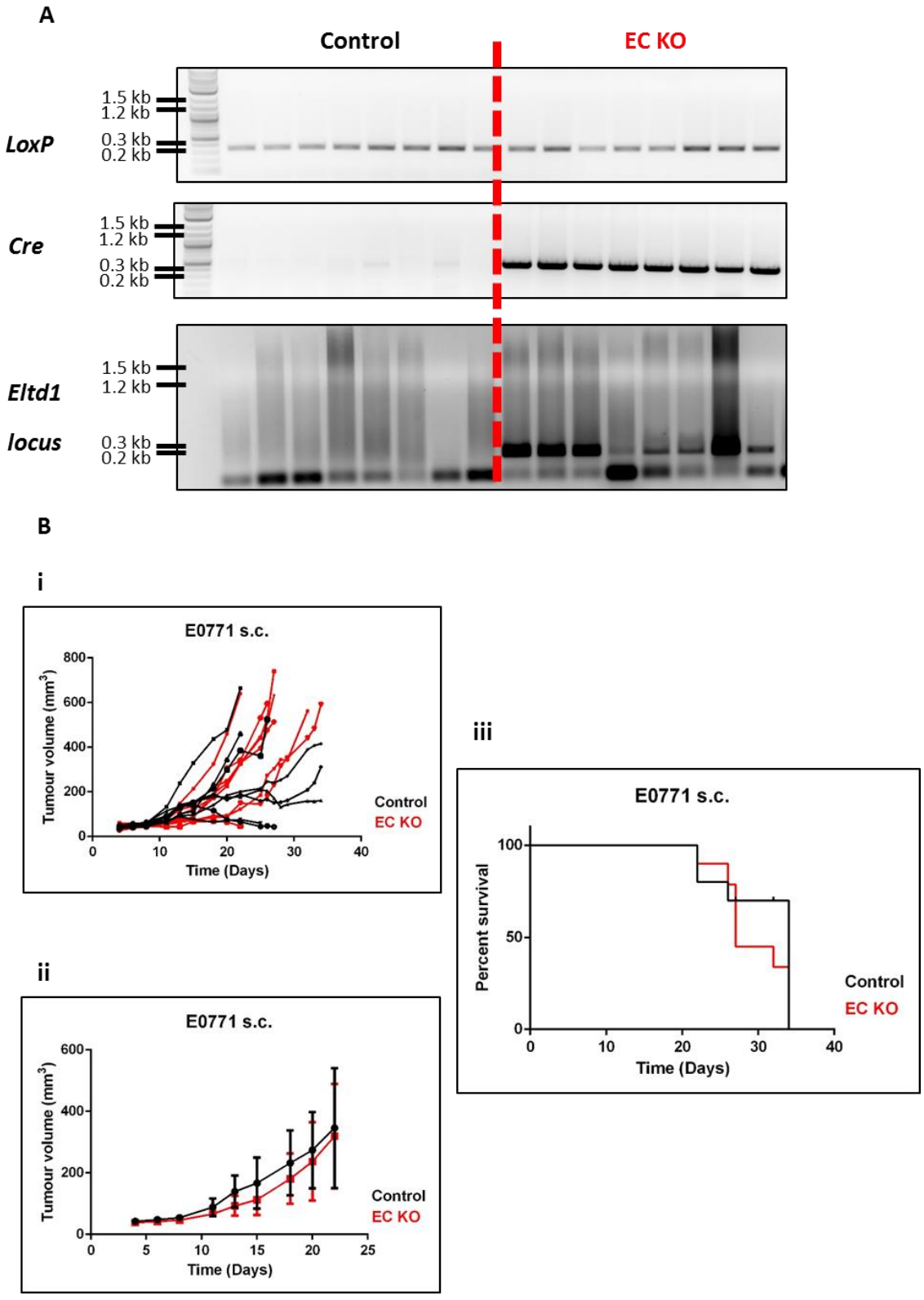

Figure 4.14: E0771 syngeneic tumour model. A) Genotyping PCR of experimental mice B) Tumour growth curve (i. raw data for individual animals, ii. average tumour volume per group, up until day 22) and iii. survival plot showed no significant difference in tumour growth and

survival outcome between inducible endothelial cell-specific *Eltd1* knockout and littermate control mice. In this experiment, eight mice were used in each group. However, two mice in the control group and one mouse in the *Eltd1* knockout group did not take up the tumour successfully and were excluded in the analysis.

4.9.3 Inducible endothelial cell-specific *Eltd1* knockout tumours had reduced microvessel density and pericyte coverage and a trend towards increased hypoxia and necrosis but there was no change in tumour proliferation.

In histological analyses, only six tumours from the control group and seven tumours from the knockout group were used as three mice (two controls and one knockout) did not develop tumours. Despite no significant difference in tumour growth curves or survival of the animals, there were significant reductions in microvessel density (CD31)(fold change= -0.21, unpaired Student's *t* test: $p = 0.048$), and pericyte coverage of the vessels (CD31/αSMA)(fold change= -0.34, unpaired Student's *t* test: $p = 0.003$), and a trend towards increased hypoxia (CA9) and necrosis in the *Eltd1* knockout group, as shown in Figures 4.15 and 4.16. Interestingly, there was a larger reduction in $Eltd1^+$ vessels than $CD31^+$ vessels which would suggest that the remaining vessels lacked Eltd1 (F01: fold change = -1.00, unpaired Student's *t* test, $p \leq 0.0001$; F04: fold change = -1.00, unpaired Student's *t* test, $p \leq 0.0001$). Ki67 analysis was done on tumour rather than vasculature and was not significantly different in the endothelial cell-specific *Eltd1* knockout tumours.

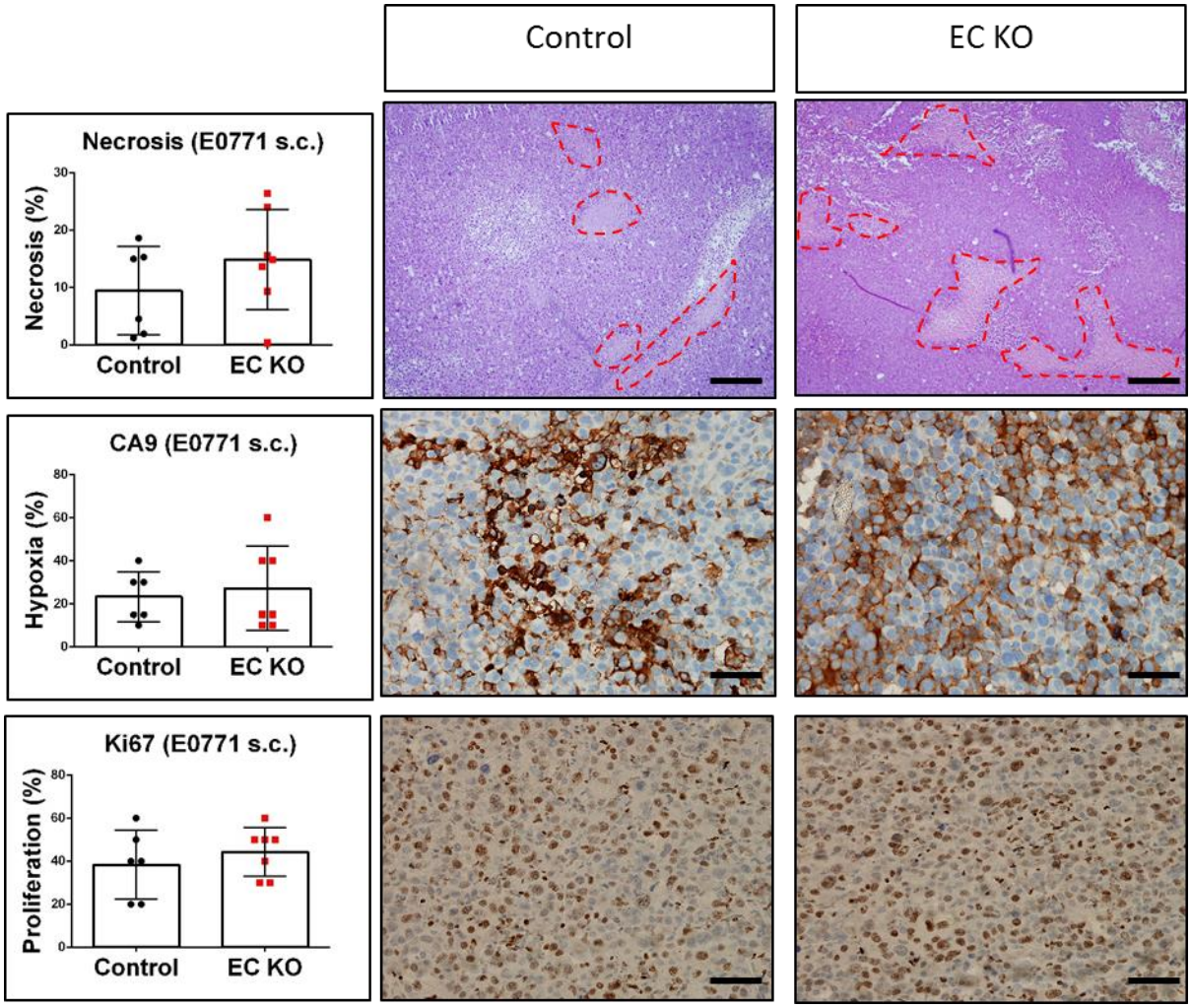

Figure 4.15: Immunohistochemical analyses of necrosis, hypoxia and proliferation in E0771 syngeneic tumour model. Immunohistochemical analysis showed a trend towards increased necrosis (H&E) and hypoxia (CA9) in the tumours of inducible endothelial cell-specific *Eltd1* knockout compared to those of littermate control mice. Six tumours in the control group and seven tumours in the knockout group were used in the analysis (Scale bar: 20 µm).

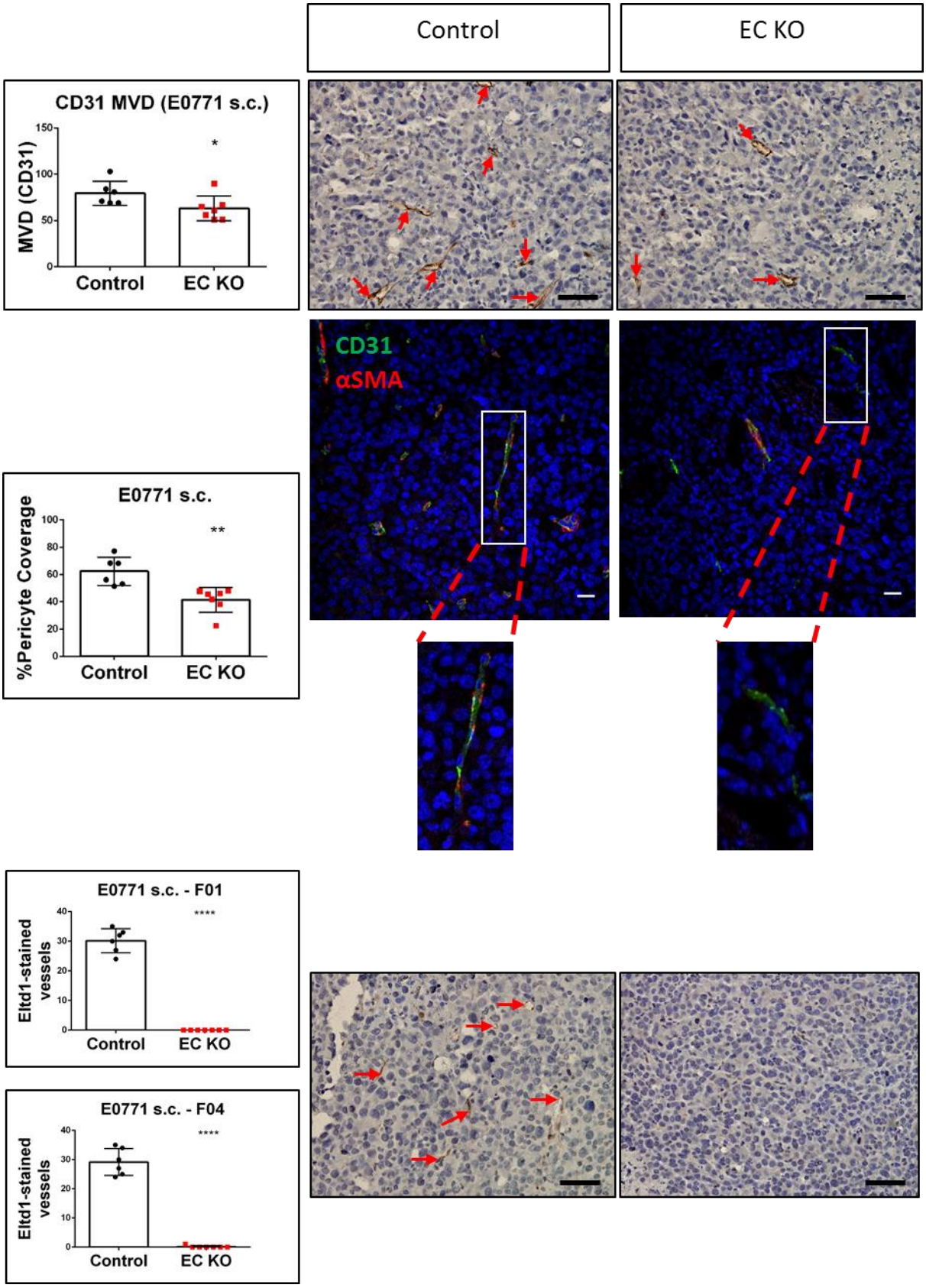
Control
EC KO
CD31 MVD (E0771 s.c.)
MVD (CD31)
150
100
50
0
*
Control
EC KO
CD31
αSMA
E0771 s.c.
%Pericyte Coverage
100
80
60
40
20
0
**
Control
EC KO
E0771 s.c. - F01
Eltd1-stained vessels
40
30
20
10
0
****
Control
EC KO
E0771 s.c. - F04
Eltd1-stained vessels
40
30
20
10
0
****
Control
EC KO

Figure 4.16: Immunohistochemical analysis of vasculature in E0771 syngeneic tumour model. Immunohistochemical analysis showed a significant reduction in microvessel density (CD31; fold change= -0.21, unpaired Student's *t* test: p = 0.048), pericyte coverage (CD31/αSMA; fold change= -0.34, unpaired Student's *t* test: p = 0.003) and Eltd1 (F01: fold change = -1.00 , unpaired Student's *t* test, $p \leq 0.0001$; F04: fold change = -1.00, unpaired Student's *t* test, $p \leq 0.0001$) in the tumours of inducible endothelial cell-specific *Eltd1* knockout group compared to those of littermate control. Six tumours in control group and seven tumours in knockout group were used in the analysis (Scale bar: 20 μm). Data represented as mean ± SD (*: $p \leq 0.05$; **: $p \leq 0.01$; ****: $p \leq 0.0001$). F01 and F04 were in-house polyclonal antibodies targeting Eltd1.

4.10 Syngeneic MC38 tumour model

4.10.1 Experimental design

To investigate whether inducible endothelial cell *Eltd1* deletion affected tumour growth *in vivo* using a different syngeneic tumour model, the syngeneic MC38 colorectal cancer model was analysed. In this study, five age-matched 6 week old male mice per group (*Eltd1*$^{fl/fl}$*;Pdgfb-Cre*$^{+/-}$ and *Eltd1*$^{fl/fl}$*;Pdgfb-Cre*$^{-/-}$) were used in the syngeneic MC38 tumour model. These mice were given intraperitoneal injection of tamoxifen, 1 mg, for 5 consecutive days. Tumour induction was conducted 10 days post tamoxifen treatment. 1 x 10^6 cells resuspended in PBS was injected subcutaneously at the back of the mice and tumour growth was recorded routinely and tumours were harvested at the endpoint at which the tumours have reached gross median dimension (GMD) of 12 mm due to the highly necrotic nature of MC38 tumours.

4.10.2 No significant difference was observed in tumour growth curves and survival plot between inducible endothelial cell-specific *Eltd1* knockout and littermate control groups

The experiment was carried out until the end point, which lasted 34 days. However, there were no significant differences in tumour growth curves, average tumour volume at day 15 and survival plots of inducible endothelial cell-specific *Eltd1* knockout tumours as compared to those of the littermate control group (Figure 4.17).

A

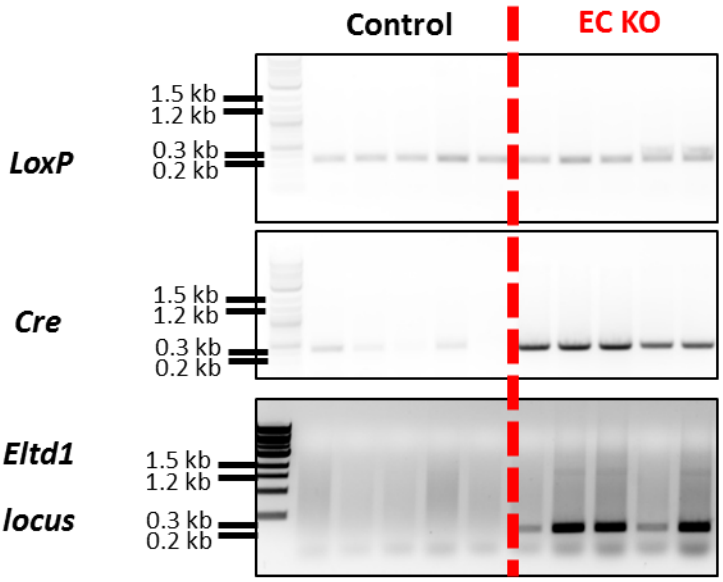
Control
EC KO
LoxP
1.5 kb
1.2 kb
0.3 kb
0.2 kb
Cre
1.5 kb
1.2 kb
0.3 kb
0.2 kb
Eltd1
locus
1.5 kb
1.2 kb
0.3 kb
0.2 kb

B

i

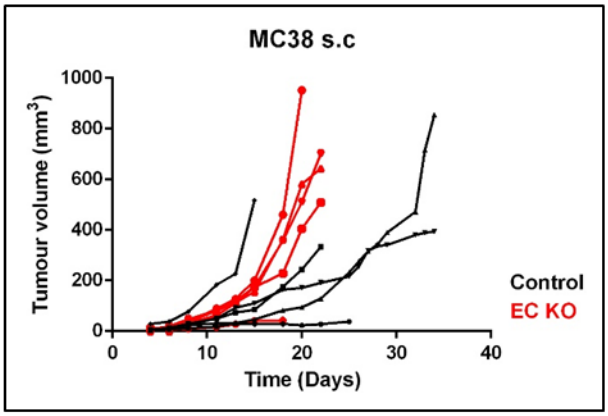
MC38 s.c
Tumour volume (mm3)
1000
800
600
400
200
0
0
10
20
30
40
Time (Days)
Control
EC KO

ii

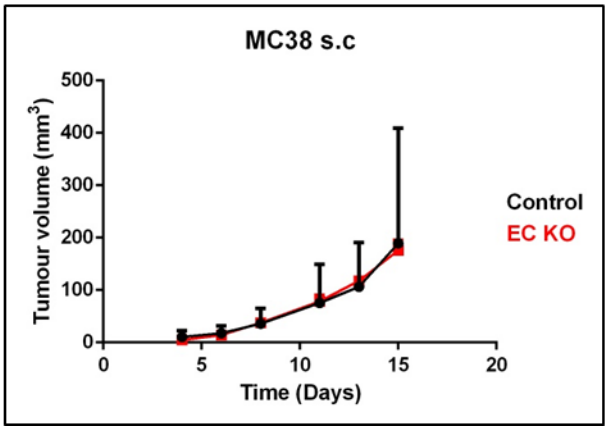
MC38 s.c
Tumour volume (mm3)
500
400
300
200
100
0
0
5
10
15
20
Time (Days)
Control
EC KO

iii

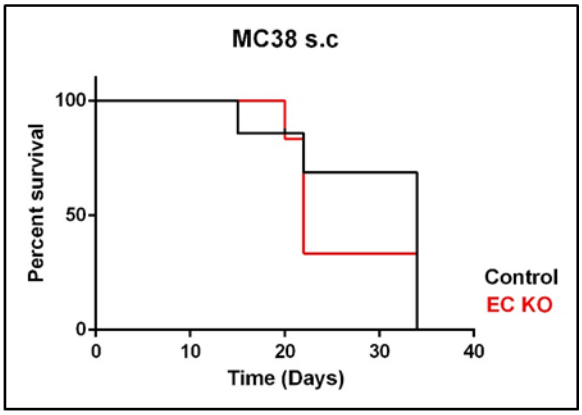
MC38 s.c
Percent survival
100
50
0
0
10
20
30
40
Time (Days)
Control
EC KO

Figure 4.17: MC38 syngeneic tumour model. A) Genotyping PCR of experimental mice B) Tumour growth curves (i. raw data and ii. Average tumour volume at day 15) and iii. survival plot showed no significant difference in tumour growth and survival between inducible endothelial cell-specific *Eltd1* knockout and littermate control mice (n=5 male mice per group). However, one mouse per group did not take up the tumour successfully and were excluded in the analysis.

4.10.3 Inducible endothelial cell-specific *Eltd1* knockout tumours had reduced microvessel density and pericyte coverage and a trend towards increased hypoxia and necrosis but there was no change in tumour proliferation

In this analysis, only 4 tumours in each group were used as 2 mice (1 in each group) did not take up the tumour successfully. Despite that there was no significant difference in tumour growth curves and survival plot in the inducible endothelial cell-specific *Eltd1* knockout mice, interestingly, there were significant reductions in microvessel density (CD31) (fold change= -0.25, unpaired Student's *t* test: $p = 0.012$), and pericyte coverage (CD31/αSMA) (fold change= -0.31, unpaired Student's *t* test: $p = 0.011$), with an uptrend in hypoxia (CA9) and necrosis in the knockout group, as shown in Figures 4.18 and 4.19.

Similarly, to the E0771 model, there was a larger reduction in $Eltd1^+$ vessels (F01: fold change = -0.98, unpaired Student's *t* test, $p= 0.0006$; F04: fold change = -0.90, unpaired Student's *t* test, $p= 0.0003$) than $CD31^+$ vessels which would suggest that the remaining vessels lacked Eltd1. Ki67 analysis was done on tumour rather than vasculature and was not significantly different in the endothelial cell-specific *Eltd1* knockout tumours.

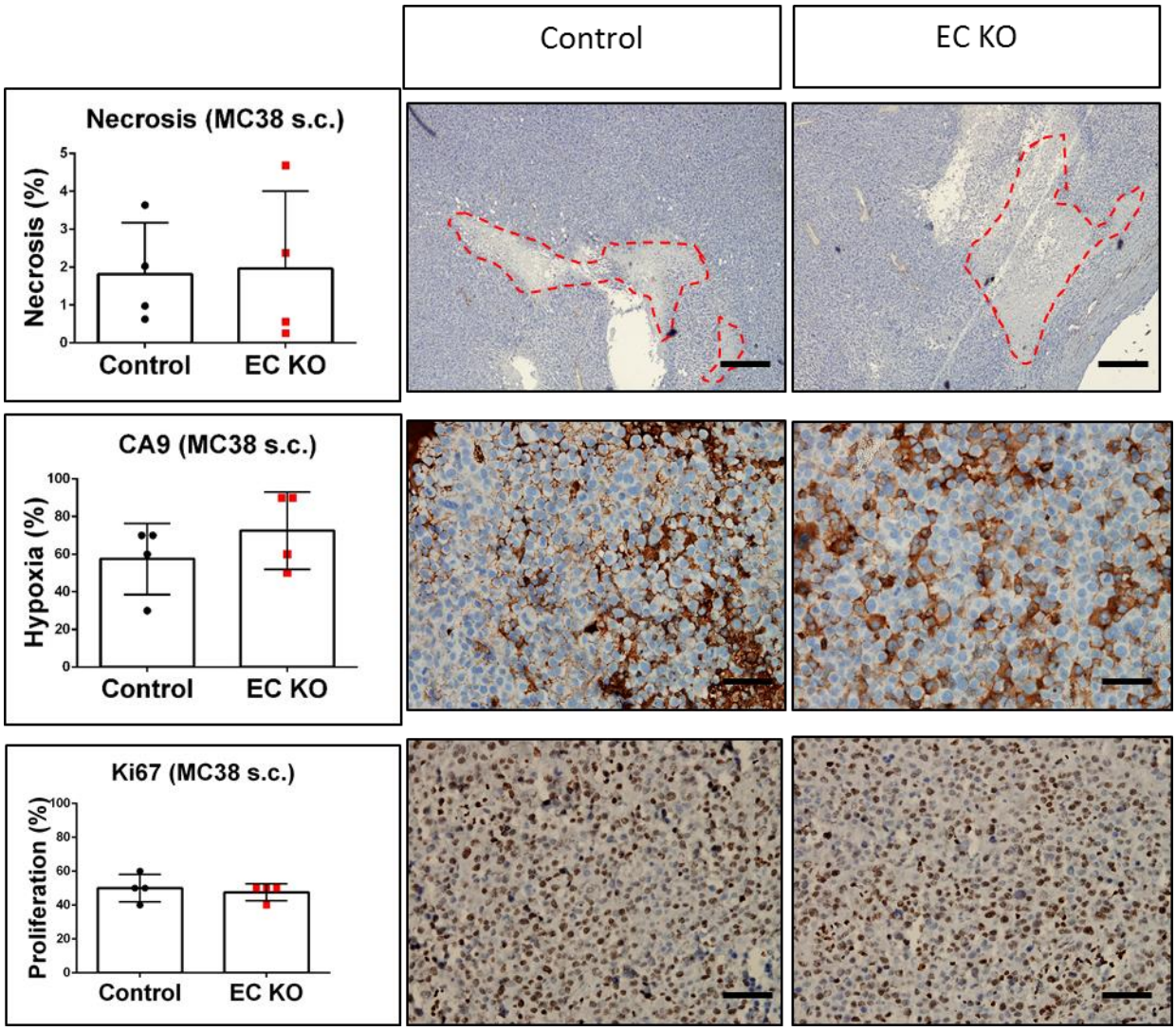

Figure 4.18: Immunohistochemical analyses of necrosis, hypoxia and proliferation in MC38 syngeneic tumour model. Immunohistochemical analysis showed a trend towards increased necrosis (H&E) and hypoxia (CA9) in the tumours of inducible endothelial cell-specific *Eltd1* knockout compared to those of littermate control mice. Four tumours in each group were used in the analysis (Scale bar: 20 µm).

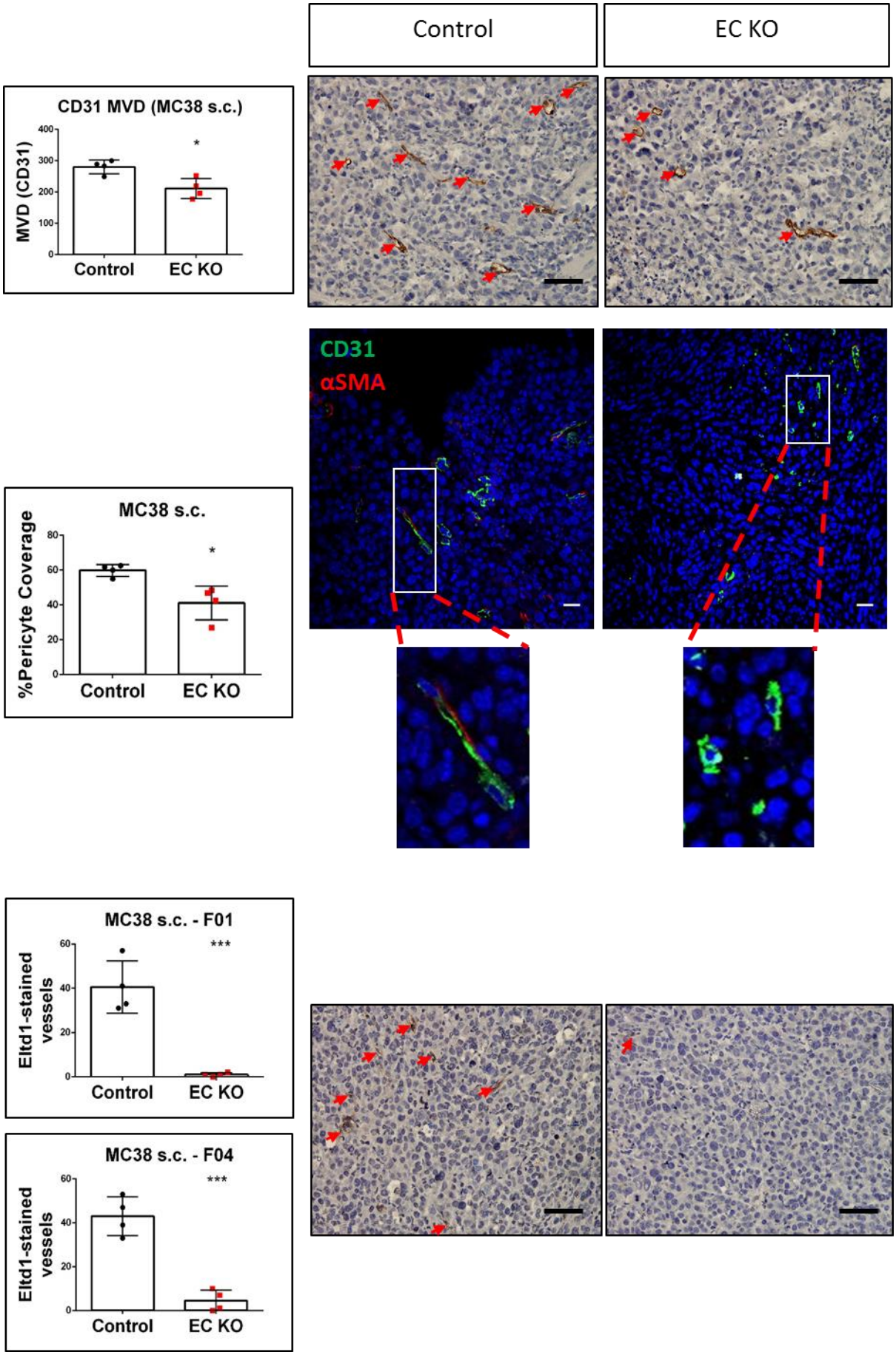
Control
EC KO
CD31 MVD (MC38 s.c.)
MVD (CD31)
400
300
200
100
0
*
Control
EC KO
CD31
αSMA
MC38 s.c.
%Pericyte Coverage
80
60
40
20
0
*
Control
EC KO
MC38 s.c. - F01
Eltd1-stained vessels
60
40
20
0
***
Control
EC KO
MC38 s.c. - F04
Eltd1-stained vessels
60
40
20
0
***
Control
EC KO

Figure 4.19: Immunohistochemical analysis of vasculature in MC38 syngeneic tumour model. Immunohistochemistry analysis showed a significant reduction in microvessel density (CD31; fold change= -0.25, unpaired Student's *t* test: $p = 0.012$), pericyte coverage (CD31/αSMA; fold change= -0.31, unpaired Student's *t* test: $p = 0.011$) and Eltd1 (F01: fold change = -0.98, unpaired Student's *t* test, $p= 0.0006$; F04: fold change = -0.90, unpaired Student's *t* test, $p= 0.0003$) in the tumours of inducible endothelial cell-specific *Eltd1* knockout group compared to those of littermate control. Four tumours in each group were used in the analysis (Scale bar: 20 µm). Data represented as mean ± SD (*: $p \leq 0.05$; **: $p \leq 0.01$; ***: $p \leq 0.001$). F01 and F04 were in-house generated polyclonal antibodies targeting Eltd1.

4.11 Discussion

In this chapter, a tamoxifen inducible *Eltd1* knockout model was generated and validated to investigate into the effects of acute endothelial cell-specific *Eltd1* depletion on mouse physiology and tumour pathology. In this inducible endothelial cell-specific *Eltd1* knockout model, a different endothelial promoter (*Pdgfb*) was used compared to that of the constitutive model (*Tie2*). This choice was made due to the report of the efficient inducible Cre-recombinase activation in the endothelium using the *PdgfbiCreER*^{T2} model (Claxton et al., 2008), also because the *Tie2-Cre* model contains other *Tie2*-expressing non-endothelial cell types, such as macrophages (Chen et al., 2016), and because there was no inducible *Tie2-Cre* strain available in Oxford.

There were varying degrees of *Eltd1* transcript reduction in different tissues (lung, kidneys, brain and heart). This could be due to the penetrance of tamoxifen or the endothelium of different tissues might consist of different proportion of *Pdgfb*$^{+}$ Cre-expressing endothelial cells where the deletion occurred.

It was observed that acute endothelial cell-specific *Eltd1* deletion did not cause any gross behavioural or phenotypic changes in the animals, compared to *Cre*$^{-/-}$ littermate controls. There were also no significant differences in body or organ weights or defects in vital organs such as the tissue architecture and vessel density. These were consistent with the observations in chronic endothelial-*Eltd1* depleted mice described in chapter 3. However, very interestingly, the *ex vivo* aortic ring assay performed using tissues from the acute endothelial cell-specific *Eltd1* depleted mice showed a significant inhibition in vascular sprouting. This had not been observed with the chronic endothelial cell-specific *Eltd1* depletion described in chapter 3. This indicates that there is a biological difference between acute and chronic endothelial-*Eltd1* depletion and could suggest that functional compensation might have occurred in the constitutive endothelial cell-specific *Eltd1* model that masked the inhibition of the sprouting phenotype caused by the loss of endothelial *Eltd1*. Furthermore, this also implied that inducible endothelial cell-specific *Eltd1* knockout model was a better model to investigate into the *in vivo* effects of endothelial-*Eltd1* depletion. More importantly, the inducible model is more relevant to the study of targeting *ELTD1* as therapy in the clinic. However, it is worth noting that the two adopted knockout models utilised different endothelial promoters, hence the difference in phenotypic observations could also

be due to the level of *Eltd1* reduction in different targeted endothelial populations. Interestingly, it has been recently reported that *Tie2-Cre* model is pan-endothelial but also targets hematopoietic cells whereas *Pdgfb-Cre* targets arterial and capillary endothelial cells but also keratinocytes and megakaryocytes (Payne et al., 2018). In addition, in all the endothelial-targeting cre lines reported, there are either incomplete coverage of the targeted endothelial population or targeting of other non-endothelial cell types (Payne et al., 2018). It could be interesting to repeat the *in vivo* experiments using inducible or constitutive endothelial-cre lines driven by different promoters, to see consistency of the phenotype and whether it is the promoter driving the Cre recombinase or the chronic versus acute *Eltd1* depletion that contributes most significantly. However, this is not feasible in this project due to the time and cost needed to generate these knockout models.

Neither of the syngeneic tumour models (E0771, breast and MC38, colon) exhibited significant differences in tumour growth curves and survival plots in the inducible endothelial cell-specific *Eltd1* knockout group. This observation was different to a previous study where a reduction in tumour growth and better survival outcome was observed in ovarian and colorectal xenografts treated with *Eltd1*-targeting siRNAs incorporated into chitosan nanoparticles *in vivo* (Masiero et al., 2013). However, there are several key differences in the experimental methodology between these studies. In our genetic knockout model, the knockout was induced before tumour cells were inoculated into the mice. This was critically different from the published work in which siRNA was delivered when the tumours had been established. Tumour-associated endothelial cells were reported to have an elevated Eltd1 expression (Masiero et al., 2013), which was unlikely to be observed in the genetic knockout model where the deletion was induced before tumour inoculation. It is possible that inhibition of the elevated levels of Eltd1 in an established tumour microenvironment is needed to impair tumour growth. In addition, other key differences between the *in vivo* tumour growth findings in the genetic knockout model compared to the siRNA-induced knockout in the published report were that xenografts were grown in immunocompromised mice which had no immune capability and the *Eltd1*-targeting siRNA delivered might not only target endothelial cells. For example, vascular smooth muscle cells in the tumour vasculature are also Eltd1 positive but would not be targeted using the genetic approach.

Despite no significant differences in tumour growth and survival outcomes, however, inducible endothelial cell-specific *Eltd1* knockout tumours showed differences in histology, with significant reductions in microvessel density (CD31) and pericyte coverage (CD31/αSMA), and a trend towards increased necrosis and hypoxia compared to those of the littermate control group. These observations were similar to that of the constitutive endothelial cell-specific *Eltd1* knockout group. The inducible endothelial cell-specific *Eltd1* knockout model might have been expected to show more significant differences in tumour growth and survival outcomes than the constitutive knockout model since there was a significant difference in the sprouting phenotype in the inducible endothelial-*Eltd1* depleted aortic rings. One plausible explanation could be that the chosen cell lines, E0771 and MC38 were too aggressive and thus grew too fast before the effect of endothelial-*Eltd1* depletion could be observed. Therefore, in the future experiments could be performed using less aggressive cell lines or fewer number of injected cancer cells. Also, not all endothelial cells behave similarly. In this case the aortic ring sprouting phenotype involved aortic endothelial cells, which have different biology compared to the tumour endothelial cells.

Nevertheless, in both knockout models, no apparent significant differences in vessel morphology and density were observed in vital organs, but significant reduction in microvessel density in the tumours grown in *Eltd1*-knockout mice was observed. This suggested that established vessels might not require *Eltd1* to maintain the vascular morphology and density. It could also be due to the insufficient reduction of *Eltd1* in the vital organs in the inducible endothelial cell-specific *Eltd1* knockout mice as the tamoxifen penetrance and efficiency might differ in different organs with the current schedule of tamoxifen induction.

In tumours harvested from both the constitutive and inducible endothelial cell-specific *Eltd1* knockout mice, there were significant reductions in microvessel density (CD31) and pericyte coverage (CD31/αSMA). This demonstrated that genetic endothelial-*Eltd1* deletion was sufficient to affect the tumour vasculature, supporting previous data from the lab which adopted *in vivo* endothelial-*Eltd1* silencing (Masiero et al., 2013). Furthermore, it showed that the effect of endothelial-*Eltd1* depletion could be observed more evidently in neovessels rather than established vessels. Interestingly, with the loss of Eltd1, there was a reduction in the pericyte coverage of $CD31^+$ vessels. This observation was consistent in two syngeneic

tumour experiments in both constitutive and inducible endothelial cell-specific *Eltd1* knockout models. This implied that there could be a crosstalk between *Eltd1*-positive endothelial cells and pericytes. And Eltd1 could serve as a means for communication between the two cell types such that the endothelial cells could signal the recruitment of pericytes.

The aortic ring angiogenesis assay performed in this chapter had variations within each experiment, though all three experiments conducted showed reduction in the sprouting area in the *Eltd1*-knockout aortas. It was later realised that the aorta is made up of endothelial cells of different biology, depending on the location of the aorta. The anatomical structure of the aorta consists of the aorta arch, descending aorta and various branches to the carotid, subclavian artery etc. And there are different blood flow patterns attributed to different hemodynamic shear stresses. Therefore, in the future it may be interesting to standardise the section of the aorta used in this assay and to track sequential aortic rings to determine whether their position affects the phenotype.

4.12 Conclusion

Acute endothelial-*Eltd1* depletion did not cause defects in mice except that acute endothelial-*Eltd1* depleted aortic rings showed significant inhibition of their vascular sprouting activity. In the syngeneic tumour models (E0771 and MC38), acute endothelial-*Eltd1* depletion in the mice prior to tumour inoculation generated tumours that exhibited significant reductions in microvessel density and pericyte coverage and a trend towards increased necrosis and hypoxia despite no significant difference in tumour growth curves and survival outcomes.

Chapter 5: Single cell genomics of acute *Eltd1*-depleted lung endothelial cells

5.1 Introduction

Over the years, there has been an increasing awareness of the cellular heterogeneity within tissues and that this exists even within subpopulations of the same cell type such as among endothelial cells or tumour cells. This can now be coupled with technological advancements which allow for information to be extracted at single cell resolution (Potter, 2018). The understanding of single cells in normal tissues could potentially shed light into normal physiology and developmental biology, while in pathological tissues, like tumours, this could enable the development of more targeted therapies with better efficacies and reduced toxicity.

Single cell sequencing technology could be utilised to investigate if Eltd1 might have different functionality in endothelial subsets. This information might then enable a better understanding of the functional role of Eltd1 in the vasculature.

Currently, there are two single-cell RNA sequencing (scRNA-seq) platforms that are frequently used (Svensson et al., 2018, Wang et al., 2019), namely Smartseq2 (Picelli et al., 2013) and 10X (10X Genomics Chromium, 10X Genomics, Pleasanton, CA). To dissect the gene expression profile of endothelial cells, Smartseq2 was chosen as this scRNA-seq platform is more sensitive for gene detection and has a lower dropout ratio compared to 10X (Wang et al., 2019). Also, as we wanted to define subpopulations, deeper sequencing was thought to be more appropriate. In Smartseq2, cells are seeded into microtiter plates where mRNA is then isolated and reverse transcribed to cDNA to be used for high-throughput sequencing for each individual cell (Stegle et al., 2015). The quantification of gene expression in each cell is then computed by reads mapped to a gene. Figure 5.1 gives an overview of Smart-seq2 library preparation (Picelli et al., 2014).

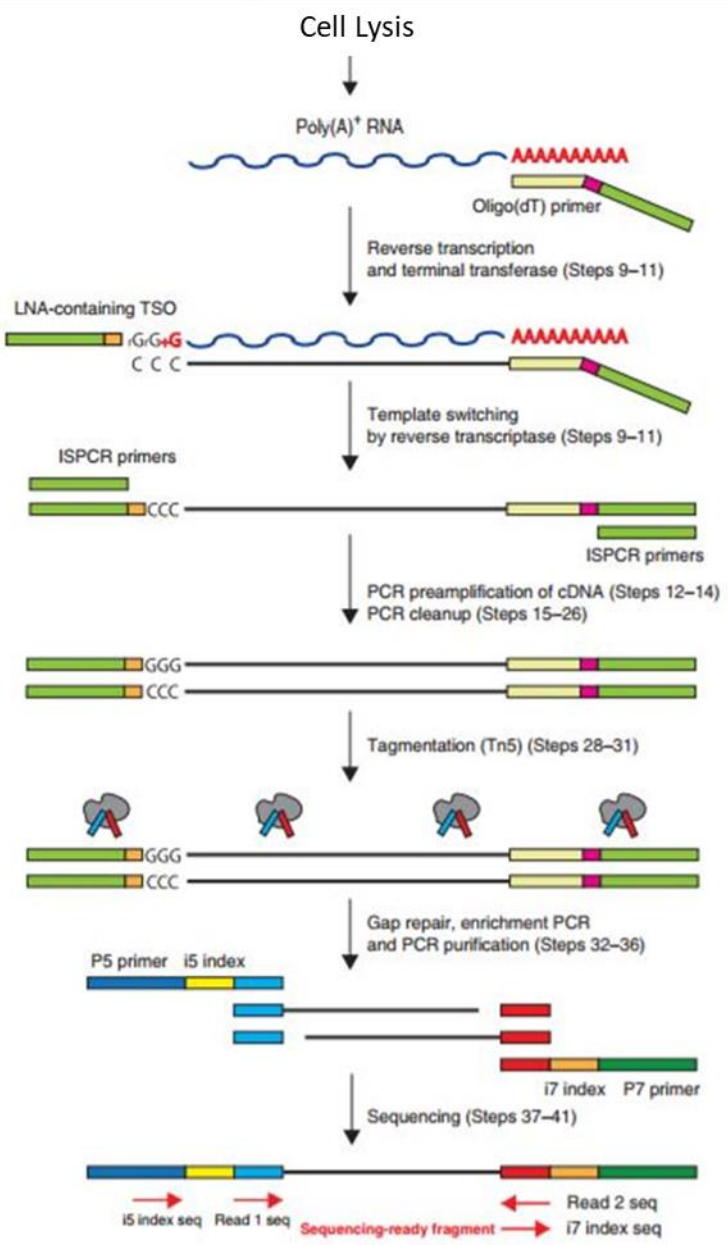

Figure 5.1: Overview of Smart-seq2 library preparation. After the cell has been lysed, the extracted RNA is then reverse transcribed to cDNA. In this protocol, template-switching oligos (TSO) that carry two riboguanosines located in the second and third positions with a modified guanosine, giving a locked nucleic acid (LNA) as the final base at the 3' end were used. This enhances the LNAs annealing to the 3' extension of the cDNA that is untemplated. Following this, the cDNA is amplified and the PCR product is later purified. Tagmentation is then used to efficiently construct sequencing libraries from the amplified cDNA. The fragments in the tagmented cDNA undergo enrichment PCR reaction and these samples are pooled and analysed in the DNA sequencer. Figure modified from Picelli et al, 2014.

The lung is a highly vascularised organ and is a common site of tumour metastasis. Moreover, mouse lungs had been reported to have a high *Eltd1* expression (Serban et al., 2015), as confirmed earlier in this thesis in Figure 5.2A. Interestingly, it was recently reported that the mouse lungs are comprised of not only of several vascular cell subsets, such as endothelial cells, pericytes and vascular smooth muscle cells etc, but also that the endothelial cell population could be further divided into a range of endothelial cell subsets such as arterial, capillary, lymphatic, continuum, and several uncharacterised subtypes of endothelial cells (He et al., 2018). From analysing the data from this study most of the lung vascular-associated cells did not express *Eltd1*, its expression being largely restricted to endothelial cells. Furthermore, mining this published data indicated that endogenous *Eltd1* expression varied between these different endothelial cell subsets, as shown in Figure 5.2B.

This chapter aims to investigate the gene expression profiles regulated by the acute loss of *Eltd1* in different subsets of lung endothelial cells.

A

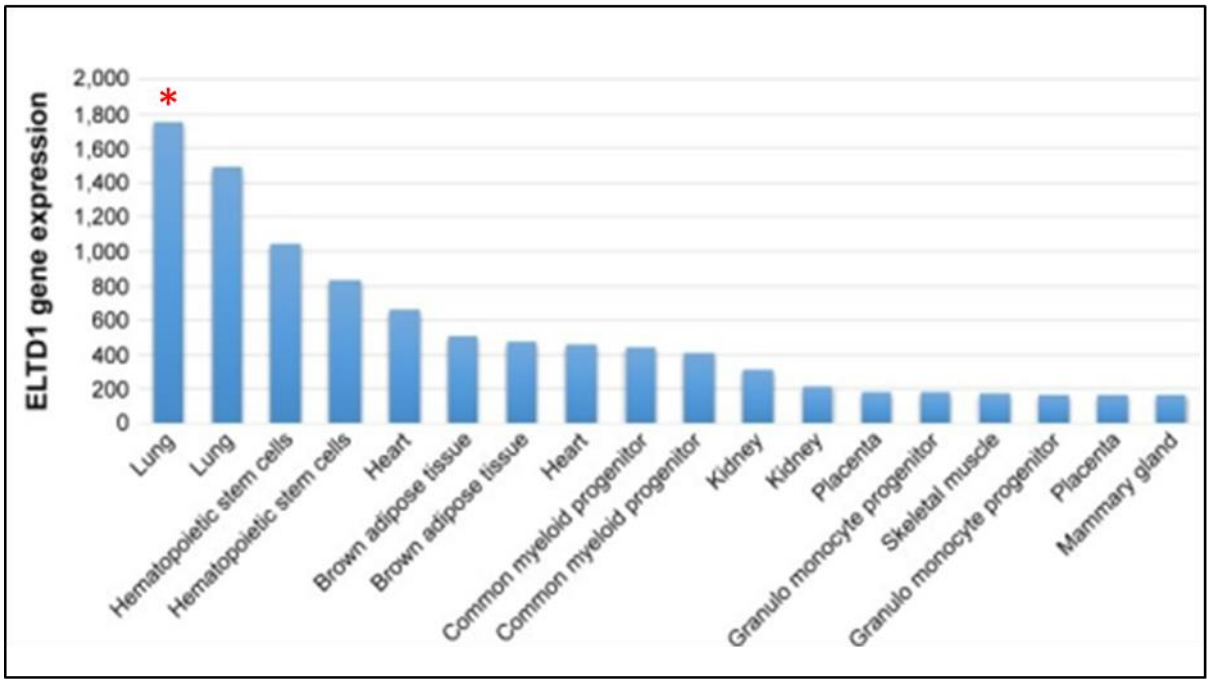

B

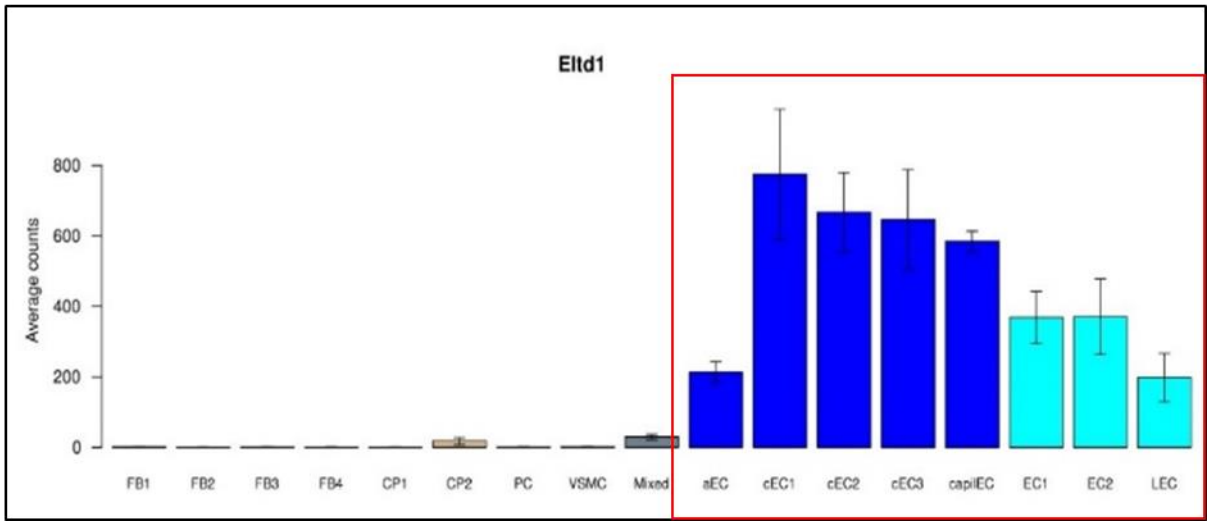

Figure 5.2: *Eltd1* expression in various mouse tissues and lung vascular-associated cell types. A) mouse tissues (Serban et al., 2015) with lungs (*) having the highest expression and B) vascular-associated cells in mouse lungs (He et al., 2018) with the endothelial cell population being highlighted. Figure 5.2B was generated from an online database (http://betsholtzlab.org/VascularSingleCells/database.html). Abbreviations: FB (Vascular fibroblast-like cells); CP (Cartilage perichondrium); PC (Pericytes); VSMC (Vascular smooth

muscle cells); EC (Endothelial cells); capil (Capillary); a (Arterial); c (Continuum); L (Lymphatic); 1,2,3,4 (Subtypes).

5.2 Experimental design

This experiment was conducted using the inducible endothelial cell-specific *Eltd1* knockout model, as described in chapter 4. Six age-matched (7 to 8 week-old) female mice, with the genotype of *Eltd1*$^{fl/fl}$*;Pdgfb-Cre*$^{+/-}$, were used in this experiment. Three mice were injected with tamoxifen to induce the endothelial-*Eltd1* deletion, the remaining three mice were the experimental controls. *Cre*$^{-/-}$ mice with tamoxifen were not used as control in this experiment as the EGFP marker from the Cre cassette was used to positively select *Pdgfb*$^{+}$ endothelial cells and thus enrich for those with *Eltd1* deletion in the tamoxifen treated group. The tamoxifen induction schedule was intraperitoneal injection of tamoxifen, 1 mg, for 5 consecutive days. This schedule was shown to be effective in inducing *Eltd1*-depletion in lung endothelial cells by RNA *in situ* hybridisation staining of lung sections and qPCR analysis of the EGFP^{+} lung endothelial cells, as previously reported in chapter 4. Ear notches were collected at the time of experiment and ear notch DNA genotyping showed the deleted *Eltd1* locus in the tamoxifen-treated group, which was indicative of *Eltd1* deletion, as shown in Figure 5.3A.

The lungs were removed from the euthanized mice at ten days after the last tamoxifen injection and the tissue was dissociated.

To ensure a good purity of endothelial cells after fluorescence-activated cell sorting (FACS), hematopoietic cells were excluded from the dissociated lung cell suspensions by selecting only the CD45-negative cells. These were then sorted for EGFP-positivity and purified further with the endothelial markers CD31 and VECadherin, as shown in Figure 5.3B. The triple positive cells were sorted singly into 96-well plates and were sent for a single cell sequencing experiment. A total of 768 lung endothelial cells from six mice were analysed, including 96 cells from each mouse and an additional 96 cells each from two of the tamoxifen-treated mice. The reason for using more cells from the tamoxifen-treated group was due to the possibility that the knockout may not occur in all endothelial cells as expected and this would increase the chances of harvesting the *Eltd1* knockout cells.

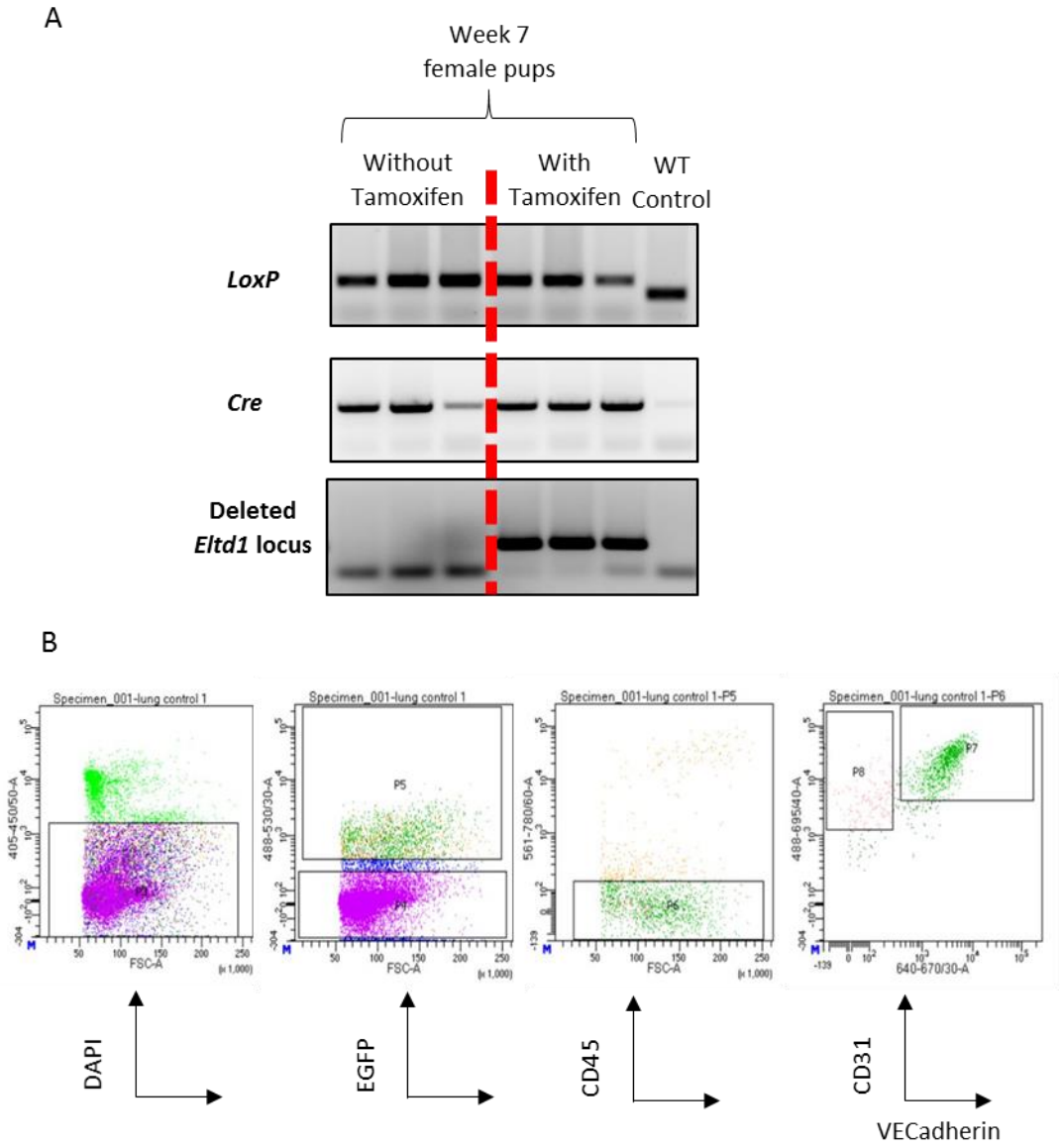

Figure 5.3: Experimental setup of sample preparation for scRNA-seq experiment. A) Ear notch DNA genotyping showed deleted *Eltd1* locus in notches from tamoxifen-treated mice but not in the untreated group. B) FACS profile of isolated cells for scRNA-seq.

5.3 Quality check of scRNA-seq data

Before commencing analysis of the single cell sequencing data, the quality of the data was inspected. This was executed by an expert bioinformatician who was experienced in analysing single cell sequencing data, Dr Dimitrios Voukantsis (University of Oxford). Cells with small library sizes and having less than 1000 genes with a non-zero count read were regarded as

poor quality and thus were excluded from the analysis. As shown in Figure 5.4, a total of 233 control cells and 351 knockout cells were used for further analysis. The downstream analysis of these data was conducted with the ongoing scientific input from Koon Hwee Ang and with specialised computational bioinformatic analysis performed by Dr Dimitrios Voukantsis, using the pipeline developed by Professor Francesca Buffa and Dr Wei Cheng. The input included a knowledge of the scientific field and further studies of the literature to refine subsequent downstream analyses and devise hypotheses that could be tested using additional analyses.

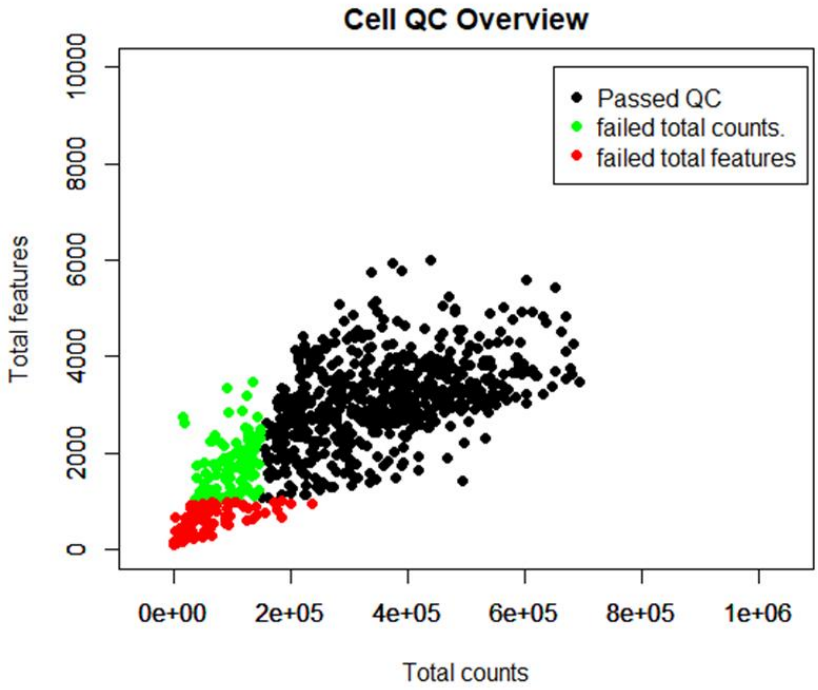

Figure 5.4: Quality control of scRNA-seq data. Total counts represents the sum of counts (transcript) per cell (library size) and total features is the number of genes with non-zero counts. Cells with small library sizes and less than 1000 genes with non-zero count read were of poor quality and were excluded in further analysis.

5.4 Characterisation of lung endothelial cell subsets

The initial analysis of pooled endothelial cells does not really exploit the power of using single cell sequencing technology. It was reported in 2018 by He *et al* that lungs in C57BL/6 mice contained different endothelial cell subsets namely, arterial, capillary, lymphatic, continuum

and other uncharacterised subtypes of endothelial cells (He et al., 2018). However, the information reported in the paper was not sufficient to enable us to independently identify these endothelial cell subtypes. Therefore, the corresponding author of the paper was contacted and we were able to obtain additional data that could facilitate this cell characterisation work and enable us to compare our findings using the published endothelial cell subsets.

By comparing our sequencing data with previously reported datasets (Vanlandewijck et al., 2018, He et al., 2018), two main endothelial cell populations were identified among our $EGFP^{+}/Cd31^{+}/VE\text{-}Cadherin^{+}$ lung cells. Namely, arterial (132 cells, 22.6 % of total cell population) and capillary endothelial cells (422 cells, 72.3 % of total cell population), as shown in Figure 5.5. There were very few cells of other identities such as, lymphatic endothelial cells, continuum endothelial cells, uncharacterised endothelial cell type, pericytes, fibroblasts and cartilage perichondrium (about 5%). The sample sizes of these rare cell types were too small to make any meaningful analyses. The focus of the work in this chapter has been on comparing the data obtained from the entire lung cell population with that from the arterial and capillary endothelial cell subsets to investigate whether Eltd1 biology might differ within endothelial cell subpopulations.

A

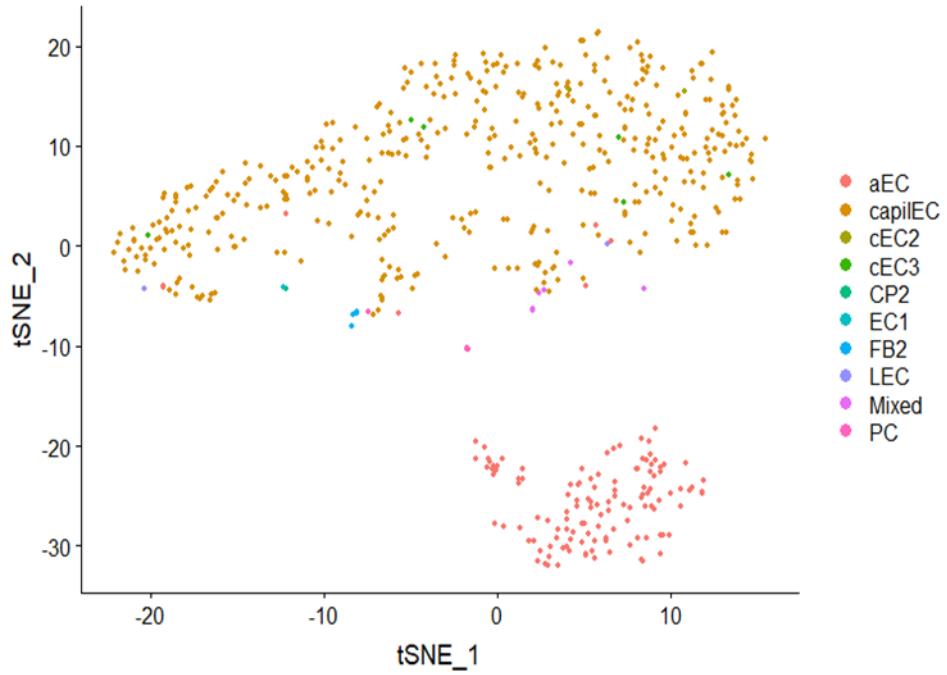
20
10
0
-10
-20
-30
tSNE_2
-20
-10
0
10
tSNE_1
aEC
capilEC
cEC2
cEC3
CP2
EC1
FB2
LEC
Mixed
PC

B

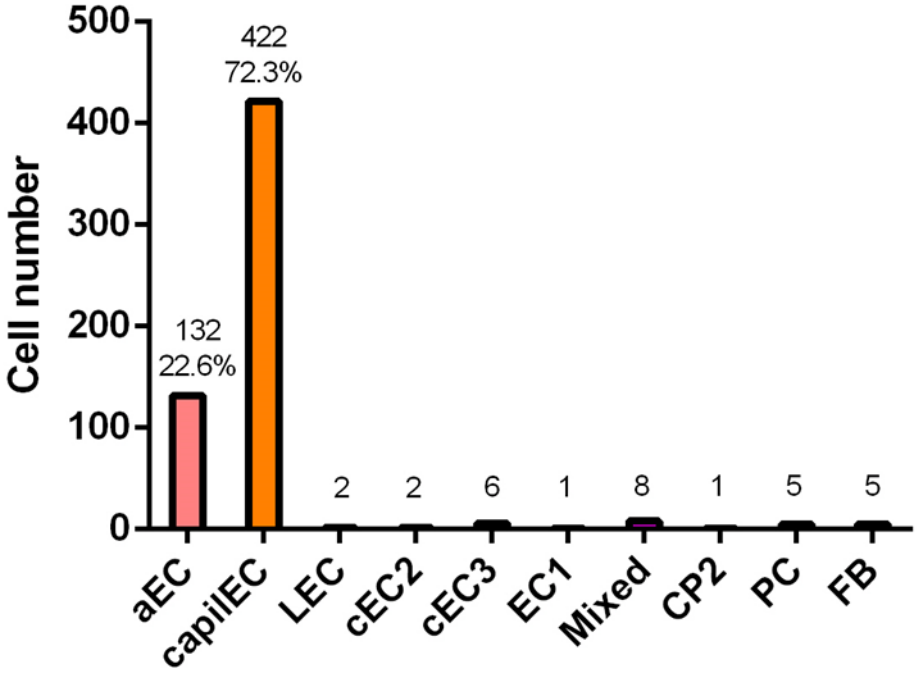
Cell number
500
400
300
200
100
0
132
22.6%
422
72.3%
2
2
6
1
8
1
5
5
aEC
capilEC
LEC
cEC2
cEC3
EC1
Mixed
CP2
PC
FB

Figure 5.5: Characterisation of endothelial cell types. A) A tSNE (t-distributed stochastic neighbour embedding) plot is a dimensionality technique that provides a graphical way to simplify a large dataset for visualisation of the data. This plot shows that within our $EGFP^{+}VECadherin^{+}Cd31^{+}$ population there were mainly two endothelial cell clusters present, namely arterial and capillary endothelial cells. B) A bar chart showing that capillary endothelial cells were the majority, with a total of 422 cells (72.3% of total cell population) and comprising 68.2% and 74.9% in control and knockout groups respectively. Arterial endothelial cells were the second significant endothelial cell subset with a total of 132 cells (22.6% of total cell population) and 25.3% and 20.8% in control and knockout groups respectively. Other cell subsets were identified such as lymphatic endothelial cells, continuum endothelial cells subtypes 1 and 2, endothelial cells subtype 1, cartilage perichondrium, pericytes and fibroblasts. However, these identified cell subsets were of too small a sample size to enable any statistically meaningful analyses as separate subpopulations.

5.5 Data analyses performed and statistical tests

After the data had been screened for quality control, a series of analyses on differential gene expression profile was conducted as described below:

1) between cells in untreated and tamoxifen-treated groups
2) between cells with and without *Eltd1* (exons 4 and 5)

Three statistical tests, namely Wilcox, edgeR and MAST tests were used to assess the significance of the differential expression of individual genes between control and *Eltd1* knockout endothelial cells.

The Wilcox-rank sum test is a non-parametric test which tests the difference in median expression between the two groups. EdgeR is based on a binomial model of gene expression and uses a generalised linear model. MAST tests for differential expression to combine test of discrete (0 vs not zero) and continuous (non-zero values) aspects of gene expression.

In all of these analyses, the differential expressed genes, that were significant in one of the statistical tests, were ranked in order of fold changes, either most upregulated or downregulated with *Eltd1*-depletion. It was observed that the genes at the lowest end of the

list ranked by log (fold change) were shown to be significant using MAST test. This gave an indication that MAST might not be a suitable statistical test in our analyses as very small fold changes, although statistically significant, might not be biologically relevant. Moreover, if the analyses were restricted to genes with differential expression that were significant in all three tests, there would be very few gene targets to work on, as shown in Figure 5.6. Hence, in the downstream analyses, we focused on genes that have either log (fold change)>2/<-2 and whose differential expression was significant in at least one test, or log (fold change)<2/>-2 and significant in both Wilcox and edgeR tests. These genes were then further investigated for literature identifying their association with endothelial biology, angiogenesis, tumour development and/or immunology. Genes related to endothelial biology and angiogenesis were further described in detail. The complete lists of differentially expressed genes with statistical significance and fold changes are provided in the Appendix 7.2 to 7.5.

5.6 Analysis of cells in untreated and tamoxifen-treated groups

5.6.1 Overview of the differentially expressed genes

As shown in Figure 5.6A, a total of 203 genes were identified as being significantly differentially expressed ($p < 0.05$) in the tamoxifen-treated total $EGFP^+/Cd31^+/VE\text{-}Cadherin^+$ lung cell population by at least one of the tests and 34 differentially regulated genes were significant in all three tests.

In lung arterial endothelial cells (Figure 5.6B) and lung capillary endothelial cells (Figure 5.6C) from the tamoxifen-treated group, 83 genes and 144 genes were significantly differentially expressed in which only 14 and 25 differentially expressed genes were significant in two tests namely, Wilcox and edgeR. The much smaller number of genes in both arterial and capillary endothelial cells reflects the much smaller sample size and corresponding loss of statistical power in the analyses.

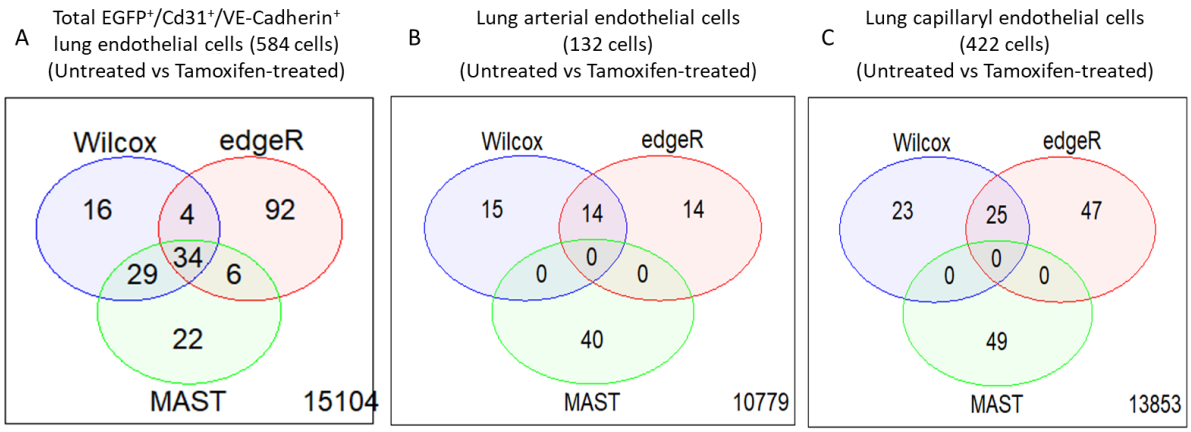

Figure 5.6: Venn diagrams of significant differential gene expression profiles using Wilcox, edgeR and MAST statistical tests. Differential gene expression profile between untreated and tamoxifen-treated A) total EGFP$^+$/Cd31$^+$/VE-Cadherin$^+$ lung endothelial cells (584 cells), B) lung arterial endothelial cells (132 cells) and C) lung capillary endothelial cells (422 cells). In the total EGFP$^+$/Cd31$^+$/VE-Cadherin$^+$ lung endothelial cells, 34 differentially regulated genes were significant in all three statistical tests (A) whereas in arterial and capillary endothelial cells, there were only 14 and 25 differentially regulated genes respectively that were significant in two statistical tests namely, Wilcox and edgeR. Colour legends: Blue (Wilcox), red (edgeR) and green (MAST).

In the total EGFP$^+$/Cd31$^+$/VE-Cadherin$^+$ lung endothelial cell population, out of the 34 differentially expressed genes between untreated and tamoxifen-treated groups that were significant in three statistical tests, 22 genes were predicted genes (Figure 5.7 and Table 5.1). Whereas in the arterial and capillary endothelial subpopulations, there were 11 predicted genes (out of 14 genes) and 16 predicted genes (out of 25 genes), as shown in Tables 5.2 and 5.3. Most of these predicted genes were pseudogenes. Pseudogenes are copies of protein-coding genes that result from genomic duplication or retrotransposition of mRNA sequences into the genome and with subsequent accumulation of mutations that lead to their degeneration (Sasidharan and Gerstein, 2008). They have been associated with potential roles in regulating the expression and function of cognate wild type genes by various ways such as, being a source of endogenous siRNAs (Tam et al., 2008) and antisense transcripts

(Zheng et al., 2007). These genes often complicate the analysis of gene expression due to their high occurrence in the genome, representing almost every coding gene and having a close sequence similarity with their cognate genes (Kalyana-Sundaram et al., 2012). Due to the lack of information of these pseudogenes that were significantly differentially expressed, it was not able to make conclusions and perform further analyses at this stage.

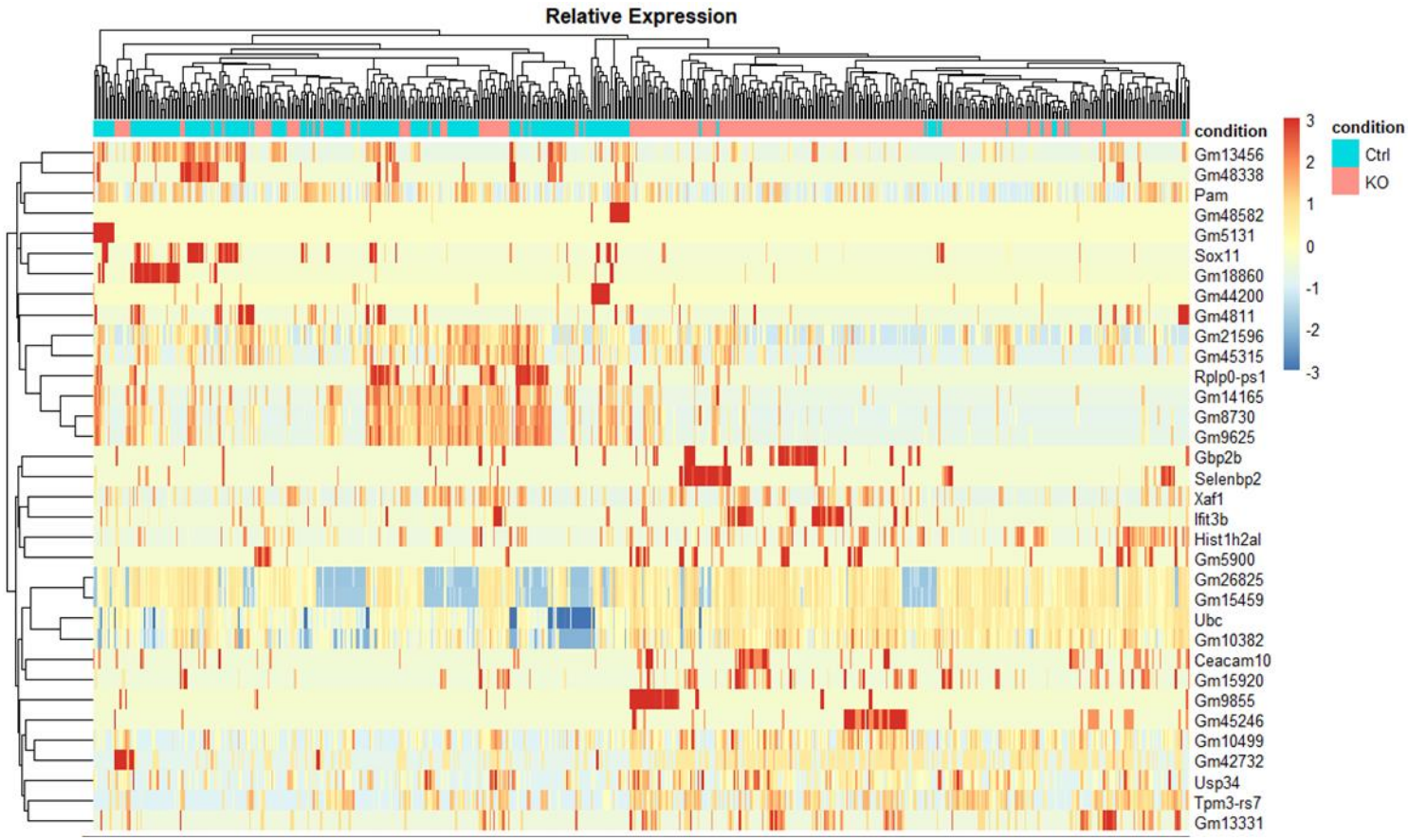

Figure 5.7: Heatmap of 34 differentially expressed genes that were significant in Wilcox, EdgeR and MAST tests. In this list, 22 genes were predicted genes which were mostly pseudogenes. Pseudogenes are copies of protein-coding genes that result from genomic duplication or retrotransposition of mRNA sequences into the genome and with subsequent accumulation of mutations that lead to their degeneration.

Expression	Symbol	Gene type	Gene description
Upregulated	*Gm9855*	Pseudo	thymine DNA glycosylase
	Gm5900	Pseudo	MAPK scaffold protein 1
	Gm15920	protein coding	-
	Gm13331	pseudo	ubiquitin-conjugating enzyme E2D
	Gm45246	pseudo	-
	Gm10499	protein coding	-
	Gm42732	predicted but unknown	-
	Gm10382	protein coding	-
	Gm15459	pseudo	heat shock protein 8
	Gm26825	protein coding	-
Downregulated	*Gm48582*	predicted but unknown	-
	Gm44200	predicted but unknown	-
	Gm18860	pseudo	CCR4-NOT transcription complex, subunit 8
	Gm13456	pseudo	eukaryotic translation elongation factor 1 alpha 1
	Gm8730	pseudo	ribosomal protein, large, P0
	Gm9625	pseudo	ribosomal protein, large, P0
	Gm48338	predicted but unknown	-
	Gm14165	pseudo	ribosomal protein, large, P0
	Gm4811	pseudo	SWI/SNF related, matrix associated, actin dependent regulator of chromatin, subfamily e, member 1
	Gm45315	predicted but unknown	-
	Gm21596	protein coding	-
	Gm5131	pseudo	Acyl-Coenzyme A dehydrogenase, medium chain

Table 5.1: List of differentially expressed predicted genes in the total EGFP$^+$/Cd31$^+$/VE-Cadherin$^+$ lung endothelial cell population between untreated and tamoxifen-treated groups.

Expression	Symbol	Gene type	Gene description
Upregulated	*Gm9855*	pseudo	thymine DNA glycosylase
	Gm15920	protein coding	-
	Gm5900	pseudo	MAPK scaffold protein 1
	Gm13331	pseudo	ubiquitin-conjugating enzyme E2D 3
	Gm10382	protein coding	-
Downregulated	*Gm48582*	predicted but unknown	-
	Gm9625	pseudo	ribosomal protein, large, P0
	Gm8730	pseudo	ribosomal protein, large, P0
	Gm13456	pseudo	eukaryotic translation elongation factor 1 alpha 1
	Gm48338	predicted but unknown	-
	Gm14165	pseudo	ribosomal protein, large, P0

Table 5.2: List of differentially expressed predicted genes in lung arterial endothelial cell population between untreated and tamoxifen-treated groups.

Expression	Symbol	Gene type	Gene description
Upregulated	*Gm5900*	pseudo	MAPK scaffold protein 1
	Gm13331	pseudo	ubiquitin-conjugating enzyme E2D 3
	Gm42732	predicted but unknown	-
	Gm15920	protein coding	-
	Gm45246	pseudo	-
	Gm10499	protein coding	-
	Gm10382	protein coding	-
Downregulated	*Gm18860*	pseudo	CCR4-NOT transcription complex, subunit 8
	Gm27194	tRNA	-
	Gm13456	pseudo	eukaryotic translation elongation factor 1 alpha 1
	Gm8730	pseudo	ribosomal protein, large, P0
	Gm9625	pseudo	ribosomal protein, large, P0
	Gm48338	predicted but unknown	-
	Gm14165	pseudo	ribosomal protein, large, P0
	Gm45315	predicted but unknown	-
	Gm21596	protein coding	-

Table 5.3: List of differentially expressed predicted genes in lung capillary endothelial cell population between untreated and tamoxifen-treated groups.

5.6.2 Differential gene expression profile of total EGFP$^+$/Cd31$^+$/VE-Cadherin$^+$ lung endothelial cells, lung arterial and capillary endothelial cells between untreated and tamoxifen-treated groups

5.6.2.1 *Eltd1* expression

5.6.2.1.1 Average Eltd1 counts

To confirm that the isolated cells were indeed endothelial cells, the expressions of *Cd31*, *VECadherin* and *Pdgfb* transcripts were also assessed, as shown in Figure 5.8. The expression levels of these genes were then matched with the expression of *Eltd1*. The majority of the cells were *Cd31*$^+$ and *VECadherin*$^+$. Interestingly, in total lung endothelial cell population (Figure 5.7A), lung arterial and capillary endothelial subpopulations, *Pdgfb* transcript expression was absent in at least 50% of the cells, both in untreated and tamoxifen-treated groups. A similar proportion of *Pdgfb*$^+$ and *Pdgfb*$^-$ cells in untreated and tamoxifen-treated groups were seen in both lung arterial (Figure 5.8B) and capillary (Figure 5.8C) endothelial cells. We suspect that this might be due to the insertion of the PAC cassette into the *Pdgfb* gene but cannot confirm this. This will be investigated in future experiments by repeating the single cell sequencing study in wildtype mice. Regarding *Eltd1* expression, there were more cells that lacked *Eltd1* expression in the knockout group compared to control.

However, *Eltd1* was not detected in a subset of cells in the untreated group, which complicated the analysis of the knockdown as cells with induced loss of *Eltd1* expression could not be distinguished from those that naturally lack *Eltd1* expression.

Eltd1 transcriptional downregulation (as a consequence of its knockout) in the EGFP$^+$/Cd31$^+$/VE-Cadherin$^+$ lung endothelial cells isolated from tamoxifen-treated mice showed significant downregulation (log (fold change) = -0.67) compared to those of untreated mice, as shown in Figure 5.9A. In endothelial cell subpopulations isolated from tamoxifen-treated mice, there was also a significant downregulation of (log (fold change) = -0.71) in the capillary endothelial cells (Figure 5.9B) but only a modest, not significant, reduction in arterial endothelial cells Figure 5.9C). This initial analysis was conducted by calculating the average counts of *Eltd1* (exons 1-16). The knockout strategy adopted in the inducible knockout mouse model used in this project, excised only exons 4 and 5 after Cre recombination. Though the expressions of exons 1 and 2 (5' to the deleted exons) and exons 7-8 (3' to the deleted exons)

had been shown to be significantly downregulated by qPCR, the downregulation was not as striking as exons 4 and 5, as shown in chapter 4. Interestingly, there was considerable cellular heterogeneity in the level of *Eltd1* expression in both control and knockout groups. This could be due to the varying degrees of *Eltd1* expression in different endothelial subsets identified from the He et al., 2018 dataset which showed that the more abundant capillary endothelial cell subset has a higher *Eltd1* expression which is important when analysing the knockout.

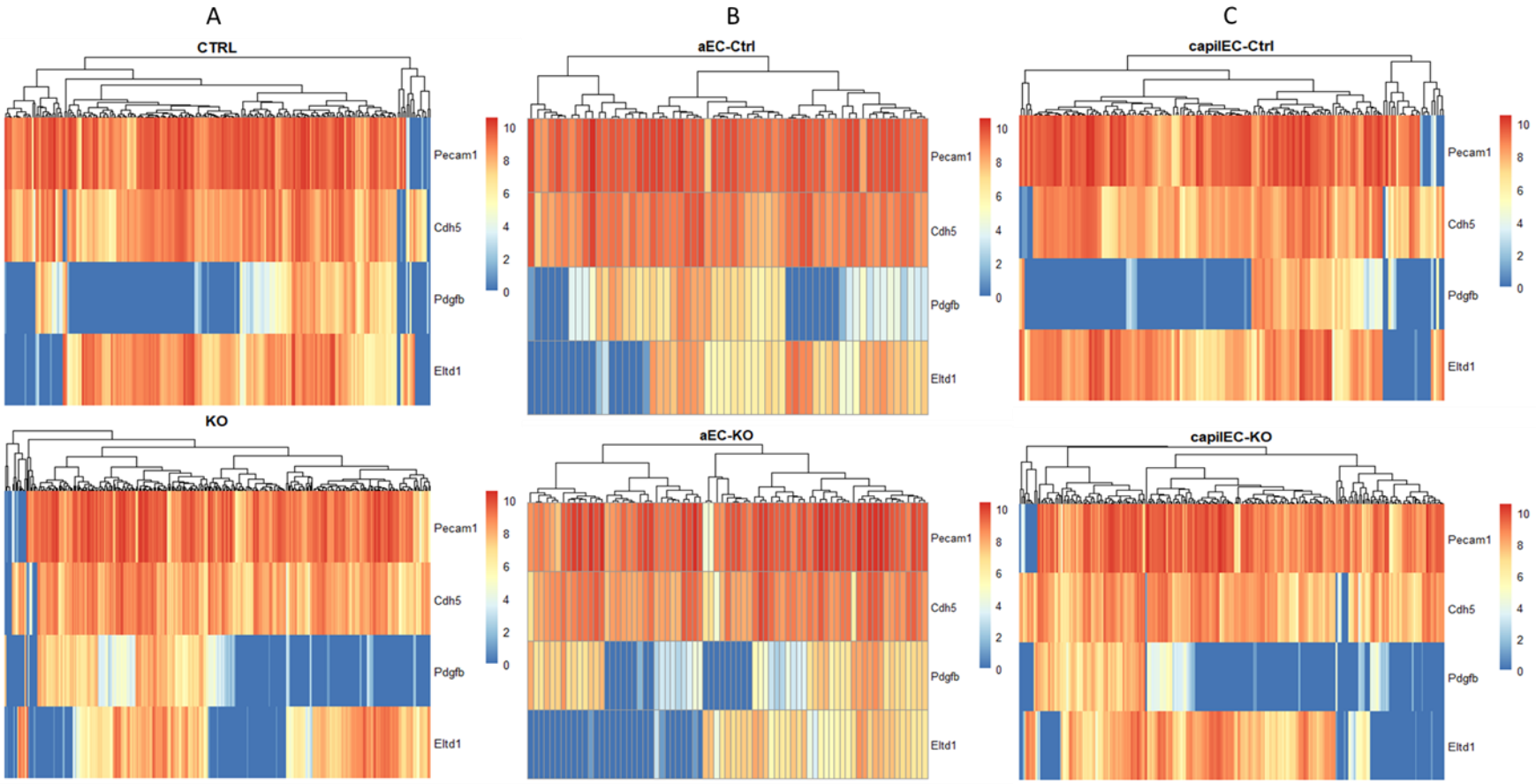

Figure 5.8: Heatmap of gene expressions in lung endothelial cells isolated from untreated (CTRL) and tamoxifen-treated (KO) mice. A) Total EGFP^{+}/Cd31^{+}/VE-Cadherin^{+} lung endothelial cells; B) lung arterial endothelial cells; C) lung capillary endothelial cells. The samples were largely of endothelial identity (CD31^{+} and VECadherin^{+}). Reduction in *Eltd1* expression was seen in total lung endothelial cells, lung arterial and capillary endothelial cells from the tamoxifen-treated group. Nomenclature: *Pecam1* (*Cd31*); *Cdh5* (*VECadherin*).

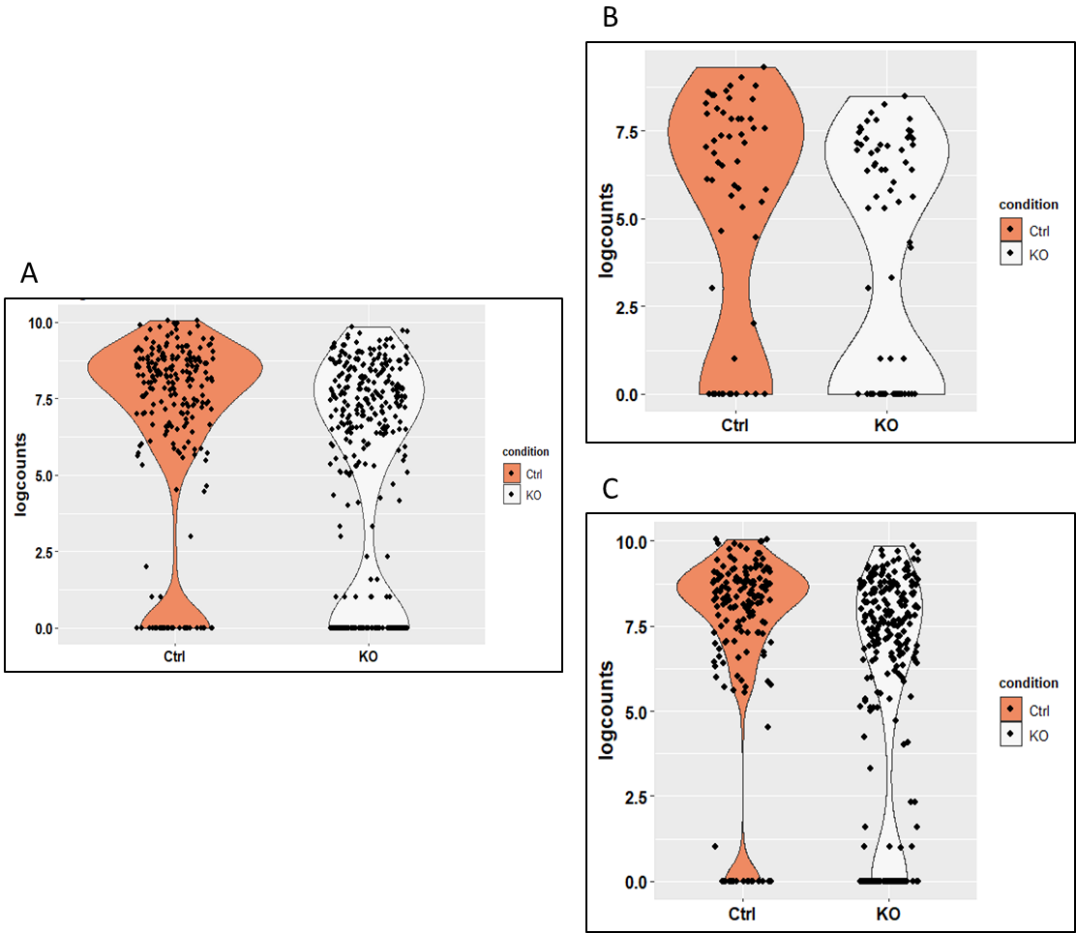

Figure 5.9: Violin plots of average *Eltd1* expression in lung endothelial cells isolated from untreated (Ctrl) and tamoxifen-treated (KO) mice. A) Total EGFP^{+}/Cd31^{+}/VE-Cadherin^{+} lung endothelial cells; B) lung arterial endothelial cells; C) lung capillary endothelial cells. Each dot represents a cell. In all three violin plots, there were cells that had endogenously undetectable levels of *Eltd1* expression, and there was cell heterogeneity in *Eltd1* expression in both untreated and tamoxifen-treated groups.

5.6.2.1.2 Raw counts of Eltd1 exons

To specifically assess the loss of exons 4 and 5 as a consequence of genetic *Eltd1* deletion, raw counts of *Eltd1* were analysed, as shown in Figures 5.10 and 5.11. It was observed that the raw counts of all exons were reduced, to varying degrees, in the tamoxifen-treated group compared to untreated. However, the reductions in exon 4 and 5 expression were considerably more marked. The varying degree of reduction in *Eltd1*expression could be due to the different basal expression of *Eltd1* in different endothelial cell subsets. The violin plots of all individual exons in cells between untreated and tamoxifen-treated groups (total lung endothelial cells, arterial endothelial cells and capillary endothelial cells) are provided in the Appendix 7.2.

In Figure 5.11A, 15.5% of the total lung endothelial cells in the untreated group did not show expression of *Eltd1*, across all exons. And this was increased to 27.4% in the tamoxifen-treated group. In lung arterial (Figure 5.10B) and capillary (Figure 5.10C) endothelial cells, there was an increase in 13% (from 25.4% to 38.4%) and 13.6% (from 10.7% to 24.3%) of cells that did not express *Eltd1* from the tamoxifen-treated group. In general, it could be observed that there was a downregulation of *Eltd1* (exons 1-16) in the tamoxifen-treated group compared to the untreated group.

Interesting in Figure 5.10, in general, endogenous expression of *Eltd1* exons 1, 5, 13 and 14 was low in the endothelial cells while there was a high expression of exon 16 in a proportion of cells. This suggests that *Eltd1* transcripts may have varying exon usage in endothelial cells.

After validating the *Eltd1* deletion in the endothelial population, we moved on to compare the differential gene expression patterns affected by *Eltd1*-depletion in the total and two endothelial subpopulations. For this analysis on the differential gene expression between cells in untreated and tamoxifen-treated groups, it is important to note that the effects were not entirely due to *Eltd1*-depletion as there may be other effects of tamoxifen and that *Eltd1* deletion was not complete

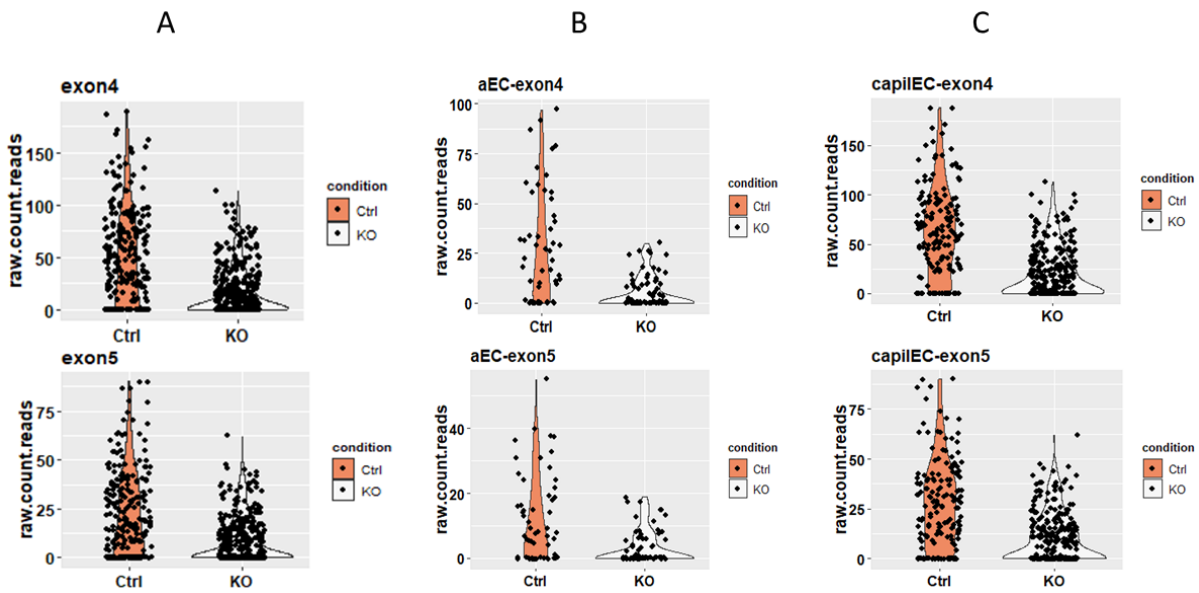

Figure 5.10: Violin plots of the raw counts of exons 4 and 5 of *Eltd1* in lung endothelial cells from untreated (Ctrl) and tamoxifen-treated (KO) groups. A) Total EGFP^{+}/Cd31^{+}/VE-Cadherin^{+} lung endothelial cells; B) lung arterial endothelial cells; C) lung capillary endothelial cells. Exons 4 and 5 showed marked reduction in the tamoxifen-treated group.

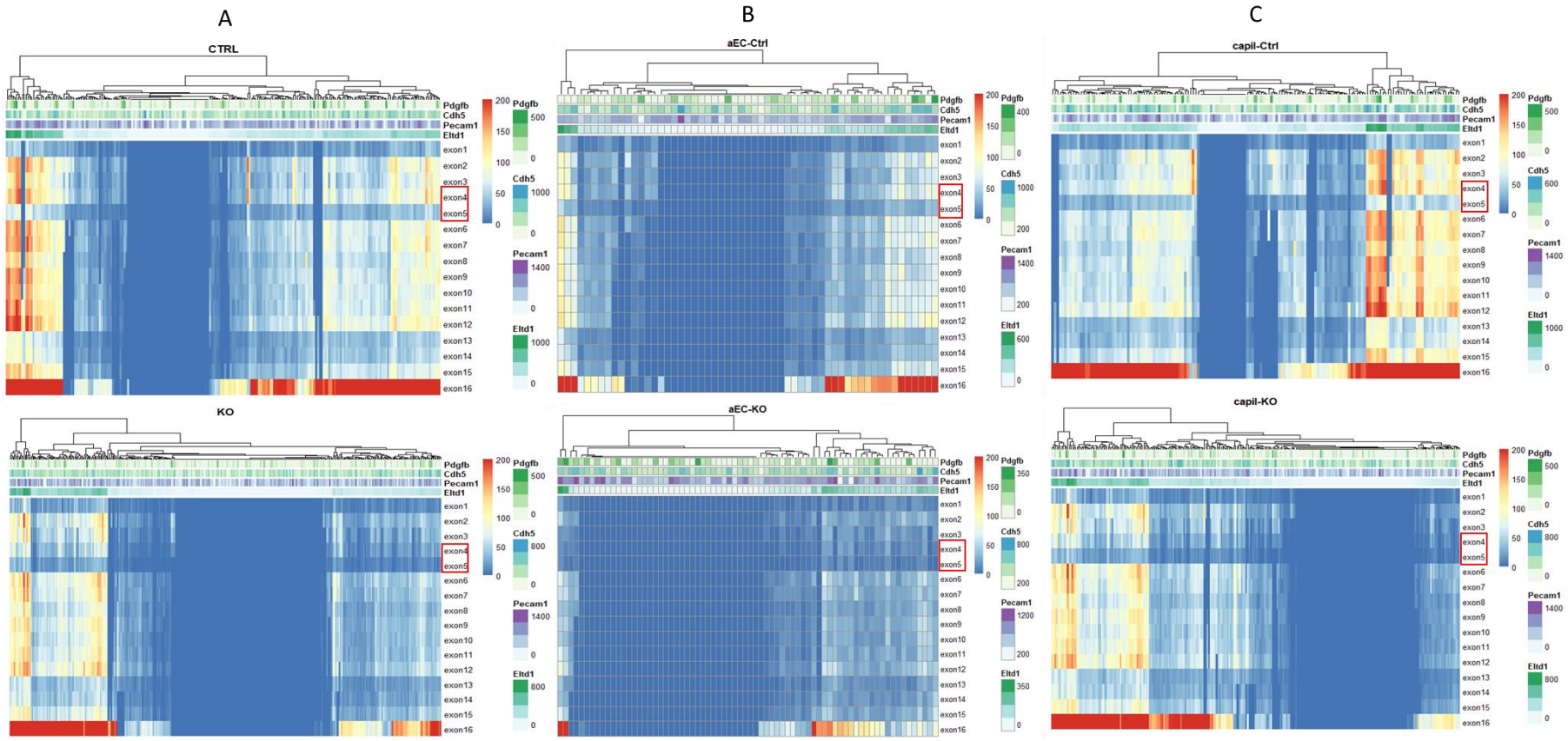

Figure 5.11: Heatmap of the expression of *Eltd1* exons (1-16) in lung endothelial cells isolated from untreated (CTRL) and tamoxifen-treated (KO) mice. A) Total EGFP^{+}/Cd31^{+}/VE-Cadherin^{+} lung endothelial cells; B) lung arterial endothelial cells; C) lung capillary endothelial cells. All exons showed varying degrees of reduction in *Eltd1* expression and a more marked reduction in exons 4 and 5 (highlighted in red). Nomenclature: *Pecam1* (*Cd31*); *Cdh5* (*VECadherin*).

5.6.2.2 Upregulated genes

5.6.2.2.1 Total lung endothelial cells

In the total $EGFP^+/Cd31^+/VE\text{-}Cadherin^+$ lung endothelial cell population, tamoxifen-induced *Eltd1*-depletion was associated with a significant, in at least one test, log(fold change) >2 upregulation of genes related to endothelial biology such as *Trpv4*, *Klf15* and Ifit3b. In addition, genes with log (fold change)<2, statistically significant, in all three tests, and are related to endothelial biology such as, *Xaf1* (Table 5.4).

Transient receptor potential vanilloid 4 (Trpv4) channels are mechanosensitive, Ca^{2+} permeable, nonselective cation channels that mediate highly localised Ca^{2+} signals in the endothelium. Endothelial Trpv4 is involved in the modulation of vascular tone by Ca^{2+}-induced Ca^{2+} release which acts on IP3 receptors (Heathcote et al., 2019). Trpv4 channels have low expression in tumour associated endothelial cells and are able to regulate tumour vessel integrity by maintaining the expression of VECadherin at points of cell to cell contact (Cappelli et al., 2019). Trpv4 channels were also a target for tumour metastasis (Cappelli et al., 2019).

Kruppel-like factor 15 (Klf15) has a role in several pathological conditions such as myocardial injury and nephropathy. Endothelial Klf15 has a protective role in TNF-α vascular endothelial dysfunction (Liu et al., 2018). Klf15 is involved in the effects of endothelin-1 on bone morphogenetic proteins endothelial cell precursor-derived regulator (BMPER) which is necessary for proper vessel formation (Helbing et al., 2010).

Interferon-induced protein with tetratricopeptide repeats 3B (Ifit3b) is an interferon-stimulated gene. It is strongly expressed in the endothelial cell biopsies from arm veins of patients suffering from systemic lupus erythematosus (SLE) whose endothelium is directly affected by interferon (Reynolds et al., 2014).

Xaf1 is a tumour suppressor gene that was shown to induce apoptosis and inhibit angiogenesis which result in the inhibition of development of hepatocellular carcinoma (Zhu et al., 2014).

In addition, there were upregulated genes associated with tumour development such as *Ncf2* (Xu et al., 2019), *Sftpb* (Lee et al., 2017), *Klf15* (Hou et al., 2019), *Intu* (Yang et al., 2017), *Ppargc1* (Li et al., 2017), *Trpv4* (Cappelli et al., 2019) and *Usp34* (Gu et al., 2019) and immunology such as *Gbp2b* (Sohrabi et al., 2018), *Ifi27l2a* (Lucas et al., 2016), *Il5ra* (Cheong

et al., 2005) (Table 5.4). Another target gene, *Selenbp2* was associated with playing a role in protecting retinal cells from oxidative stress (Ishikawa et al., 2010).

5.6.2.2.2 Lung arterial endothelial cells

In the arterial endothelial subpopulation, tamoxifen-induced *Eltd1*-depletion was associated with a single upregulated gene related to endothelial biology, *Fn1* (Table 5.5), whose altered expression was not detectable in the whole $EGFP^+/Cd31^+/VE\text{-}Cadherin^+$ population.

Fibronectin (Fn1), together with angiopoietin-1, modulates the cross talk between Tie2 and integrin signalling pathways which is important in the coordination of adhesion and migration of endothelial cells in response to the extracellular matrix (Dalton et al., 2016). This is interesting as adhesion GPCRs have similar roles.

In addition, some of the *Eltd1* regulated arterial endothelial genes have been associated with tumour development such as *Cop1*(Shao et al., 2013) and *Fn1* (Xu et al., 2015), and immunology such as, *Ifi27l2a* (Lucas et al., 2016).

5.6.2.2.3 Lung capillary endothelial cells

In the larger capillary endothelial subpopulation, tamoxifen-induced *Eltd1*-depletion was associated with upregulated genes related to endothelial biology such as *Ifit3b* and *Cgn* (Table 5.5).

Cingulin (Cgn) constitutes the cytoplasmic component of tight junctions. It has been shown to be expressed in the endothelial cells of skin, brain and lung. Its overexpression in HUVECs led to tight junction formation and strengthening of barrier function of the endothelium to low and high molecular weight tracers (Schossleitner et al., 2016).

In addition, some genes have been associated with tumour development such as, *P3h3* (Shah et al., 2009), *Cgn* (Citi et al., 1991), *MSI312* (Saleembhasha and Mishra, 2019), *Prkn* (Zijlstra et al., 1999) and *Usp34* (Gu et al., 2019), and immunology such as, *Gbp2b* (Sohrabi et al., 2018).

5.6.2.3 Downregulated genes

5.6.2.3.1 Total lung endothelial cells

In the total $EGFP^+/Cd31^+/VE\text{-}Cadherin^+$ cell population, tamoxifen-induced *Eltd1*-depletion was associated with downregulated genes (of log (fold change) <-2) related to endothelial

biology such as *Kcnk3*, *Trpc6*, *Prom1*, *Aqp7*, *Cyp26b1*, *Igfbp3* and *Esrα* (Table 5.1). In addition, a gene that was differentially expressed, with a log (fold change)>-2 but significant in two statistical tests and associated with angiogenesis such as *Sox11*.

Potassium channel subfamily K member 3 (Kcnk3) expression and function in pulmonary smooth muscle cells and endothelial cells has been shown to be significantly reduced in pulmonary arterial hypertension. Furthermore, Kcnk3 inhibition led to increased vasoconstriction and inflammation, contributing to the disease development (Antigny et al., 2016).

Transient receptor potential cation channel, subfamily C, member 6 (Trpc6) is expressed in endothelial cells and is able to regulate leukocyte transendothelial migration by mediating increased Ca^{2+} ion concentration (Weber et al., 2015).

Prominin-1 (Prom1)/CD133-positive pulmonary vascular endothelial cells have been shown to be 'tissue-resident' endothelial progenitor cells and these cells contribute to neovasculogenesis and homeostasis in pulmonary vascular tissues (Sekine et al., 2016).

Aquaporin (Aqp7) has been shown to have expression in the capillary endothelium of adipose tissue, cardiac and striated muscles and its expression is increased in the white adipose tissue in response to streptozotocin-induced diabetes mellitus which supports the role of Aqp7 in glycogen metabolism (Skowronski et al., 2007).

Cytochrome P450, family 26, subfamily b, polypeptide 1 (Cyp26b1) encodes an enzyme that is involved in the specific inactivation of all-trans retinoic acid to hydroxylated forms. The upregulation Cyp26b1 expression has been reported to induce angiogenesis (Messner et al., 2013).

Insulin-like growth factor binding protein 3 (Igfbp3) is the carrier protein for various circulating insulin-like factors such as, IGF-I and IGF-II). Its upregulation was reported to modulate the interaction of IGFs with the receptors at the site of hypoxic-ischemic injury in rat brains (Lee et al., 1999).

Estrogen receptor α (Esrα), together with 17-beta estradiol, have been demonstrated to modulate VEGFA expression in adipose tissue leading to increased angiogenesis, reduced inflammation and improved function of adipose tissue(Fatima et al., 2017).

SRY[sex determining region-Y]-box11 (SOX11) was demonstrated to promote angiogenesis via transcriptional regulation of PDGFA in mantle cell lymphoma (MCL). And the increased angiogenesis due to Sox11 led to a more aggressive phenotype (Palomero et al., 2014).

Moreover, some genes have been associated with tumour development such as, *Ltbp2* (Wang et al., 2018), *Aqp7* (Wang et al., 2015), *Slc25a43* (Lytovchenko and Kunji, 2017);*, Slc26a8* (Marín-Aguilera et al., 2015) and *Prom1* (Ding et al., 2013), as shown in Table 5.5.

5.6.2.3.2 Lung arterial endothelial cells

In the smaller arterial endothelial subpopulation, tamoxifen-induced *Eltd1*-depletion was not associated with downregulated genes related to endothelial biology (Table 5.5). It seems likely that there were insufficient numbers of cells analysed to detect the relatively small changes in gene expression. *Fancc* (Palagyi et al., 2010) and *Rab6b* (Sciabica et al., 2008) has been associated with tumour development.

5.6.2.3.3 Lung capillary endothelial cells

In the capillary endothelial subpopulation, tamoxifen-induced *Eltd1*-depletion was associated with downregulated genes related to endothelial biology such as *Prom1*, *Aqp7*, *Notch2*, *Cyp26b1, Esrα* and *Sox11* (Table 5.1). Interestingly, *Notch2* was the only gene whose differential expression was not also detectable in the $EGFP^+/Cd31^+/VE\text{-}Cadherin^+$ population.

Notch2 has been reported to be a target of miR-29a/b and the overexpression of miR-29a/b led to downregulation of Notch2 which inhibited high glucose-induced endothelial-mesenchymal transition (EndoMT) (Zhang et al., 2019).

In addition, some genes were associated with tumour development such as, *Prom1* (Ding et al., 2013), Slc25a43 (Lytovchenko and Kunji, 2017), Cyp26b1 (Brown et al., 2014) and *Notch2* (Garcia and Kandel, 2012) (Table 5.5).

Function associations	Gene expression and description		
	Total cell population	**Arterial endothelial cells**	**Capillary endothelial cells**
Endothelial biology, **Angiogenesis**	***Trpv4*** *(Transient Receptor Potential Cation Channel Subfamily V Member 4)*; ***Klf15*** *(Kruppel like factor 15)*; ***Ifit3b*** *(Interferon induced protein with tetratricopeptide repeats 3)*; ***Xaf1*** *(XIAP associated factor 1)*	***Fn1*** *(fibronectin 1)*	***Ifit3b***; ***Cgn*** *(cingulin)*
Tumour development	***Ncf2*** *(neutrophil cytosolic factor 2)*; ***Sftpb*** *(surfactant associated protein B)*; ***Klf15***; ***Intu*** *(inturned planar cell polarity protein)*; ***Ppargc1a*** (peroxisome proliferative activated receptor, gamma, coactivator 1 alpha); ***Trpv4***; ***Usp34*** *(ubiquitin specific peptidase 34)*	***Cop1*** *(COP1, E3 ubiquitin ligase)*; ***Fn1*** *(fibronectin 1)*	***P3h3*** *(prolyl 3 hydroxylase 3)*; ***MSl312*** *(MSL3 like 2)*; ***Cgn***; ***Prkn*** *(parkin RBR E3 ubiquitin protein ligase);* ***Usp34*** *(ubiquitin specific peptidase 34)*

Immunology	***Gbp2b*** *(guanylate binding protein 2b)*; ***Ifi27l2a*** (interferon, alpha-inducible protein 27 like 2A); ***Il5ra*** *(interleukin 5 receptor, alpha)*	***Ifi27l2a***	***Gbp2b***

Table 5.4: Upregulated genes related to endothelial biology, angiogenesis, tumour development and immunology. Genes in **black** are of log (fold change) >2 and significant in at least one statistical test while genes in **red** are of log (fold change) <2 and significant in all three tests.

Function associations	Gene expression and description		
	Total cell population	**Arterial endothelial cells**	**Capillary endothelial cells**
Endothelial biology, **Angiogenesis**	***Kcnk3*** *(potassium channel, subfamily K, member 3)*; ***Trpc6*** *(transient receptor potential cation channel, subfamily C, member 6)*; ***Prom1*** *(prominin 1)*; ***Aqp7*** *(aquaporin 7)*; ***Cyp26b1*** *(cytochrome P450, family 26, subfamily b, polypeptide 1)*; ***Igfbp3*** *(insulin-like growth factor binding protein 3)*; ***Esrα*** (estrogen receptor 1, alpha); ***Sox11*** *(SRY[sex determining region Y]-box 11)*	-	***Prom1***; ***Aqp7***; ***Notch2***; ***Cyp26b1***; ***Esrα;*** ***Sox11***
Tumour development	***Ltbp2*** *(latent transforming growth factor beta binding protein 2)*; ***Aqp7***; ***Slc25a43*** *(solute carrier family 25, member 43)*;	***Fancc*** *(Fanconi anemia, complementation group C);* ***Rab6b*** *(RAB6B, member RAS oncogene family)*	***Prom1***; ***Slc25a43***; ***Cyp26b1***; ***Notch2***

	Prom1; ***Slc26a8*** *(solute carrier family 26, member 8)*		

Table 5.5: Downregulated genes related to endothelial biology, angiogenesis and tumour development. Genes in **black** are of log (fold change) >2 and significant in at least one statistical test while genes in **red** are of log (fold change) <2 and significant in all three tests.

5.6.3 Pathway analyses of total lung endothelial cells, lung arterial and capillary endothelial cells from untreated and tamoxifen-treated group

5.6.3.1 Total lung endothelial cells

From the GO (gene ontology) enrichment analyses illustrated in Figure 5.12, tamoxifen treatment (induced *Eltd1* deletion) in total lung endothelial cells altered patterns of genes involved in multiple processes, including the response to interferon beta, homeostasis and transport of calcium ion, regulation of carbohydrate metabolic process, DNA repair etc.

Tamoxifen treatment (induced *Eltd1* deletion) was associated with both the VEGF and Notch signalling pathways that play important roles in angiogenesis, as shown in Figure 5.13. In the VEGF signalling pathway, *Eltd1* depletion resulted in the upregulation of *PKC*, *CALN*, *Rac* and downregulation of *SPK* and *PI3K*. The regulation of VEGF-induced microvascular permeability is dependent on Rac. The upregulation of *Rac* could suggest an increase in microvascular permeability.

In the Notch signalling pathway, tamoxifen treatment (induced *Eltd1* deletion) also led to the downregulation of *Notch* and *Deltex*. From previously published data (Masiero et al., 2013), it was reported that VEGF treatment in HUVECs led to an increase in ELTD1 expression. And DLL4 treatment resulted in a decrease in ELTD1 expression. However, this was done on HUVECs which might not be the same for other types of endothelial cells from a different tissue source.

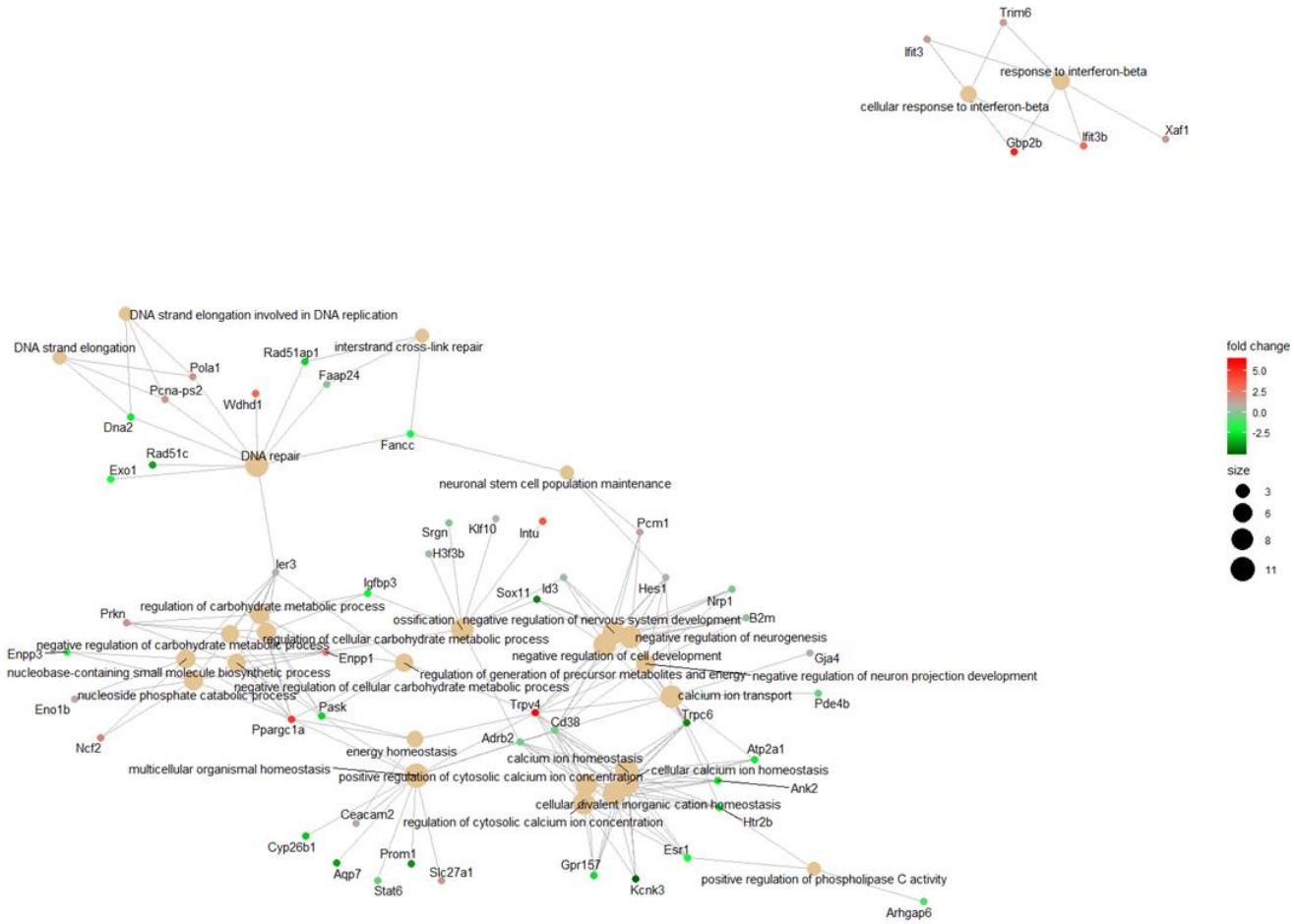

Figure 5.12: Biological processes and the differential expression of associated genes in total lung endothelial population in the tamoxifen-treated group compared to untreated group. Generated from Gene Ontology (GO) enrichment analysis.

A

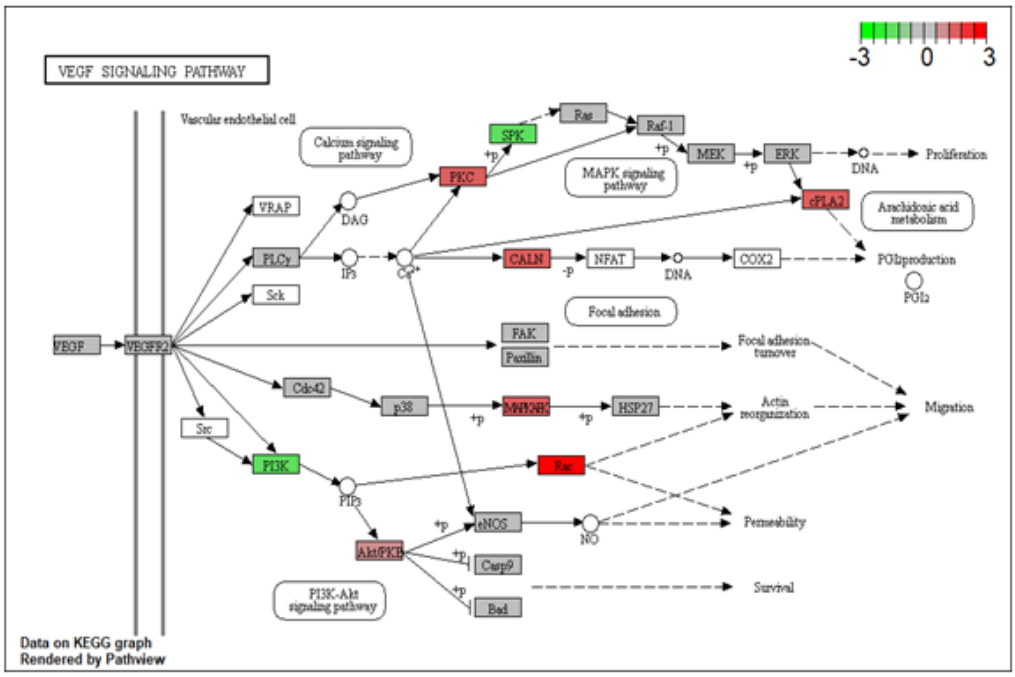

B

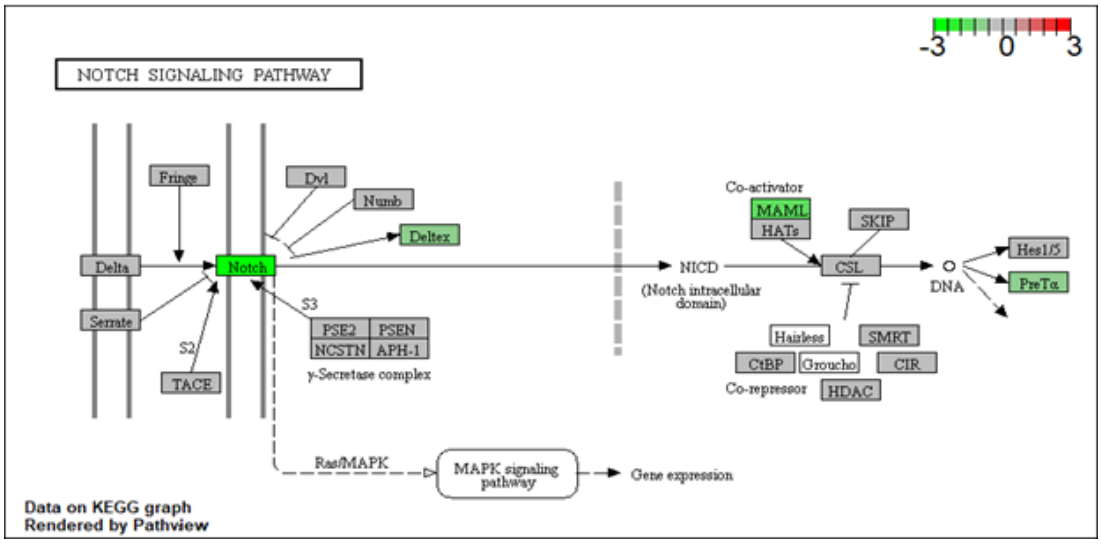

Figure 5.13: Pathway analyses (VEGF and Notch signalling) in in total lung endothelial population in the tamoxifen-treated group compared to untreated group. Figure generated from Kegg pathway enrichment analysis and KEGG module enrichment analysis.

5.6.3.2 Lung arterial endothelial cells

Due to the relatively small number of differentially expressed genes within the subpopulation of lung arterial endothelial cells, there were no outputs from Kegg pathway enrichment analysis and KEGG module enrichment analysis.

From the GO enrichment analysis shown in Figure 5.14, tamoxifen treatment (induced *Eltd1* deletion) in lung arterial endothelial cells was associated with functions in ubiquitin-like protein ligase binding and protease binding.

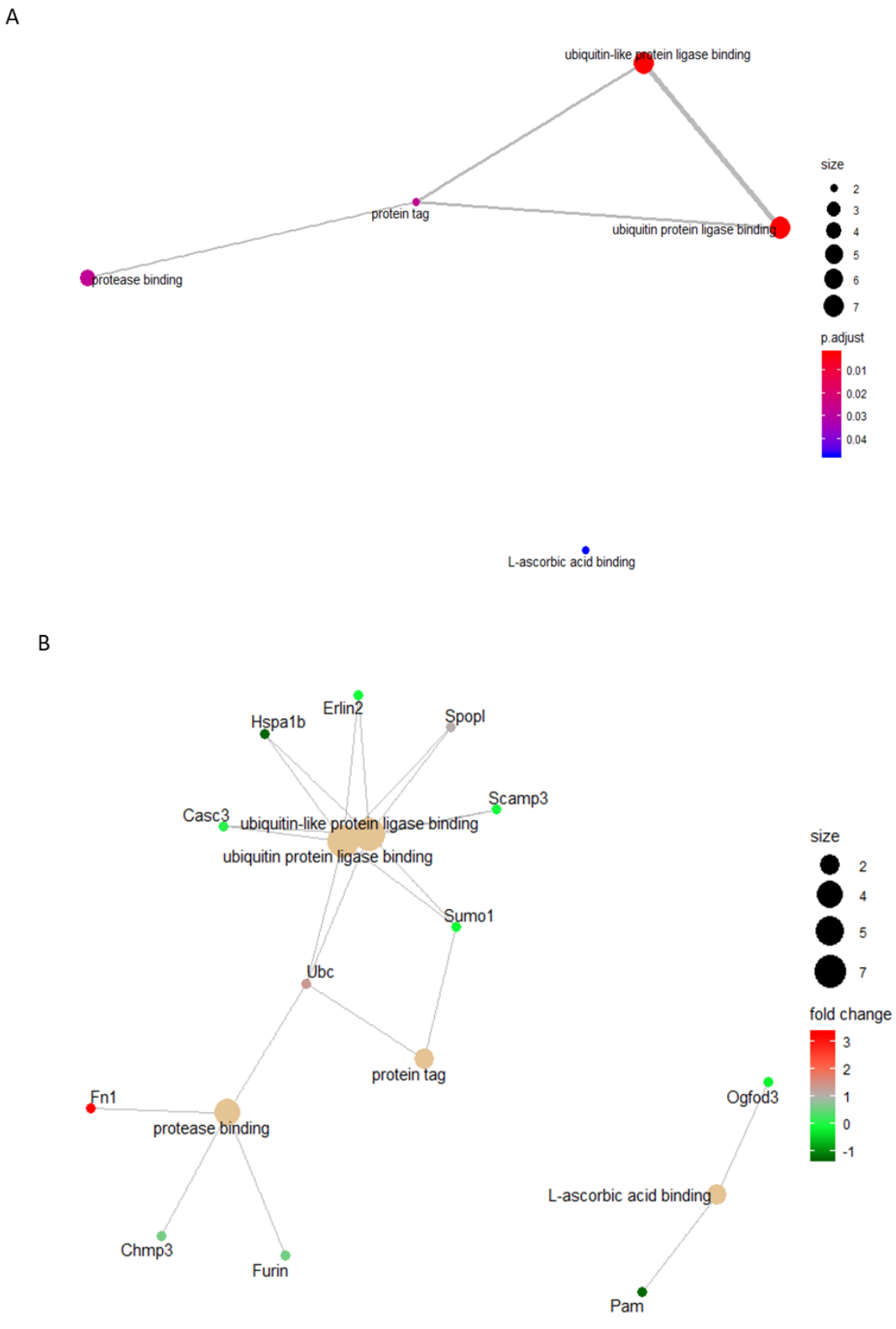

Figure 5.14: Biological processes and the expression of associated genes in lung arterial endothelial population in the tamoxifen-treated group compared to untreated group. Generated from Gene Ontology (GO) enrichment analysis.

5.6.3.3 Lung capillary endothelial cells

Due to the relatively small differentially expressed gene sets and population of lung arterial endothelial cells, there were no outputs from GO enrichment analysis, Kegg pathway enrichment analysis and KEGG module enrichment analysis.

Gene set enrichment analysis was done on the differentially gene expression profiles of lung capillary endothelial cells as shown in Table 5.6. This analysis utilised curated published gene signatures to visualise the potential functional implications of the differentially gene expression profiles. It showed that tamoxifen treatment (induced *Eltd1* deletion) could potentially affect pathways such as interferon pathway, tumour associated pathway, stem cell associated pathway etc. Interestingly response to tamoxifen came up in the list. There were several reports on the half-life of tamoxifen and it was mentioned to be about 12 hours (Robinson et al., 1991) while in this sequencing experiment, the lungs were harvested after 10 days. But unfortunately, there was not a $Cre^{-/-}$ control treated with tamoxifen to rule out the effect of tamoxifen on gene expression.

Tamoxifen treatment (induced *Eltd1* deletion) in lung capillary endothelial cells implicated both the VEGF and Notch signalling pathways as shown in Figure 5.15. In the VEGF signalling pathway, tamoxifen treatment (induced *Eltd1* deletion) was associated with the upregulation of *CALN* and *Akt/PKB* and downregulation of *SPK* and *eNOS*. The downregulation of *eNOS* could lead to a reduction in nitric oxide which could reduce microvascular permeability. In the Notch signalling pathway, tamoxifen treatment (induced *Eltd1* deletion) was also associated with *Notch*, *Delta* and *Deltex*.

Pathway	NES
MOSERLE_IFNA_RESPONSE	2.2901
HECKER_IFNB1_TARGETS	2.26622
FARMER_BREAST_CANCER_CLUSTER_1	2.18703
SEITZ_NEOPLASTIC_TRANSFORMATION_BY_8P_DELETION_UP	2.1323
REACTOME_INTERFERON_ALPHA_BETA_SIGNALING	2.12408
KRASNOSELSKAYA_ILF3_TARGETS_UP	2.12205
DAUER_STAT3_TARGETS_DN	2.10893
BOWIE_RESPONSE_TO_TAMOXIFEN	2.09028
BOWIE_RESPONSE_TO_EXTRACELLULAR_MATRIX	2.08282
BROWNE_INTERFERON_RESPONSIVE_GENES	2.03567
DER_IFN_ALPHA_RESPONSE_UP	2.02907
GRANDVAUX_IRF3_TARGETS_UP	2.01917
XU_AKT1_TARGETS_6HR	2.01465
ZHANG_INTERFERON_RESPONSE	2.01174
REACTOME_PLATELET_CALCIUM_HOMEOSTASIS	-1.9295
FONTAINE_PAPILLARY_THYROID_CARCINOMA_U	-2.0173
REACTOME_PRE_NOTCH_PROCESSING_IN_GOLGI	-2.0667

Table 5.6: Gene Set Enrichment Analysis (GSEA). Pathways implicated by the differential gene expression profiles in lung capillary endothelial population in the tamoxifen-treated group compared to untreated group, using Gene Set Enrichment Analysis (GSEA). Abbreviation: NES (Normalised enrichment scores).

A

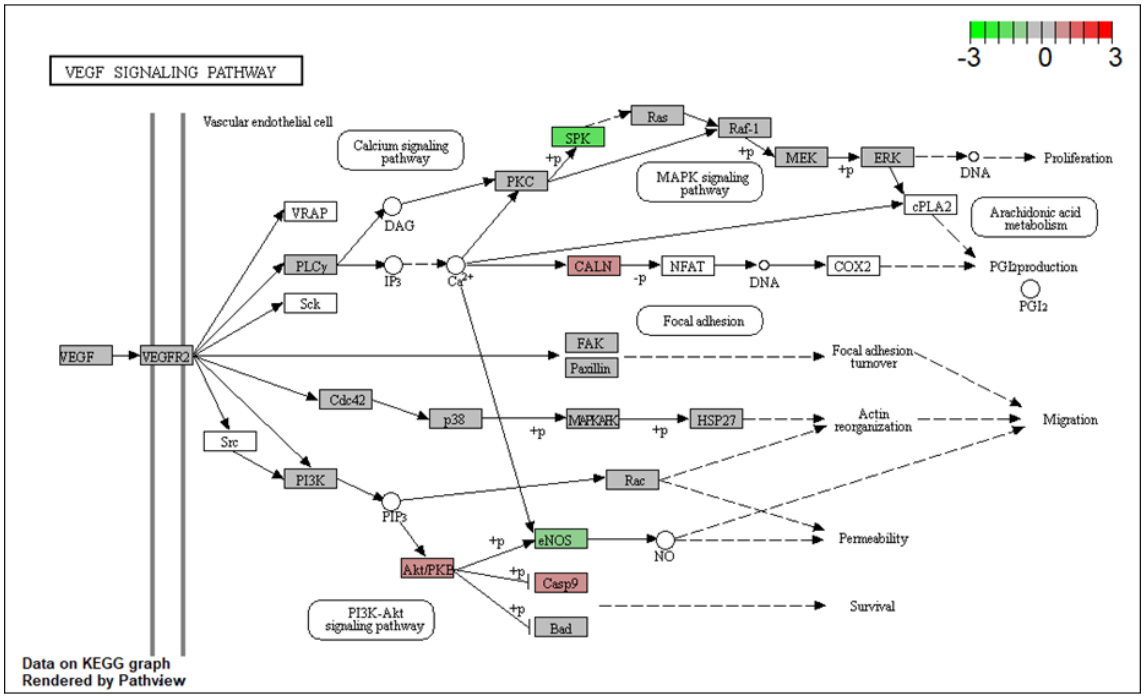

B

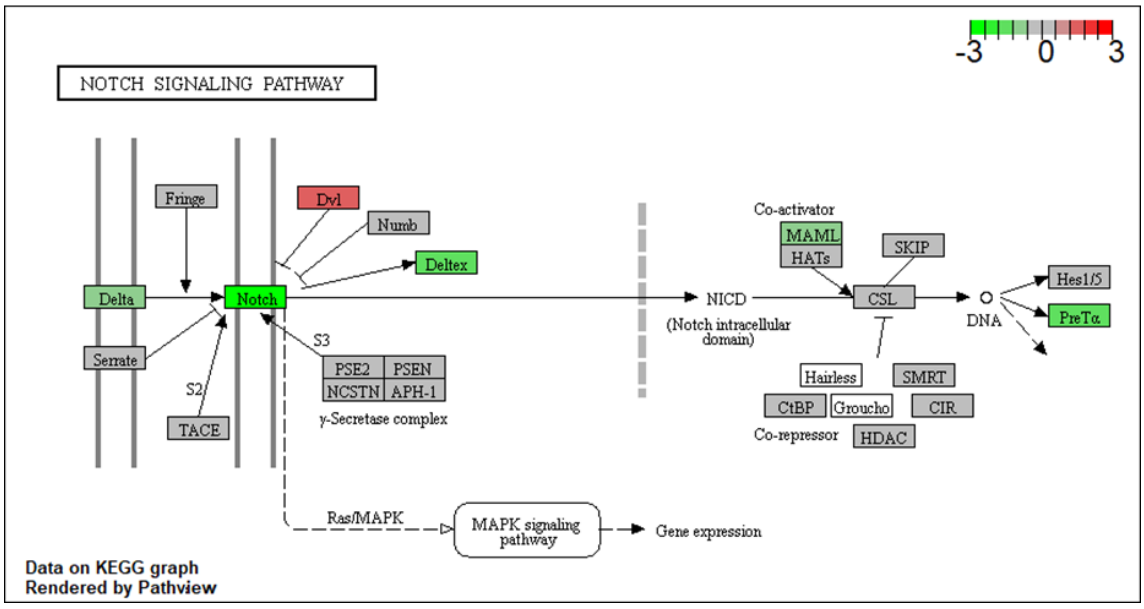

Figure 5.15: Pathway analyses (VEGF and Notch signalling) in lung capillary endothelial population in the tamoxifen-treated group compared to untreated group. Figure generated from Kegg pathway enrichment analysis and KEGG module enrichment analysis.

5.6.4 Conclusion

It was observed that the differentially expressed gene profile caused by tamoxifen treatment (induced *Eltd1* deletion) in lung arterial endothelial cells was different from lung capillary endothelial cells.

However, there were some limitations in this analysis. First, though there was a significant reduction in *Eltd1* expression in the tamoxifen-treated group, the knockout was not complete even the designed deletion strategy at exons 4 and 5. There were heterogeneity of cells in the level of *Eltd1* expression in both untreated and tamoxifen-treated groups. Secondly, in this experiment, there was not a $Cre^{-/-}$ control group with tamoxifen treatment, hence the effect of tamoxifen on the differential gene expression profile could not be ruled out.

To address the first limitation, it would be useful to perform the follow up analysis to compare the differential gene profile of the cells with and without *Eltd1* expression (exons 4 and 5) in untreated and tamoxifen-treated groups.

In addition, we also combined the *Eltd1*-depleted (all exons) cells from both untreated and tamoxifen-treated groups and compared with the rest. However, it was later thought that this analysis could be skewed due to the deletion strategy adopted in this model being focused on only exons 4 and 5. The list of differentially expressed genes in this analysis is provided in the Appendix 7.4 for reference.

5.7 Analysis of differential gene expression profile between cells with and without *Eltd1* (exons 4 and 5)

Since our adopted knockout strategy entailed the deletion of exons 4 and 5, and there were many cells in the tamoxifen-treated group that had much reduced expression of *Eltd1* exons, the analysis could be more stringent if only cells without the expression of exons 4 and 5 were considered. In this analysis, cells without exons 4 and 5 (n=390 cells) were compared with cells expressing one or both exons (n=189 cells), as shown in Figure 5.16.

Considering there is a very low expression of exon 5 in most cells in both untreated and tamoxifen-treated groups, a separate analysis was done on cells without exon 4 (n=387 cells) and cells with exon 4 (n=192 cells). The differential gene expression profile was very similar to that of the analysis on cells without exons 4 and 5 (Data not shown).

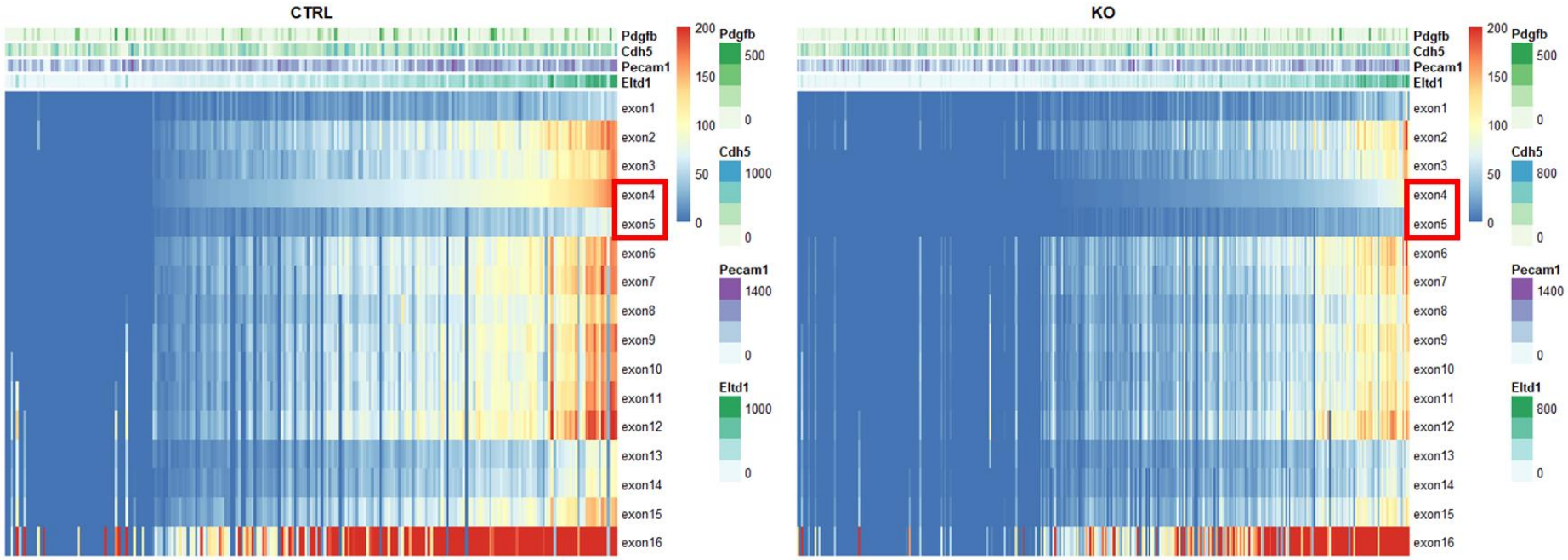

Figure 5.16: Analysis of cells with and without *Eltd1* exons 4 and 5. Heatmap was ranked by increasing *Eltd1* exon 4 expression. Cells without *Eltd1* exons 4 and 5 (n=390 cells) were pooled together and compared with the remaining cells (n=189 cells). Abbreviations: CTRL (Untreated group); KO (Tamoxifen-treated group).

5.7.1 Overview of differentially expressed genes

In the total EGFP$^+$/Cd31$^+$/VE-Cadherin$^+$ lung endothelial cell population, arterial and capillary endothelial subpopulations, there were no differentially expressed genes significant in all three statistical tests (Figure 5.17). In the total EGFP$^+$/Cd31$^+$/VE-Cadherin$^+$ lung endothelial cell population, 5 out of the 14 differentially expressed genes were predicted genes, significant in Wilcox and edgeR tests.

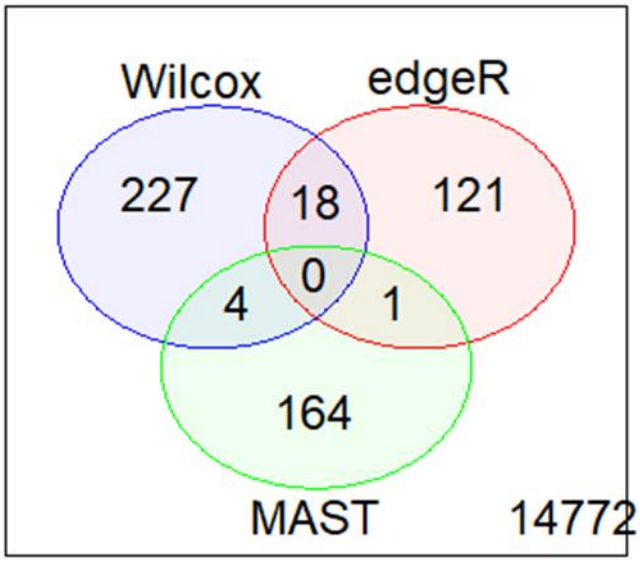

Figure 5.17: Venn diagrams of significant differential gene expression profiles using Wilcox, edgeR and MAST statistical tests. Differential gene expression profile between *Eltd1*-depleted (exons 4 and 5) total EGFP$^+$/Cd31$^+$/VE-Cadherin$^+$ lung endothelial cells (390 cells) compared to control cells (189 cells). In the total EGFP$^+$/Cd31$^+$/VE-Cadherin$^+$ lung endothelial cells, there was no differentially expressed gene that was significant in all three statistical tests. 18 differentially regulated genes were significant in Wilcox and edgeR while 4 genes were significant I Wilcox and MAST and only one gene was significant in both edgeR and MAST tests. Colour legends: Blue (Wilcox), red (edgeR) and green (MAST).

5.7.2 Differential gene expression profile of *Eltd1*-depleted (exons 4 and 5) total EGFP$^+$/Cd31$^+$/VE-Cadherin$^+$ lung endothelial cells

5.7.2.1 Upregulated genes

5.7.2.1.1 Total lung endothelial cells

In the total cell population, *Eltd1*-depletion (exons 4 and 5) was associated with upregulated genes related to endothelial biology such as *Rac2*, *Cgn* and *Il18r1* (Table 5.7).

Rac2 is a hematopoietic specific GTPase and is involved in endothelial integrin signalling. It has been reported that Rac2 expression in endothelial cells is necessary for postnatal neovascularisation (De et al., 2009).

Interleukin 18 receptor 1 (Il18r1) expression, together with interleukin 18, in endothelial cells, smooth muscle cells and mononuclear phagocytes have been reported to constitute a paracrine proinflammatory pathway during atherogenesis (Gerdes et al., 2002).

In addition, *Nox4* (Tang et al., 2018), *Cyp2e1* (Leung et al., 2013), *Eaf2* (Zang et al., 2016) and *Lars2* (Zhou et al., 2009) were associated with tumour development while *Il18r1* (Gerdes et al., 2002) was reported to be implicated in immunology. Lars 2 inactivation was discovered in nasopharyngeal carcinoma.

5.7.2.2 Downregulated gene

5.7.2.2.1 Total lung endothelial cells

In the total cell population, *Eltd1*-depletion (exons 4 and 5) was associated with downregulated genes related to endothelial biology such as *Trpc6*, *Lef1*, *Aqp7* and *Esrβ* (Table 5.7).

Lymphoid enhancer binding factor 1 (Lef1) has been reported to be target gene of the Wnt-beta-catenin pathway I endothelial cells in which Lef1 regulates the expression of matrix metalloproteinase-2 and facilitates endothelial cell invasion (Planutiene et al., 2011)
Estrogen receptor β (Esrβ) has been reported to play a key role in the mechanism that Notch1 functions, in the presence of 17β-estradiol, which is important in protecting the vascular endothelium against tumour necrosis factor α (TNF α)-induced inflammation (Fortini et al., 2017).

Some genes such as, *Esrβ* (Bowers et al., 2015) and *Alox12* (Mashima and Okuyama, 2015) were reported to be associated with tumour development.

Function Associations	Gene expression and description	
	Total lung endothelial cells	
	Up	Down
Endothelial biology, Angiogenesis	***Rac2*** *(Rac family small GTPase 2);* ***Cgn*** *(cingulin);* ***Il18r1*** *(interleukin18 receptor 1)*	***Trpc6*** *(transient receptor potential cation channel, subfamily C, member 6);* ***Lef1*** *(lymphoid enhancer binding factor 1);* ***Aqp7*** (aquaporin 7)*;* ***Esrβ*** *(estrogen receptor 2, beta)*
Tumour development	***Nox4*** *(NADPH oxidase 4)*; ***Cyp2e1*** *(cytochrome P450, family 2, subfamily e, polypeptide 1)*; ***Eaf2*** *(ELL associated factor 2)*; ***Lars2*** *(leucyl-tRNA synthetase, mitochondria)*	***Alox12*** *(arachidonate 12-lipoxygenase)*; ***Esrβ***
Immunology	***Il18r1***	-

Table 5.7: Upregulated genes related to endothelial biology, angiogenesis, tumour development and immunology. Genes in **black** are of log(fold change)>2 and significant in at least one statistical test while genes in **red** are of log(fold change)<2 and significant in all three tests.

5.7.3 Pathway analyses of *Eltd1*-depleted (exons 4 and 5) total lung endothelial cells

5.7.3.1 Total lung endothelial cells

The GO (gene ontology) enrichment analyses, as illustrated in Figure 5.18, showed that *Eltd1*-depletion (exons 4 and 5) in total lung endothelial cells affected repertoire of genes involved in multiple processes, including branching in blood vessel morphogenesis, regulation of vasculature development, regulation of angiogenesis, sprouting angiogenesis and endothelium development.

The genes that were involved in these processes, as shown in Figure 5.19 and consistent with our expression data with a logFC of more than 2 were *Lef1* (logFC=-3.16), *Rac2* (logFC=3.24), and *Esrβ* (logFC=-4.57).

In VEGF and Notch signalling pathways, *Eltd1*-depletion was shown to have an effect on genes in these pathways, as shown in Figure 5.20. In the VEGF signalling pathway, *Eltd1* depletion resulted in the downregulation of most genes in the pathway such as, *VEGFR2*, and downstream targets like *Cdc42*, *Rac* etc.

In the Notch signalling pathway, *Eltd1*-depletion also led to the downregulation of *Dvl* and *Deltex* and upregulation of *Serrate* and *TACE*. .

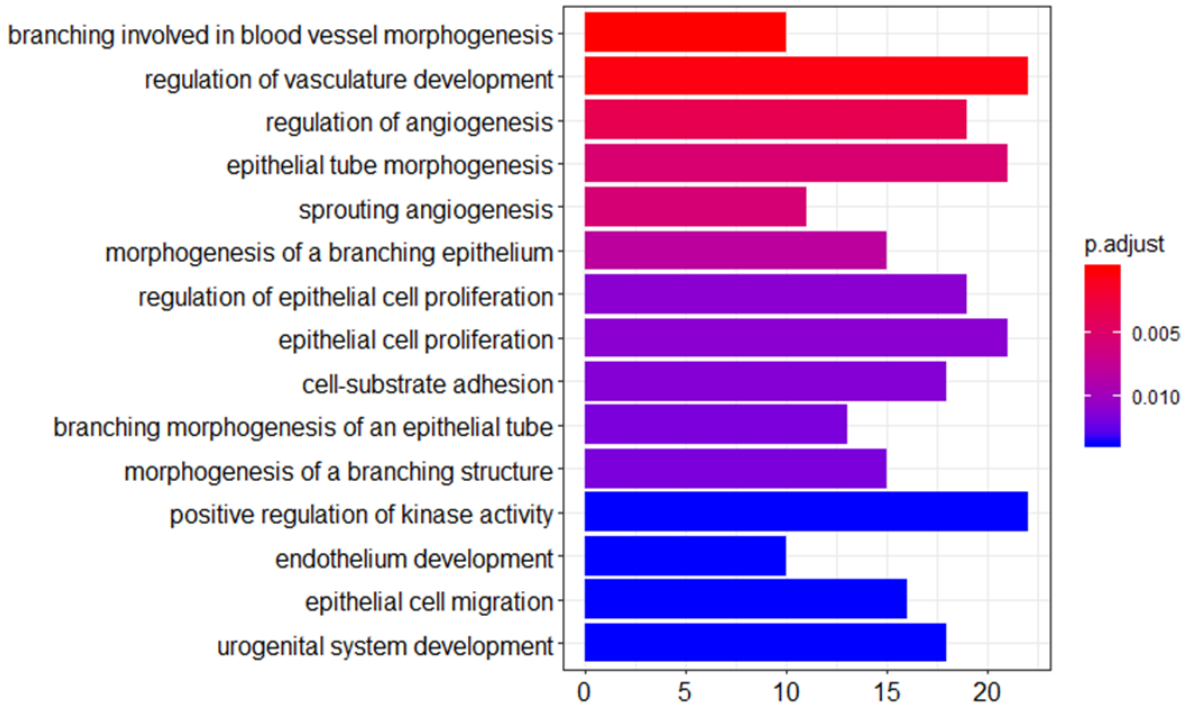

Figure 5.18: Biological processes impacted by the loss of *Eltd1* (exons 4 and 5) in total endothelial population. Generated from Gene Ontology (GO) enrichment analysis.

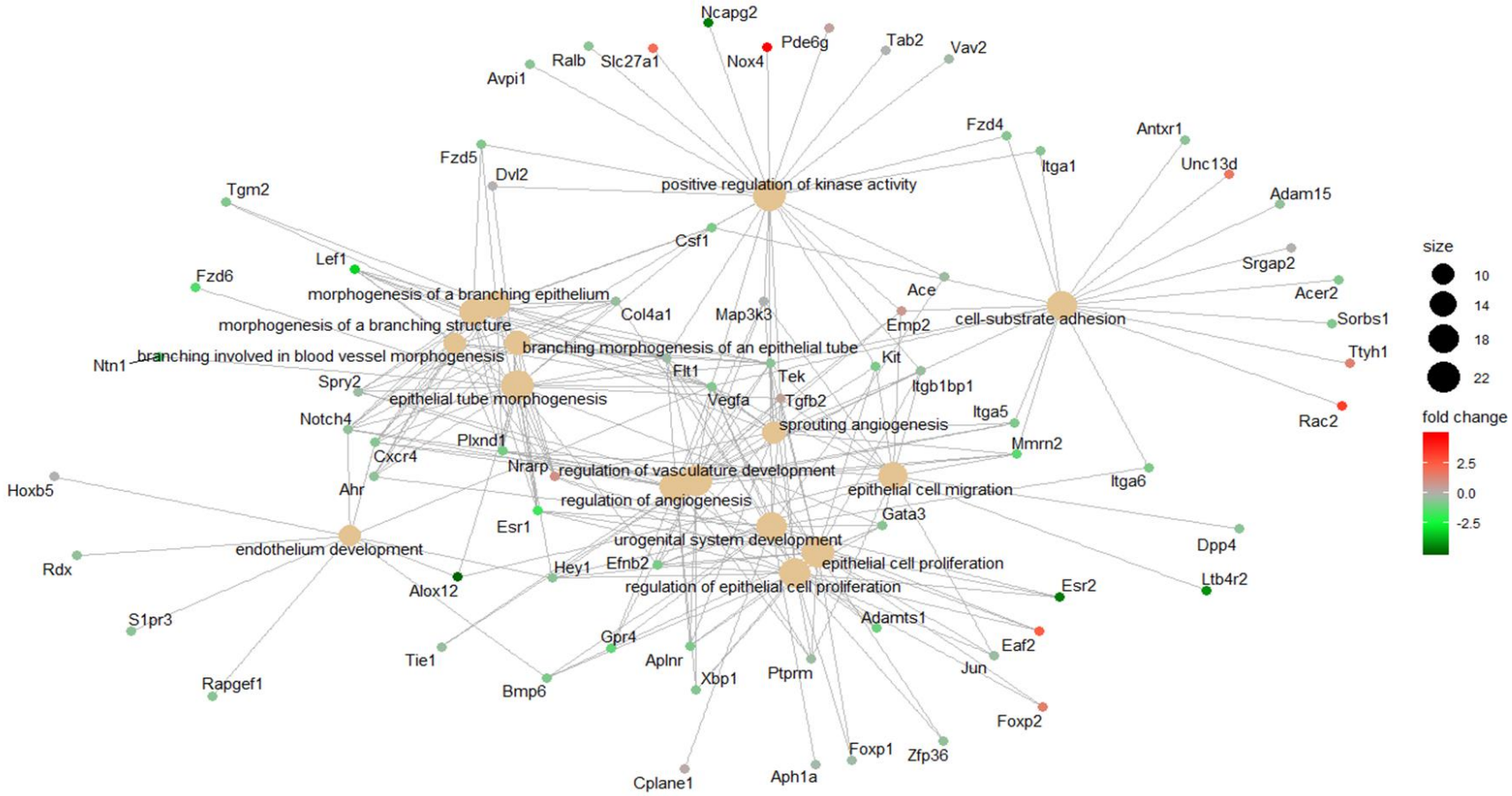

Figure 5.19: Biological processes and the expression of associated genes in *Eltd1*-depleted (exons 4 and 5) total lung endothelial population. Generated from Gene Ontology (GO) enrichment analysis.

A

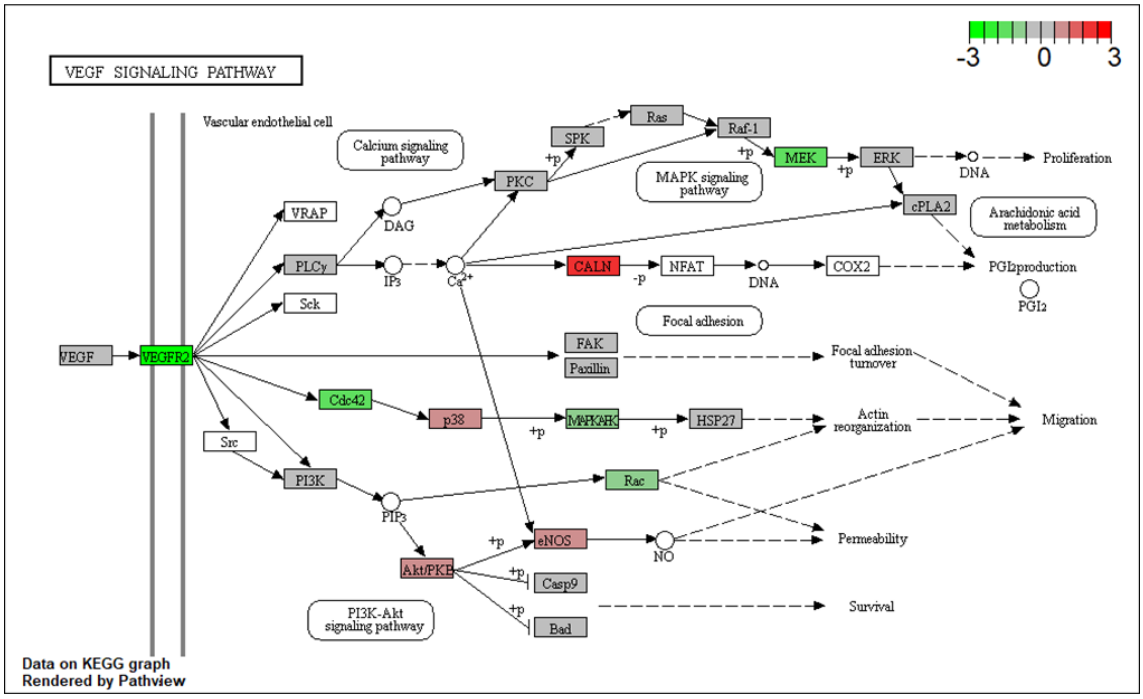

B

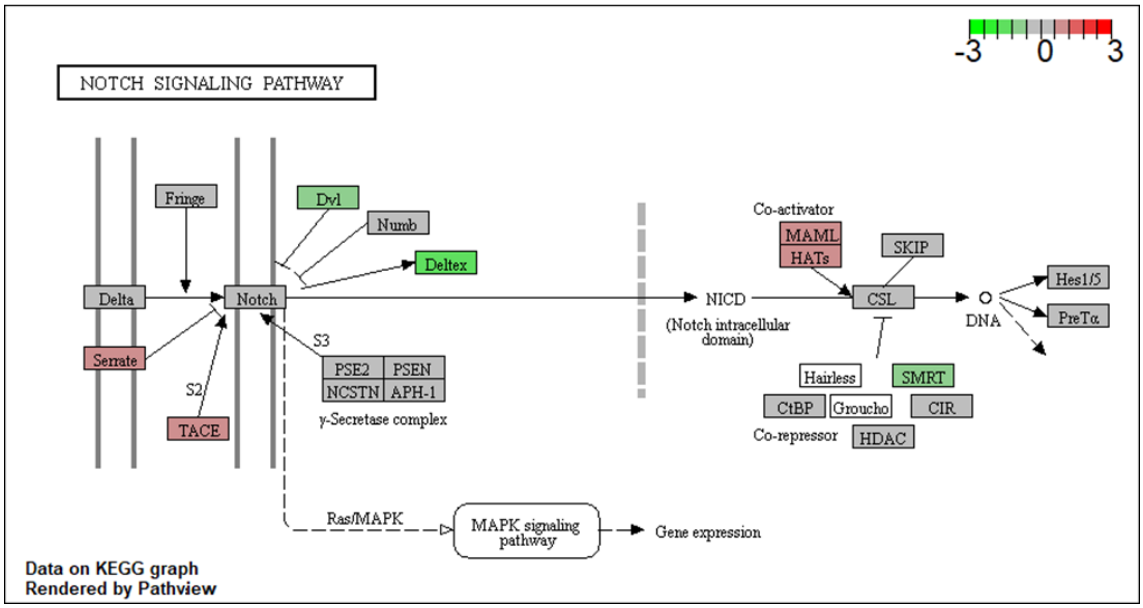

Figure 5.20: Pathway analyses (VEGF and Notch signalling) in *Eltd1*-depleted (exons 4 and 5) in total lung endothelial population. Figure generated from Kegg pathway enrichment analysis and KEGG module enrichment analysis.

5.7.4 Conclusion

The analysis of cells with *Eltd1*-depletion (exons 4 and 5) enriched pathways related to endothelial biology compared to the analysis performed in section 5.6 which had more noise due to the issue of having cells with variable *Eltd1*-depletion. In addition, the VEGF and Notch signalling pathway analyses demonstrated different effects. In the VEGF signalling pathway, this analysis showed downregulation of *VEGFR2* not observed in the previous analysis. Also, in the Notch pathway, there was no change in the *Notch* expression but in the previous analysis, *Notch* was downregulated.

5.8 Discussion

Single cell sequencing of *ex vivo* isolated lung endothelial cells has demonstrated the complexity in this biological system by revealing the heterogeneity of endothelial cells. This was manifested both in terms of *Eltd1* expression levels and the changes in gene expression on its depletion. *Ex vivo* isolated cells have been exposed to a complex microenvironment and to other cell types in the tissue. In comparison with sequencing from *in vitro* cell cultures where these features are absent and thus might not recapitulate the relevant physiological or pathological contexts.

The single cell sequencing performed managed to sequence more than 10,000 genes per cell which demonstrated that the technique has worked efficiently in this study. In this experiment, a control group of tamoxifen-treated *Eltd1*$^{fl/fl}$*;Pdgfb-Cre*$^{-/-}$ mice would have been useful to exclude the potential effects of tamoxifen (in addition to *Eltd1* depletion) on changes in the differential gene expression profile of lung endothelial cells. However, due to the relative high cost of single cell sequencing experiment, we chose to use only *Eltd1*$^{fl/fl}$*;Pdgfb-Cre*$^{+/-}$mice as the EGFP signal provided a better chance of isolating *Eltd1*-depleted cells. Moreover, it was previously reported that the half-life of tamoxifen was about 12 hours (Robinson et al., 1991), it was thought that the residual tamoxifen would be minimal. However, from the differential gene expression profile of total lung endothelial cells between untreated and tamoxifen-treated group, *Esrα* was downregulated and gene signature corresponding to the response to tamoxifen came up in the lung capillary endothelial cells. In addition, the analysis of *Eltd1*-depleted (exons 4 and 5) lung endothelial cells showed *Esrβ* being downregulated. Both *Esrα* and *Esrβ* have been independently reported to be expressed in lung endothelial cells (Vegeto et al., 2010). A further control group would include wildtype mice to exclude any effects of genetic manipulation and include the effects of tamoxifen.

From the flow cytometry studies, on hindsight, it was shown that EGFP$^+$ cells were largely Cd31$^+$ and VECadherin$^+$ (>80%), and that the proportion of EGFP$^-$;Cd31$^+$;VECadherin$^+$ cells was very small (<5%). However, it is still a useful marker as it is the reporter for Cre-expressing cells where the *Eltd1* deletion occurred.

In general, these cells have very low endogenous expression of *Eltd1* exons 1, 5, 13 and 14. Interestingly, exon 16 has the highest expression amongst all other exons which might be attributed to exon 16 being the largest whereas exons 1, 5, 13 and 14 are much reduced in

size (Figure 5.20). Larger exons may possibly higher counts (transcripts) as smaller exons may not generate counts as effectively. There could also be differential use of exons in the transcript. Exons 4 and 5 code for the second and third EGF domains, with these domains possibly having a functional role. The low counts for exon 5 might indicate that many *Eltd1* transcripts naturally lack this exon, although transcripts lacking this exon have not been previously reported (Figure 5.20). This might also indicate that the third EGF domain may not be as functionally important as the second in endothelial cells. The importance of the second EGF domain is supported by it being retained in ELTD1 from all orthologous species (Favara et al., 2019a).

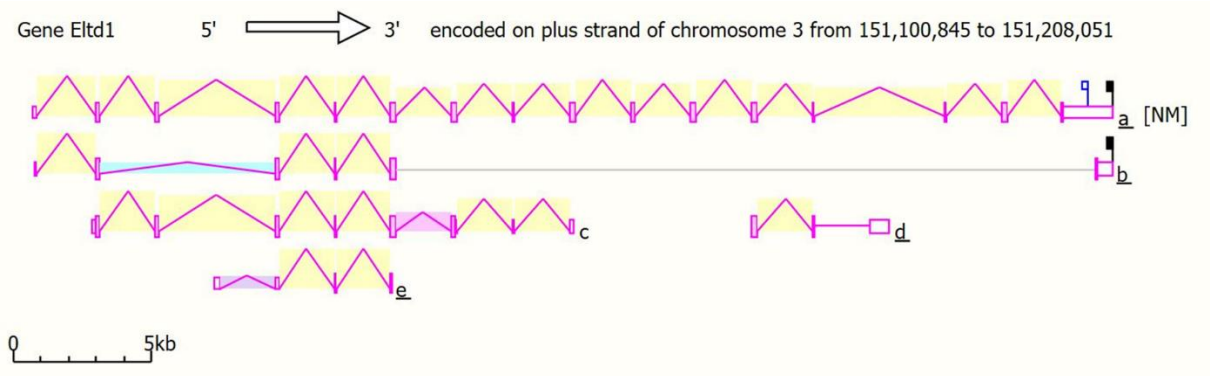

Figure 5.21: Murine Eltd1 transcripts. There are five reported transcripts in which the length of the bar is proportional to the exon size while intron height is reflective of the number of cDNAs supporting each intron. It can be seen that the transcript 'a' contains 16 exons, where the exon 1 is on the 5' end and exon 16 on the 3' end. Out of all the exons, exon 16 is the largest. Figure generated from AceView.

Tamoxifen-induced deletion of *Eltd1* exons 4 and 5 resulted in a marked downregulation of *Eltd1* expression. Evidently, this deletion has led to the reduction in the expression of other exons presumably due to premature nonsense mediated decay of the downstream mRNA and this gave confidence in that the tamoxifen induction protocol generated an inducible endothelial cell-specific *Eltd1* knockout model. Even when an exon 4&5 deleted *Eltd1* transcript was retained, the protein product lacking the EGF domains and having a premature stop codon would not be functional.

In the analyses performed, it could be seen that the refinement of the analyses resulted in pathways significantly associated with endothelial biology and angiogenesis. It reflects the importance of the analytical approach to filter out pathways that might be caused by the noise in the data.

The analysis of total lung endothelial cells was conducted prior to the characterisation of endothelial cell subsets. Out of 584 cells, 18 cells were not of endothelial identity and this small sample size was not likely to cause a drastic change in the differential gene expression profile. Our analysis showed that the lung endothelial cell preparation yielded greater number of capillary than arterial endothelial cells and that *Eltd1* expression in capillary endothelial cells was higher than that of arterial endothelial cells. Within each endothelial subpopulation, there was heterogeneity in *Eltd1* expression. These observations were consistent with data mined from a previously published study of lung endothelial cells (He et al., 2018). Interestingly, in both subpopulations, there were subsets of endogenously *Eltd1*-deficient cells. This existence of a population of endothelial cells that naturally lack *Eltd1* expression may be inferred to be resistant to *Eltd1*-targeted therapy. Additionally, this population of cells complicate our analyses in differential gene expressions in the inability to identify individual cells that naturally lack *Eltd1* from those in which the loss of its expression was induced.

Both *Eltd1*-depleted lung arterial and capillary endothelial cells had different differential gene expression profiles in all the analyses performed. This might suggest *Eltd1* is involved in different functional pathways in arterial versus capillary endothelial cells but might also be reflective of the different relative abundance of the two populations.

The two analyses have highlighted genes associated with endothelial biology and angiogenesis including upregulated genes such as, *Rac2*, *Fn1*, *Cgn*, *Ifit3b*, *Il18r1* and *Xaf1*, and down regulated genes like *Trpc6*, Prom1, *Esrα*, *Esrβ*, *Lef1*, *Notch2, Sox11*.

A spheroid model comprising of *ELTD1*-silenced HUVECs was previously shown to have inhibited endothelial cell sprouting (Masiero et al., 2013) and acute *Eltd1*-depleted aortas were also shown to have reduction in the sprouting area. *Fn1* was upregulated while *Lef1* was downregulated in the *Eltd1*-depleted lung endothelial cells. Fn1 is implicated in the coordination of endothelial migration and adhesion in response to extracellular matrix while

Lef1 was reported to facilitate endothelial cell invasion. These two genes could potentially play a role in the sprouting phenotype of *Eltd1*-depleted endothelial cells.

As an adhesion GPCR, Eltd1 has been hypothesised to have a role in cell-to-cell contact. In the *Eltd1*-depleted lung endothelial cells, *Cgn* was upregulated. *Cgn* has been shown to play a role in regulating vessel integrity. This suggest that *Eltd1* could be involved in cell contact via Cgn-dependent mechanism.

Additionally, some of the differentially expressed genes were related to endothelial function in inflammation such as *Kcnk3*, *Trpc6, Ifit3b, Il18r1* and Esrβ. *Ifit3b* and *Il18r1* were upregulated while the others were downregulated with *Eltd1*-depletion. It would be interesting in the future to investigate whether Eltd1 might be involved in inflammatory responses to certain stimuli.

Rac2, *Prom1* and *Esrα* have been implicated in neovascularisation. In *Eltd1*-depleted lung endothelial cells, *Rac2* was upregulated while *Prom1* and *Esrα* were downregulated. It would be assumed that all drivers of angiogenesis would reduce in abundance with the depletion of *Eltd1*. It could be seen that the biological system is complex and that a balance of promoters and inhibitors is tightly regulated.

Notch2 has been reported to inhibit high glucose-induced endothelial mesenchymal transition (EndoMT) and was downregulated with *Eltd1*-depletion. Could *Eltd1* play a role in the endothelial mesenchymal transition observed in endothelial cells?

In the VEGF signalling pathway, *Eltd1*-depletion led to the downregulation of *VEGFR2* and some downstream targets such as *Cdc42* and *Rac*. This coincides with a recent paper that reported that *in vivo* treatment of Eltd1-targeted antibody led to a reduced level of VEGFR2 by immunohistochemistry of mouse tumours (Ziegler et al., 2019).

Interestingly, the differential gene expression profile of *Eltd1*-depletion in lung endothelial cells did not match with that of *ELTD1*-silenced HUVECs. In the microarray experiment performed, *ELTD1* silencing in HUVECs resulted in the upregulation of *DLL4* and *ACLY*, and downregulation of *JAG1* and *HES2*. However, these were not observed in the profile of *Eltd1*-depleted lung endothelial cells. There are several reasons why this might be the case. First, it could be due to the different species having a different biology associated with *Eltd1*-

depletion. This is not surprising, as in chapter 1, it has been shown that the *Eltd1* expression in human tissues are not the same as those in mice. Secondly, although HUVECs are a primary cell line, these cells being cultured *in vitro* in tissue culture flasks for a period of time without other cell types is presumably sufficient to alter their biology. The lung endothelial cells, on the other hand, were freshly isolated and sent for sequencing experiment within hours. These could possibly retain the physiology of the cells better and therefore a more physiologically relevant tool to assess the effect of *Eltd1* depletion.

However, there are limitations to this analysis. Firstly, the relatively small sample size, especially in the endothelial subsets, and small gene changes have made it difficult to perform pathway analyses. The high cost of the single cell sequencing experiment was the main limiting factor. Secondly, the analysis of endothelial subpopulations was based solely on the gene signatures from a published report as this studied a much larger number of lung endothelial cells (He et al., 2018). It would be ideal to compare our finding with the signatures from other studies, but there have not yet been many reports on the characterisation of endothelial subsets at the single cell level.

At this stage, the sequencing data could only provide us with hints on the biological consequences of endothelial-*Eltd1* depletion. The endothelial subsets have been characterised by relatively large gene signatures. It is possible to select a few top ranked genes that are expressed in high abundance in a specific subset and isolate these cells by flow cytometry. With these isolated genes, qPCR analysis could be performed to validate these target genes and perhaps perform functional assays to characterise the phenotype of *Eltd1*$^{-}$ cells. Alternatively, immunohistochemistry on lung sections or flow cytometry for cell surface markers could be performed to assess the expression level of these target genes at the protein level.

5.9 Conclusion

In summary, the single cell sequencing on lung endothelial cells demonstrated the complexity in lung endothelial Eltd1 expression and function and posed further questions: What is the role of the heterogeneity in the endothelial function? Does this heterogeneity change in pathological context, like cancer? These questions remained unanswered and would be interesting for further investigation.

Chapter 6: Final discussion and future plans

The work in this thesis focused on developing mouse models with genetic loss of endothelial-*Eltd1* and utilising these models to study its role on physiology, tumour vasculature and gene expression pattern in lung endothelial cell subsets. There are several advantages of using mouse models in these investigations. Firstly, the *in vivo* mouse models provide a means to study physiological and pathological mechanism in a complex organism which cannot be recapitulated fully in an *in vitro* system such as, complex interactions of different cell types and exposure to different stresses like hemodynamic stress. Secondly, *in vivo* mouse models could provide preclinical screening and safety testing for *Eltd1*-targeting.

6.1 *In vivo* effects of endothelial-*Eltd1* depletion

To investigate the *in vivo* effects of chronic and acute endothelial-*Eltd1* depletion, both constitutive and inducible endothelial cell-specific *Eltd1* knockout models were generated using *Tie2-Cre* and *Pdgfb-Cre* mice respectively. Notably, the Cre recombinase expression was driven by different endothelial promoters in the two models. This raises the possibility that the *Eltd1* knockout may not occur in identical endothelial cell population in both models.

The inducible model was more relevant for the clinical setting, where all the normal organs will have developed with physiological Eltd1 expression levels in the vasculature, providing a better tool to assess the therapeutic efficacy of *in vivo* endothelial-*Eltd1* targeting. In hindsight, it would be better to have had the inducible Cre driven by the same endothelial promoter as the constitutive Cre for comparative analysis of the phenotypes that arise from acute and chronic endothelial-*Eltd1* depletion. However, due to the availability of the mice and some disadvantages of *Tie2-Cre,* such as the presence of, *Tie2*-expressing macrophages, hematopoietic cells and mature pericytes (Teichert et al., 2017), we selected the inducible *Pdgfb-Cre* model which was shown to be efficient and its expression in non-endothelial cells such as keratinocytes (Payne et al., 2018), were unlikely to play a critical role in the functional investigation conducted in this DPhil project.

The knockout strategy adopted in the generation of these models was designed to delete *Eltd1* exons 4 and 5, encoding the second and third EGF domains that are likely to have a

functional role in ligand binding by this aGPCR. Insertion of a premature stop codon and frameshift mutation subsequently should lead to the loss in expression of the bulk of the protein. This was a different design compared to the previously published report by Xiao and colleagues (2012), which retained the bulk of the extracellular domain.

During the autocatalytic cleavage of the aGPCRs at the GPS, and additional proteolysis events within the extracellular domain of these receptors, the NTF or smaller fragments may be dissociated and released into circulation. There have been reported circulating NTFs for various aGPCRs such as BAI1 (Kaur et al., 2005), CD97 (Gray et al., 1996), GPR116 (Abe et al., 2002) and GPR126 (Moriguchi et al., 2004). Theoretically, these circulating NTFs could interact with molecules over large distances from where they were released. For instance, soluble fragment of CD97 stimulates tumour angiogenesis *in vitro* and *in vivo* via binding of integrins and chondroitin sulfate, a component of the extracellular matrix (Wang et al., 2005). Additionally, these fragments could also be found at sites of inflammation (Hamann et al., 1999). Therefore, the knockout strategy adopted in this DPhil project would be a better design as it deleted the bulk of the Eltd1 protein, including the extracellular domain or NTF.

6.1.1 Effects of endothelial-*Eltd1* depletion on mouse physiology

In both constitutive and inducible endothelial cell-specific *Eltd1* knockout mouse models, the mice developed normally with the absence of any behavioural or physiological abnormalities. Interestingly, inducible endothelial-*Eltd1* depleted aortic rings showed significant reduction in the sprouting area which was not observed in the constitutive model. This suggested that there might be a functional compensatory mechanism in the constitutive endothelial-*Eltd1* model, a phenomenon which has also been reported in other gene knockout models such as the knockout of the ribosomal gene *Rpl22* (El-Brolosy and Stainier, 2017). In the future, RNA sequencing of constitutive and inducible *Eltd1*-depleted aortic endothelial cells could be performed to identify the genes that were significantly differentially regulated. This could shed light onto the signalling pathway/s that may have compensated for the constitutive loss of *Eltd1* expression, and also perhaps provide clues as to the noncanonical signalling pathway regulated by *Eltd1*. Moreover, the aortic ring phenotype could be an important finding linking Eltd1 to the functional role of aGPCRs in the adhesion to matrix components. It would also be interesting to conduct a proteomic study to find whether Eltd1 resides in the extracellular

matrix (Ghajar et al., 2013b) or staining Eltd1 in the matrix to localise its expression in the sprouts.

A previously published report (Masiero et al., 2013) showed that *eltd1*-silencing by morpholinos in zebrafish led to a severe vascular phenotype, hence constitutive endothelial-*Eltd1* was not feasible in this model as the eggs would not be viable. The constitutive endothelial-*Eltd1* knockout mouse model developed normally and did not show significant differences in normal physiology. This was unlike observations in the zebrafish, suggesting that the role of *Eltd1* in different species has changed during evolution. It has been reported that mice and zebrafish have the same Eltd1 variant of EGF domains. However, mammals have an increased repertoire of aGPCRs and angiogenic genes compared to zebrafish which could suggest functional redundancy of the receptor(Favara et al., 2019b). This could help explain the difference in phenotype of *Eltd1*-depletion in mice and zebrafish.

The constitutive model knocked out *Eltd1* in endothelial cells starting from developing embryos. This is not wholly biologically relevant for testing the safety of a therapeutic targeting of endothelial-*Eltd1* in the clinic as this would not be given during human development. Also, the suggestion of functional compensation after long term Eltd1 depletion, as indicated by the absence of any aortic ring phenotype in the constitutive model, could suggest that there might be a possible relapse from repeated administration of Eltd1-targeted therapies in patients. On the other hand, the inducible model also showed a good safety profile. This mimicked the clinic setting more closely and was a better model for studying the safety of Eltd1-targeted therapies.

In summary, the observations in both constitutive and inducible endothelial cell-specific *Eltd1* knockout models showed that chronic and acute endothelial-*Eltd1* targeting exhibited a good safety profile with no evidence of any short or long-term toxicity.

6.1.2 Effects of endothelial-*Eltd1* depletion on tumour development and angiogenesis

The growth of syngeneic tumour models (E0771 and MC38) in constitutive and inducible endothelial cell-specific *Eltd1* knockout mouse models was analysed to further investigate the role of endothelial *Eltd1* in tumour development and angiogenesis in immunocompetent syngeneic models. In all of the performed tumour experiments, despite histological

differences in the vasculature, there were no significant differences in tumour growth curves and survival outcomes in both *Eltd1* knockout models.

These observations were different from those reported in the previous study (Masiero et al., 2013) in which *Eltd1* silencing resulted in a significant reduction in tumour growth and improved survival outcome. It is important to note that there were several key differences in the experimental design. Firstly, in this DPhil project, the mice were induced with tamoxifen to create endothelial-*Eltd1* knockout prior to the inoculation of tumour cells. However, in the published report, the mice were given *Eltd1* siRNA-embedded chitosan nanoparticles after the xenografts reached a certain tumour volume. Hence, in this regard, different questions were asked. Our experimental design investigated tumour growth in the absence of endothelial-*Eltd1* compared to those in controls whereas the previous study assessed the effects of endothelial-*Eltd1* targeting in an established tumour. Secondly, the chitosan nanoparticles might affect a wider range of other cell types, such as smooth muscle cells whereas the genetic deletion could be more endothelial cell-specific. Furthermore, growth of the syngeneic tumour models in inducible global *Eltd1* knockout using *Rosa26-Cre* showed similar results as the inducible endothelial-*Eltd1* knockout, suggesting that endothelial-*Eltd1* might play a predominant role in tumour vasculature. Thirdly, the previous study conducted xenograft studies in immunocompromised mice while our study was conducted in syngeneic tumour models in immunocompetent mice. There has been an increasing awareness that endothelial cells play a role in the immune response as these cells function as sensors in the bloodstream in detecting pathogens and endogenous metabolite-related cues. These in turn stimulate the endothelial cells to secrete pro-inflammatory chemokines and cytokines which attract immune cells(Mai et al., 2013, Al-Soudi et al., 2017). Endothelial-*Eltd1* could potentially participate in the intratumoural immune activity. This could be further pursued in future investigation.

The involvement of non-endothelial Eltd1 in the vasculature is not known and could be explored by several methods. For example, the *Eltd1* siRNAs in nanoparticles could be administered to the *Eltd1* genetic knockout and control models to assess whether they are able to alter the growth of these murine syngeneic tumour models and importantly if they have any additive effects when combined with endothelial-*Eltd1* deletion. It could also be interesting to cross the *Eltd1* knockout mice with immunocompromised mice and conduct the

same human xenograft experiments where siRNA was able to significantly impair tumour growth (Masiero et al., 2013). If in both experiments, additive effects of siRNA and genetic loss of endothelial-*Eltd1* were observed, it could suggest that the siRNA delivery targeted non-endothelial *Eltd1*-expressing cell types that play a role in the tumour vasculature.

It could be useful to perform orthotopic tumour experiment in future as the experiments performed were subcutaneous tumour inoculation. Orthotopic tumours give a more relevant microenvironment of the cancer type. Additionally, it will be important to compare Eltd1 expression in matched tissue and tumour samples by immunohistochemistry in our models and this will help in future experimental designs on Eltd1-targeted therapies.

The *in vivo* experiments using inducible endothelial cell-specific *Eltd1* knockout model have been designed to study the effects of endothelial-*Eltd1* on the tumour growth after tumour cell inoculation. It could be interesting to induce endothelial-*Eltd1* depletion by tamoxifen in an established tumour to investigate into its effect on existing tumour vasculature. This could be particularly important if Eltd1 was also upregulated in the tumour environment.

The immature and perhaps leaky vessels observed in both endothelial cell-specific *Eltd1* knockout tumour models could help explain the correlation of higher ELTD1 expression with better prognosis in patients (Masiero et al., 2013). If ELTD1 is involved in the permeability of vessels such that the loss of ELTD1 leads to leaky vessels, then drug delivery will potentially be impeded which then could lead to poorer response of patients to therapy and their worse prognosis. An *in vivo* experiment with the endothelial-*Eltd1* knockout mice, studying vessel permeability or involving delivering of a chemotherapeutic drug, for instance doxorubicin (which can be imaged to identify leakage from vessels), could be performed to address this. Better perfused vessels might aid the metastatic spread of the tumour cells. However, in the syngeneic tumour models, no gross micro- or macro-metastases were found. This might be due to the short time frame of the experiment. Leaky vessels might contribute to the engraftment of tumour cells in various sites. The metastatic potential of the tumour cells could be different in the endothelial cell-specific *Eltd1* knockout mice. To investigate this, tumour cells could be injected *in vivo* via tail vein of the mice and the number and nature of the micro- and macro-metastases could be analysed.

The loss of endothelial-*Eltd1* was sufficient to lead to a reduction in microvessel density in the tumours. However, reduction in microvessel density was not observed in the vital organs of both constitutive and inducible endothelial cell-specific *Eltd1* knockout mice. This suggested that the effect of endothelial loss of *Eltd1* might only be in newly formed vessels and not in established mature vessels. ELTD1 was reported to be involved in sprouting in a 3-dimensional HUVEC spheroid assay. ELTD1-knockout HUVEC spheroids showed inhibition in sprouting in Matrigel as compared to those of control (Masiero et al., 2013). Consistent with these results, inducible endothelial cell-specific *Eltd1* depleted aortic rings also showed inhibition in sprouting in Matrigel. Therefore, Eltd1 might play a role in early angiogenesis, particularly in the biology of endothelial cells such as migration and invasion into matrix and tube formation. To further substantiate this, an *in vivo* wound healing assay could be performed to explore the role of *Eltd1*-expressing endothelial cells in wound recovery.

Furthermore, the endothelial loss of *Eltd1* in the tumours resulted in a reduction in pericyte coverage of existing vessels. This suggested that endothelial-*Eltd1* might be involved in the recruitment of mural cells supporting the newly formed vessels. *In vitro* coculture of endothelial cells and pericytes/smooth muscle cells could be performed to study the mechanisms of communication between ELTD1-expressing endothelial and smooth muscle cells. For instance, an experiment using the Transwell cell culture system could be conducted by seeding ELTD1-knockdown HUVECs and smooth muscle cells separated by a thin porous membrane and analysing various parameters, such as the migratory ability of either cell type, and compared with control HUVECs (Truskey, 2010).

To summarise, both genetic and drug-induced *Eltd1* deletion in the endothelium gave similar results indicating that endothelial-*Eltd1* played a role in the tumour vasculature *in vivo*.

6.2 Differential gene expressions of isolated *Eltd1*-depleted murine lung endothelial cells

Single cell sequencing of lung endothelial cells showed heterogeneity in *Eltd1*-expressing lung arterial and capillary endothelial cell subsets. Lung capillary endothelial cells were found to have higher *Eltd1* expression than lung arterial endothelial cells. These findings were consistent with the sequencing data mined from a previously published report (He et al., 2018). The differential gene expression profiles of acute *Eltd1*-depleted lung arterial and capillary endothelial cell subsets were found to be different. This demonstrated that different

endothelial subsets might have different biology and *Eltd1* might play different functional roles in the pathways of both endothelial cell subsets. Moreover, both capillary and arterial endothelial subpopulations were similarly targeted by tamoxifen-induced *Eltd1* deletion.

Various analyses were performed to assess the differential gene profiles between *Eltd1*$^{+}$ and *Eltd1*$^{-}$ lung endothelial cells. The analyses between cells with and without *Eltd1* (exons 4 and 5) demonstrated the effect of *Eltd1*-depletion on VEGF and Notch signalling pathways, both of which are important angiogenic signalling pathways. Interestingly, *Eltd1*-depletion led to a downregulation of *VEGFR2*, *Cdc42* and *Rac* in the VEGF signalling pathway. This relationship between Eltd1 and VEGFR2 was consistent with a recent report which showed that anti-Eltd1 antibody treatment resulted in a reduction in VEGFR2 levels by immunohistochemical analysis of the tumours (Ziegler et al., 2019). However, in the Notch signalling pathway, *Eltd1*-depletion downregulated *Deltex*, *Dvl*, *Delta* and upregulated *Serrate* and *TACE*. This was different from the data generated from the microarray of *ELTD1*-silenced HUVECs in which showed an upregulation of *DLL4*. This could be due to the endothelial cells having been derived from different species and organs. It could reflect different methodologies, siRNA versus genetic deletion. It could be also due to the HUVECs being cultured *in vito* for a period of time while the lung endothelial cells were sent for sequencing within hours of harvest, hence that could retain the physiological behaviour better.

In the analysis of *Eltd1*-depleted lung endothelial cells between untreated and tamoxifen-treated groups, *Xaf1* was upregulated while *Sox11* and *Prom1* were downregulated. *Xaf1* was reported to inhibit angiogenesis (Zhu et al., 2014) while *Sox11* (Palomero et al., 2014) and *Prom1* (Sekine et al., 2016). The anti-angiogenic properties of the loss *Eltd1* might be attributed by the upregulation of *Xaf1* and downregulation of *Sox11* and *Prom1.*

The genes that were shown to be differentially expressed could provide hints on the consequences of endothelial-*Eltd1* deletion and thus the functional role of Eltd1. For instance, genes associated with endothelial function in inflammation such as *Ifit3b* and *Il18r1*.This suggested Eltd1 might be involved in the inflammatory response which is one of the benefits of using the syngeneic tumour models in immunocompetent mice as described in section 6.1. In addition, there were genes associated with barrier function such as *Cgn*. This raises the possibility that Eltd1 may have a role in maintaining vessel integrity. Although the vessel density and morphology in vital organs of endothelial-*Eltd1* depleted mice did not show

significant differences compared to those of control, there could be subtle differences in the tight junction protein localisation and arrangement. This could be further explored by immunostaining of tight junction proteins in *Eltd1*-silenced endothelial cells. Furthermore, the functional impact on the tight junctions could be assessed by measuring the flux of FITC-dextran across the endothelium (Larre et al., 2013).

Also, interestingly endothelial loss of *Eltd1* resulted in a downregulation of *Kcnk3*, which was reported to increased vasoconstriction in pulmonary artery (Antigny et al., 2016). It is possible that this might be the same in the aorta. If so, it is tempting to speculate that this could be a contributing factor to the increased cardiac hypertrophy due to pressure overload in Eltd1 knockout mice (Xiao et al., 2012). In this case, it would be interesting to perform the aortic banding experiment on the endothelial cell-specific *Eltd1* knockout mice and analyse the cardiac vasculature and aorta. Additionally, it could be attempted to restore Kcnk3 expression to check if the phenotype due to *Eltd1*-depletion could be rescued. Alternatively, *Eltd1* expression and phenotype caused by its loss could be assessed in *Kcnk3* knockout mice.

These genes could be further validated by qPCR and immunohistochemistry in lung tissues. Also, the expression of the *Eltd1*-regulated genes could be modified in an *in vitro* endothelial cell culture to identify those with most important contribution to endothelial-*Eltd1* phenotype.

However, the small sample size and small gene changes observed in the endothelial cell subsets posed difficulties in conducting pathway analyses. Different analytical tools (Gene Set Enrichment Analysis and GO enrichment analysis) were used to allow the visualisation of pathways altered by endothelial *Eltd1* depletion. But it is important to point out that these analyses only provide possibilities for hypothesis building that need further experimental investigation. Isolation of lung arterial and capillary endothelial cells would be a good approach in studying the impact of *Eltd1* depletion. As the endothelial subpopulations were identified by distinct gene signatures. It may be possible to identify differentially expressed molecules that are expressed on the cell surface as markers for these endothelial cell types and sort them using fluorescence-activated cell sorting. These cells could be cultured and used for functional characterisation, comparing the phenotype effected by the loss of *Eltd1*.

The single cell sequencing experiment demonstrated the diversity of endothelial cell populations in the lungs and that *Eltd1* expression varied across all endothelial cell subsets, which reaffirmed the mined data in the dataset (He et al., 2018). To add to the complexity, within each endothelial cell subset, there was also heterogeneity in *Eltd1* expression. This posed a number of interesting questions, is the *Eltd1* heterogeneity important for the functional role of each endothelial cell subset? Will this heterogeneity change in different organs or in tumours? Do the gradations in *Eltd1* expression reflect the cellular endothelial localisation within distinct areas of a tissue? How would the differential gene expression profiles differ in both *Eltd1*-depleted endothelial cell subsets in different organs and tumour microenvironment?

These questions could be further explored by conducting single cell sequencing on the endothelial cells derived from other organs such as kidney and heart. Comparative analyses between endothelial cells derived from different organs could give insights into whether they contain similar proportions of endothelial cell subsets and on the effects of *Eltd1* depletion and common pathways that are involved in the endothelial biology in different organs. Also by comparing the gene expression profiles of *Eltd1*-depleted endothelial cells in normal tissue and pathological tissue, such as tumours, it might be possible to identify pathways that affect the altered vascularity that has been identified during syngeneic cancer growth.

6.3 Concluding remarks

This study has used a genetic approach that has provided further evidence of the role of endothelial *Eltd1* in angiogenesis and development of the tumour vasculature. It has also resulted in the creation of two endothelial cell-specific *Eltd1* knockout models (both constitutive and inducible) and the generation and validation of murine *Eltd1* polyclonal antibodies. These will be valuable tools for ongoing studies in the laboratory. New findings include the significant differences in the vasculature of endothelial-*Eltd1* depleted tumours, angiogenesis-associated gene targets and new hypotheses of Eltd1's role in endothelial biology, including differential expression levels and altered patterns of gene regulation in arterial and capillary endothelial subpopulations, from single cell sequencing of *Eltd1*-depleted lung endothelial cells. In addition, aortic sprout inhibition observed in acute but not chronic *Eltd1* knockout aortas suggested that prolonged depletion could induce a functional

compensatory mechanism that could be therapeutically relevant if drugs targeting ELTD1 require repeated and/or prolonged administration. In summary, the work performed in this thesis has provided the project with useful tools and hypotheses that require further investigation.

Bibliography

ABE, J., FUKUZAWA, T. & HIROSE, S. 2002. Cleavage of Ig-Hepta at a "SEA" module and at a conserved G protein-coupled receptor proteolytic site. *J Biol Chem,* 277**,** 23391-8.

AGRAWAL, A., PERGADIA, M. L., SACCONE, S. F., LYNSKEY, M. T., WANG, J. C., MARTIN, N. G., STATHAM, D., HENDERS, A., CAMPBELL, M., GARCIA, R., BROMS, U., TODD, R. D., GOATE, A. M., RICE, J., KAPRIO, J., HEATH, A. C., MONTGOMERY, G. W. & MADDEN, P. A. 2008. An autosomal linkage scan for cannabis use disorders in the nicotine addiction genetics project. *Arch Gen Psychiatry,* 65**,** 713-21.

AL-SOUDI, A., KAAIJ, M. H. & TAS, S. W. 2017. Endothelial cells: From innocent bystanders to active participants in immune responses. *Autoimmunity Reviews,* 16**,** 951-962.

ANDERSON, K. D., PAN, L., YANG, X. M., HUGHES, V. C., WALLS, J. R., DOMINGUEZ, M. G., SIMMONS, M. V., BURFEIND, P., XUE, Y., WEI, Y., MACDONALD, L. E., THURSTON, G., DALY, C., LIN, H. C., ECONOMIDES, A. N., VALENZUELA, D. M., MURPHY, A. J., YANCOPOULOS, G. D. & GALE, N. W. 2011. Angiogenic sprouting into neural tissue requires Gpr124, an orphan G protein-coupled receptor. *Proc Natl Acad Sci U S A,* 108**,** 2807-12.

ANTIGNY, F., HAUTEFORT, A., MELOCHE, J., BELACEL-OUARI, M., MANOURY, B., RUCKER-MARTIN, C., PECHOUX, C., POTUS, F., NADEAU, V., TREMBLAY, E., RUFFENACH, G., BOURGEOIS, A., DORFMULLER, P., BREUILS-BONNET, S., FADEL, E., RANCHOUX, B., JOURDON, P., GIRERD, B., MONTANI, D., PROVENCHER, S., BONNET, S., SIMONNEAU, G., HUMBERT, M. & PERROS, F. 2016. Potassium Channel Subfamily K Member 3 (KCNK3) Contributes to the Development of Pulmonary Arterial Hypertension. *Circulation,* 133**,** 1371-85.

ARAC, D., AUST, G., CALEBIRO, D., ENGEL, F. B., FORMSTONE, C., GOFFINET, A., HAMANN, J., KITTEL, R. J., LIEBSCHER, I., LIN, H. H., MONK, K. R., PETRENKO, A., PIAO, X., PROMEL, S., SCHIOTH, H. B., SCHWARTZ, T. W., STACEY, M., USHKARYOV, Y. A., WOBUS, M., WOLFRUM, U., XU, L. & LANGENHAN, T. 2012. Dissecting signaling and functions of adhesion G protein-coupled receptors. *Ann N Y Acad Sci,* 1276**,** 1-25.

BAKER, M., ROBINSON, S. D., LECHERTIER, T., BARBER, P. R., TAVORA, B., D'AMICO, G., JONES, D. T., VOJNOVIC, B. & HODIVALA-DILKE, K. 2011. Use of the mouse aortic ring assay to study angiogenesis. *Nat Protoc,* 7**,** 89-104.

BALDWIN, J. M. 1994. Structure and function of receptors coupled to G proteins. *Curr Opin Cell Biol,* 6**,** 180-90.

BENJAMIN, L. E., GOLIJANIN, D., ITIN, A., PODE, D. & KESHET, E. 1999. Selective ablation of immature blood vessels in established human tumors follows vascular endothelial growth factor withdrawal. *J Clin Invest,* 103**,** 159-65.

BERGERS, G. & HANAHAN, D. 2008. Modes of resistance to anti-angiogenic therapy. *Nat Rev Cancer,* 8**,** 592-603.

BERTOLINI, F., MANCUSO, P., SHAKED, Y. & KERBEL, R. S. 2007. Molecular and cellular biomarkers for angiogenesis in clinical oncology. *Drug Discov Today,* 12**,** 806-12.

BJARNADOTTIR, T. K., FREDRIKSSON, R., HOGLUND, P. J., GLORIAM, D. E., LAGERSTROM, M. C. & SCHIOTH, H. B. 2004. The human and mouse repertoire of the adhesion family of G-protein-coupled receptors. *Genomics,* 84**,** 23-33.

BOUABE, H. & OKKENHAUG, K. 2013. Gene targeting in mice: a review. *Methods Mol Biol,* 1064**,** 315-36.

BOWERS, L. W., WIESE, M., BRENNER, A. J., ROSSI, E. L., TEKMAL, R. R., HURSTING, S. D. & DEGRAFFENRIED, L. A. 2015. Obesity Suppresses Estrogen Receptor Beta Expression in Breast Cancer Cells via a HER2-Mediated Pathway. *PLoS One,* 10**,** e0145452.

BROWN, G. T., CASH, B. G., BLIHOGHE, D., JOHANSSON, P., ALNABULSI, A. & MURRAY, G. I. 2014. The expression and prognostic significance of retinoic acid metabolising enzymes in colorectal cancer. *PLoS One,* 9**,** e90776.

BYRNE, A. M., BOUCHIER-HAYES, D. J. & HARMEY, J. H. 2005. Angiogenic and cell survival functions of vascular endothelial growth factor (VEGF). *J Cell Mol Med,* 9**,** 777-94.

CAPASSO, M., DURRANT, L. G., STACEY, M., GORDON, S., RAMAGE, J. & SPENDLOVE, I. 2006. Costimulation via CD55 on human CD4+ T cells mediated by CD97. *J Immunol,* 177**,** 1070-7.

CAPPELLI, H. C., KANUGULA, A. K., ADAPALA, R. K., AMIN, V., SHARMA, P., MIDHA, P., PARUCHURI, S. & THODETI, C. K. 2019. Mechanosensitive TRPV4 channels stabilize VE-cadherin junctions to regulate tumor vascular integrity and metastasis. *Cancer Lett,* 442**,** 15-20.

CARMELIET, P. & JAIN, R. K. 2000. Angiogenesis in cancer and other diseases. *Nature,* 407**,** 249-57.

CARMELIET, P. & JAIN, R. K. 2011a. Molecular mechanisms and clinical applications of angiogenesis. *Nature,* 473**,** 298-307.

CARMELIET, P. & JAIN, R. K. 2011b. Principles and mechanisms of vessel normalization for cancer and other angiogenic diseases. *Nat Rev Drug Discov,* 10**,** 417-27.

CHEN, L., LI, J., WANG, F., DAI, C., WU, F., LIU, X., LI, T., GLAUBEN, R., ZHANG, Y., NIE, G., HE, Y. & QIN, Z. 2016. Tie2 Expression on Macrophages Is Required for Blood Vessel Reconstruction and Tumor Relapse after Chemotherapy. *Cancer Res,* 76**,** 6828-6838.

CHEONG, H. S., KIM, L. H., PARK, B. L., CHOI, Y. H., PARK, H.-S., HONG, S.-J., CHOI, B. W., PARK, C.-S. & SHIN, H. D. 2005. Association analysis of interleukin 5 receptor alpha subunit (IL5RA) polymorphisms and asthma. *Journal Of Human Genetics,* 50**,** 628.

CHURCHMAN, A. T. & SIOW, R. C. 2009. Isolation, culture and characterisation of vascular smooth muscle cells. *Methods Mol Biol,* 467**,** 127-38.

CITI, S., AMOROSI, A., FRANCONI, F., GIOTTI, A. & ZAMPI, G. 1991. Cingulin, a specific protein component of tight junctions, is expressed in normal and neoplastic human epithelial tissues. *The American journal of pathology,* 138**,** 781-789.

CLAXTON, S., KOSTOUROU, V., JADEJA, S., CHAMBON, P., HODIVALA-DILKE, K. & FRUTTIGER, M. 2008. Efficient, inducible Cre-recombinase activation in vascular endothelium. *Genesis,* 46**,** 74-80.

DALTON, A. C., SHLAMKOVITCH, T., PAPO, N. & BARTON, W. A. 2016. Constitutive Association of Tie1 and Tie2 with Endothelial Integrins is Functionally Modulated by Angiopoietin-1 and Fibronectin. *PLoS One,* 11**,** e0163732.

DE, P., PENG, Q., TRAKTUEV, D. O., LI, W., YODER, M. C., MARCH, K. L. & DURDEN, D. L. 2009. Expression of RAC2 in endothelial cells is required for the postnatal neovascular response. *Exp Cell Res,* 315**,** 248-63.

DIETERICH, L. C., MELLBERG, S., LANGENKAMP, E., ZHANG, L., ZIEBA, A., SALOMAKI, H., TEICHERT, M., HUANG, H., EDQVIST, P. H., KRAUS, T., AUGUSTIN, H. G., OLOFSSON, T., LARSSON, E., SODERBERG, O., MOLEMA, G., PONTEN, F., GEORGII-HEMMING, P., ALAFUZOFF, I. & DIMBERG, A. 2012. Transcriptional profiling of human glioblastoma vessels indicates a key role of VEGF-A and TGFbeta2 in vascular abnormalization. *J Pathol,* 228**,** 378-90.

DING, B. S., JAMES, D., IYER, R., FALCIATORI, I., HAMBARDZUMYAN, D., WANG, S., BUTLER, J. M., RABBANY, S. Y. & HORMIGO, A. 2013. Prominin 1/CD133 endothelium sustains growth of proneural glioma. *PLoS One,* 8**,** e62150.

EICHSTAEDT, C. A., ANTAO, T., PAGANI, L., CARDONA, A., KIVISILD, T. & MORMINA, M. 2014. The Andean adaptive toolkit to counteract high altitude maladaptation: genome-wide and phenotypic analysis of the Collas. *PLoS One,* 9**,** e93314.

EL-BROLOSY, M. A. & STAINIER, D. Y. R. 2017. Genetic compensation: A phenomenon in search of mechanisms. *PLoS genetics,* 13**,** e1006780-e1006780.

FATIMA, L. A., CAMPELLO, R. S., SANTOS, R. S., FREITAS, H. S., FRANK, A. P., MACHADO, U. F. & CLEGG, D. J. 2017. Estrogen receptor 1 (ESR1) regulates VEGFA in adipose tissue. *Sci Rep,* 7**,** 16716.

FAVARA, D. M., BANHAM, A. H. & HARRIS, A. L. 2014. A review of ELTD1, a pro-angiogenic adhesion GPCR. *Biochem Soc Trans,* 42**,** 1658-64.

FAVARA, D. M., BANHAM, A. H. & HARRIS, A. L. 2019b. ADGRL4/ELTD1 is a highly conserved angiogenesis-associated orphan adhesion GPCR that emerged with the first vertebrates and comprises 3 evolutionary variants. *BMC Evolutionary Biology,* 19**,** 143.

FIELD, K. M., JORDAN, J. T., WEN, P. Y., ROSENTHAL, M. A. & REARDON, D. A. 2015. Bevacizumab and glioblastoma: scientific review, newly reported updates, and ongoing controversies. *Cancer,* 121**,** 997-1007.

FLICEK, P., AMODE, M. R., BARRELL, D., BEAL, K., BILLIS, K., BRENT, S., CARVALHO-SILVA, D., CLAPHAM, P., COATES, G., FITZGERALD, S., GIL, L., GIRON, C. G., GORDON, L., HOURLIER, T., HUNT, S., JOHNSON, N., JUETTEMANN, T., KAHARI, A. K., KEENAN, S., KULESHA, E., MARTIN, F. J., MAUREL, T., MCLAREN, W. M., MURPHY, D. N., NAG, R., OVERDUIN, B., PIGNATELLI, M., PRITCHARD, B., PRITCHARD, E., RIAT, H. S., RUFFIER, M., SHEPPARD, D., TAYLOR, K., THORMANN, A., TREVANION, S. J., VULLO, A., WILDER, S. P., WILSON, M., ZADISSA, A., AKEN, B. L., BIRNEY, E., CUNNINGHAM, F., HARROW, J., HERRERO, J., HUBBARD, T. J., KINSELLA, R., MUFFATO, M., PARKER, A., SPUDICH, G., YATES, A., ZERBINO, D. R. & SEARLE, S. M. 2014. Ensembl 2014. *Nucleic Acids Res,* 42**,** D749-55.

FOLKMAN, J. 1971. Tumor angiogenesis: therapeutic implications. *N Engl J Med,* 285**,** 1182-6.

FORTINI, F., VIECELI DALLA SEGA, F., CALICETI, C., AQUILA, G., PANNELLA, M., PANNUTI, A., MIELE, L., FERRARI, R. & RIZZO, P. 2017. Estrogen receptor beta-dependent Notch1 activation protects vascular endothelium against tumor necrosis factor alpha (TNFalpha)-induced apoptosis. *J Biol Chem,* 292**,** 18178-18191.

FOUAD, Y. A. & AANEI, C. 2017. Revisiting the hallmarks of cancer. *American journal of cancer research,* 7**,** 1016-1036.

FREDRIKSSON, R., LAGERSTROM, M. C., LUNDIN, L. G. & SCHIOTH, H. B. 2003. The G-protein-coupled receptors in the human genome form five main families. Phylogenetic analysis, paralogon groups, and fingerprints. *Mol Pharmacol,* 63**,** 1256-72.

GARCIA, A. & KANDEL, J. J. 2012. Notch: a key regulator of tumor angiogenesis and metastasis. *Histology and histopathology,* 27**,** 151-156.

GERDES, N., SUKHOVA, G. K., LIBBY, P., REYNOLDS, R. S., YOUNG, J. L. & SCHONBECK, U. 2002. Expression of interleukin (IL)-18 and functional IL-18 receptor on human vascular endothelial cells, smooth muscle cells, and macrophages: implications for atherogenesis. *J Exp Med,* 195**,** 245-57.

GHAJAR, C. M., PEINADO, H., MORI, H., MATEI, I. R., EVASON, K. J., BRAZIER, H., ALMEIDA, D., KOLLER, A., HAJJAR, K. A., STAINIER, D. Y. R., CHEN, E. I., LYDEN, D. & BISSELL, M. J. 2013b. The perivascular niche regulates breast tumour dormancy. *Nature cell biology,* 15**,** 807-817.

GHOSH, E., KUMARI, P., JAIMAN, D. & SHUKLA, A. K. 2015. Methodological advances: the unsung heroes of the GPCR structural revolution. *Nat Rev Mol Cell Biol,* 16**,** 69-81.

GOEL, S., DUDA, D. G., XU, L., MUNN, L. L., BOUCHER, Y., FUKUMURA, D. & JAIN, R. K. 2011. Normalization of the vasculature for treatment of cancer and other diseases. *Physiol Rev,* 91**,** 1071-121.

GRAY, J. X., HAINO, M., ROTH, M. J., MAGUIRE, J. E., JENSEN, P. N., YARME, A., STETLER-STEVENSON, M. A., SIEBENLIST, U. & KELLY, K. 1996. CD97 is a processed, seven-transmembrane, heterodimeric receptor associated with inflammation. *J Immunol,* 157**,** 5438-47.

GREAVES, M. & MALEY, C. C. 2012. Clonal evolution in cancer. *Nature,* 481**,** 306-313.

GRIFFIOEN, A. W. & MOLEMA, G. 2000. Angiogenesis: potentials for pharmacologic intervention in the treatment of cancer, cardiovascular diseases, and chronic inflammation. *Pharmacol Rev,* 52**,** 237-68.

GU, Z., LIN, C., HU, J., XIA, J., WEI, S. & GAO, D. 2019. USP34 Regulated Human Pancreatic Cancer Cell Survival via AKT and PKC Pathways. *Biol Pharm Bull,* 42**,** 573-579.

HAMANN, J., AUST, G., ARAC, D., ENGEL, F. B., FORMSTONE, C., FREDRIKSSON, R., HALL, R. A., HARTY, B. L., KIRCHHOFF, C., KNAPP, B., KRISHNAN, A., LIEBSCHER, I., LIN, H. H., MARTINELLI, D. C., MONK, K. R., PEETERS, M. C., PIAO, X., PROMEL, S., SCHONEBERG, T., SCHWARTZ, T. W., SINGER, K., STACEY, M., USHKARYOV, Y. A., VALLON, M., WOLFRUM, U., WRIGHT, M. W., XU, L., LANGENHAN, T. & SCHIOTH, H. B. 2015. International Union of Basic and Clinical Pharmacology. XCIV. Adhesion G protein-coupled receptors. *Pharmacol Rev,* 67**,** 338-67.

HAMANN, J., WISHAUPT, J. O., VAN LIER, R. A., SMEETS, T. J., BREEDVELD, F. C. & TAK, P. P. 1999. Expression of the activation antigen CD97 and its ligand CD55 in rheumatoid synovial tissue. *Arthritis Rheum,* 42**,** 650-8.

HANAHAN, D. & FOLKMAN, J. 1996. Patterns and emerging mechanisms of the angiogenic switch during tumorigenesis. *Cell,* 86**,** 353-64.

HANLON, C. D. & ANDREW, D. J. 2015. Outside-in signaling--a brief review of GPCR signaling with a focus on the Drosophila GPCR family. *J Cell Sci,* 128**,** 3533-42.

HARKENSEE, C., OKA, A., ONIZUKA, M., MIDDLETON, P. G., INOKO, H., NAKAOKA, H., GENNERY, A. R., ANDO, K. & MORISHIMA, Y. 2013. Microsatellite scanning of the immunogenome associates MAPK14 and ELTD1 with graft-versus-host disease in hematopoietic stem cell transplantation. *Immunogenetics,* 65**,** 417-27.

HARRIS, A. L. 2002. Hypoxia--a key regulatory factor in tumour growth. *Nat Rev Cancer,* 2**,** 38-47.

HE, L., VANLANDEWIJCK, M., MAE, M. A., ANDRAE, J., ANDO, K., DEL GAUDIO, F., NAHAR, K., LEBOUVIER, T., LAVINA, B., GOUVEIA, L., SUN, Y., RASCHPERGER, E., SEGERSTOLPE, A., LIU, J., GUSTAFSSON, S., RASANEN, M., ZARB, Y., MOCHIZUKI, N., KELLER, A., LENDAHL, U. & BETSHOLTZ, C. 2018. Single-cell RNA sequencing of mouse brain and lung vascular and vessel-associated cell types. *Sci Data,* 5**,** 180160.

HEATHCOTE, H. R., LEE, M. D., ZHANG, X., SAUNTER, C. D., WILSON, C. & MCCARRON, J. G. 2019. Endothelial TRPV4 channels modulate vascular tone by Ca(2+) -induced Ca(2+) release at IP3 receptors. *Br J Pharmacol*.

HELBING, T., VOLKMAR, F., GOEBEL, U., HEINKE, J., DIEHL, P., PAHL, H. L., BODE, C., PATTERSON, C. & MOSER, M. 2010. Kruppel-like factor 15 regulates BMPER in endothelial cells. *Cardiovasc Res,* 85**,** 551-9.

HELFRICH, I. & SCHADENDORF, D. 2011. Blood vessel maturation, vascular phenotype and angiogenic potential in malignant melanoma: one step forward for overcoming anti-angiogenic drug resistance? *Mol Oncol,* 5**,** 137-49.

HERBERT, J. M., STEKEL, D., SANDERSON, S., HEATH, V. L. & BICKNELL, R. 2008. A novel method of differential gene expression analysis using multiple cDNA libraries applied to the identification of tumour endothelial genes. *BMC Genomics,* 9**,** 153.

HOU, Z., O'CONNOR, C., FRUHAUF, J., ORR, S., KIM, S., GANGJEE, A. & MATHERLY, L. H. 2019. Regulation of differential proton-coupled folate transporter gene expression in human tumors: transactivation by KLF15 with NRF-1 and the role of Sp1. *Biochem J,* 476**,** 1247-1266.

HUANG, Y. S., CHIANG, N. Y., HU, C. H., HSIAO, C. C., CHENG, K. F., TSAI, W. P., YONA, S., STACEY, M., GORDON, S., CHANG, G. W. & LIN, H. H. 2012. Activation of myeloid cell-specific adhesion class G protein-coupled receptor EMR2 via ligation-induced translocation and interaction of receptor subunits in lipid raft microdomains. *Mol Cell Biol,* 32**,** 1408-20.

ISHIKAWA, K., YOSHIDA, S., KADOTA, K., NAKAMURA, T., NIIRO, H., ARAKAWA, S., YOSHIDA, A., AKASHI, K. & ISHIBASHI, T. 2010. Gene Expression Profile of Hyperoxic and Hypoxic Retinas in a Mouse Model of Oxygen-Induced Retinopathy. *Investigative Ophthalmology & Visual Science,* 51**,** 4307-4319.

JAIN, R. K. 2005. Normalization of tumor vasculature: an emerging concept in antiangiogenic therapy. *Science,* 307**,** 58-62.

JAIN, R. K., DUDA, D. G., CLARK, J. W. & LOEFFLER, J. S. 2006. Lessons from phase III clinical trials on anti-VEGF therapy for cancer. *Nat Clin Pract Oncol,* 3**,** 24-40.

JAIN, R. K., DUDA, D. G., WILLETT, C. G., SAHANI, D. V., ZHU, A. X., LOEFFLER, J. S., BATCHELOR, T. T. & SORENSEN, A. G. 2009. Biomarkers of response and resistance to antiangiogenic therapy. *Nat Rev Clin Oncol,* 6**,** 327-38.

KALYANA-SUNDARAM, S., KUMAR-SINHA, C., SHANKAR, S., ROBINSON, D. R., WU, Y.-M., CAO, X., ASANGANI, I. A., KOTHARI, V., PRENSNER, J. R., LONIGRO, R. J., IYER, M. K., BARRETTE, T., SHANMUGAM, A., DHANASEKARAN, S. M., PALANISAMY, N. & CHINNAIYAN, A. M. 2012. Expressed pseudogenes in the transcriptional landscape of human cancers. *Cell,* 149**,** 1622-1634.

KAN, A., LE, Y., ZHANG, Y. F., DUAN, F. T., ZHONG, X. P., LU, L. H., LING, Y. H. & GUO, R. P. 2018. ELTD1 Function in Hepatocellular Carcinoma is Carcinoma-Associated Fibroblast-Dependent. *J Cancer,* 9**,** 2415-2427.

KAUR, B., BRAT, D. J., DEVI, N. S. & VAN MEIR, E. G. 2005. Vasculostatin, a proteolytic fragment of brain angiogenesis inhibitor 1, is an antiangiogenic and antitumorigenic factor. *Oncogene,* 24**,** 3632-42.

KISANUKI, Y. Y., HAMMER, R. E., MIYAZAKI, J., WILLIAMS, S. C., RICHARDSON, J. A. & YANAGISAWA, M. 2001. Tie2-Cre transgenic mice: a new model for endothelial cell-lineage analysis in vivo. *Dev Biol,* 230**,** 230-42.

KOIRALA, S., JIN, Z., PIAO, X. & CORFAS, G. 2009. GPR56-regulated granule cell adhesion is essential for rostral cerebellar development. *J Neurosci,* 29**,** 7439-49.

KOS, M. & DABROWSKI, A. 2002. Tumour's angiogenesis--the function of VEGF and bFGF in colorectal cancer. *Ann Univ Mariae Curie Sklodowska Med,* 57**,** 556-61.

KWAKKENBOS, M. J., KOP, E. N., STACEY, M., MATMATI, M., GORDON, S., LIN, H. H. & HAMANN, J. 2004. The EGF-TM7 family: a postgenomic view. *Immunogenetics,* 55**,** 655-66.

LANGENHAN, T., AUST, G. & HAMANN, J. 2013. Sticky signaling--adhesion class G protein-coupled receptors take the stage. *Sci Signal,* 6**,** re3.

LARRE, M. I., FLORES-MALDONADO, C. & CEREIJIDO, M. 2013. Methods to Study Tight Junctions. *In:* MARTIN, T. A. & JIANG, W. G. (eds.) *Tight Junctions in Cancer Metastasis.* Dordrecht: Springer Netherlands.

LAU, J., CHEUNG, J., NAVARRO, A., LIANOGLOU, S., HALEY, B., TOTPAL, K., SANDERS, L., KOEPPEN, H., CAPLAZI, P., MCBRIDE, J., CHIU, H., HONG, R., GROGAN, J., JAVINAL, V., YAUCH, R., IRVING, B., BELVIN, M., MELLMAN, I., KIM, J. M. & SCHMIDT, M. 2017. Tumour and host cell PD-L1 is required to mediate suppression of anti-tumour immunity in mice. *Nat Commun,* 8**,** 14572.

LEE, K. T., BYUN, M. J., KANG, K. S., PARK, E. W., LEE, S. H., CHO, S., KIM, H., KIM, K. W., LEE, T., PARK, J. E., PARK, W., SHIN, D., PARK, H. S., JEON, J. T., CHOI, B. H., JANG, G. W., CHOI, S. H., KIM, D. W., LIM, D., PARK, H. S., PARK, M. R., OTT, J., SCHOOK, L. B., KIM, T. H. & KIM, H. 2011. Neuronal genes for subcutaneous fat thickness in human and pig are identified by local genomic sequencing and combined SNP association study. *PLoS One,* 6**,** e16356.

LEE, S., KIM, D., KANG, J., KIM, E., KIM, W., YOUN, H. & YOUN, B. 2017. Surfactant Protein B Suppresses Lung Cancer Progression by Inhibiting Secretory Phospholipase A2 Activity and Arachidonic Acid Production. *Cell Physiol Biochem,* 42**,** 1684-1700.

LEE, W. H., WANG, G. M., YANG, X. L., SEAMAN, L. B. & VANNUCCI, S. I. 1999. Perinatal hypoxia-ischemia decreased neuronal but increased cerebral vascular endothelial IGFBP3 expression. *Endocrine,* 11**,** 181-8.

LEEMANS, J. C., TE VELDE, A. A., FLORQUIN, S., BENNINK, R. J., DE BRUIN, K., VAN LIER, R. A., VAN DER POLL, T. & HAMANN, J. 2004. The epidermal growth factor-seven transmembrane (EGF-TM7) receptor CD97 is required for neutrophil migration and host defense. *J Immunol,* 172**,** 1125-31.

LEFKOWITZ, R. J. 2000. The superfamily of heptahelical receptors. *Nat Cell Biol,* 2**,** E133-6.

LEUNG, T., RAJENDRAN, R., SINGH, S., GARVA, R., KRSTIC-DEMONACOS, M. & DEMONACOS, C. 2013. Cytochrome P450 2E1 (CYP2E1) regulates the response to oxidative stress and migration of breast cancer cells. *Breast cancer research : BCR,* 15**,** R107-R107.

LI, J. D., FENG, Q. C., QI, Y., CUI, G. & ZHAO, S. 2017. PPARGC1A is upregulated and facilitates lung cancer metastasis. *Exp Cell Res,* 359**,** 356-360.
LI, J. L. & HARRIS, A. L. 2009. Crosstalk of VEGF and Notch pathways in tumour angiogenesis: therapeutic implications. *Front Biosci (Landmark Ed),* 14**,** 3094-110.
LI, W. & GAO, F. B. 2003. Actin filament-stabilizing protein tropomyosin regulates the size of dendritic fields. *J Neurosci,* 23**,** 6171-5.
LIEBSCHER, I., SCHON, J., PETERSEN, S. C., FISCHER, L., AUERBACH, N., DEMBERG, L. M., MOGHA, A., COSTER, M., SIMON, K. U., ROTHEMUND, S., MONK, K. R. & SCHONEBERG, T. 2014. A tethered agonist within the ectodomain activates the adhesion G protein-coupled receptors GPR126 and GPR133. *Cell Rep,* 9**,** 2018-26.
LIN, H. H., CHANG, G. W., DAVIES, J. Q., STACEY, M., HARRIS, J. & GORDON, S. 2004. Autocatalytic cleavage of the EMR2 receptor occurs at a conserved G protein-coupled receptor proteolytic site motif. *J Biol Chem,* 279**,** 31823-32.
LIU, B., XU, L., YU, X., LI, W., SUN, X., XIAO, S., GUO, M. & WANG, H. 2018. Protective effect of KLF15 on vascular endothelial dysfunction induced by TNFalpha. *Mol Med Rep,* 18**,** 1987-1994.
LU, S., LIU, S., WIETELMANN, A., KOJONAZAROV, B., ATZBERGER, A., TANG, C., SCHERMULY, R. T., GRONE, H. J. & OFFERMANNS, S. 2017. Developmental vascular remodeling defects and postnatal kidney failure in mice lacking Gpr116 (Adgrf5) and Eltd1 (Adgrl4). *PLoS One,* 12**,** e0183166.
LUCAS, T. M., RICHNER, J. M. & DIAMOND, M. S. 2016. The Interferon-Stimulated Gene Ifi27l2a Restricts West Nile Virus Infection and Pathogenesis in a Cell-Type- and Region-Specific Manner. *Journal of virology,* 90**,** 2600-2615.
LYTOVCHENKO, O. & KUNJI, E. R. S. 2017. Expression and putative role of mitochondrial transport proteins in cancer. *Biochimica et Biophysica Acta (BBA) - Bioenergetics,* 1858**,** 641-654.
MAI, J., VIRTUE, A., SHEN, J., WANG, H. & YANG, X.-F. 2013. An evolving new paradigm: endothelial cells--conditional innate immune cells. *Journal of hematology & oncology,* 6**,** 61-61.
MARÍN-AGUILERA, M., REIG, Ò., LOZANO, J. J., JIMÉNEZ, N., GARCÍA-RECIO, S., ERILL, N., GABA, L., TAGLIAPIETRA, A., ORTEGA, V., CARRERA, G., COLOMER, A., GASCÓN, P. & MELLADO, B. 2015. Molecular profiling of peripheral blood is associated with circulating tumor cells content and poor survival in metastatic castration-resistant prostate cancer. *Oncotarget,* 6**,** 10604-10616.
MASHIMA, R. & OKUYAMA, T. 2015. The role of lipoxygenases in pathophysiology; new insights and future perspectives. *Redox Biol,* 6**,** 297-310.
MASIERO, M., SIMOES, F. C., HAN, H. D., SNELL, C., PETERKIN, T., BRIDGES, E., MANGALA, L. S., WU, S. Y., PRADEEP, S., LI, D., HAN, C., DALTON, H., LOPEZ-BERESTEIN, G., TUYNMAN, J. B., MORTENSEN, N., LI, J. L., PATIENT, R., SOOD, A. K., BANHAM, A. H., HARRIS, A. L. & BUFFA, F. M. 2013. A core human primary tumor angiogenesis signature identifies the endothelial orphan receptor ELTD1 as a key regulator of angiogenesis. *Cancer Cell,* 24**,** 229-41.
MATSUSHITA, H., LELIANOVA, V. G. & USHKARYOV, Y. A. 1999. The latrophilin family: multiply spliced G protein-coupled receptors with differential tissue distribution. *FEBS Lett,* 443**,** 348-52.
MCNAMARA, M. G., SAHEBJAM, S. & MASON, W. P. 2013. Emerging biomarkers in glioblastoma. *Cancers (Basel),* 5**,** 1103-19.
MESSNER, B., KERN, J., WIEDEMANN, D., SCHWAIGER, S., TURKCAN, A., PLONER, C., TROCKENBACHER, A., AUMAYR, K., BONAROS, N., LAUFER, G., STUPPNER, H., UNTERGASSER, G. & BERNHARD, D. 2013. 5-Methoxyleoligin, a lignan from Edelweiss, stimulates CYP26B1-dependent angiogenesis in vitro and induces arteriogenesis in infarcted rat hearts in vivo. *PLoS One,* 8**,** e58342.
MORIGUCHI, T., HARAGUCHI, K., UEDA, N., OKADA, M., FURUYA, T. & AKIYAMA, T. 2004. DREG, a developmentally regulated G protein-coupled receptor containing two conserved proteolytic cleavage sites. *Genes Cells,* 9**,** 549-60.

NECHIPORUK, T., URNESS, L. D. & KEATING, M. T. 2001. ETL, a novel seven-transmembrane receptor that is developmentally regulated in the heart. ETL is a member of the secretin family and belongs to the epidermal growth factor-seven-transmembrane subfamily. *J Biol Chem,* 276**,** 4150-7.

NICOLAIDIS, S. 2015. Biomarkers of glioblastoma multiforme. *Metabolism,* 64**,** S22-7.

ODA, K., SHIRATSUCHI, T., NISHIMORI, H., INAZAWA, J., YOSHIKAWA, H., TAKETANI, Y., NAKAMURA, Y. & TOKINO, T. 1999. Identification of BAIAP2 (BAI-associated protein 2), a novel human homologue of hamster IRSp53, whose SH3 domain interacts with the cytoplasmic domain of BAI1. *Cytogenet Cell Genet,* 84**,** 75-82.

PALAGYI, A., NEVELING, K., PLINNINGER, U., ZIESCH, A., TARGOSZ, B.-S., DENK, G. U., OCHS, S., RIZZANI, A., MEIER, D., THASLER, W. E., HANENBERG, H., DE TONI, E. N., BASSERMANN, F., SCHÄFER, C., GÖKE, B., SCHINDLER, D. & GALLMEIER, E. 2010. Genetic inactivation of the Fanconi anemia gene FANCC identified in the hepatocellular carcinoma cell line HuH-7 confers sensitivity towards DNA-interstrand crosslinking agents. *Molecular cancer,* 9**,** 127-127.

PALOMERO, J., VEGLIANTE, M. C., RODRÍGUEZ, M. L., EGUILEOR, Á., CASTELLANO, G., PLANAS-RIGOL, E., JARES, P., RIBERA-CORTADA, I., CID, M. C., CAMPO, E. & AMADOR, V. 2014. SOX11 promotes tumor angiogenesis through transcriptional regulation of PDGFA in mantle cell lymphoma. *Blood,* 124**,** 2235.

PATAN, S., MUNN, L. L. & JAIN, R. K. 1996. Intussusceptive microvascular growth in a human colon adenocarcinoma xenograft: a novel mechanism of tumor angiogenesis. *Microvasc Res,* 51**,** 260-72.

PAYNE, S., DE VAL, S. & NEAL, A. 2018. Endothelial-Specific Cre Mouse Models. *Arterioscler Thromb Vasc Biol,* 38**,** 2550-2561.

PEKOW, J., DOUGHERTY, U., HUANG, Y., GOMETZ, E., NATHANSON, J., COHEN, G., LEVY, S., KOCHERGINSKY, M., VENU, N., WESTERHOFF, M., HART, J., NOFFSINGER, A. E., HANAUER, S. B., HURST, R. D., FICHERA, A., JOSEPH, L. J., LIU, Q. & BISSONNETTE, M. 2013. Gene signature distinguishes patients with chronic ulcerative colitis harboring remote neoplastic lesions. *Inflamm Bowel Dis,* 19**,** 461-70.

PETROVA, V., ANNICCHIARICO-PETRUZZELLI, M., MELINO, G. & AMELIO, I. 2018. The hypoxic tumour microenvironment. *Oncogenesis,* 7**,** 10.

PICELLI, S., BJORKLUND, A. K., FARIDANI, O. R., SAGASSER, S., WINBERG, G. & SANDBERG, R. 2013. Smart-seq2 for sensitive full-length transcriptome profiling in single cells. *Nat Methods,* 10**,** 1096-8.

PICELLI, S., FARIDANI, O. R., BJORKLUND, A. K., WINBERG, G., SAGASSER, S. & SANDBERG, R. 2014. Full-length RNA-seq from single cells using Smart-seq2. *Nat Protoc,* 9**,** 171-81.

PLANUTIENE, M., PLANUTIS, K. & HOLCOMBE, R. F. 2011. Lymphoid enhancer-binding factor 1, a representative of vertebrate-specific Lef1/Tcf1 sub-family, is a Wnt-beta-catenin pathway target gene in human endothelial cells which regulates matrix metalloproteinase-2 expression and promotes endothelial cell invasion. *Vasc Cell,* 3**,** 28.

PORTO NETO, L. R., BUNCH, R. J., HARRISON, B. E. & BARENDSE, W. 2011. DNA variation in the gene ELTD1 is associated with tick burden in cattle. *Anim Genet,* 42**,** 50-5.

POTTER, S. S. 2018. Single-cell RNA sequencing for the study of development, physiology and disease. *Nat Rev Nephrol,* 14**,** 479-492.

PRADEEP, C. R., SUNILA, E. S. & KUTTAN, G. 2005. Expression of vascular endothelial growth factor (VEGF) and VEGF receptors in tumor angiogenesis and malignancies. *Integr Cancer Ther,* 4**,** 315-21.

PROMEL, S., LANGENHAN, T. & ARAC, D. 2013. Matching structure with function: the GAIN domain of adhesion-GPCR and PKD1-like proteins. *Trends Pharmacol Sci,* 34**,** 470-8.

RAK, J. & KERBEL, R. S. 1997. bFGF and tumor angiogenesis--back in the limelight? *Nat Med,* 3**,** 1083-4.

RAY, M. K., FAGAN, S. P. & BRUNICARDI, F. C. 2000. The Cre-loxP system: a versatile tool for targeting genes in a cell- and stage-specific manner. *Cell Transplant,* 9**,** 805-15.

REGARD, J. B., SATO, I. T. & COUGHLIN, S. R. 2008. Anatomical profiling of G protein-coupled receptor expression. *Cell,* 135**,** 561-71.

REYNOLDS, J. A., RAY, D. W., ZEEF, L. A. H., O'NEILL, T., BRUCE, I. N. & ALEXANDER, M. Y. 2014. The effect of type 1 IFN on human aortic endothelial cell function in vitro: relevance to systemic lupus erythematosus. *Journal of interferon & cytokine research : the official journal of the International Society for Interferon and Cytokine Research,* 34**,** 404-412.

ROBINSON, S. P., LANGAN-FAHEY, S. M., JOHNSON, D. A. & JORDAN, V. C. 1991. Metabolites, pharmacodynamics, and pharmacokinetics of tamoxifen in rats and mice compared to the breast cancer patient. *Drug Metabolism and Disposition,* 19**,** 36.

SALEEMBHASHA, A. & MISHRA, S. 2019. Long non-coding RNAs as pan-cancer master gene regulators of associated protein-coding genes: a systems biology approach. *PeerJ,* 7**,** e6388-e6388.

SASIDHARAN, R. & GERSTEIN, M. 2008. Genomics: protein fossils live on as RNA. *Nature,* 453**,** 729-31.

SCHIOTH, H. B. & FREDRIKSSON, R. 2005. The GRAFS classification system of G-protein coupled receptors in comparative perspective. *Gen Comp Endocrinol,* 142**,** 94-101.

SCHOSSLEITNER, K., RAUSCHER, S., GROGER, M., FRIEDL, H. P., FINSTERWALDER, R., HABERTHEUER, A., SIBILIA, M., BROSTJAN, C., FODINGER, D., CITI, S. & PETZELBAUER, P. 2016. Evidence That Cingulin Regulates Endothelial Barrier Function In Vitro and In Vivo. *Arterioscler Thromb Vasc Biol,* 36**,** 647-54.

SCIABICA, K., WU, Y., GUTIERREZ, M. & LUO, J. 2008. Cancer biomarker candidate identification using novel, quantitative multiplex gene expression profiling. *Cancer Research,* 68**,** 1654.

SEIFERT, J. R. & MLODZIK, M. 2007. Frizzled/PCP signalling: a conserved mechanism regulating cell polarity and directed motility. *Nat Rev Genet,* 8**,** 126-38.

SEKINE, A., NISHIWAKI, T., NISHIMURA, R., KAWASAKI, T., URUSHIBARA, T., SUDA, R., SUZUKI, T., TAKAYANAGI, S., TERADA, J., SAKAO, S., TADA, Y., IWAMA, A. & TATSUMI, K. 2016. Prominin-1/CD133 expression as potential tissue-resident vascular endothelial progenitor cells in the pulmonary circulation. *Am J Physiol Lung Cell Mol Physiol,* 310**,** L1130-42.

SERBAN, F., ARTENE, S. A., GEORGESCU, A. M., PURCARU, S. O., TACHE, D. E., ALEXANDRU, O. & DRICU, A. 2015. Epidermal growth factor, latrophilin, and seven transmembrane domain-containing protein 1 marker, a novel angiogenesis marker. *Onco Targets Ther,* 8**,** 3767-74.

SERBAN, F., DAIANU, O., TATARANU, L. G., ARTENE, S. A., EMAMI, G., GEORGESCU, A. M., ALEXANDRU, O., PURCARU, S. O., TACHE, D. E., DANCIULESCU, M. M., SFREDEL, V. & DRICU, A. 2017. Silencing of epidermal growth factor, latrophilin and seven transmembrane domain-containing protein 1 (ELTD1) via siRNA-induced cell death in glioblastoma. *J Immunoassay Immunochem,* 38**,** 21-33.

SHAH, R., SMITH, P., PURDIE, C., QUINLAN, P., BAKER, L., AMAN, P., THOMPSON, A. M. & CROOK, T. 2009. The prolyl 3-hydroxylases P3H2 and P3H3 are novel targets for epigenetic silencing in breast cancer. *Br J Cancer,* 100**,** 1687-96.

SHAO, J., TENG, Y., PADIA, R., HONG, S., NOH, H., XIE, X., MUMM, J. S., DONG, Z., DING, H.-F., COWELL, J., KIM, J., HAN, J. & HUANG, S. 2013. COP1 and GSK3β Cooperate to Promote c-Jun Degradation and Inhibit Breast Cancer Cell Tumorigenesis. *Neoplasia,* 15**,** 1075-IN11.

SILVA, J. P., LELIANOVA, V., HOPKINS, C., VOLYNSKI, K. E. & USHKARYOV, Y. 2009. Functional cross-interaction of the fragments produced by the cleavage of distinct adhesion G-protein-coupled receptors. *J Biol Chem,* 284**,** 6495-506.

SINGH, H., TAHIR, T. A., ALAWO, D. O., ISSA, E. & BRINDLE, N. P. 2011. Molecular control of angiopoietin signalling. *Biochem Soc Trans,* 39**,** 1592-6.

SKOWRONSKI, M. T., LEBECK, J., ROJEK, A., PRAETORIUS, J., FUCHTBAUER, E. M., FROKIAER, J. & NIELSEN, S. 2007. AQP7 is localized in capillaries of adipose tissue, cardiac and striated muscle: implications in glycerol metabolism. *Am J Physiol Renal Physiol,* 292**,** F956-65.

SOHRABI, Y., VOLKOVA, V., KOBETS, T., HAVELKOVÁ, H., KRAYEM, I., SLAPNIČKOVÁ, M., DEMANT, P. & LIPOLDOVÁ, M. 2018. Genetic Regulation of Guanylate-Binding Proteins 2b and 5 during Leishmaniasis in Mice. *Frontiers in Immunology,* 9.

STEGLE, O., TEICHMANN, S. A. & MARIONI, J. C. 2015. Computational and analytical challenges in single-cell transcriptomics. *Nat Rev Genet,* 16**,** 133-45.

STOVEKEN, H. M., HAJDUCZOK, A. G., XU, L. & TALL, G. G. 2015. Adhesion G protein-coupled receptors are activated by exposure of a cryptic tethered agonist. *Proc Natl Acad Sci U S A,* 112**,** 6194-9.

SVENSSON, V., VENTO-TORMO, R. & TEICHMANN, S. A. 2018. Exponential scaling of single-cell RNA-seq in the past decade. *Nat Protoc,* 13**,** 599-604.

TAM, O. H., ARAVIN, A. A., STEIN, P., GIRARD, A., MURCHISON, E. P., CHELOUFI, S., HODGES, E., ANGER, M., SACHIDANANDAM, R., SCHULTZ, R. M. & HANNON, G. J. 2008. Pseudogene-derived small interfering RNAs regulate gene expression in mouse oocytes. *Nature,* 453**,** 534-8.

TANDLE, A. & LIBUTTI, S. K. 2003. Antiangiogenic therapy: targeting vascular endothelial growth factor and its receptors. *Clin Adv Hematol Oncol,* 1**,** 41-8.

TANG, C. T., GAO, Y. J. & GE, Z. Z. 2018. NOX4, a new genetic target for anti-cancer therapy in digestive system cancer. *J Dig Dis,* 19**,** 578-585.

TANG, Y., HARRINGTON, A., YANG, X., FRIESEL, R. E. & LIAW, L. 2010. The contribution of the Tie2+ lineage to primitive and definitive hematopoietic cells. *Genesis,* 48**,** 563-7.

TEICHERT, M., MILDE, L., HOLM, A., STANICEK, L., GENGENBACHER, N., SAVANT, S., RUCKDESCHEL, T., HASANOV, Z., SRIVASTAVA, K., HU, J., HERTEL, S., BARTOL, A., SCHLERETH, K. & AUGUSTIN, H. G. 2017. Pericyte-expressed Tie2 controls angiogenesis and vessel maturation. *Nature Communications,* 8**,** 16106.

THURSTON, G. & KITAJEWSKI, J. 2008. VEGF and Delta-Notch: interacting signalling pathways in tumour angiogenesis. *Br J Cancer,* 99**,** 1204-9.

TOWNER, R. A., JENSEN, R. L., COLMAN, H., VAILLANT, B., SMITH, N., CASTEEL, R., SAUNDERS, D., GILLESPIE, D. L., SILASI-MANSAT, R., LUPU, F., GILES, C. B. & WREN, J. D. 2013. ELTD1, a potential new biomarker for gliomas. *Neurosurgery,* 72**,** 77-90; discussion 91.

TRUSKEY, G. A. 2010. Endothelial Cell Vascular Smooth Muscle Cell Co-Culture Assay For High Throughput Screening Assays For Discovery of Anti-Angiogenesis Agents and Other Therapeutic Molecules. *International journal of high throughput screening,* 2010**,** 171-181.

UHLEN, M., OKSVOLD, P., FAGERBERG, L., LUNDBERG, E., JONASSON, K., FORSBERG, M., ZWAHLEN, M., KAMPF, C., WESTER, K., HOBER, S., WERNERUS, H., BJORLING, L. & PONTEN, F. 2010. Towards a knowledge-based Human Protein Atlas. *Nat Biotechnol,* 28**,** 1248-50.

USUI, T., SHIMA, Y., SHIMADA, Y., HIRANO, S., BURGESS, R. W., SCHWARZ, T. L., TAKEICHI, M. & UEMURA, T. 1999. Flamingo, a seven-pass transmembrane cadherin, regulates planar cell polarity under the control of Frizzled. *Cell,* 98**,** 585-95.

VAN BEIJNUM, J. R., NOWAK-SLIWINSKA, P., HUIJBERS, E. J., THIJSSEN, V. L. & GRIFFIOEN, A. W. 2015. The great escape; the hallmarks of resistance to antiangiogenic therapy. *Pharmacol Rev,* 67**,** 441-61.

VANLANDEWIJCK, M., HE, L., MAE, M. A., ANDRAE, J., ANDO, K., DEL GAUDIO, F., NAHAR, K., LEBOUVIER, T., LAVINA, B., GOUVEIA, L., SUN, Y., RASCHPERGER, E., RASANEN, M., ZARB, Y., MOCHIZUKI, N., KELLER, A., LENDAHL, U. & BETSHOLTZ, C. 2018. A molecular atlas of cell types and zonation in the brain vasculature. *Nature,* 554**,** 475-480.

VEGETO, E., CUZZOCREA, S., CRISAFULLI, C., MAZZON, E., SALA, A., KRUST, A. & MAGGI, A. 2010. Estrogen receptor-alpha as a drug target candidate for preventing lung inflammation. *Endocrinology,* 151**,** 174-84.

VOLYNSKI, K. E., SILVA, J. P., LELIANOVA, V. G., ATIQUR RAHMAN, M., HOPKINS, C. & USHKARYOV, Y. A. 2004. Latrophilin fragments behave as independent proteins that associate and signal on binding of LTX(N4C). *Embo j,* 23**,** 4423-33.

WALLGARD, E., LARSSON, E., HE, L., HELLSTROM, M., ARMULIK, A., NISANCIOGLU, M. H., GENOVE, G., LINDAHL, P. & BETSHOLTZ, C. 2008. Identification of a core set of 58 gene transcripts with broad and specific expression in the microvasculature. *Arterioscler Thromb Vasc Biol,* 28**,** 1469-76.

WALTER, S., ATZMON, G., DEMERATH, E. W., GARCIA, M. E., KAPLAN, R. C., KUMARI, M., LUNETTA, K. L., MILANESCHI, Y., TANAKA, T., TRANAH, G. J., VOLKER, U., YU, L., ARNOLD, A., BENJAMIN, E. J., BIFFAR, R., BUCHMAN, A. S., BOERWINKLE, E., COUPER, D., DE JAGER, P. L., EVANS, D. A., HARRIS, T. B., HOFFMANN, W., HOFMAN, A., KARASIK, D., KIEL, D. P., KOCHER, T., KUNINGAS, M., LAUNER, L. J., LOHMAN, K. K., LUTSEY, P. L., MACKENBACH, J., MARCIANTE, K., PSATY, B. M., REIMAN, E. M., ROTTER, J. I., SESHADRI, S., SHARDELL, M. D., SMITH, A. V., VAN DUIJN, C., WALSTON, J., ZILLIKENS, M. C., BANDINELLI, S., BAUMEISTER, S. E., BENNETT, D. A., FERRUCCI, L., GUDNASON, V., KIVIMAKI, M., LIU, Y., MURABITO, J. M., NEWMAN, A. B., TIEMEIER, H. & FRANCESCHINI, N. 2011. A genome-wide association study of aging. *Neurobiol Aging,* 32**,** 2109.e15-28.

WANG, J., FENG, L., ZHU, Z., ZHENG, M., WANG, D., CHEN, Z. & SUN, H. 2015. Aquaporins as diagnostic and therapeutic targets in cancer: how far we are? *Journal of translational medicine,* 13**,** 96-96.

WANG, J., LIANG, W. J., MIN, G. T., WANG, H. P., CHEN, W. & YAO, N. 2018. LTBP2 promotes the migration and invasion of gastric cancer cells and predicts poor outcome of patients with gastric cancer. *Int J Oncol,* 52**,** 1886-1898.

WANG, T., WARD, Y., TIAN, L., LAKE, R., GUEDEZ, L., STETLER-STEVENSON, W. G. & KELLY, K. 2005. CD97, an adhesion receptor on inflammatory cells, stimulates angiogenesis through binding integrin counterreceptors on endothelial cells. *Blood,* 105**,** 2836-44.

WANG, X., HE, Y., ZHANG, Q., REN, X. & ZHANG, Z. 2019. Direct Comparative Analysis of 10X Genomics Chromium and Smart-seq2. *bioRxiv***,** 615013.

WEBER, E. W., HAN, F., TAUSEEF, M., BIRNBAUMER, L., MEHTA, D. & MULLER, W. A. 2015. TRPC6 is the endothelial calcium channel that regulates leukocyte transendothelial migration during the inflammatory response. *J Exp Med,* 212**,** 1883-99.

WU, C., OROZCO, C., BOYER, J., LEGLISE, M., GOODALE, J., BATALOV, S., HODGE, C. L., HAASE, J., JANES, J., HUSS, J. W., 3RD & SU, A. I. 2009. BioGPS: an extensible and customizable portal for querying and organizing gene annotation resources. *Genome Biol,* 10**,** R130.

XIAO, J., JIANG, H., ZHANG, R., FAN, G., ZHANG, Y., JIANG, D. & LI, H. 2012. Augmented cardiac hypertrophy in response to pressure overload in mice lacking ELTD1. *PLoS One,* 7**,** e35779.

XU, T., YU, W., LI, Q., LI, X., SHI, Y., CAO, B., ZHANG, Y., WANG, S., ZHANG, Y., WANG, T. & HUANG, B. 2019. MicroRNA-524 inhibits the progress of glioma via the direct targeting of NCF2. *Am J Transl Res,* 11**,** 1605-1615.

XU, X., LIU, Z., ZHOU, L., XIE, H., CHENG, J., LING, Q., WANG, J., GUO, H., WEI, X. & ZHENG, S. 2015. Characterization of genome-wide TFCP2 targets in hepatocellular carcinoma: implication of targets FN1 and TJP1 in metastasis. *Journal of experimental & clinical cancer research : CR,* 34**,** 6-6.

YANG, N., LEUNG, E. L., LIU, C., LI, L., EGUETHER, T., JUN YAO, X. J., JONES, E. C., NORRIS, D. A., LIU, A., CLARK, R. A., ROOP, D. R., PAZOUR, G. J., SHROYER, K. R. & CHEN, J. 2017. INTU is essential for oncogenic Hh signaling through regulating primary cilia formation in basal cell carcinoma. *Oncogene,* 36**,** 4997-5005.

ZANG, Y., DONG, Y., YANG, D., XUE, B., LI, F., GU, P., ZHAO, H., WANG, S., ZHOU, S., YING, R., WANG, Z. & SHAN, Y. 2016. Expression and prognostic significance of ELL-associated factor 2 in human prostate cancer. *International urology and nephrology,* 48**,** 695-700.

ZHANG, J., ZENG, Y., CHEN, J., CAI, D., CHEN, C., ZHANG, S. & CHEN, Z. 2019. miR-29a/b cluster suppresses high glucose-induced endothelial-mesenchymal transition in human retinal microvascular endothelial cells by targeting Notch2. *Exp Ther Med,* 17**,** 3108-3116.

ZHENG, D., FRANKISH, A., BAERTSCH, R., KAPRANOV, P., REYMOND, A., CHOO, S. W., LU, Y., DENOEUD, F., ANTONARAKIS, S. E., SNYDER, M., RUAN, Y., WEI, C. L., GINGERAS, T. R., GUIGO, R., HARROW, J. & GERSTEIN, M. B. 2007. Pseudogenes in the ENCODE regions: consensus annotation, analysis of transcription, and evolution. *Genome Res,* 17**,** 839-51.

ZHOU, W., FENG, X., LI, H., WANG, L., ZHU, B., LIU, W., ZHAO, M., YAO, K. & REN, C. 2009. Inactivation of LARS2, located at the commonly deleted region 3p21.3, by both epigenetic and genetic mechanisms in nasopharyngeal carcinoma. *Acta Biochim Biophys Sin (Shanghai),* 41**,** 54-62.

ZHU, L. M., SHI, D. M., DAI, Q., CHENG, X. J., YAO, W. Y., SUN, P. H., DING, Y., QIAO, M. M., WU, Y. L., JIANG, S. H. & TU, S. P. 2014. Tumor suppressor XAF1 induces apoptosis, inhibits angiogenesis and inhibits tumor growth in hepatocellular carcinoma. *Oncotarget,* 5**,** 5403-15.

ZIEGLER, J., PODY, R., COUTINHO DE SOUZA, P., EVANS, B., SAUNDERS, D., SMITH, N., MALLORY, S., NJOKU, C., DONG, Y., CHEN, H., DONG, J., LERNER, M., MIAN, O., TUMMALA, S., BATTISTE, J., FUNG, K. M., WREN, J. D. & TOWNER, R. A. 2017. ELTD1, an effective anti-angiogenic target for gliomas: preclinical assessment in mouse GL261 and human G55 xenograft glioma models. *Neuro Oncol,* 19**,** 175-185.

ZIEGLER, J., ZALLES, M., SMITH, N., SAUNDERS, D., LERNER, M., FUNG, K. M., PATEL, M., WREN, J. D., LUPU, F., BATTISTE, J. & TOWNER, R. A. 2019. Targeting ELTD1, an angiogenesis marker for glioblastoma (GBM), also affects VEGFR2: molecular-targeted MRI assessment. *Am J Nucl Med Mol Imaging,* 9**,** 93-109.

ZIGMOND, E., HALPERN, Z., ELINAV, E., BRAZOWSKI, E., JUNG, S. & VAROL, C. 2011. Utilization of murine colonoscopy for orthotopic implantation of colorectal cancer. *PLoS One,* 6**,** e28858.

ZIJLSTRA, A., MCCABE, N. R. & SCHELLING, M. E. 1999. Expression and assembly of the angiogenic marker B-fibronectin by endothelial cells in vitro: regulation by confluency. *Angiogenesis,* 3**,** 77-87.

Conference posters related to thesis

Poster presentations

1. Poster presentation: ADGRL4/ELTD1 in Angiogenesis. Department of Oncology Annual Oncology Student Symposium, St. Anne's College, University of Oxford, 23rd June 2016.
2. Poster presentation: ADGRL4/ELTD1, An Adhesion G Protein-Coupled Receptor Involved in Angiogenesis. 11th World Congress for Microcirculation, Vancouver, 9th – 13th September 2018.
3. Poster presentation: The role of ELTD1/ADGRL4 in tumour angiogenesis. National Cancer Research Institute, Glasgow, 4th – 6th November 2018

Talks

1. Biology of ELTD1/ADGRL4 and its involvement in tumour development and angiogenesis. Annual Oncology Student Symposium, St. Anne's College, University of Oxford, 13th July 2017.
2. Biology of ELTD1/ADGRL4 and its involvement in tumour development and angiogenesis. WIMM Student Day, Weatherall Institute of Molecular Medicine, University of Oxford, 22nd February 2018.

Appendix

7.1 Violin plots of acute *Eltd1*-depleted lung endothelial cells

7.1.1 Combined analysis

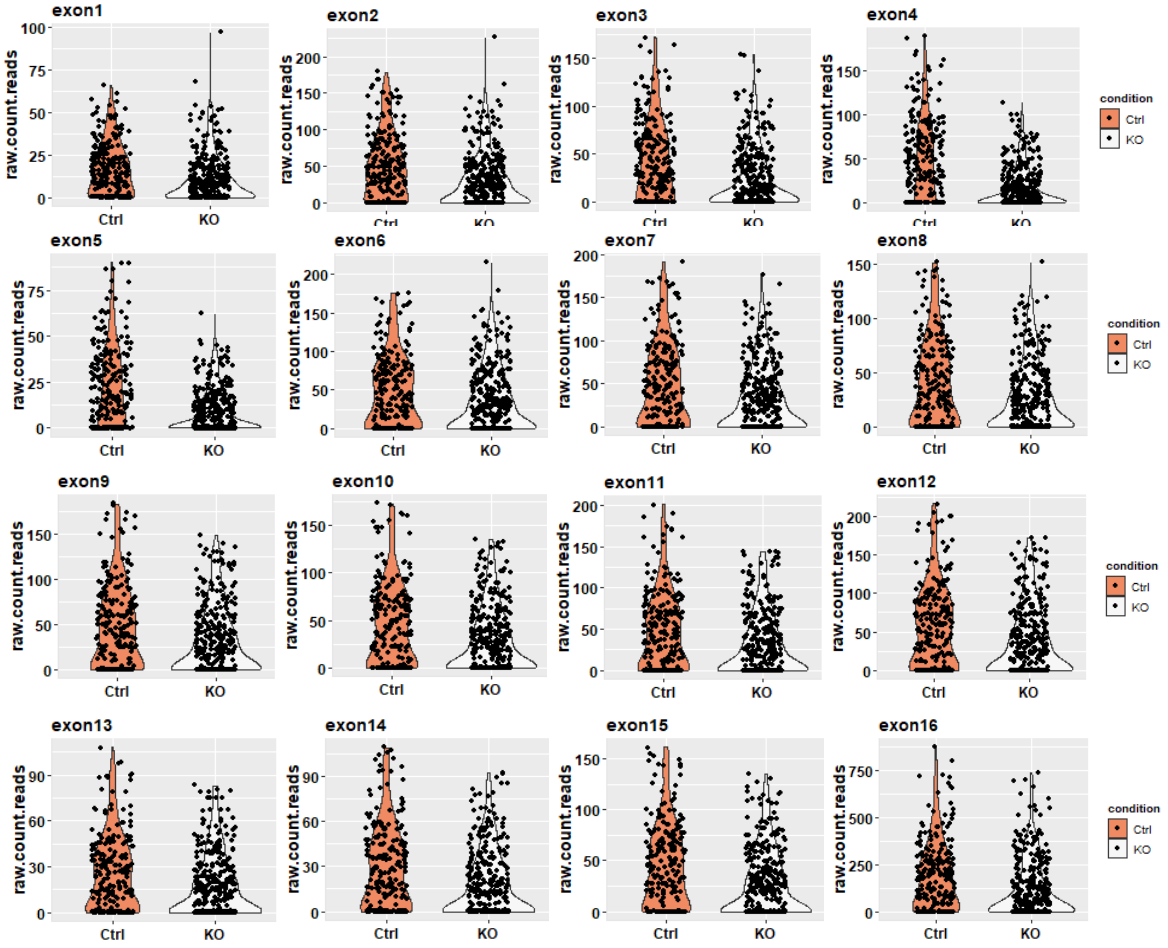

Figure 7.1: Violin plots of *Eltd1* exons 1-16 in total lung endothelial cells isolated from untreated (Ctrl) and tamoxifen-treated (KO) mice.

7.1.2 Lung arterial endothelial cells

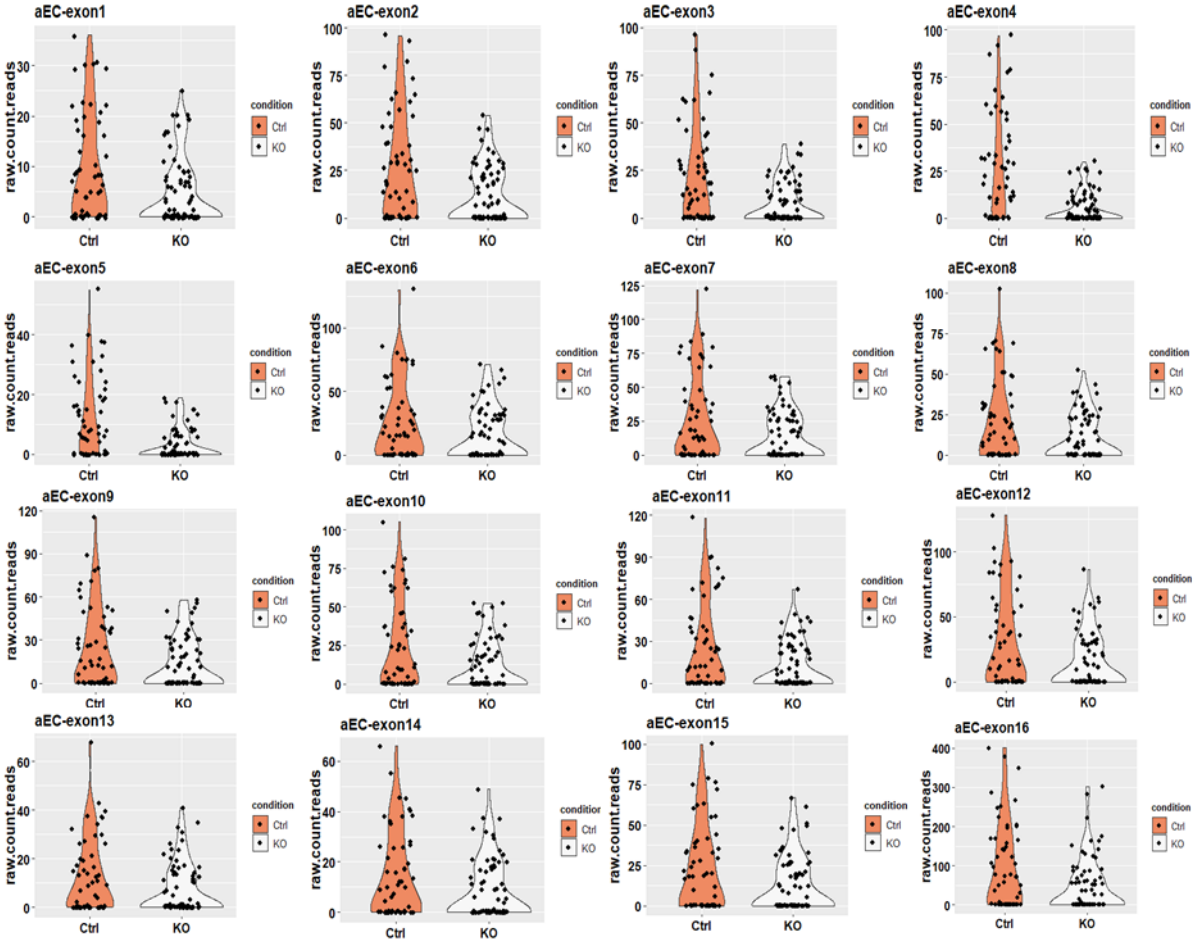

Figure 7.2: Violin plots of *Eltd1* exons 1-16 in lung arterial endothelial cells isolated from untreated (Ctrl) and tamoxifen-treated (KO) mice.

7.1.3 Lung capillary endothelial cells

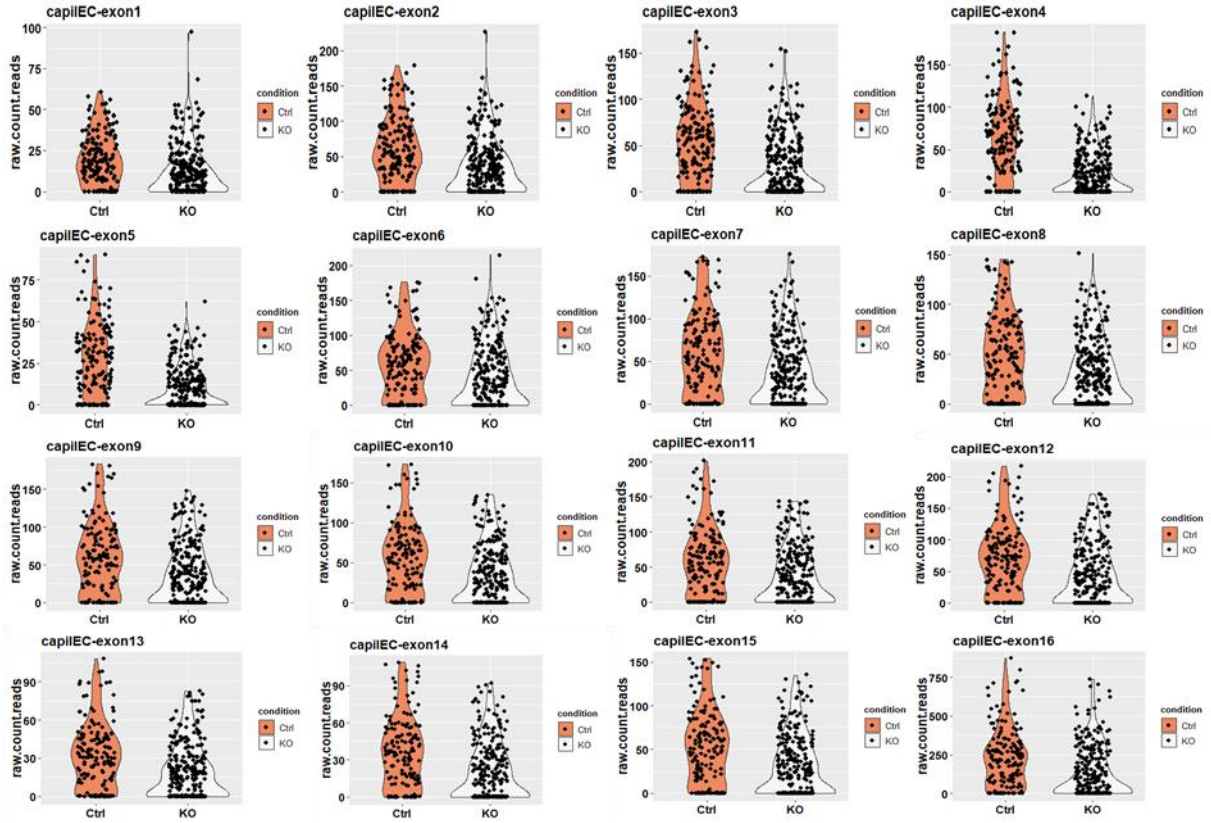

Figure 7.3: Violin plots of *Eltd1* exons 1-16 in lung capillary endothelial cells isolated from untreated (Ctrl) and tamoxifen-treated (KO) mice.

7.2 Differential gene expression profile of lung endothelial cells from untreated and tamoxifen-treated mice

7.2.1 Combined analysis

7.2.1.1 Upregulated genes

Gene symbol	pval.adjj.wilcox	pval.adj.edgeR	pval.adj.MAST	log(Fold Change)
Trpv4	0.13	0.0034	0.026	6.21
Klf15	0.44	0.0028	0.0013	5.71
Sftpb	0.70	0.023	0.58	5.33
Gbp2b	1.68E-07	4.70E-05	1.58E-10	5.31
Ppargc1a	0.54	0.0014	0.40	4.63
Intu	0.89	0.0015	0.61	3.88
Ociad2	0.69	0.0073	0.75	3.87
Cyp2e1	0.99	0.020	0.90	3.83
Dcst1	0.95	0.020	0.75	3.72
Gm9855	6.76E-05	2.70E-10	1.32E-08	3.64
Gstcd	0.49	0.0047	0.23	3.60
Ifi27l2a	0.00020	0.068	2.43E-05	3.57
Gm45223	0.79	5.46E-06	0.40	3.38
Gm47111	0.79	0.038	0.35	3.36
Wdhd1	0.99	0.025	0.78	3.36
Zfp607a	1.0	0.00071	0.42	3.26
Ifit3b	0.0038	0.00044	0.00013	3.23
Gm15506	0.54	0.0026	0.49	3.15
Slc12a8	0.95	0.0092	0.64	2.97
Gm39556	0.93	0.045	0.62	2.95
Gm5900	2.16E-09	7.75E-17	6.86E-13	2.85
Il5ra	0.33	0.011	0.34	2.84
Gm44699	0.84	0.0063	0.83	2.84
Hook2	0.36	9.86E-08	0.41	2.81
Ahrr	1.0	0.048	0.90	2.79
Tdg-ps	0.33	1.55E-05	2.11E-06	2.72
Gm38161	0.31	0.0046	0.13	2.69
Mpzl2	0.98	0.026	0.88	2.64
Gm15920	2.37E-14	1.77E-11	2.36E-18	2.58
Gm49410	1	0.013	0.92	2.55
Enpp1	0.93	0.045	0.86	2.47
Cux2	0.59	0.033	0.55	2.43
Ncf2	0.83	0.029	0.84	2.38
N4bp2	0.79	0.015	0.82	2.37
Gm37204	0.68	8.78E-06	0.72	2.36

Snx32	0.59	1.0	0.029	2.29
Gm45641	0.019	0.087	0.017	2.22
Selenbp2	0.012	0.016	0.0078	2.20
5930420M18 Rik	0.80	0.0043	0.61	2.17
Ms4a1	0.97	0.0015	0.98	2.17
4930578M01 Rik	0.81	0.011	0.80	2.10
Gm13331	1.78E-17	5.86E-16	2.61E-21	2.08
Gm47113	0.33	0.015	0.38	2.03
H2-DMb2	0.92	0.038	0.92	2.02
Ccdc141	0.71	0.0014	0.77	2.01
Gm2788	0.90	0.0083	0.91	1.99
Matn2	1.0	0.00046	0.65	1.98
Slc23a1	0.86	0.023	0.73	1.96
Pola1	0.99	0.043	0.71	1.90
Prkn	0.92	0.00015	0.82	1.88
Gm43511	0.97	0.013	0.78	1.88
Cfb	0.31	0.018	0.13	1.83
Gm45246	3.74E-08	4.47E-14	1.88E-12	1.80
Kptn	0.073	1.00	0.048	1.80
Tpm3-rs7	3.37E-18	2.11E-07	1.06E-20	1.75
Gm10499	3.66E-20	2.12E-21	2.24E-18	1.73
Gm38299	0.82	0.0019	0.86	1.72
Slc27a1	0.39	0.0092	0.47	1.71
Cdk5rap1	0.022	1.0	0.014	1.70
1110003F10Rik	0.31	0.019	0.13	1.70
Cables2	0.010	0.99	0.018	1.69
Gm42732	1.16E-28	2.63E-13	1.45E-33	1.67
Pcna-ps2	0.59	0.045	0.22	1.67
Gm42566	0.22	0.037	0.22	1.66
Ube2c	0.31	0.020	0.13	1.63
Gm4117	0.72	0.00069	0.72	1.60
Hist1h2al	9.24E-05	0.0046	0.00083	1.52
Xaf1	0.00020	0.048	0.00058	1.45
Ifit3	0.0023	0.43	0.011	1.42
Trim6	0.42	0.0078	0.22	1.42
Pcm1	0.98	0.69	0.013	1.33
Ifi44	0.041	1.0	0.032	1.31
Ubc	2.55E-48	4.32E-36	4.96E-46	1.29
Akt2-ps	0.14	0.0028	0.024	1.24
Usp34	1.61E-14	0.0082	3.76E-16	1.19
Sirt5	0.22	0.011	0.46	1.18

Gm42726	0.46	0.037	0.46	1.13
Zfp459	0.90	0.025	0.79	1.09
Ceacam10	0.00025	0.00014	0.00010	1.05
Gm10382	1.93E-19	2.18E-14	7.52E-18	0.96
Ttyh1	0.75	0.0041	0.86	0.96
Eno1b	2.41E-06	0.30	2.35E-07	0.95
B3gnt3	0.031	1.0	0.063	0.93
Ceacam2	5.00E-06	0.31	1.07E-06	0.89
Gja4	0.021	0.99	0.13	0.75
Gm26809	0.0017	0.043	0.11	0.75
Gm45551	0.023	0.095	0.055	0.73
D130062J10Rik	0.71	0.0029	0.75	0.71
Rps17	0.0051	0.54	0.020	0.68
Gm15459	2.79E-07	0.0094	2.59E-10	0.65
ENSMUSG00000115801	0.0034	0.0043	0.063	0.65
Klf10	0.015	1.00	0.012	0.62
Rplp0	0.00031	0.17	0.018	0.61
Gm26825	4.94E-06	0.034	5.26E-10	0.58
Sgk1	0.0095	1.0	0.16	0.53
Mindy1	0.079	1.0	0.016	0.52
Socs3	0.034	1.0	0.034	0.47
Ier3	0.041	1.0	0.11	0.46
Hes1	0.012	1.0	0.020	0.43
H3f3b	1.73E-06	0.0083	0.17	0.37
Spopl	5.01E-18	1.0	1.33E-32	0.35
Rps3a3	0.10	1.0	0.014	0.33
Id3	0.0017	0.45	0.43	0.30
Gm17275	0.027	1.0	0.59	0.25
B2m	0.0041	0.049	0.57	0.14
Faap24	0.31	1.00	0.049	0.04

Table 7.1: Upregulated genes in total lung endothelial cells isolated from untreated and tamoxifen-treated mice. The *p* value of the differentially expressed genes were colour coded to indicate significance ($p < 0.05$). Blue (Wilcox test); yellow (edgeR) and green (MAST).

7.3.1.2 Downregulated genes

Gene symbol	pval.adjj.wilcox	pval.adj.edgeR	pval.adj.MAST	log(Fold Change)
Ltbp2	0.10	7.04E-07	0.0057	-7.30
Gm48582	0.0051	7.60E-07	0.0025	-5.99
Kcnk3	0.17	0.015	0.15	-4.86
Sox11	2.21E-13	2.32E-06	1.44E-13	-4.18
Trpc6	0.07	0.048	0.17	-4.12
Prom1	0.93	2.85E-05	0.79	-4.00
Fbxo17	0.93	0.0014	0.16	-3.98
1700048O20 Rik	0.59	0.00094	0.43	-3.97
Aqp7	0.83	6.24E-06	0.54	-3.77
Zbtb33	0.34	0.025	0.38	-3.70
Rad51c	0.70	0.0039	0.25	-3.55
Dennd1c	0.92	0.0095	0.82	-3.54
Cyp26b1	6.37E-08	0.108	3.28E-07	-3.10
Gm44200	0.0020	1.61E-07	0.0028	-3.04
Gm38120	0.84	1.69E-07	0.64	-2.96
Gm47138	0.93	0.029	0.78	-2.95
Gm18860	7.27E-09	4.22E-14	3.39E-10	-2.95
Fam161b	0.84	0.0024	0.70	-2.94
Slc26a8	0.70	0.0066	0.81	-2.93
Slc25a43	0.83	0.0093	0.69	-2.81
Gm2822	0.39	1.89E-05	0.34	-2.80
Rad51ap1	0.98	8.78E-05	0.80	-2.78
Pask	1.0	0.044	0.78	-2.76
Dlgap5	0.84	0.0050	0.88	-2.68
Gm26703	0.76	0.00025	0.40	-2.64
Ank2	0.97	0.031	0.31	-2.61
Gpr157	1.0	0.011	0.90	-2.57
Gm49328	0.66	0.0020	0.62	-2.53
Frrs1	0.00054	0.38	1.78E-05	-2.46
Gm44199	0.027	0.28	0.11	-2.44
Atp2a1	0.94	0.001	0.34	-2.40
Dna2	0.59	4.74E-06	0.55	-2.37
Tarsl2	0.93	0.0046	0.51	-2.36
Htr2b	0.048	1.0	0.16	-2.36
Dnali1	0.93	0.0011	0.96	-2.31
Trim36	0.98	1.95E-05	0.66	-2.22
Igfbp3	0.078	1.0	0.0022	-2.15
Esr1	0.95	2.57E-05	0.95	-2.10

Gm16536	0.033	0.9999499	0.11	-2.10
Gm13456	8.75E-16	2.52E-13	1.62E-20	-2.07
Gm8730	3.73E-20	2.70E-10	3.20E-21	-2.06
Fancc	0.20	0.79	0.020	-2.04
Selplg	1.0	0.050	0.78	-1.99
A730020E08 Rik	0.75	0.0053	0.70	-1.93
Gm9625	2.73E-20	4.67E-12	5.83E-21	-1.92
Saa3	0.98	0.0014	0.84	-1.90
Gm38699	0.61	0.036	0.60	-1.90
Exo1	0.80	0.023	0.82	-1.83
Gm26724	0.42	0.0011	0.012	-1.80
Gm34121	0.91	0.0044	0.80	-1.70
Gm20589	0.58	0.0016	0.63	-1.51
4930442H23 Rik	0.63	0.00051	0.55	-1.48
Gm43503	0.77	0.023	0.76	-1.42
Gm48338	1.28E-08	7.67E-08	3.94E-08	-1.35
Enpp3	0.61	0.029	0.68	-1.30
Gm35769	0.33	0.048	0.19	-1.28
Gm14165	9.28E-14	6.34E-11	1.69E-14	-1.27
Pam	5.01E-06	0.00019	1.12E-06	-1.26
Gm13123	0.00054	0.053	0.0025	-1.24
Rplp0-ps1	2.15E-06	4.73E-05	1.16E-05	-1.23
Gm26862	0.0040	0.41	0.019	-1.21
AA465934	0.022	1.0	0.055	-1.08
Arhgap6	0.034	1.0	0.063	-1.04
Gm4811	0.0052	0.033	0.020	-0.98
Slc5a10	0.43	0.019	0.304	-0.90
Wsb2-ps	1.69E-06	1.0	1.47E-05	-0.87
Per1	0.0010	1.0	0.0057	-0.80
Mfap1b	0.58	1.0	0.024	-0.78
Gm27194	1.52E-08	1.0	9.89E-08	-0.73
Gtf2a2	0.27	1.0	0.036	-0.68
Gm5869	0.033	0.055	0.057	-0.68
Adgrl4	1.90E-05	0.11	0.00010	-0.68
Pde4b	0.0051	0.42	0.00068	-0.66
Gm45315	0.00057	0.011	0.00021	-0.62
Gm21596	0.00013	0.0015	2.95E-05	-0.61
Phactr2	0.0081	0.33	0.0051	-0.60
Stat6	0.49	1.0	0.034	-0.59
Phldb2	0.014	1.0	0.11	-0.56
Adrb2	0.16	1.0	0.034	-0.54
Gm27206	0.99	1.0	0.031	-0.52

Rab35	0.94	1.0	0.011	-0.51
Gm5131	0.010	0.0039	0.0034	-0.51
Cd38	0.013	1.0	0.0059	-0.48
Gm46432	3.46E-07	0.51	4.00E-08	-0.46
Scaf11	0.029	1.0	0.057	-0.42
Gm16133	0.011	1.0	0.010	-0.39
Nhlrc2	0.084	1.0	0.0055	-0.37
Sparc	0.024	0.64	0.18	-0.37
Gm42928	0.13	0.51	0.046	-0.30
Nrp1	0.39	1.0	0.020	-0.28
Gm18194	2.68E-07	1.0	5.73E-08	-0.28
Srgn	0.58	1.0	0.024	-0.19
Klf2	0.17	1.0	0.020	-0.19
Gm7180	0.0055	1.0	0.013	-0.18
Dpysl2	0.20	0.69	0.017	-0.17
Pcdhga4	0.90	1.0	0.032	-0.04
Tulp2	0.31	1.0	0.039	-0.01

Table 7.2: Downregulated genes in total lung endothelial cells isolated from untreated and tamoxifen-treated mice. The *p* value of the differentially expressed genes were colour coded to indicate significance ($p < 0.05$). Blue (Wilcox test); yellow (edgeR) and green (MAST).

7.3.2 Lung arterial endothelial cells

7.3.2.1 Upregulated genes

Gene symbol	pval.adjj.wilcox	pval.adj.edgeR	pval.adj.MAST	log(Fold Change)
Adh1	0.051	3.57E-05	0.95	7.09
BC002059	0.20	0.0018	0.92	6.25
Ifi27l2a	0.29	0.011	0.92	5.75
Chadl	0.29	0.011	0.81	5.41
Gm16559	0.073	0.00018	0.61	4.43
Gm9855	0.028	1.38E-05	0.98	4.39
Dtnb	0.43	0.00097	0.95	4.37
Gm15920	0.00059	5.74E-08	0.77	3.39
Tdg-ps	0.20	0.0088	0.83	3.38
Fn1	0.85	0.016	0.82	3.29
Gm5900	0.0037	1.16E-05	0.71	3.15
Cop1	0.035	0.64	0.62	2.43
Olfr975	0.29	0.034	0.45	2.26

Gm13331	0.00048	0.0095	0.88	1.88
Ceacam10	0.012	0.014	0.96	1.74
Gm45246	0.099	0.018	0.91	1.59
Xaf1	0.035	1.0	0.69	1.55
Tpm3-rs7	0.0013	0.32	0.48	1.52
Eno1b	0.036	1.0	0.70	1.37
Ubc	1.51E-13	1.00E-13	0.69	1.36
Ceacam2	0.0009	0.17	0.64	1.33
Vps13a	1.0	1.0	0.05	1.26
Tmem107	0.73	1.0	0.00053	1.24
Noct	0.042	0.10	0.77	1.09
Spopl	2.45E-07	1.0	0.63	1.07
Gm10382	3.92E-05	0.00028	0.86	1.06
Mxra7	0.042	0.92	0.45	0.94
Spef1	0.76	1.0	0.0050	0.86
Gm26792	1.0	1.0	0.0036	0.64
Chmp3	0.78	1.0	0.049	0.61
Furin	0.68	1.0	0.036	0.57
Rtraf	0.93	1.0	0.044	0.51
Rbm28	0.88	1.0	0.0020	0.50
Tatdn3	0.91	1.0	0.00053	0.35
Prr14	0.82	1.0	0.0040	0.32
B2m	0.042	0.12	1.0	0.30
Crip1	0.79	1.0	0.0039	0.30
Psmb6	0.90	1.0	0.017	0.19
Rab13	0.97	1.0	0.021	0.17
mt-Cytb	0.90	1.0	0.037	0.16
Mrpl17	0.95	1.0	0.0026	0.11
Casc3	1.0	1.0	2.17E-09	0.09
Gm7097	0.93	1.0	0.021	0.08
Wwtr1	0.83	1.0	0.00053	0.07
Prps1	0.98	1.0	6.28E-06	0.06
Ergic3	0.89	1.0	0.0048	0.06

Table 7.3: Upregulated genes in lung arterial endothelial cells isolated from untreated and tamoxifen-treated mice. The *p* value of the differentially expressed genes were colour coded to indicate significance ($p < 0.05$). Blue (Wilcox test); yellow (edgeR) and green (MAST).

7.3.2.2 Downregulated genes

Gene symbol	pval.adjj.wilcox	pval.adj.edgeR	pval.adj.MAST	log(Fold Change)
Gm48582	0.017	6.04E-06	0.60	-8.10
Rab6b	0.017	6.04E-06	0.59	-7.14
Fancc	0.042	0.14	0.96	-5.00
Ccdc14	0.74	0.022	0.50	-4.47
Tfcp2	0.93	0.044	0.88	-3.38
Gm18860	0.073	0.0018	0.89	-3.19
Rhbdd3	0.83	0.028	0.69	-2.40
Gm9625	9.59E-06	0.00018	0.92	-2.10
Gm8730	2.10E-05	0.00046	0.83	-2.07
Gm13456	0.017	0.021	0.61	-2.04
Seh1l	0.035	1.0	0.63	-1.96
Frrs1	0.0032	1.0	0.79	-1.91
Gm48338	0.032	0.017	0.94	-1.58
Rplp0-ps1	0.028	0.074	0.68	-1.56
Ccdc134	0.58	1.0	0.036	-1.42
Gm14165	0.00056	0.043	0.38	-1.41
Hspa1b	0.046	1.0	0.82	-1.27
Pam	0.012	0.14	0.98	-1.22
Tsga10	0.87	1.0	0.036	-1.10
Vamp1	0.83	1.0	0.014	-1.00
Bmt2	0.88	1.0	0.023	-0.79
Gm45053	0.93	1.0	0.039	-0.64
Chst2	0.43	1.0	0.050	-0.55
Dcun1d1	0.92	1.0	0.00053	-0.45
Hcfc1	0.82	1.0	6.28E-06	-0.45
Brcc3	0.97	1.0	0.0021	-0.36
Vamp2	0.84	1.0	0.012	-0.31
Adamtsl5	0.88	1.0	0.0039	-0.27
Ttc14	0.88	1.0	0.00041	-0.24
Slc8a1	1.0	1.0	0.00074	-0.20
Ogfod3	0.88	1.0	0.017	-0.20
Asb8	1.0	1.0	0.022	-0.16
Sumo1	0.91	1.0	0.0050	-0.11
Gm29434	0.97	1.0	5.01E-11	-0.11
Erlin2	0.99	1.0	0.0018	-0.09
Tmem68	0.96	1.0	0.0090	-0.05
Scamp3	0.99	1.0	4.09E-06	-0.04

Table 7.4: Downregulated genes in lung arterial endothelial cells isolated from untreated and tamoxifen-treated mice. The *p* value of the differentially expressed genes were colour

coded to indicate significance ($p < 0.05$). Blue (Wilcox test); yellow (edgeR) and green (MAST).

7.3.3 Lung capillary endothelial cells

7.3.3.1 Upregulated genes

Gene symbol	pval.adjj.wilcox	pval.adj.edgeR	pval.adj.MAST	log(Fold Change)
Msl3l2	0.40	0.0039	0.97	5.73
Tecpr2	0.82	0.026	0.94	5.62
Gbp2b	1.93E-05	0.0014	0.94	5.12
Zfp30	0.50	0.0094	0.84	4.81
Mmachc	0.53	0.047	0.97	4.48
P3h3	0.90	0.0040	0.34	4.44
Ifit3b	0.022	0.00015	0.86	4.40
Gm16287	0.76	0.028	0.99	3.88
Cgn	0.86	0.00064	0.90	3.74
Gm26733	0.43	0.047	0.91	3.72
Gm15506	0.65	0.021	0.82	3.43
Gm9855	0.12	0.00057	0.97	3.38
Gm45223	0.92	0.0011	0.99	3.31
Zfp26	0.67	0.042	0.88	2.98
Gm5900	2.67E-05	4.17E-10	0.89	2.80
Gm38042	0.96	0.00067	0.99	2.80
Gm13331	2.98E-11	2.05E-17	0.82	2.65
Tsacc	0.40	0.028	0.98	2.57
Hook2	0.62	0.00014	0.84	2.50
Gm42732	1.15E-25	7.63E-21	0.98	2.49
Gm37204	0.89	0.0012	0.92	2.45
Gm15920	1.67E-08	4.85E-05	0.93	2.39
Prkn	0.98	0.0065	0.99	2.15
Gm45246	4.99E-05	1.05E-08	0.91	1.87
Gm10499	1.95E-16	2.24E-17	0.94	1.87
Gm38299	0.95	0.037	0.86	1.84
E330034L11Rik	0.86	1.0	1.26E-30	1.74
Tpm3-rs7	5.24E-11	0.00050	0.54	1.71
Ifit3	0.040	0.63	0.97	1.70
Hist1h2al	0.00014	0.046	0.87	1.69
Akt2-ps	0.35	0.024	0.84	1.39
Pus7	0.96	1.0	0.012	1.33
Usp34	5.64E-14	0.037	0.99	1.32

Gbp11	0.99	1.0	5.06E-19	1.31
Ubc	7.90E-30	3.03E-19	0.87	1.23
Ttyh1	0.88	0.022	0.89	1.13
Nagpa	0.47	1.0	0.030	1.10
Tarbp2	0.92	1.0	1.58E-06	0.96
Gm10382	2.47E-10	9.73E-07	0.92	0.86
Gm45551	0.011	0.17	0.65	0.85
Smg6	0.76	1.0	0.00047	0.82
Gm26809	0.0011	0.11	0.99	0.80
Pbx2	0.69	1.0	0.00024	0.78
Eno1b	0.0063	1.0	0.97	0.77
Gls	0.94	1.0	0.0023	0.77
Sspn	0.92	1.0	0.012	0.74
Add1	0.0052	0.92	0.99	0.73
Ceacam2	0.010	1.0	0.97	0.65
Gm15459	0.00035	0.15	0.87	0.63
Shroom3	0.95	1.0	1.52E-10	0.63
D130040H23Rik	1.0	1.0	0.017	0.59
2310031A07Rik	0.98	1.0	0.0017	0.54
Gm26825	0.0041	0.39	0.82	0.54
Ints6l	0.98	1.0	0.034	0.46
Chd9	0.55	1.0	0.027	0.45
Pcbd2	0.88	1.0	0.015	0.45
Nutf2	0.84	1.0	0.017	0.42
Vav3	1.0	1.0	0.017	0.42
H3f3b	0.00017	0.13	0.91	0.36
Cgas	0.99	1.0	9.25E-30	0.34
Msrb3	0.93	1.0	0.030	0.32
Fgfrl1	0.96	1.0	2.28E-05	0.30
Cdca8	0.99	1.0	0.046	0.29
Mkrn1	0.98	1.0	4.26E-06	0.27
BC037039	0.94	1.0	6.65E-13	0.23
Spopl	1.13E-08	1.0	0.89	0.21
Timm8b	1.0	1.0	0.046	0.16
Wdr31	0.98	1.0	1.87E-11	0.15
Sbf1	0.99	1.0	6.79E-11	0.079
Zfp281	0.95	1.0	0.0026	0.019
Cdk14	1.0	1.0	2.55E-13	0.0084

Table 7.5: Upregulated genes in lung capillary endothelial cells isolated from untreated and tamoxifen-treated mice. The *p* value of the differentially expressed genes were colour coded to indicate significance ($p < 0.05$). Blue (Wilcox test); yellow (edgeR) and green (MAST).

7.3.3.2 Downregulated genes

Gene symbol	pval.adjj.wilcox	pval.adj.edgeR	pval.adj.MAST	log(Fold Change)
Prom1	0.99	0.00024	0.97	-4.41
Pmm1	0.83	0.0065	0.72	-4.38
Notch2	0.42	0.00021	0.76	-4.38
Sox11	8.37E-11	0.00015	0.96	-4.35
Aqp7	0.96	1.35E-05	0.92	-4.20
Dennd1c	0.95	0.047	0.96	-3.83
Efcc1	0.92	0.00015	0.90	-3.24
Slc25a43	0.89	0.018	0.78	-3.20
ENSMUSG00000117499	0.54	0.0092	1.0	-3.20
Cyp26b1	1.85E-07	0.17	0.98	-3.19
Gm38120	1.0	4.04E-05	0.92	-3.07
Gm26703	0.88	0.0031	0.74	-2.99
Gm18860	1.29E-05	1.05E-08	0.87	-2.92
Rad51ap1	1.0	0.0019	0.80	-2.89
Dna2	0.70	0.0000019	0.97	-2.88
Atp2a1	0.94	0.0038	0.93	-2.85
Gm43813	0.99	0.032	0.87	-2.74
Gm44200	0.17	0.00026	0.92	-2.69
Esr1	0.98	0.00011	0.98	-2.58
Tuba1c	0.53	0.0019	0.97	-2.55
Mpv17l	0.98	0.022	0.54	-2.52
Gm2822	0.29	0.00083	0.86	-2.27
A730020E08Rik	0.92	0.029	0.89	-2.23
Gm27194	1.51E-05	0.012	0.97	-2.18
Syt12	0.91	0.00083	0.99	-2.10
Gm13456	2.86E-11	1.05E-08	0.92	-2.08
Gm8730	8.91E-12	0.00013	0.92	-2.02
Gm32856	0.97	0.0048	0.94	-1.93
Gm20589	0.63	0.00081	0.96	-1.90
Wsb2-ps	0.00018	0.029	0.89	-1.89
Gm43088	0.93	0.0033	0.99	-1.89
Gm9625	2.45E-11	4.85E-05	0.98	-1.80
4930442H23Rik	0.88	0.0040	0.79	-1.75
Ptcra	0.64	0.038	0.76	-1.61
Gm26862	0.0024	0.28	0.91	-1.42
Gm48338	4.14E-05	0.00016	1.0	-1.34
Gm13123	0.011	0.37	0.89	-1.31
Zfp300	0.96	1.0	8.60E-05	-1.25
Pam	0.021	0.037	0.98	-1.21

Gm14165	2.44E-06	5.56E-05	0.96	-1.19
Smim13	1.0	1.0	1.01E-10	-1.18
L3mbtl3	0.65	1.0	0.0011	-1.10
Rplp0-ps1	0.021	0.063	0.49	-1.09
Gmeb1	1.0	1.0	6.56E-15	-1.05
Dusp6	0.031	1.0	0.87	-0.99
Togaram1	0.88	1.0	2.28E-08	-0.93
Gm45315	5.65E-05	0.0044	0.99	-0.81
Pde4b	0.013	0.55	0.76	-0.80
Gm4419	0.84	0.022	0.96	-0.76
Adgrl4	6.95E-06	0.14	0.99	-0.72
Hic1	0.99	1.0	0.030	-0.68
Gm48273	0.58	1.0	0.0011	-0.66
Phldb2	0.018	1.0	0.79	-0.64
Gm21596	0.0063	0.043	0.91	-0.60
Per1	0.021	1.0	0.72	-0.58
Fam20b	0.95	1.0	7.03E-08	-0.58
Nhlrc2	0.032	1.0	0.96	-0.56
Myo6	0.41	1.0	5.45E-05	-0.54
Nup210l	0.98	1.0	7.03E-08	-0.48
Atp13a2	0.87	1.0	0.0063	-0.37
Gm18194	3.78E-05	1.0	0.51	-0.36
Nmnat1	0.93	1.0	3.32E-06	-0.35
Sgcb	0.96	1.0	2.48E-06	-0.35
Sparc	0.011	0.74	0.94	-0.35
Fam53b	0.97	1.0	0.013	-0.32
Polr3e	1.0	1.0	7.72E-06	-0.32
Mtpn	0.83	1.0	0.00015	-0.29
Zfp809	0.92	1.0	0.0023	-0.27
Gm46432	0.00018	1.0	1.0	-0.25
Bag1	0.90	1.0	1.07E-15	-0.22
Gm44123	0.98	1.0	1.56E-16	-0.20
Jcad	0.92	1.0	0.00014	-0.18
Srp72	0.95	1.0	1.87E-11	-0.10

Table 7.6: Downregulated genes in lung capillary endothelial cells isolated from untreated and tamoxifen-treated mice. The *p* value of the differentially expressed genes were colour coded to indicate significance ($p < 0.05$). Blue (Wilcox test); yellow (edgeR) and green (MAST).

7.4 Differential gene expression profile in acute *Eltd1* knockout (all exons) lung endothelial cells

7.4.1 Combined analysis

7.4.1.1 Upregulated genes

Gene symbol	Pval.adjj.wilcox	pval.adj.edgeR	pval.adj.MAST	log(Fold Change)
Sftpb	0.33	0.00027	0.55	6.18
Scd1	0.34	0.0013	0.99	6.09
Ociad2	0.25	2.24E-09	1.0	5.04
Lyz2	0.019	0.057	0.71	4.37
Gm31517	0.65	0.00013	0.72	4.14
Tmem163	0.46	0.026	0.57	4.03
Blnk	0.95	0.00012	0.89	4.03
Mpzl2	0.90	2.24E-09	0.63	3.99
Ppl	0.77	0.0034	0.96	3.96
Gm15396	0.50	3.46E-07	0.41	3.91
Emb	0.78	1.11E-05	0.89	3.90
Dcst1	0.94	0.0037	0.76	3.85
Il5ra	0.76	0.00015	0.91	3.74
A530017D24Rik	0.63	0.043	0.92	3.63
Rac2	0.71	6.03E-05	0.91	3.63
Tmem200a	0.97	0.039	0.75	3.58
Prss8	0.94	0.00052	0.79	3.55
A830018L16Rik	0.97	0.00050	0.84	3.53
D230049E03Rik	0.47	0.0020	0.33	3.49
Cgn	0.86	0.00015	0.93	3.49
Gm15675	0.94	0.0019	0.44	3.35
Ms4a1	0.70	4.42E-12	0.75	3.33
H2-DMb2	0.82	1.17E-08	0.45	3.31
Enpp1	0.51	2.31E-05	0.97	3.27
B4galnt1	0.19	0.30	9.79E-05	3.10
Gm16576	0.22	0.33	0.027	3.08
Gm7591	0.55	0.0038	0.84	3.03
Trmt61a	0.021	0.43	0.71	3.02
Tc2n	0.56	0.00018	0.82	3.02
Dlgap5	1.0	0.0018	0.96	2.96
Gimap3	0.70	0.025	0.98	2.86
Slc23a1	0.84	1.31E-05	0.49	2.83
Pi16	0.58	0.00079	1.0	2.81
Ckap2	0.93	2.37E-05	0.96	2.77

Myh14	0.030	0.67	0.67	2.75
Prss35	0.85	0.039	0.69	2.69
Ncf2	0.93	0.045	0.39	2.68
Gstt1	0.032	0.71	0.94	2.68
Eaf2	0.80	0.026	0.97	2.62
Gm38042	0.68	0.00013	0.86	2.47
Lrrc8e	0.53	0.0024	0.40	2.44
4732416N19Rik	0.52	1.11E-05	0.78	2.43
Rapgef4os1	0.60	0.00018	0.67	2.43
Dnali1	0.36	0.00099	0.62	2.42
Pi15	0.74	0.0054	0.077	2.36
Tjp3	0.85	0.0018	0.90	2.33
Saa3	1.0	1.72E-05	0.82	2.31
A530040E14Rik	0.66	0.039	0.78	2.28
Slc16a7	0.92	0.033	0.98	2.27
Gm48871	0.89	0.0029	0.79	2.24
Slc27a1	0.94	0.00012	0.85	2.24
Tmem82	0.58	9.18E-05	0.87	2.19
3110039I08Rik	1.0	0.045	0.57	2.08
ENSMUSG00000117187	0.96	0.0020	0.68	2.06
Gm36955	0.84	0.033	0.88	2.04
Zfp459	0.81	1.62E-06	0.90	1.84
Gm37834	0.75	0.0045	0.57	1.80
Unc13d	0.79	9.08E-05	0.97	1.75
Gal3st3	0.97	0.022	0.67	1.69
Foxp2	0.93	0.013	0.70	1.69
Dhtkd1	0.61	4.47E-06	0.87	1.60
Ttyh1	0.93	3.61E-08	0.93	1.52
Dhfr	0.73	1.0	0.024	1.34
Slc5a6	0.85	0.011	0.66	1.27
Eef1akmt3	0.41	0.025	0.95	1.24
Gm17259	0.88	0.0029	0.84	1.22
Ccdc78	0.85	0.031	0.52	1.14
Rpl36al	0.31	0.014	0.97	1.13
Ercc5	0.85	1.0	0.0086	1.01
Adck2	0.60	1.0	0.024	0.77
Gm10767	0.51	0.039	0.27	0.66
Slx4	0.69	1.0	0.046	0.62
Gm29530	0.77	1.0	0.013	0.60
Emp2	0.02	0.78	0.88	0.58
Zdhhc9	0.48	1.0	0.031	0.57
Zan	0.87	1.0	0.013	0.50
Mid1ip1	0.87	1.0	0.0039	0.50
Gm45236	0.93	1.0	0.00072	0.49

Ppp2r3d	0.98	1.0	0.019	0.48
Cat	0.63	1.0	0.030	0.47
Lrmda	0.99	1.0	0.045	0.47
Gm5915	0.98	1.0	0.032	0.46
Gm16153	0.70	1.0	0.0093	0.46
Gm5814	0.50	0.73	0.044	0.45
Dynlrb1	0.050	1.0	0.99	0.44
Hspd1	0.93	1.0	0.037	0.43
Fth1	0.00080	0.0011	0.89	0.41
Stpg1	0.78	1.0	0.0078	0.41
Card6	0.94	1.0	0.0093	0.38
Sdc2	0.84	1.0	0.0086	0.38
Tmem70	0.92	1.0	0.00083	0.31
2310022A10Rik	0.86	1.0	0.019	0.30
Gm10252	0.00026	0.00079	0.96	0.26
Tab2	0.95	1.0	0.0047	0.25
Abracl	0.86	1.0	0.028	0.24
Myl12a	0.012	0.28	0.86	0.23
2010007H06Rik	0.70	1.0	0.035	0.23
Ica1	0.96	1.0	0.0050	0.22
Cnrip1	0.93	1.0	0.041	0.20
Ftl1	0.0017	0.059	0.99	0.20
E130208F15Rik	0.74	1.0	1.31E-07	0.19
Tnfrsf18	0.71	1.0	0.0093	0.18
Sumo1	1.0	1.0	0.038	0.18
Gm26699	0.038	1.0	0.86	0.17
B3gnt9	0.86	1.0	8.07E-05	0.16
Rps15a	0.93	1.0	0.036	0.16
Aspscr1	0.93	1.0	0.030	0.12
Ubb	0.00055	0.21	0.76	0.11
Dvl2	0.92	1.0	0.0035	0.10
Eif2d	0.88	1.0	0.0086	0.10
Daglb	0.46	1.0	0.013	0.09
Gm13441	0.89	1.0	0.018	0.08
Tmlhe	0.89	1.0	0.032	0.07
Dynll1	0.57	1.0	6E-130	0.06
Fam177a	0.93	1.0	0.031	0.06
Trim6	0.038	1.0	0.95	0.06
Cwc27	0.99	1.0	0.0012	0.03
Coq8a	0.87	1.0	0.0068	0.02
B230207O21Rik	0.90	1.0	0.037	0.02
Dnajb4	0.89	1.0	0.036	0.02
Ypel3	0.81	1.0	9.44E-07	0.02
Snrnp25	0.93	1.0	2.06E-05	0.02

Table 7.7: Upregulated genes in *Eltd1*-depleted (all exons) total lung endothelial cells. The *p* value of the differentially expressed genes were colour coded to indicate significance ($p < 0.05$). Blue (Wilcox test); yellow (edgeR) and green (MAST).

7.4.1.2 Downregulated genes

Gene symbol	pval.adjj.wilcox	pval.adj.edgeR	pval.adj.MAST	log(Fold Change)
Adgrl4	1.03E-67	0	0.18	-11.12
Zfp28	0.098	0.0033	0.75	-6.45
Zfp275	0.39	0.029	0.77	-5.66
Ppm1l	0.34	0.011	0.95	-5.54
Pcdhb4	0.48	0.043	0.85	-5.44
Crocc	0.28	0.013	0.19	-5.40
Slc46a3	0.39	0.047	0.43	-5.33
Pcdhb12	0.44	0.013	0.74	-5.31
Ido1	0.24	0.014	0.95	-5.26
Rassf2	0.34	0.015	0.92	-5.18
Zfp94	0.21	0.015	0.57	-5.17
Zfp946	0.26	0.039	0.98	-5.06
Gm14221	0.27	0.026	0.59	-5.03
Sesn2	0.44	0.017	0.68	-5.02
Slc29a4	0.39	0.017	0.88	-4.97
Cdca7	0.36	0.018	0.73	-4.94
Alox12	0.51	0.043	0.94	-4.90
Inhbb	0.36	0.021	0.40	-4.74
Kank4	0.18	0.025	0.68	-4.65
Trpc6	0.34	0.023	0.79	-4.64
B3gnt6	0.44	0.023	0.90	-4.60
Eri2	0.41	0.024	0.48	-4.56
Gm37446	0.44	0.024	0.96	-4.55
3830408C21Rik	0.24	0.024	0.96	-4.53
BC024063	0.39	0.027	0.86	-4.35
Mbd5	0.26	0.030	0.93	-4.33
Pcdhgc4	0.44	0.029	0.56	-4.26
Crym	0.34	0.029	0.97	-4.23
Gm37297	0.44	0.030	1.0	-4.20
Cep112	0.26	0.031	0.81	-4.14
Trim59	0.44	0.036	0.99	-3.95
Dsn1	0.55	0.039	1.0	-3.89
Wee1	0.41	0.038	0.46	-3.88

Dancr	0.44	0.039	0.51	-3.83
Cdc45	0.34	0.039	0.98	-3.80
Lalba	0.39	0.039	0.33	-3.79
Gbp11	0.41	0.039	0.62	-3.76
Aldh5a1	0.41	0.042	0.45	-3.68
Majin	0.39	0.043	0.80	-3.62
BC018473	0.33	0.043	0.70	-3.60
Ctxn1	0.41	0.043	0.70	-3.57
Gm26545	0.28	0.043	0.84	-3.57
B230334C09Rik	0.36	0.049	0.86	-3.43
Nsl1	0.60	0.035	0.49	-3.41
Aqp7	0.40	0.038	0.40	-3.28
Lef1	0.62	0.048	0.94	-3.28
Hykk	0.36	0.00021	0.99	-3.25
Zfp940	0.51	0.0037	0.74	-3.18
Gm35021	0.23	0.043	0.79	-3.10
Tchp	0.53	2.00E-09	0.94	-3.04
Efcc1	0.76	0.040	0.87	-2.95
Nek4	0.39	0.00016	0.95	-2.76
Gm43061	0.26	0.047	0.99	-2.73
Gm43668	0.85	0.0082	0.99	-2.67
Snrnp35	0.55	0.99	0.0039	-2.65
Gm43379	0.13	0.0023	0.96	-2.65
Elp6	0.65	0.00040	0.99	-2.52
Zfp626	0.54	0.018	0.99	-2.48
Hspa1l	0.12	0.0060	0.95	-2.33
Gm10501	0.58	0.036	0.82	-2.11
Matn2	0.19	0.020	0.99	-1.99
Tgs1	0.046	0.64	0.58	-1.93
Gm49395	0.035	0.0028	0.87	-1.85
Fzd6	0.024	0.67	0.81	-1.75
Esrra	0.23	0.0069	0.82	-1.75
Racgap1	0.89	0.00049	0.97	-1.73
Sntb1	0.024	0.73	0.67	-1.65
Slc7a11	0.18	0.039	0.089	-1.60
Prkn	0.58	0.064	0.037	-1.57
Zfp292	0.041	1.0	0.43	-1.53
Gpr68	0.97	0.62	0.0015	-1.52
Mmrn2	0.030	0.64	0.45	-1.49
1500004A13Rik	0.77	0.73	2.06E-05	-1.42
Mctp1	0.0039	1.0	0.88	-1.31
Gpr4	0.041	1.0	0.58	-1.31
Gm10734	0.00095	0.40	0.86	-1.30
Pan3	0.0039	0.10	0.81	-1.29

Gm43503	0.20	0.043	0.37	-1.27
Gm19710	0.023	0.30	0.76	-1.24
Bik	0.019	1.0	0.71	-1.23
Pelo	0.00055	0.62	0.95	-1.21
Ntn1	0.018	1.0	0.86	-1.18
Dnaja3	0.019	0.88	0.71	-1.14
Adgra3	0.0035	0.91	0.84	-1.08
Rapgef1	0.010	0.91	0.80	-1.07
Klhl23	0.88	1.0	0.012	-1.06
Cul4a	0.043	1.0	0.97	-1.03
Mcam	0.0024	0.33	0.90	-1.03
Ivns1abp	0.014	0.69	0.93	-1.02
Ubap2l	0.019	0.57	0.63	-1.01
Adamts1	0.0018	0.83	0.94	-1.00
1700060J05Rik	0.019	0.42	0.93	-0.98
Kit	0.00012	0.19	0.078	-0.97
Ubald1	0.014	1.0	0.47	-0.97
Plcb4	0.033	0.86	0.77	-0.94
Cebpd	0.0041	0.36	0.62	-0.93
Slc44a1	0.019	1.0	0.56	-0.90
Irf2bp2	0.032	1.0	0.94	-0.89
Gm31834	0.049	0.60	0.96	-0.88
Dll4	0.015	0.89	0.81	-0.88
Gm14207	0.0084	0.55	0.94	-0.87
Glp1r	0.00055	0.47	0.95	-0.87
Rasgrp3	0.0099	0.76	0.97	-0.84
Ccrl2	0.024	0.94	0.84	-0.83
Uqcrc2	0.030	1.0	0.76	-0.83
Aplnr	0.0085	0.95	0.93	-0.81
Efnb2	0.0096	0.43	0.99	-0.80
Drc3	0.92	1.0	0.019	-0.80
Cd93	0.00026	0.27	0.59	-0.78
Gm6627	0.048	0.15	0.94	-0.77
Itga6	0.0029	0.78	0.63	-0.77
Tmem268	0.69	1.0	0.027	-0.76
Rnf144a	0.00095	0.77	0.98	-0.76
Cltc	0.024	0.66	0.90	-0.75
H2-Q5	0.014	0.52	0.91	-0.74
Gbp7	0.014	1.0	0.96	-0.74
Gm26616	0.33	1.0	0.00078	-0.73
Gm10138	0.0085	0.86	0.017	-0.73
Prr14l	0.45	1.0	0.0022	-0.73
Marcksl1	0.13	1.0	0.0086	-0.72
Atp1a1	0.0052	1.0	0.96	-0.72

Gm13889	0.0050	1.0	0.80	-0.71
Ptprb	0.00095	0.32	0.86	-0.70
H2-Q6	0.00098	0.45	0.89	-0.70
Slc35d1	0.67	1.0	0.000030	-0.69
Antxr2	0.042	1.0	0.13	-0.69
Ewsr1	0.0039	0.60	0.75	-0.68
Acer2	0.0031	0.44	0.86	-0.67
Gm43328	0.53	1.0	0.014	-0.67
Lyve1	0.0067	1.0	0.97	-0.66
Ptprg	0.039	1.0	0.86	-0.66
Bmp6	0.0018	0.61	0.98	-0.66
Fzd4	0.017	1.0	0.85	-0.66
Irf1	0.0017	0.69	0.91	-0.65
Polr3k	0.53	1.0	1.26E-07	-0.65
Tor1aip2	0.0096	1.0	0.58	-0.65
Vegfa	0.0041	0.91	0.92	-0.65
Gm17334	0.0041	0.46	0.70	-0.65
Pde4b	0.0083	0.80	0.91	-0.63
Cpsf2	0.51	1.0	0.0034	-0.62
Itga1	0.00026	0.32	0.79	-0.61
Cmtm3	0.037	1.0	0.66	-0.61
Tmem184b	0.029	0.94	0.79	-0.60
Gbp4	0.19	1.0	0.015	-0.60
Tek	0.0024	0.39	0.93	-0.60
Notch4	0.030	1.0	0.87	-0.59
Entpd1	0.041	1.0	0.76	-0.59
Spns2	0.019	0.84	0.62	-0.59
H2-Q10	0.019	0.60	0.97	-0.58
Ptprm	0.0097	0.75	0.93	-0.58
Elk3	0.0090	0.46	0.95	-0.57
Gpihbp1	0.0043	0.36	0.58	-0.57
Matr3	0.026	1.0	0.96	-0.56
Cdk17	0.0043	0.38	0.69	-0.56
Vps50	0.60	1.0	0.028	-0.56
Cemip2	0.0084	1.0	0.90	-0.55
2310057M21Rik	0.92	1.0	0.025	-0.54
Pan2	0.41	1.0	0.031	-0.53
Ndufb3	0.15	1.0	0.035	-0.53
Ehd1	0.025	1.0	0.87	-0.53
Txndc5	0.0041	1.0	0.15	-0.52
Plvap	0.038	0.47	0.40	-0.52
Podxl	0.050	0.73	0.067	-0.52
Vaultrc5	0.88	1.0	0.029	-0.51
Mfsd1	0.39	1.0	0.0020	-0.51

Xbp1	0.026	1.0	0.88	-0.49
Jmy	0.39	1.0	0.039	-0.49
Sfpq	0.017	1.0	0.94	-0.48
Pofut2	0.20	1.0	0.018	-0.48
Tie1	0.0031	0.23	0.90	-0.48
Slc3a2	0.021	0.75	0.97	-0.47
Mfsd11	0.021	0.85	0.73	-0.45
Jun	0.008	0.10	0.94	-0.44
Fbxw17	0.90	1.0	0.0045	-0.44
Cyyr1	0.015	0.61	0.37	-0.44
Mybbp1a	0.012	1.0	0.79	-0.43
Spry2	0.074	1.0	0.032	-0.40
Junos	0.015	0.10	0.47	-0.40
Gm11651	0.013	0.043	0.97	-0.40
Alkbh3	0.62	1.0	0.030	-0.40
Ece1	0.024	0.38	0.60	-0.39
Dock9	0.048	1.0	0.89	-0.39
Cfap54	0.96	1.0	0.026	-0.38
Poldip3	0.72	1.0	0.00027	-0.36
Gm42547	0.93	1.0	0.00011	-0.36
Ace	0.023	0.14	0.70	-0.36
Pum2	0.93	1.0	0.045	-0.28
Vrk1	0.89	1.0	0.016	-0.27
Tspan6	0.90	1.0	0.00085	-0.25
Aph1a	0.53	1.0	0.041	-0.24
Gm49534	0.47	1.0	0.029	-0.23
Arhgap28	0.60	1.0	0.00020	-0.23
Gm11960	0.64	1.0	0.00059	-0.20
Commd7	0.73	1.0	0.030	-0.19
Golga1	0.76	1.0	0.014	-0.18
Cd72	0.82	1.0	0.017	-0.16
Pelp1	0.94	1.0	0.0019	-0.15
Tspan2	0.81	1.0	0.031	-0.14
Itgb1bp1	0.26	1.0	0.0093	-0.14
Fzd5	0.79	1.0	0.0045	-0.13
Pde6g	0.81	1.0	0.028	-0.12
Rhbdd3	0.0022	1.0	0.80	-0.12
Mxd3	0.85	1.0	3.72E-06	-0.11
Sag	0.41	1.0	0.030	-0.11
Srgap2	0.70	1.0	0.030	-0.09
Mrnip	0.93	1.0	0.028	-0.08
Ctsd	0.90	1.0	0.028	-0.08
Gm17080	0.79	1.0	6.59E-06	-0.08
Exoc7	0.74	1.0	0.028	-0.06

Rnf130	0.63	1.0	2.44E-05	-0.05
B3galnt2	0.43	1.0	0.00027	-0.03
Eif6	0.78	1.0	0.013	-0.03
1600020E01Rik	0.57	1.0	0.022	-0.03
Gm36236	0.81	1.0	0.031	-0.01
Gm17036	0.83	1.0	0.030	0.00
Mrpl48-ps	0.80	1.0	0.038	0.00
Map3k3	0.86	1.0	0.019	0.00

Table 7.8: Downregulated genes in *Eltd1*-depleted (all exons) total lung endothelial cells.

The *p* value of the differentially expressed genes were colour coded to indicate significance ($p < 0.05$). Blue (Wilcox test); yellow (edgeR) and green (MAST).

7.4.2 Lung arterial endothelial cells

7.4.2.1 Upregulated genes

Gene symbol	pval.adjj.wilcox	pval.adj.edgeR	pval.adj.MAST	log(Fold Change)
Mamld1	0.70	0.025	0.77	6.63
4933404O12Rik	0.72	0.043	0.88	6.47
Rhpn2	0.74	0.035	0.97	6.02
Cd83	0.70	0.026	0.80	5.77
Cchcr1	0.70	0.035	0.93	5.59
Lrrc51	0.66	0.016	0.99	5.56
Strip2	0.68	0.025	0.96	4.74
Gm10425	0.78	0.026	0.77	4.04
H2-T-ps	0.86	0.035	0.96	2.04
Ly6c2	0.79	0.026	0.88	1.98
Tmem94	0.80	0.035	1.0	1.61
C130012C08Rik	1.0	1.0	0.0031	0.74

Table 7.9: Upregulated genes in *Eltd1*-depleted (all exons) lung arterial endothelial cells.

The *p* value of the differentially expressed genes were colour coded to indicate significance ($p < 0.05$). Blue (Wilcox test); yellow (edgeR) and green (MAST).

7.4.2.2 Downregulated genes

Gene symbol	pval.adjj.wilcox	pval.adj.edgeR	pval.adj.MAST	log(Fold Change)
Adgrl4	4.67E-17	1.08E-83	0.94	-10.29
Sparcl1	0.70	0.043	1.0	-7.41
Thnsl2	0.70	0.035	0.79	-7.35
Naglu	0.70	0.045	0.91	-6.82
Nrarp	0.66	0.025	0.88	-6.55
Mcub	0.66	0.025	0.78	-6.53
Gm38287	0.70	0.035	0.84	-6.10
Elp6	0.84	0.031	0.93	-3.82
Tchp	0.91	0.035	1.0	-3.40
Mid1ip1	0.80	1.0	3.24E-30	-0.21

Table 7.10: Downregulated genes in *Eltd1*-depleted (all exons) lung arterial endothelial cells. The *p* value of the differentially expressed genes were colour coded to indicate significance ($p < 0.05$). Blue (Wilcox test); yellow (edgeR) and green (MAST).

7.4.3 Lung capillary endothelial cells

7.4.3.1 Upregulated genes

Gene symbol	pval.adjj.wilcox	pval.adj.edgeR	pval.adj.MAST	log(Fold Change)
S1pr3	0.066	5.91E-07	0.78	6.59
Adcy2	0.42	6.52E-07	0.98	6.49
Arhgap24	0.66	7.06E-06	0.97	6.37
Aox1	0.87	3.00E-10	0.92	5.95
Gramd2	0.35	0.020	0.96	5.63
Lamb3	0.35	0.0064	0.92	5.57
Ptges	0.42	6.42E-06	0.78	5.43
Tmem200a	0.92	4.89E-06	1.0	5.34
Gm31517	0.84	7.23E-06	0.99	5.31
Cetn4	0.41	4.08E-05	0.92	5.27
A530017D24Rik	0.45	0.0017	0.97	5.08
Auts2	0.92	0.0082	0.99	4.74
Dennd1c	0.91	0.00039	0.92	4.72
Dcst1	0.78	0.012	0.98	4.67
Rgs14	0.45	0.0015	0.99	4.49
Gm38042	0.74	4.64E-16	0.97	4.16

D230049E03Rik	0.60	0.0050	0.98	4.12
Foxp4	0.66	0.011	0.96	4.08
Pfkfb1	0.82	0.042	0.99	3.90
A830018L16Rik	0.78	0.0086	0.92	3.74
Chrm1	0.66	0.0014	0.97	3.68
Gm7591	0.56	0.0015	0.93	3.62
Gm30074	0.23	0.00025	0.99	3.62
Cfap100	0.74	0.028	0.96	3.53
Pi16	0.91	0.00050	0.89	3.46
Eaf2	0.52	0.0070	0.98	3.28
Pde1a	0.96	4.08E-05	0.97	3.24
Cgn	0.77	0.029	0.84	3.06
Rapgef4os1	0.75	0.00034	0.92	2.99
Mpv17l	0.88	0.0066	0.97	2.95
Slitrk6	0.42	0.0011	0.75	2.93
3110039I08Rik	0.92	0.0015	0.87	2.87
Gm36955	0.91	0.0043	0.96	2.77
4732416N19Rik	0.62	0.00018	0.92	2.54
Gm38366	0.36	0.00089	0.99	2.39
Gm16185	0.88	0.0015	0.98	2.37
Klf12	0.92	0.0065	0.98	2.37
Exph5	0.60	0.0014	0.95	2.36
Gm37834	0.68	0.0041	0.97	2.21
Farp2	0.92	0.024	0.95	2.13
Ttyh1	0.95	1.32E-10	0.97	2.09
Gm8807	0.89	0.022	0.83	2.09
2310016G11Rik	0.070	0.00025	0.95	1.98
Gm17259	0.99	2.60E-05	1.0	1.93
Gm32834	0.23	0.013	1.0	1.74
Rpl36al	0.82	0.0086	0.99	1.45
Gm42732	0.26	0.0045	0.99	1.15
Gm15564	0.58	0.0094	0.95	1.15
D130062J10Rik	0.55	0.0012	0.98	1.03
Gm10767	0.67	0.035	0.99	0.89
Sptbn1	0.30	0.014	0.98	0.63
Gm23935	0.29	0.0078	0.73	0.61
Fth1	0.072	0.0013	0.98	0.58
mt-Rnr2	0.23	0.0070	0.98	0.55
mt-Atp8	0.074	4.08E-05	0.91	0.53
Myl12a	0.074	0.023	0.96	0.46
Tmsb4x	0.0056	3.12E-07	0.99	0.45
mt-Cytb	0.095	0.014	0.68	0.44
Mir6236	0.19	0.0058	0.81	0.42
Gm10252	0.011	6.56E-05	0.74	0.41

ENSMUSG00000106106	0.23	0.0072	0.64	0.35
Ftl1	0.072	0.0032	0.91	0.34
Gm42418	0.21	0.0030	0.92	0.33
Ubb	0.010	0.00075	0.92	0.26
Vps72	0.94	1.0	1.97E-76	0.24

Table 7.11: Upregulated genes in *Eltd1*-depleted (all exons) lung capillary endothelial cells. The *p* value of the differentially expressed genes were colour coded to indicate significance ($p < 0.05$). Blue (Wilcox test); yellow (edgeR) and green (MAST).

7.4.3.2 Downregulated genes

Gene symbol	pval.adjj.wilcox	pval.adj.edgeR	Pval.adj.MAST	Log(Fold Change)
Adgrl4	1.26E-40	3.3E-281	0.82	-11.24
Slc35b4	0.21	0.0071	0.99	-7.35
Mpp5	0.21	0.0070	0.99	-6.29
Fam69a	0.22	0.0094	1.0	-6.17
Tnfrsf12a	0.29	0.044	0.82	-5.87
Mettl26	0.21	0.029	0.73	-5.87
1110012L19Rik	0.28	0.035	0.92	-5.49
Fnip2	0.37	0.0086	0.84	-5.04
Gm49066	0.24	0.021	0.80	-4.80
Gm13856	0.24	0.021	0.99	-4.48
Ift80	0.29	0.032	0.82	-4.32
Atg2b	0.60	0.020	0.98	-4.20
Dtnb	0.41	0.0030	0.98	-3.76
Gm10033	0.41	0.021	0.82	-3.54
Gm44187	0.27	0.027	0.87	-3.50
Elp6	0.89	0.00039	0.87	-3.50
C230062I16Rik	0.21	0.028	0.84	-3.16
Gm43379	0.23	0.017	1.0	-3.07
Tchp	0.63	3.04E-05	0.99	-3.02
Nek4	0.33	0.0086	0.97	-2.88
Coa4	0.55	0.027	0.96	-2.38

Table 7.12: Downregulated genes in *Eltd1*-depleted (all exons) lung capillary endothelial cells. The *p* value of the differentially expressed genes were colour coded to indicate significance ($p < 0.05$). Blue (Wilcox test); yellow (edgeR) and green (MAST).

7.5 Differential gene expression profile in acute *Eltd1*-depleted (exons 4 and 5) lung endothelial cells

7.5.1 Combined analysis

7.5.1.1 Upregulated genes

Gene.symbol	pval.adj.wilcox	pval.adj.edgeR	pval.adj.MAST	log(Fold Change)
Sftpb	0.37	0.0015	0.19	5.74
Scd1	0.50	0.0059	0.94	5.58
Nox4	0.64	0.00036	0.67	4.76
Cyp2e1	0.49	8.99E-05	0.85	4.74
Ociad2	0.19	9.25E-07	0.96	4.63
Cbr2	0.42	0.049	0.71	4.39
Gm26903	0.019	0.026	0.99	3.96
Cetn4	0.51	0.0010	0.62	3.88
Gm31517	0.94	0.0010	0.80	3.79
Wfdc2	0.044	0.14	0.92	3.74
Gm44699	0.70	3.02E-07	0.42	3.74
Il18r1	0.12	0.14	0.0051	3.66
Tbc1d16	0.72	0.038	0.69	3.65
Mpzl2	0.80	3.02E-07	0.63	3.64
Gm47138	0.19	0.00056	0.64	3.62
Ppl	0.80	0.0073	0.79	3.61
Blnk	0.92	0.0042	0.87	3.60
Gm15396	0.80	6.76E-05	0.42	3.44
A530017D24Rik	0.63	0.049	0.42	3.41
Dcst1	0.99	0.026	0.69	3.37
Il5ra	0.89	0.0040	0.90	3.31
Emb	0.75	0.0010	0.69	3.31
Nebl	0.0092	0.35	0.92	3.28
Rac2	0.69	0.0010	0.85	3.24
Prss8	0.95	0.0046	0.91	3.15
A830018L16Rik	0.89	0.0051	0.94	3.15
D230049E03Rik	0.72	0.010	0.31	3.07
Cfap100	0.63	0.011	0.96	3.05
Ms4a1	0.68	5.69E-10	0.98	3.04
Gstt1	0.012	0.48	0.89	3.04
Gm16287	0.99	0.0078	0.83	2.95
B4galnt1	0.19	0.37	7.09E-07	2.94
Gm15675	0.81	0.019	0.20	2.92
Cgn	0.87	0.0052	0.97	2.91

Enpp1	0.77	0.00055	0.96	2.90
Gm37204	0.71	7.07E-11	0.65	2.88
H2-DMb2	0.55	1.07E-05	0.38	2.85
Celf2	0.58	0.49	0.0043	2.84
Trmt61a	0.042	0.55	0.97	2.82
Myh14	0.040	0.61	0.83	2.81
Gm16576	0.27	0.56	0.014	2.66
Tc2n	0.57	0.0034	0.94	2.63
Dlgap5	0.89	0.014	0.84	2.62
Gm7591	0.80	0.037	0.98	2.61
Pi16	0.99	0.0012	1.0	2.59
Ckap2	0.63	4.34E-05	0.84	2.58
Slc23a1	0.60	0.00012	0.19	2.56
Pde1a	0.72	0.030	0.62	2.55
Ccdc141	0.98	2.59E-07	0.75	2.51
Abcc9	0.76	0.019	0.85	2.49
Eaf2	0.70	0.026	0.75	2.41
Efcc1	0.96	0.036	0.92	2.40
4732416N19Rik	0.50	1.14E-05	0.84	2.30
Gm43340	0.90	0.0060	0.68	2.23
Gm43790	0.84	0.024	0.95	2.18
Rapgef4os1	0.50	0.0010	0.70	2.16
Lrrc8e	0.48	0.012	0.30	2.13
Gm38042	0.89	0.0020	0.70	2.12
Slc16a7	0.75	0.028	1.0	2.09
Gm47113	0.98	0.026	0.42	2.06
Pi15	0.82	0.024	0.10	2.05
Dnali1	0.23	0.014	0.68	2.02
Slc27a1	0.87	0.0011	0.66	1.98
Tmem88b	0.96	0.042	0.92	1.97
Tjp3	0.85	0.019	0.96	1.97
Saa3	0.98	0.00056	0.89	1.96
Tmem82	0.66	0.0020	0.84	1.86
Gm36955	0.99	0.048	0.96	1.82
Gm48871	0.84	0.047	0.76	1.81
Pqlc3	0.23	1.0	0.031	1.80
ENSMUSG00000117187	0.98	0.021	0.72	1.74
Matn2	0.40	0.0050	0.77	1.70
Unc13d	0.80	4.64E-05	1.0	1.70
Gal3st3	0.43	0.0025	0.74	1.68
Gm6266	0.65	0.026	0.95	1.62
Slfn3	0.81	0.53	0.01	1.60
Fam171b	0.59	1.0	0.038	1.54
S1pr3	0.014	1.0	0.98	1.51

Gm37834	0.78	0.030	0.22	1.48
Zfp459	0.96	0.00047	0.90	1.44
Foxp2	0.99	0.042	0.82	1.43
E330009J07Rik	0.026	1.0	1.0	1.42
Ttyh1	0.63	4.14E-07	0.60	1.38
Gm32834	0.035	0.52	0.08	1.37
Dhtkd1	0.83	0.00056	0.82	1.28
Sult5a1	0.78	0.014	0.99	1.25
Tmeff2	0.012	0.86	0.63	1.14
Smim1	0.32	1.0	0.010	1.13
Gm15564	0.022	5.54E-05	0.76	1.08
Ccdc78	0.48	0.025	0.28	1.07
Gm17259	0.93	0.023	0.94	1.00
Dhfr	0.94	1.0	0.0049	0.97
Dnajb14	0.96	0.033	0.63	0.93
P3h3	0.96	1.0	0.010	0.90
Gpx3	0.035	0.77	0.85	0.88
Gm12473	0.82	1.0	0.040	0.88
Olfr1124	0.045	0.18	0.87	0.87
Cpq	0.99	1.0	0.0090	0.84
Naip5	0.0028	1.0	0.14	0.83
Zan	0.85	1.0	0.035	0.72
Emp2	0.00095	0.43	0.68	0.66
D130062J10Rik	0.63	0.022	0.50	0.64
Rnf157	0.92	1.0	0.0013	0.61
Hint1	0.025	0.56	0.71	0.60
Gm23935	0.022	1.14E-05	0.96	0.58
Rpl36	0.044	0.20	0.92	0.57
Asns	0.68	1.0	0.041	0.54
Gm45236	0.92	1.0	2.96E-05	0.52
Lars2	0.0018	0.0041	0.99	0.52
Gm29530	0.73	1.0	0.0010	0.49
Ercc5	0.97	1.0	0.0046	0.48
Gm9959	0.93	1.0	0.0072	0.47
Ftl1-ps1	0.014	0.075	0.69	0.47
Fth1	8.28E-06	1.07E-05	0.77	0.46
Tmem70	0.96	1.0	8.87E-05	0.44
Metrnl	0.87	1.0	0.041	0.43
Tgfb2	0.99	1.0	0.020	0.40
mt-Rnr2	0.22	0.0073	0.21	0.38
Grina	0.72	1.0	0.038	0.38
Mid1ip1	0.92	1.0	0.00017	0.37
Adck2	0.86	1.0	0.020	0.36
Pde6g	0.98	1.0	0.0083	0.36

Gm5814	0.84	1.0	0.010	0.34
Gm17661	0.98	1.0	0.0042	0.34
mt-Atp8	0.038	0.0026	0.95	0.32
Zdhhc9	0.54	1.0	0.05	0.31
ENSMUSG00000106106	0.018	4.34E-05	0.70	0.31
mt-Cytb	0.019	0.0092	0.10	0.31
Gm42418	0.014	1.05E-06	0.46	0.31
Tmsb4x	0.0019	0.00030	0.60	0.31
Creg1	0.87	1.0	0.013	0.30
Dcdc2c	0.94	1.0	0.010	0.29
Gm10252	1.68E-05	2.17E-05	0.71	0.28
Calm2	0.014	0.76	0.67	0.26
Mir6236	0.035	0.021	0.75	0.26
Sdc2	0.71	1.0	0.0014	0.26
Myl12a	0.00085	0.079	0.938	0.26
Rwdd1	0.94	1.0	0.015	0.24
Mrpl48-ps	0.93	1.0	0.020	0.24
Tuba1a	0.043	0.94	0.834	0.23
Dbi	0.94	1.0	0.0014	0.23
Ftl1	0.00030	0.0066	0.96	0.22
Gm28959	0.93	1.0	0.041	0.22
Calm1	0.016	0.59	1.0	0.20
Abracl	0.49	1.0	0.0012	0.20
Gm13070	0.92	1.0	0.0043	0.19
Fkbp1a	0.0010	0.56	0.98	0.18
Dynll1	0.21	1.0	7.0E-117	0.17
Ubb	7.27E-06	0.0031	0.93	0.16
Cuedc1	0.90	1.0	0.045	0.15
Sumo1	0.86	1.0	0.0012	0.14
Crip2	0.0044	0.76	0.96	0.14
E130208F15Rik	0.79	1.0	1.18E-08	0.14
Msl2	0.97	1.0	0.0010	0.14
Slc52a2	1.0	1.0	0.014	0.12
Ica1	0.93	1.0	0.0099	0.11
Gm16153	0.97	1.0	0.0017	0.09
Cplane1	0.92	1.0	0.015	0.09
Aspscr1	0.98	1.0	0.00026	0.08
Card6	0.98	1.0	0.0014	0.08
Daglb	0.66	1.0	0.0014	0.08
B2m	0.040	1.0	0.92	0.08
Tcf12	0.79	1.0	0.010	0.07
Efhc1	0.85	1.0	0.0039	0.07
Galk1	0.94	1.0	0.0014	0.06
Acot13	0.68	1.0	0.013	0.06

2310022A10Rik	0.88	1.0	0.0022	0.06
Ypel3	0.76	1.0	2.02E-07	0.06
Poldip3	0.93	1.0	3.07E-05	0.06
Gm24265	0.33	1.0	0.013	0.05
Exoc7	0.74	1.0	0.037	0.05
Psmb9	0.65	1.0	0.020	0.05
Fam177a	0.85	1.0	0.00029	0.05
Dnajb4	0.87	1.0	0.033	0.04
Rnf130	0.72	1.0	1.85E-08	0.03
Eif6	0.80	1.0	0.0083	0.03
Gm43328	0.75	1.0	0.030	0.03
Lrrc14b	0.53	1.0	0.031	0.03
Lrmda	0.97	1.0	0.014	0.02
Stpg1	0.94	1.0	0.020	0.02
Atf1	0.96	1.0	0.018	0.01
Slx4	0.78	1.0	0.0034	0.01

Table 7.13: Upregulated genes in *Eltd1*-depleted (exons 4 and 5) total lung endothelial cells. The *p* value of the differentially expressed genes were colour coded to indicate significance ($p < 0.05$). Blue (Wilcox test); yellow (edgeR) and green (MAST).

7.5.1.2 Downregulated genes

Gene.symbol	pval.adj.wilcox	pval.adj.edgeR	pval.adj.MAST	Log(Fold Change)
Zfp28	0.029	0.041	0.51	-5.73
Ppm1l	0.17	0.0009	0.98	-5.72
Inhbb	0.19	0.0020	0.96	-4.92
Alox12	0.47	0.024	0.95	-4.91
Trpc6	0.17	0.0022	0.59	-4.82
Eri2	0.24	0.0024	0.26	-4.75
Esr2	0.39	0.027	1.0	-4.57
Ncapg2	0.77	0.033	0.095	-4.52
Zfp202	0.46	0.018	0.70	-4.38
Foxd2os	0.35	0.035	0.70	-4.28
Ltb4r2	0.32	0.037	0.90	-4.24
Chaf1b	0.74	0.033	0.20	-4.20
Trim59	0.27	0.0046	0.70	-4.13
Zfp169	0.38	0.023	0.84	-4.00
ENSMUSG00000116815	0.74	0.047	0.46	-3.83
Dsn1	0.81	0.012	0.90	-3.82
Majin	0.22	0.0066	0.78	-3.80

B230334C09Rik	0.19	0.0081	0.87	-3.60
Adgrl4	7.67E-68	8.74E-45	0.17	-3.49
Tigd3	0.45	0.047	0.92	-3.46
Acsm3	0.45	0.045	0.96	-3.38
Lef1	0.78	0.024	0.89	-3.16
Gm26835	0.97	0.042	0.94	-3.11
Tchp	0.73	1.04E-13	0.86	-3.07
Aqp7	0.49	0.028	0.16	-3.07
Slc12a8	0.73	0.026	0.70	-2.99
Gnat1	0.63	0.024	0.95	-2.88
Tmem95	0.57	0.50	0.0048	-2.79
Usp49	0.54	0.012	0.31	-2.73
Gm37503	0.27	0.024	0.89	-2.64
Elp6	0.61	4.84E-06	0.93	-2.63
Pabpc4l	0.27	0.025	0.90	-2.58
N4bp2	0.71	0.022	1.0	-2.57
B130021K23Rik	0.79	0.022	0.91	-2.39
Ltb4r1	0.083	0.0059	0.43	-2.33
Gm43379	0.28	0.0042	0.89	-2.31
ENSMUSG00000116995	0.29	0.0089	1.0	-2.25
Gm8463	0.24	0.039	0.81	-2.19
Hspa1l	0.10	0.024	0.67	-2.00
Tas1r3	0.82	0.026	0.98	-1.99
Slc5a3	0.046	1.0	0.24	-1.96
Nhsl2	0.0042	0.86	0.86	-1.96
C78334	0.36	0.92	0.0027	-1.94
Il13ra1	0.041	0.90	0.76	-1.93
Tgs1	0.020	0.48	0.36	-1.91
Snrnp35	0.72	1.0	0.0043	-1.89
Gm2788	0.45	0.042	0.13	-1.88
Clp1	0.043	1.0	0.88	-1.84
Snord7	0.11	0.014	1.0	-1.83
Zfp292	0.012	0.56	0.17	-1.80
Gm16054	0.012	0.76	0.87	-1.75
Esr1	0.75	0.032	0.93	-1.74
Racgap1	0.89	3.83E-05	0.50	-1.72
Slc19a2	0.32	1.0	0.020	-1.70
Klhl23	0.62	1.0	0.0028	-1.66
Prkn	0.85	0.025	0.0050	-1.56
Csrnp1	0.0031	0.56	0.68	-1.53
Gm43274	0.24	0.044	0.98	-1.52
Prss12	0.031	1.0	0.99	-1.47
1500004A13Rik	0.64	0.53	3.46E-09	-1.45
1700019L13Rik	0.014	0.068	0.85	-1.45

Bik	0.0023	0.70	0.88	-1.45
Pdk1	0.041	1.0	0.70	-1.43
Hmg20a	0.029	0.87	0.92	-1.41
Asb3	0.25	1.0	0.020	-1.41
Fzd6	0.018	0.83	0.82	-1.40
Gch1	0.010	0.81	1.0	-1.39
Esrra	0.072	0.026	0.95	-1.37
Setdb1	0.10	0.012	0.36	-1.37
Osmr	0.017	1.0	0.98	-1.29
Mmrn2	0.007	0.71	0.88	-1.28
Klhl28	0.40	1.0	0.0040	-1.28
1700086O06Rik	0.072	0.049	0.73	-1.24
Gpr68	0.56	0.92	0.024	-1.23
Ntn1	0.0018	0.75	0.78	-1.22
Smarcd1	0.024	1.0	0.90	-1.21
Gpr4	0.044	1.0	0.59	-1.18
Pdcl	0.021	1.0	0.34	-1.13
Sft2d2	0.014	1.0	0.72	-1.09
Gm26799	0.051	0.018	0.96	-1.08
Slc35b3	0.043	1.0	0.51	-1.06
Gm14654	0.020	0.21	0.84	-1.06
Adamts1	0.00021	0.55	0.65	-1.06
Tmem268	0.68	1.0	0.015	-1.04
Gm44065	0.048	1.0	0.96	-1.02
5430405H02Rik	0.033	1.0	0.92	-1.01
Marcksl1	0.010	1.0	0.014	-1.00
Gm37091	0.012	0.14	0.90	-1.00
Nrarp	0.034	1.0	0.94	-1.00
Sntb1	0.044	1.0	0.77	-0.99
5830408C22Rik	0.048	0.051	1.0	-0.98
Glp1r	3.26E-07	0.17	0.96	-0.98
Tor1b	0.040	1.0	0.94	-0.98
Gm38287	0.042	1.0	1.0	-0.98
Tmem185b	0.030	1.0	0.48	-0.97
Tgif2	0.013	1.0	0.59	-0.96
Mctp1	0.013	1.0	0.84	-0.95
Slc39a11	0.52	1.0	0.022	-0.94
St7l	0.11	0.49	0.016	-0.94
Plxnd1	0.017	1.0	0.52	-0.93
Pelo	0.00058	0.90	0.97	-0.92
Gm42547	0.87	1.0	9.64E-09	-0.91
1700060J05Rik	0.011	0.43	0.99	-0.90
Ivns1abp	0.018	0.75	0.95	-0.90
Irf2bp2	0.0069	0.92	0.84	-0.89

Efnb2	0.0028	0.16	0.86	-0.89
Cebpd	0.0019	0.29	0.39	-0.89
Tor4a	0.040	1.0	0.69	-0.88
Iigp1	0.048	1.0	0.52	-0.88
Fpgs	0.018	0.81	0.43	-0.86
Antxr2	0.00085	0.72	0.21	-0.86
Gm31834	0.019	0.51	0.96	-0.85
Gm26759	0.012	0.85	0.78	-0.84
Jam2	0.021	1.0	0.58	-0.84
Spidr	0.012	1.0	0.64	-0.83
Zc3h7a	0.010	0.55	0.98	-0.83
Dusp6	0.044	1.0	1.0	-0.83
Kbtbd2	0.030	1.0	0.95	-0.83
Agfg2	0.220	1.0	0.020	-0.83
Itga6	0.00017	0.50	0.09	-0.82
Csf1	0.021	1.0	0.89	-0.82
Strip1	0.031	1.0	0.67	-0.81
Mospd2	0.049	1.0	0.92	-0.81
Aplnr	0.0014	0.77	0.98	-0.81
Rcan1	0.010	1.0	0.95	-0.80
Mansc1	0.048	1.0	0.69	-0.80
Gm26616	0.44	1.0	8.54E-05	-0.80
Mfsd1	0.14	1.0	0.00076	-0.79
Ubald1	0.032	1.0	0.83	-0.79
Ubap2l	0.031	0.81	0.62	-0.79
Kit	3.53E-05	0.34	0.020	-0.79
Drc3	0.96	1.0	0.021	-0.78
Gm20412	0.021	0.77	1.0	-0.77
Bmp6	1.01E-05	0.20	0.79	-0.77
Gm15758	0.018	0.77	0.89	-0.77
Sep-11	0.0087	1.0	0.91	-0.75
Itga5	0.010	1.0	0.82	-0.75
Rnf144a	0.00012	0.62	0.99	-0.75
Cdc42ep4	0.021	1.0	1.00	-0.75
Gls	0.050	1.0	0.91	-0.75
Ddx24	0.010	1.0	0.30	-0.75
Gm4070	0.045	0.87	0.92	-0.74
Acer2	9.73E-05	0.18	0.84	-0.74
Sorbs1	0.0069	0.71	0.92	-0.74
Atp6v1a	0.041	1.0	0.58	-0.73
Tgm2	0.021	0.83	0.98	-0.73
Mcam	0.0096	0.76	0.74	-0.73
ENSMUSG00000116811	0.041	0.12	0.05	-0.72
Pofut2	0.034	1.0	0.17	-0.72

Zbtb21	0.042	1.0	0.77	-0.72
Fzd5	0.99	1.0	0.05	-0.71
H2-Q5	0.0030	0.47	1.0	-0.71
Vegfa	0.00045	0.57	0.95	-0.71
Gm20481	0.038	0.92	1.0	-0.71
Xbp1	2.85E-05	0.24	0.96	-0.70
Gm10734	0.0013	1.0	0.30	-0.69
Rasgrp3	0.0019	0.91	0.80	-0.69
Oxr1	0.049	1.0	0.89	-0.69
Gm37415	0.29	1.0	0.04	-0.69
Sertad1	0.033	1.0	0.89	-0.69
Cfap54	0.89	1.0	0.0062	-0.68
Uba1	0.018	1.0	0.64	-0.67
Plcb4	0.018	1.0	0.84	-0.67
Cxcr4	0.39	1.0	0.024	-0.67
Fam84b	0.048	1.0	0.71	-0.67
Cemip2	0.00044	0.85	0.98	-0.66
Fzd4	0.0027	0.77	0.95	-0.66
A930028N01Rik	0.037	0.85	0.99	-0.66
Nod1	0.044	1.0	0.84	-0.66
Ctsc	0.039	1.0	0.83	-0.65
Tspan6	0.54	1.0	6.38E-05	-0.65
Rapgef1	0.021	1.0	0.76	-0.65
Fam171a1	0.0074	1.0	0.92	-0.64
Tek	3.13E-05	0.18	0.71	-0.64
Gm14207	0.045	0.94	0.86	-0.63
Gata3	0.049	1.0	0.81	-0.63
Itfg1	0.043	1.0	0.96	-0.63
Gm15629	0.045	0.90	0.81	-0.62
Avpi1	0.019	1.0	0.79	-0.62
Ptprb	9.77E-05	0.36	0.87	-0.62
Ccdc85a	0.041	1.0	0.94	-0.62
Itga1	1.34E-05	0.18	0.80	-0.62
Gm13889	0.0069	1.0	0.88	-0.61
Cd93	0.00044	0.53	0.32	-0.61
Antxr1	0.044	1.0	0.83	-0.61
Pim3	0.012	1.0	0.77	-0.60
Cmtm3	0.013	1.0	0.86	-0.59
Ralb	0.022	1.0	0.66	-0.59
Entpd1	0.013	1.0	0.61	-0.59
Atf7ip	0.012	1.0	0.86	-0.58
Sparcl1	0.041	1.0	0.46	-0.58
Ephx1	0.013	1.0	0.91	-0.58
Tor1aip2	0.018	1.0	0.60	-0.58

Lyve1	0.0074	1.0	0.99	-0.58
Atp1a1	0.0035	1.0	1.0	-0.58
Mbnl1	0.0069	0.91	0.89	-0.58
Dpp4	0.012	0.85	0.53	-0.57
Hey1	0.018	1.0	0.99	-0.57
H2-Q10	0.0084	0.50	0.73	-0.57
Plcb1	0.0037	1.0	0.78	-0.57
Ascc3	0.63	1.0	0.0043	-0.57
Mat2a	0.041	1.0	0.83	-0.56
Gm44710	0.0069	1.0	0.99	-0.56
Ctu2	0.042	1.0	0.89	-0.56
Gbp7	0.0082	1.0	0.88	-0.55
Notch4	0.019	1.0	0.89	-0.54
Pde4b	0.012	0.91	0.85	-0.53
Ahr	0.040	0.85	0.83	-0.53
Gm28192	0.041	1.0	0.78	-0.53
Ano6	0.033	1.0	0.33	-0.53
Ppp1r15a	0.045	1.0	0.78	-0.53
Zfp36	0.048	0.81	0.82	-0.52
Itm2c	0.041	1.0	0.90	-0.52
Txndc5	0.00032	0.81	0.33	-0.52
4731419I09Rik	0.020	1.0	0.84	-0.52
H2-Q6	0.0029	0.81	0.76	-0.52
Tor1aip1	0.19	1.0	0.02	-0.52
Btg2	0.038	0.92	0.95	-0.52
Atp2a3	0.019	0.81	0.74	-0.52
Rdx	0.020	0.85	0.72	-0.51
Lifr	0.012	0.86	1.0	-0.51
Zxdb	0.34	1.0	0.050	-0.51
Gm9910	0.049	1.0	0.94	-0.50
Snw1	0.012	1.0	0.66	-0.50
Slc35d1	0.52	1.0	2.43E-09	-0.50
Tln1	0.026	1.0	0.87	-0.50
Adam15	0.042	1.0	0.74	-0.50
Irf1	0.0036	1.0	1.0	-0.50
Ndfip2	0.027	1.0	0.82	-0.49
Tmc6	0.30	1.0	0.0032	-0.49
Cdr2l	0.022	1.0	0.89	-0.49
6330409D20Rik	0.016	0.57	0.17	-0.49
Casc4	0.038	0.90	0.76	-0.48
Pxdc1	0.036	1.0	0.87	-0.48
Arhgef2	0.048	1.0	0.14	-0.48
Gm28221	0.0087	1.0	0.28	-0.48
Gpr182	0.022	1.0	0.68	-0.48

Tmem184b	0.028	1.0	0.87	-0.48
Mfsd11	0.0019	0.61	0.94	-0.47
Ewsr1	0.022	1.0	0.89	-0.47
Lxn	0.012	1.0	0.16	-0.47
Ehd1	0.031	1.0	0.56	-0.46
Gm17334	0.0028	0.91	0.77	-0.46
Matr3	0.033	1.0	0.83	-0.46
Slc3a2	0.0048	0.65	1.0	-0.45
Nfkbia	0.014	0.48	0.97	-0.45
Uqcrc2	0.048	1.0	0.83	-0.44
Prr14l	0.38	1.0	0.0016	-0.44
Col4a1	0.021	0.35	0.95	-0.44
Spns2	0.014	1.0	0.77	-0.44
Ece1	0.00073	0.13	0.60	-0.43
Gm12184	0.047	0.81	0.78	-0.43
Phactr2	0.040	1.0	0.62	-0.42
Zfp330	0.38	1.0	0.041	-0.42
Sbds	0.029	1.0	0.95	-0.42
Fli1	0.22	1.0	0.05	-0.42
Gm11651	0.0018	0.012	0.67	-0.41
Coq8a	0.72	1.0	5.40E-05	-0.41
Efnb1	0.044	1.0	0.69	-0.41
Atp1b3	0.022	1.0	1.0	-0.40
Srsf9	0.047	1.0	0.88	-0.40
Tie1	0.0038	0.38	0.74	-0.40
Polr3k	0.57	1.0	2.24E-06	-0.40
Junos	0.0036	0.05	0.69	-0.39
Itgb1bp1	0.11	1.0	0.009	-0.39
Ncald	0.021	1.0	0.66	-0.39
Afap1l1	0.018	0.58	0.96	-0.39
Eif1a	0.43	1.0	0.022	-0.39
Dhdh	0.70	1.0	0.014	-0.38
Mkl2	0.22	1.0	0.026	-0.38
Jun	0.0087	0.18	0.98	-0.38
Casp6	0.047	1.0	0.74	-0.38
Gm27184	0.050	1.0	0.72	-0.37
Elk3	0.027	1.0	0.70	-0.37
Ptprm	0.028	1.0	0.95	-0.37
Cdk17	0.0069	0.94	0.93	-0.37
Vrk1	0.96	1.0	0.040	-0.36
1700021J08Rik	0.91	1.0	0.049	-0.35
Gm36236	0.53	1.0	0.006	-0.35
Spry2	0.012	1.0	0.027	-0.34
Flt1	0.042	1.0	1.0	-0.34

Ace	0.012	0.11	0.97	-0.34
Mfge8	0.036	1.0	1.0	-0.34
Snrnp25	0.87	1.0	2.08E-05	-0.33
Gbp2	0.23	1.0	0.035	-0.33
Foxp1	0.034	1.0	0.96	-0.33
Pan2	0.41	1.0	0.017	-0.33
Rad21	0.017	1.0	0.94	-0.32
Mybbp1a	0.022	1.0	0.96	-0.32
Casd1	0.55	1.0	0.0038	-0.32
Fmo2	0.010	1.0	0.88	-0.31
Adgrf5	0.022	0.11	0.92	-0.31
B230207O21Rik	0.71	1.0	0.00014	-0.31
Vav2	0.36	1.0	0.031	-0.31
Atxn1	0.51	1.0	0.014	-0.30
Elovl5	0.044	1.0	0.95	-0.30
Rhbdd3	0.0036	1.0	0.68	-0.29
Calcrl	0.048	0.079	0.87	-0.29
Rprd1b	0.048	1.0	0.97	-0.29
Commd7	0.58	1.0	0.0045	-0.29
Sfpq	0.02	1.0	0.76	-0.26
Asap2	0.01	1.0	0.97	-0.26
Eif2d	0.53	1.0	0.028	-0.25
Zmym5	0.49	1.0	0.015	-0.25
Man1a2	0.77	1.0	0.00029	-0.25
B3galnt2	0.29	1.0	5.91E-05	-0.24
Tspan2	0.52	1.0	0.0040	-0.24
Fkbp3	0.55	1.0	0.033	-0.23
Cpsf2	0.53	1.0	8.87E-05	-0.23
Pelp1	0.92	1.0	0.00097	-0.23
Aph1a	0.56	1.0	0.011	-0.23
Trim6	0.019	1.0	0.97	-0.23
Plec	0.42	1.0	0.043	-0.22
Ddx10	0.74	1.0	0.044	-0.21
Tnfrsf18	0.73	1.0	0.016	-0.20
2310057M21Rik	0.95	1.0	0.041	-0.20
Gm10138	0.015	1.0	0.0036	-0.19
Dennd2c	0.95	1.0	0.0059	-0.18
Fgfrl1	0.72	1.0	0.026	-0.16
Scfd1	0.27	1.0	0.0066	-0.14
Capza2	0.48	1.0	0.041	-0.14
Gm9939	0.75	1.0	0.016	-0.13
Ctsd	0.69	1.0	0.0032	-0.13
Cd72	0.94	1.0	0.041	-0.13
Map3k3	0.67	1.0	0.0034	-0.12

Yipf3	0.95	1.0	0.017	-0.11
Gm11960	0.54	1.0	0.00019	-0.11
Gm17080	0.58	1.0	4.22E-08	-0.11
Ssr1	0.63	1.0	0.010	-0.11
Gm24303	0.72	1.0	0.031	-0.10
Tab2	0.90	1.0	0.00018	-0.10
Ssrp1	0.52	1.0	0.010	-0.09
Gm26699	0.023	1.0	0.826	-0.08
Ndufb3	0.26	1.0	0.030	-0.08
Hinfp	0.90	1.0	0.0067	-0.07
Hoxb5	0.96	1.0	0.0036	-0.06
Dvl2	0.72	1.0	0.0006	-0.06
Cdk14	0.51	1.0	0.0013	-0.06
Srgap2	0.93	1.0	0.0036	-0.04
Mxd3	0.78	1.0	3.86E-07	-0.04
Cwc27	0.93	1.0	5.40E-05	-0.04
Rab33b	0.84	1.0	0.0040	-0.03
Gm24362	0.91	1.0	0.0012	-0.03
Arhgap28	0.80	1.0	0.0012	-0.03
Glb1l	0.84	1.0	0.0036	-0.03
1700016B15Rik	0.71	1.0	0.044	-0.02

Table 7.14: Downregulated genes in *Eltd1*-depleted (exons 4 and 5) total lung endothelial cells. The *p* value of the differentially expressed genes were colour coded to indicate significance ($p < 0.05$). Blue (Wilcox test); yellow (edgeR) and green (MAST).